

PROCEEDINGS OF FIRST INTERNATIONAL CONFERENCE ON SMART SYSTEMS AND GREEN ENERGY TECHNOLOGIES

(ICSGET-2022)

P. Sanjeevikumar
Abdelkrim Haqiq
M. A. Jabbar
MD Asif



River Publishers

Title of the Proceedings: Proceedings of First International Conference on Smart Systems and Green Energy Technologies

TABLE OF CONTENTS

Sl. No	Paper Id	Title of the Paper	Authors
1.	106	Detection and tracking maximum power point of a PV system under PSC using cuckoo search algorithm (CSA) MPPT`	V. Joshi Manohar, S. Saravanan, K. Mahesh, M. Dilip Kumar
2.	157	Design of solar powered high step up non-isolated converter with low switching stress.	B. Nagi Reddy and B Poojitha
3.	516	Control Techniques for Bipolar Bidirectional Converter for Interfacing Renewable Energy Storage System to DC Micro-grid	Srikanth Nunavath and Patil Mounica
4.	553	A Neuro-Fuzzy method for forecasting electricity consumption in the agricultural sector for India	S. Saravanan, Devineni Gireesh Kumar, Sainadh Singh Kshatri, Nagineni Venkata Sireesha, R. Muneeswar, K. Vijaya Bhaskar Reddy
5.	576	Fuzzy Logic Control of Switched Reluctance Motor for Electric Vehicles Applications	Mohammed Mateen, S. Saravanan, D. Gireesh Kumar, K. Vijaya Bhaskar Reddy, K. Mahesh, P. Chandrababu
6.	581	Power Sharing Strategy Based on Inverted Droop Controlled Microgrid	Prabaakaran K, Senthil Kumar R, Srividhya R, Praveen G, Dinesh Kumar R, Sanjai T P
7.	605	Implementation of Leader Follower Approach in Quadcopter	Pandiyarajan.R, Chandravadhana, Vivek. T, Agnishwar Jayaprakash
8.	782	A low-cost IoT-based system for monitoring the health of individual soldiers and tracking their real-time whereabouts in combat zones	A.S.S. Murugan, R. Harshavardhan, N. Karuppiah and P. Manoj Kumar
9.	873	Improved load frequency control of 2-area power system using nature inspired algorithm	Pasalapudi Sai Pavan Kumar, Idamakanti Kasireddy, DSNM Rao, Ch. Phani Kumar
10.	1245	Analysis and Simulation of Fuel Cell Powered Integrated Converter with Single Active Switch	C. V Vijay Kumar, T Sanjana and B Nagi Reddy
11.	2353	Power Optimization Scheme in Electric Vehicle Using Induction Motor Based FOPID	B. Akhil Raj, Devineni Gireesh Kumar,

		Control Strategy	Nagineeni Venkata Sireesha, S. Saravanan, DSNM RAO, R. Muneeshwar, Ranjith Kumar Gatla
12.	2544	Design of IOT Based Real Time Geo-Fencing Model for the Realization of High Security System	Shuvendra Kumar Tripathy, Kaliprasanna Swain, Gopinath Palai
13.	2563	Design and study of a double – boost non-isolated converter with continuous input current	A Gopalakrishna and G Priyanka
14.	2625	Enhancing Smart Farming Techniques by Applying Prediction Techniques through IoT and Machine Learning	Rudraraju Vandana, SV Vaishnavi, G. Surya Prabhav, R. Karthikeyan
15.	2770	IOT Based Renewable Energy Monitoring System	Venkata Suresh Yarava and Hari Shankar Jain
16.	2904	Finger Print Based Intelligent Locker System	Senthil Kumar R, Prabaakaran K, Mohammed Ovaiz A, Suguna R, Shanmugapriya M and Naresh Kumar S
17.	2932	Fully Automated Sun Drying System for Food Grains	Senthil Kumar R, Harshvardhan Naidu S, Suguna R, Raghunandhan R, Poovendan V and Sri Sai Vatsan R
18.	3203	Performance Assessment of SMA Based MPPT Controller for PV System Considering Random PSC	A Suresh Kumar, V Usha Reddy
19.	4100	Performance Enhancement of Partial Shaded Photovoltaic System with the Novel Snake ladder Pattern Array Configuration Scheme	P. Keerti and B. Praveen Kumar
20.	4115	Android Based Campus Solution (AICS) for Department Management	Geerthik. S, Ranganathan. L, Anand. T, Sajitha. L. P
21.	4146	Enhanced Machine Learning Technique for Multi-Stages Alzheimer's Disease Classification	S Bhavya Sri, S Keerthi, Md Hassan, R. Karthikeyan
22.	5358	Fuzzy Logic Controlled Hierarchical Power Management Scheme for A Solid-State Transformer (SST) Interfaced D.C Micro Grid	Udutha Satheesh and B. Raja Gopal Reddy
23.	5467	Design and Implementation of a Low-Cost Fully Automated Solar-Powered Mower Vehicle	R. Harshvardhan, A. S. S. Murugan, D. Obulesu and N. Karupiah
24.	6065	Synthesis of Micro-encapsuled Beeswax using in-situ polymerization and its characterization	K. Vijayrakesh, S. Muthuvel, G. R. Gopinath, R. Sudhakar Pandian, G.R. Rajesh

			Kanna
25.	6562	A New Two Switch Non-Inverted Buck-Boost Converter for PV System	J. N Bhanutej, U Hemalatha and B Nagireddy
26.	6614	Energy Forecasting using Hybridization of CSO with LSTM	P. Elumalaivasan, T. Munirathinam, G. Sasi, R. Rajesh, R. Pradeep, B. Rajmohan
27.	6979	Monitoring and Security Based Smart Wastebin for Real Time Application	Shuvendra Kumar Tripathy, G. Palai, K. P. Swain
28.	7368	Modelling and Implementation of SEPIC Converter for Electric Vehicle Application	Sunil Kumar Chava, Udayini Vanga and Srilekha Akula
29.	7599	Smart Anomaly Detection and Classification for Validation Process of Watch Gears using LABVIEW	Boobalan S, Sanjeeve R, Thaqib K, Vignesh R S and Vignesh S
30.	7933	An Effective Rapid Electric Vehicle Charger Using a Quasi-Direct Boost - Buck Converter	J Sreedhar and U Prashanth
31.	8507	Design of IoT Based Smart, Portable and Low-Cost Massage Band	J. Naga Vishnu Vardhan, K. Deekshitha, S. Tejaswini Harshitha, K. Devi Saranya, S. Harika, G. Srinivasa Rao
32.	8931	Comparative study on Sudoku using Backtracking algorithm	T Navya, T J Mounika, S Tharun, Kaladevi R, Hariharan S, Bhanuprasad A
33.	9588	Composite and Microencapsulated Phase Change Materials: A Brief Review	Ashok Kumar B J, Muthuvel S, Rajini N, Gopinath G R, Sudhakara Pandian R and Rajesh Kanna G R
34.	9665	Hardware Implementation of Electric Spring Converter in a PV and Wind based Smart grid for Power Quality Improvement	M. S. G. Smitha and Md. Asif

Detection and Tracking Maximum Power Point of a PV system under PSC using Cuckoo Search Algorithm (CSA)

V. Joshi Manohar¹, S. Saravanan², K. Mahesh², M. Dilip Kumar³

¹Department of EEE, Presidency University, Itgalpur, Rajankunte, Bengaluru, India

²Department of EEE, B V Raju Institute of Technology, Narsapur, Telangana, India.

³Department of EEE, Marri Laxman Reddy Institute of Technology, Dundigal, Telangana.

Email: mahesh.k@bvr.it.ac.in

Abstract

This research suggests using the Cuckoo search (CS) MPPT approach (MPPT). Using the array's maximum power point might make the system more expensive and less effective. The proposed solution is easy and cheap. PSC may cause the PV array's P-V curve to have several peaks. A conference this enormous has only occurred once in human history. The circumstances make traditional MPPT approaches less effective. For this, a two-stage MPPT approach was created. Continuous sampling of the array's P-V characteristic is utilised to discover the partition shading condition (PSC) and global maximum power point (GMPP) (MPP). An open loop makes the suggested technique straightforward and inexpensive to implement. Cuckoo search MPPT controller controls the Boost converter's duty cycle for optimal performance (CS). Fast and stable, it performs well as a dynamic partial shadow MPPT. This research addresses classic MPPT difficulties using CSA MPPT (such as incremental conductance MPPT, P and O MPPT, and PSO MPPT). To implement system simulation findings, MATLAB/SIMULINK is used.

Keywords. Photovoltaic (PV), Maximum Power Point Tracking (MPPT), Cuckoo search (CS) MPPT, Partial Shading Condition (PSC).

1. INTRODUCTION

As the world's population grows and the world's supply of fossil fuels depletes, we must find new ways to meet our energy needs. The potential of this new technology has drawn the attention of solar power experts. You can use the sun's power by using photovoltaic cells (PV). In the event that you can afford it, get equipment that needs little to no upkeep. When it comes to photovoltaic (PV) systems, the temperature and intensity of the sun's radiation may either help or hurt them. Solar radiation for photovoltaic (PV) systems is at its most efficient when it is 25 degrees Celsius and delivers 1000 watts per square metre. By comparing the voltage output and the current usage, you can figure out how much power the module puts out. The P-V curve in PV systems can only be converted at a single point. A D'P and DC-DC converter-based MPPT system is also available. Solar power controllers may be beneficial in certain situations. The MPPT system's instructions to the converter have been updated. Keeping the MPP away from the operation is essential. Consequently, PV modules are capable of producing large quantities of electricity. A possible link exists

between the quantity of sunshine that solar panels get and the temperature that they experience (UI). which shows that the PV module's cells may generate large amounts of electricity in a short length of time without being damaged. It's possible to keep tabs on the MPP in this way. It's also possible to buy FSC controllers or fractional open-circuit voltage and current versions shaded, energy is lost. A hot spot may be extinguished by using an anti-polarity diode. The P-V curve of a circuit with a bypass diode has multiple power peaks. Hardware and software safeguards may be used to disguise sections of a structure. Improved PV module interfaces and DC-to-DC converters are two examples of this. Large and sophisticated systems need a long amount of time to test. For example, traditional technology might benefit from the use of soft computing. Fuzzy logic and artificial neural networks are two examples of this ever-evolving technology. MPPT also makes use of metaheuristics. Algorithms pollinate flowers. Toward the end of this study, we constructed an autonomous bee colony ABC (ABC). When the parameters of the governing equations are changed, these strategies become progressively complex to implement. This approach needs fewer tuning parameters since it has a better track record of regularity and regular convergence.

2. PROPOSED METHODOLOGY

A) Components of Grid connected PV System

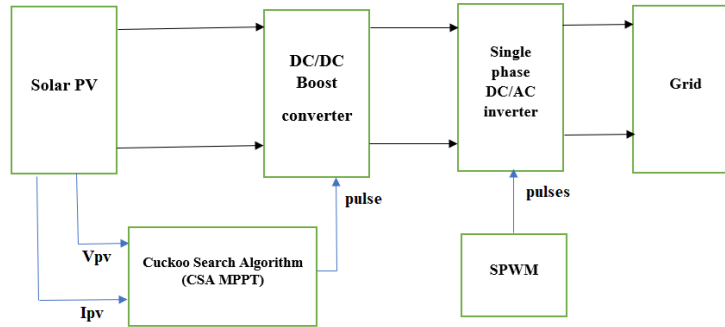


Figure. 1 Three basic components of grid-connected PV systems

PV solar cells, power converters, and a grid interface control system. One of the primary goals of a PV grid-connected system is to regulate the flow of power between the renewable energy source and the utility grid, while also maintaining a high-power quality factor for the PV inverter grid connection. Maximum power point tracking (MPPT) is a way to get the most power out of photovoltaic (PV) solar systems no matter what the weather is like. In PV systems, there are different MPPT algorithms that can be used to reach the MPP. Depending on the weather, these algorithms can be easy or hard to understand. The best is CSA MPPT.

We have the following equation for the current in a solar cell:

$$I = I_{ph} - I_o [e^{q(V + I.R_s)/nkT} - 1] - (V + I.R_s)/R_{sh} \quad (1)$$

Where V_T signifies Voltage at the terminal

I_{ph} signifies the isolation current
 V signifies voltage of the cell
 I signify current of the cell I_o signifies opposite saturation current.

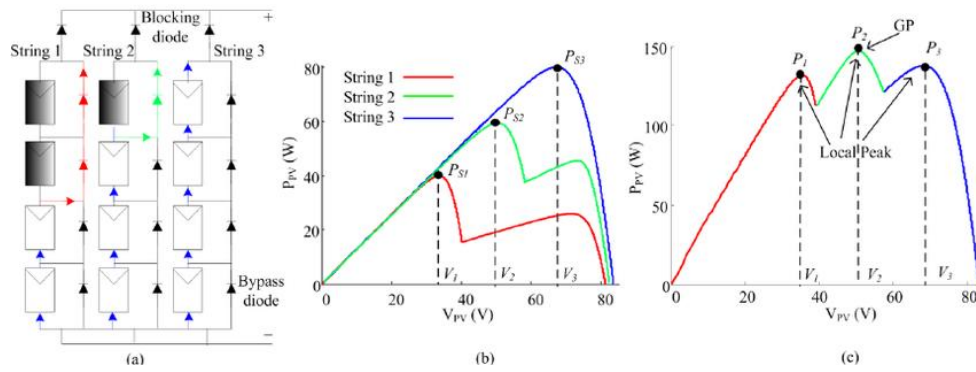


Figure. 2 (a) Sample partial shaded string structure. (b) PV Curve (c) Peak powers

R_{sh} is Parallel Resistance
 R_s signifies Series Resistance
 q signifies basic charge
 n signifies ideality factor of diode

T signifies complete Temperature

V and $P-V$ appearances of the dappled Figure. 2 (a) Sample shaded string structure. (b) I-string.

B) Boost Converter

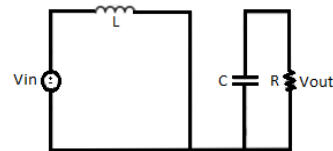
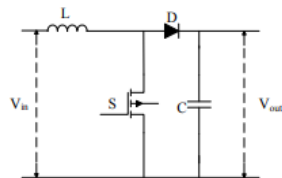


Figure. 3 Boost converter Construction Figure. 4 Alternate Mechanism of boost converter

PV systems need a dc-dc converter because the PV panel doesn't put out enough voltage. A step-up converter, also called a boost converter, increases the value of the dc voltage that goes into it. The energy that is put in is temporarily stored, and then it comes out as a higher voltage at the output. This information is stored in inductors and capacitors. The capacitor smooths out the wave form of the voltage at the output. To cut down on switching Power losses, the MPPT controller sends a switching pulse to a switching device. Here are the specs for how a boost converter presented in figure.3. The boost converter works in two ways, depending on how the reactive parts are charged and drained. During the first mode of operation, the switching device is turned on and the inductor is charged to a certain level of

energy. When the switch is in the "off" position, the reactive component is sent to the output to power the load. To power the load, the stored energy in the inductor is fed into an input voltage that drives the power diode and charges the capacitor. This means, as the name suggests, that the output voltage is higher than the input voltage. During this time, the average output voltage of the system is lower than the average input voltage. This cycle happens again and again until the MOSFET is turned back on. As the inductor's maximum value gets closer to zero, less current flows through it. If the inductor charge current is less than the current needed to provide the output when the switch is off, the converter won't boost the output to the right amount. In order to keep the converter from going into a mode called "discontinuous conduction," the values of the inductor and capacitor must be carefully calculated.

C) DC-AC Converter (Inverter)

By connecting an inverter to the DC-DC buck-boost converter's DC voltage output, power can be sent back into the grid. Grid Side Converter (GSC) is the common name for a three-phase inverter used for DC-to-AC conversion. Figure. 5 shows the three-phase inverter.

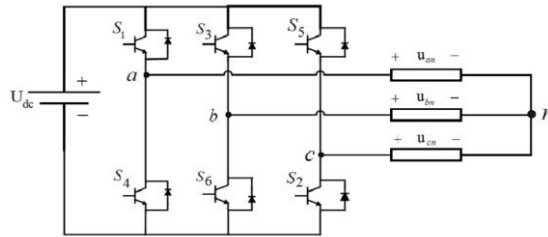


Figure. 5 Basic circuit of Three Phase Inverter

3. CONTROL METHODOLOGY

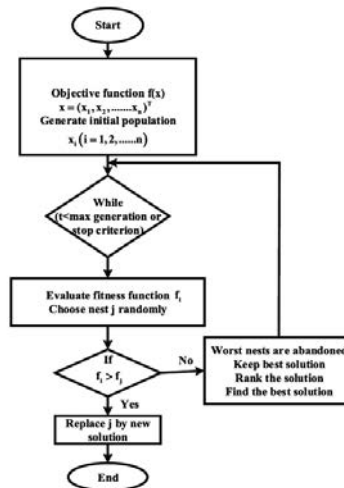


Figure. 6 Cuckoo Search Algorithm

In this project, MPPT with cuckoo search is suggested. The initial random PV voltage solution, V_a , in the cuckoo search method is equal to $[0, 25, 0]$. According to the CS technique, V_a denotes the nest. In order to determine a person's level of power Fitness.

$$P_a = V_a * I_a \quad (2)$$

As soon as you've found the best current solution, you'll "select a random nest and produce a new solution via random walk as." The flow graph of proposed Cuckoo search algorithm is shown in figure.7.

4. RESULTS & ANALYSIS

To verify the performance of the proposed GMPPT algorithm, an experimental setup is developed and the proposed MPPT method is applied to it. Fig. 7 to 11 shows the experimental setup. The setup comprises a boost converter that is paralleled with eight batteries with total 96 V to keep its output voltage (V_o) constant. It is noteworthy that because V_o is used in determination of desired duty cycle, its transients do not deteriorate efficiency of the proposed method.

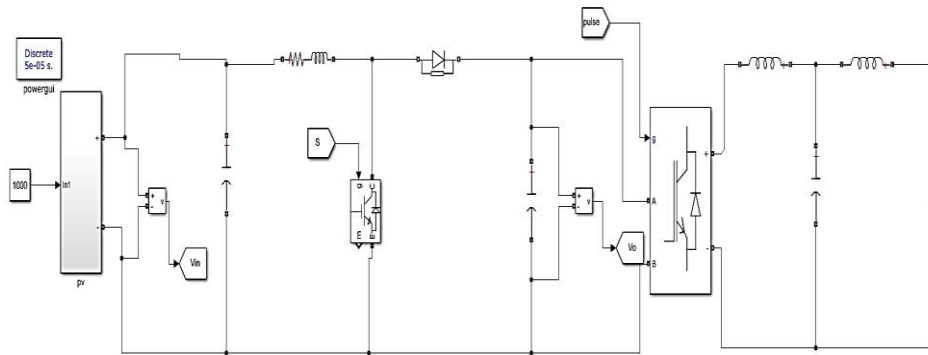


Figure. 7 MATLAB/SIMULINK circuit diagram of the proposed system

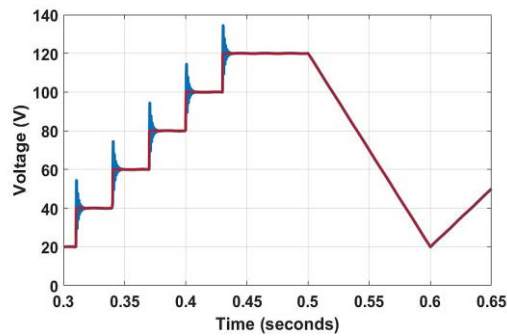


Figure. 8 When a step or ramp command is sent, the switching and averaging state space models of the PV system's boost converter respond accordingly.

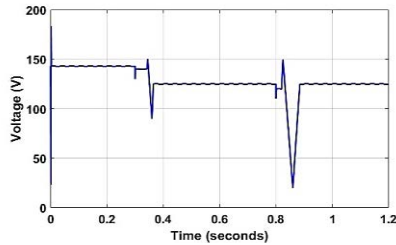


Figure. 9 Array Voltage

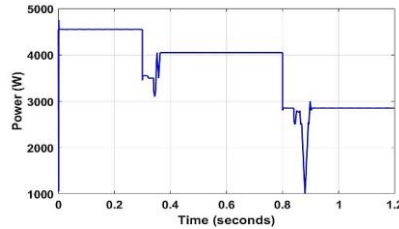


Figure. 10 Array power

5. CONCLUSION

A photovoltaic (PV) system that is connected to the grid and has a low distribution voltage is demonstrated in this article. It is suitable for use in households, in places of business, and even by individual consumers. The Cuckoo Search Method (CSA) and a boost converter topology are both used in the operation of a Maximum Power Point Tracking (MPPT) algorithm (CSA). The findings of a MATLAB/Simulink simulation show how the performance of photovoltaic (PV) systems and the grid shifts over time and in response to variations in irradiation. CSA MPPT is superior to INC and P&O when it comes to the monitoring of radiation conditions that are subject to fast change. The CSA methodology outperformed INC and P&O in terms of obtaining the TMPP more quickly and effectively than the other two ways due to the fact that there were no drifting problems involved.

REFERENCES

- [1] Bouazza Fekkak, Mohamed Mena, Bouziane Boussahoua, "Control of transformer less grid-connected PV system using average models of power electronics converters with MATLAB/Simulink", *Solar Energy*, Vol. 173, 2018, pp. 804-813.
- [2] Sadeq D. Al-Majidi, Maysam F. Abbod, Hamed S. Al-Raweshidy, "A novel maximum power point tracking technique based on fuzzy logic for photovoltaic systems", *International Journal of Hydrogen Energy*, Vol. 43, no. 31, 2018, pp. 14158-14171
- [3] S. Saravanan, K. Karunanithi, S. Pragaspathy, "A Novel Topology for Bidirectional Converter with High Buck Boost Gain", *Journal of Circuits, Systems and Computers*, Vol. 29, no. 14, pp. 2050222-1 – 2050222-27, 2020.
- [4] B. P. Kumar et al., "Performance Enhancement of Partial Shaded Photovoltaic System with the Novel Screw Pattern Array Configuration Scheme," *IEEE Access*, Vol. 10, pp. 1731-1744, 2022.

Design of solar powered high step up non-isolated converter with low switching stress

B. Nagi Reddy^{1,*}, B. Poojitha¹

¹Department of EEE, Vignana Bharathi Institute of Technology, Hyderabad, India

*Email: nagireddy208@gmail.com

Abstract

This article proposes a design of solar powered high step up non-isolated converter with low switching stress. The proposed circuit is designed by merging the traditional switched-inductor (SI) boost converter with a boosting cell. The design of new non-isolated boost DC-DC converter is made to control the DC output of the renewable systems particularly for solar. The proposed converter has various benefits such as providing a high efficiency, simplified control, low voltage stress on the active switches and high step-up voltage gain, which makes it suitable for solar energy applications. Additionally, the suggested configuration enables the shared ground connection between supply and load. The performance of the modified non-isolated converter is evaluated under study state conditions. Operation principles of the suggested topology are shown in detail. To confirm the effectiveness, the theoretical analysis of proposed topology is verified by simulation result. The converter achieved 96% efficiency for the proposed design.

Keywords. DC-DC converter, solar, continuous input current, low stresses, high voltage gain.

1. INTRODUCTION

The challenges of climate change and global warming, both of which are caused by the vastly growing emissions of greenhouse gases, have evolved into significant concerns in the modern world. Photovoltaic (PV) cells, fuel cells, and wind turbines are examples of renewable energy generating technologies that have recently gained favour as potential alternatives. Car high-intensity discharge lights, power supplies, hybrid automobiles, and telecom power systems are just a few examples [1] of the many applications for these lamps. It is possible for a basic boost circuit to attain a boundless voltage gain when the duty ratio is set to 1. Only in theory can this happen. There are large conduction losses in the controlled switch

and diode reverse recovery losses due to high duty cycles [2]. Furthermore, the voltage stress of switch is rather high, which indicates that the switch voltage stress is same as the output voltage. It is possible to get a large voltage gain in flyback, forward, half & full bridges, and push-pull topologies by increasing the number of turns on the transformer [3]. Flyback, complete bridge, and push-pull are other forms of isolated converters.

There are, however, several difficult issues, such as the secondary transformer winding leakage inductance and parasitic capacitance, high spikes in voltage and current, and greater voltage stress on the switching electronics. These issues worsen the system's performance by increasing switching losses due to excessive power dissipation and noise [4]. The switching devices can also be damaged by large voltage spikes, which are also present. By altering the connected inductor's turn's ratio, coupled inductors-based dc-dc converters may also achieve significant voltage gains [5]. They are very easy to manage. This may be accomplished by changing the connected inductor's turn ratio correctly. Voltage spikes occur across the power switches when many inductors are coupled together. In addition to this, the losses caused by leakage inductance bring the converter efficiency down. Because of this, more snubber circuits are necessary, which results in more complicated circuitry [6]. To produce high voltage gain, boost converters can also be used in a cascading or quadratic configuration [7]. In this configuration, two or more boost converters are cascaded together. Cascading boost converters, on the other hand, increase the number of stages, which necessitates a larger board area to house the increased number of switches and gate driver circuits, resulting in a lower power density. Cascading boost converters also increase the size of the board.

When employing many stages, the voltage gain may be enhanced. However, this results in a rise in the total number of circuit components, which leads to more complicated power and control circuits. In addition, the price of the circuit is huge, and its efficiency drops as the aggregate of steps needed to reach a greater voltage grows. In this paper, a novel transformer-less boost converter (TBC) is developed to lower the voltage between switches while still achieving wide step-up voltage. The proposed converter has various benefits such as providing a high efficiency, simplified control, low switching voltage stress on the devices and high step-up voltage gain, which makes it appropriate for solar energy applications [8]. Because of this, the suggested converter requires a lower number of diodes than the traditional SI boost circuit does. This is because the two active switches in the given configuration evenly divide the entire output voltage, which in turn halves the voltage stress that is placed on the switches. So, switches rated for low voltage could be used in the design of the proposed TBC structure. In addition, by employing TBC, a greater voltage gain may be accomplished without an increase in the number of components used in the present SI boost circuit. Also, the converter that was suggested can connect both the load and the supply to a single ground.

2. PROPOSED TBC CONVERTER

Wide voltage gains than standard boost converter may be achieved by utilising SI boost circuit, which incorporates extra switching circuitry. When the voltage gain is raised, however, it causes a large rise in voltage stress on the switches, which leads to a greater development of total output voltage on the switch. With two switches, voltage stress on the switches is minimised in a transformer less active switched inductor circuit. The converter, on the other hand, can only handle floating loads. Figure 1 depicts the circuitry of TBC, a suggested solution to address these limitations. Lower stress on the switches and a larger voltage gain are achieved by using the TBC. Modifying the SIBC's power circuitry is all that is required to create the circuitry. Two diodes D_a and D_b , active switches S_a and S_b , two capacitors C_a and C_b , two inductors L_a and L_b with identical ratings (L), and a load R make up the proposed TBC circuitry. The traditional SI boost circuit's intermediate diodes have been replaced with a capacitor and an active switch. A parallel charging and sequential discharging of energy components are used in the suggested TBC. A series discharge is used to charge the output filter capacitor when the power is turned off, while a parallel discharge is used to charge the other side of the capacitor when it is turned on.

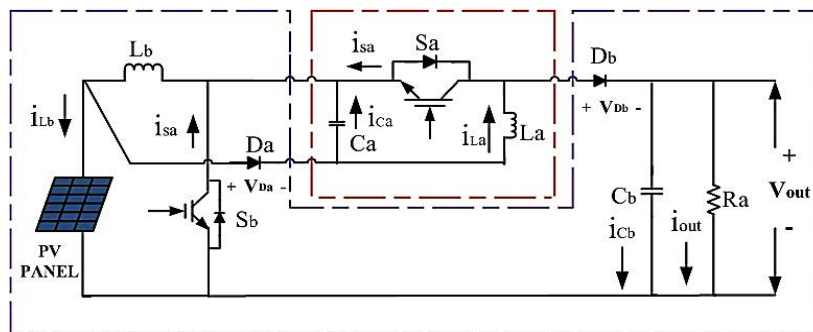


Figure 1. Designed TBC Converter

As a result of this, the suggested TBC reduces the voltage stress on the two active switches to half of what it would otherwise be. This means that the proposed TBC's power circuitry may make use of switches with low voltage ratings. Despite the fact that TBC has the same number of components as a SIBC converter, it has a larger voltage gain. Using this suggested circuit

$$L_a = L_b = L \quad (1)$$

The internal resistance of semiconductor devices and inductors, as well as a capacitor that is very big to maintain a stable voltage, are ignored while studying the characteristics of the circuit's continuous conduction mode (CCM). Time t_0-t_A is the switching duration for mode I in fig. 2 and 3, respectively, which illustrates characteristic TBC waveforms in CCM mode (i.e., ON period).

2.1 Basic operation

There are two modes of CCM operation for the suggested TBC: one in which both switches are on, and one in which both switches are off.

Mode I (Period t_0-t_A): -As seen in figure 2, mode I of TBC has an analogous circuit. Switch S_b charges inductor L_b , while input supply (V_{PV}) charges inductor L_a via diode D_a and switches S_a and S_b , while input supply (V_{PV}) charges capacitance C_a via diodes D_a and switch S_b . Note that the energy elements L_a , L_b , and C_a , are charged in the parallel-paths and the output filter capacitor C_b discharges through a load. In this mode, diode D_a is in forward bias and D_b is in reverse bias. Inductors and capacitors have voltages and currents that may be stated as

$$v'_L = v'_{La} = v'_{Lb} \approx V_{PV}, v'_{Cb} = V_0 \quad (2)$$

$$i'_{PV} = i'_{La} + i'_{Lb} + i'_{Ca}, i'_{Cb} = -i_0 \quad (3)$$

In this case, the superscript is mode I and the subscript are the element.

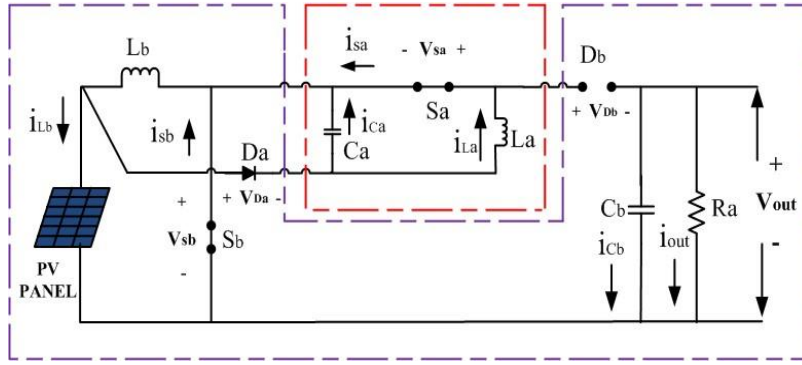


Figure 2. Mode I operation of TBC topology

Mode II (Period t_A-t_B): - TBC mode II comparable circuit is shown in Figure 3. The energy elements L_a , L_b , and C_a , are charged in the series-path with the supply voltage V_{PV} ; electrical power is provided to the load resistance through a diode for the time being the filter capacitor C_b charges. Diode D_a will be reverse biased and D_b is in forward bias, in this stage. Voltages and currents that may be stated as

$$v''_L = v''_{La} = v''_{Lb} \approx V_{PV} - \frac{V_0}{2}, v''_{Cb} = V_0 \quad (4)$$

$$i''_{PV} = i''_{La} = i''_{Lb} = i''_L, i''_{Cb} \approx i''_L - i_0 \quad (5)$$

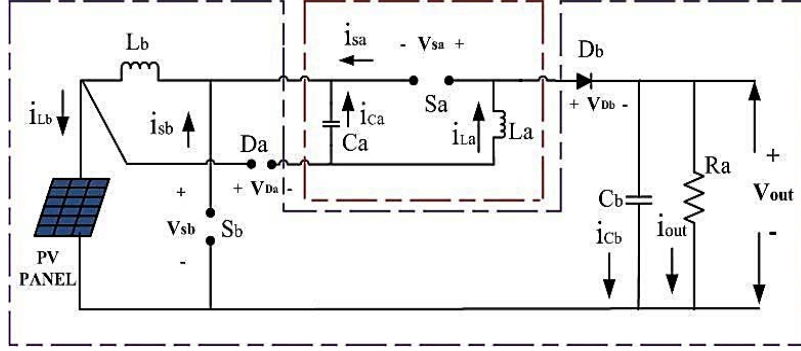


Figure 3. Mode 2 operation of TBC topology

Mode II is represented by a superscript and a lowercase subscript, respectively. The voltage gain of TBC may be written as follows using the inductor volt second balancing principle:

$$\frac{V_o}{V_{PV}} = \frac{2}{1-d} \quad (6)$$

where V_G and d are the voltage gain and duty ratio, respectively. It is clear from equation (6) that the voltage gain of the TBC is superior to that of the traditional converters.

2.2 Inductors design

$$L_a = L_b = \frac{DV_{PV}}{f_s \Delta I_{La}} \quad (7)$$

For $D = 0.6$, $V_{PV} = 24V$, $f_s = 60 \text{ kHz}$ and $\Delta I_{a\&b} = 0.5$, the values of L_a & L_b are given by L_a & $L_b = 480 \mu\text{H}$.

2.3 Capacitors design

$$C_a = \frac{P_{in}(1-D)}{V_{in}f_s \Delta V_{Ca}} \quad (8)$$

$$C_b = \frac{P_o D}{f_s \Delta V_{Cb} V_o} \quad (9)$$

For $D = 0.6$, $V_o = 120V$, $f_s = 60 \text{ kHz}$ and $\Delta V_{Ca} = 2A$, $\Delta V_{Cb} = 1A$. The value of C_a , C_b are given by $C_a = 27.78 \mu\text{F}$, $C_b = 16.67 \mu\text{F}$.

3. SIMULATION RESULTS

The projected converter is designed for an output power of 200W, with an output voltage of 120V. With the input voltage of 24V, the required output voltage

with a gain of 5, can be produced at a duty ratio of 60%. The load resistance is calculated using basic formula as 72Ω . To reduce the converter size, it is advisable to take higher switching frequencies (f_s), however for the proposed simulation and design 60 kHz frequency is considered. The proposed converter contains four energy elements which includes two inductors and two capacitors. With the considerable current and voltage ripples on the inductors and capacitors respectively, the energy component values are calculated and are observed in table 1. Figure 4 represents the input DC voltage waveform along with the input current plotted using MATLAB simulation. A 24V DC input voltage is considered as the output of fuel cell to design the proposed converter which can be observed in fig. 4. Similarly, it can be observed that the input current waveform is continuous and it has a ripple of 5A.

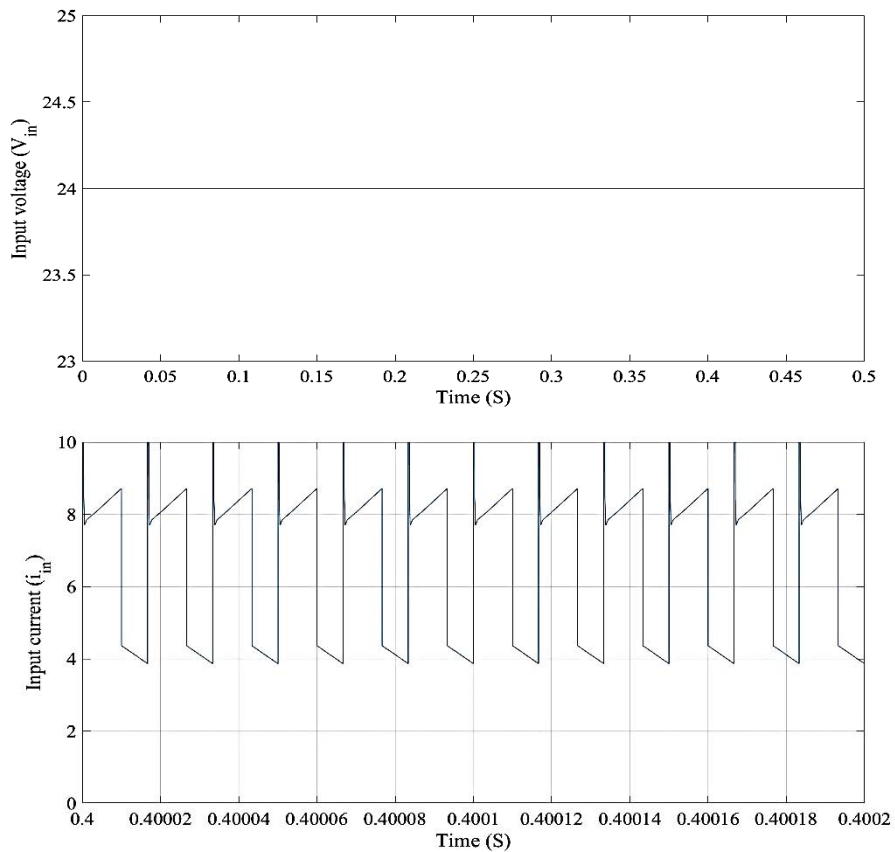


Figure 4. Simulated waveform of the input DC voltage with a voltage 24V and continuous input current with 5 A ripple as considered for design

The simulated voltage waveform of capacitor 1 (C_1) is shown in fig. 5. The charging and discharging phenomenon can be observed in the simulation results (fig. 5), with a considerable peak ripple of 2V.

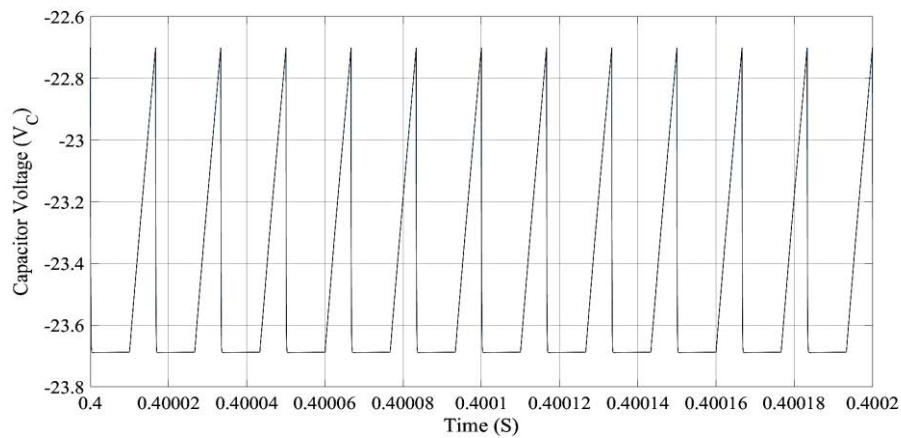


Figure 5. Simulated waveform of the capacitor 1 voltage with a peak ripple of 2V

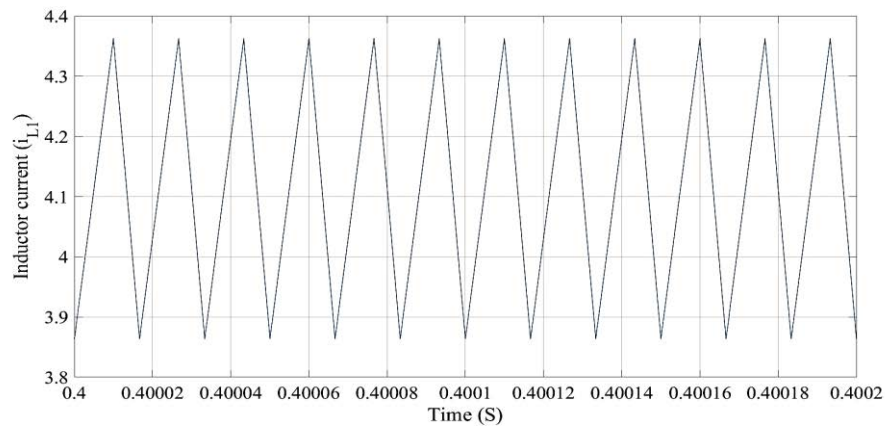


Figure 6. Inductor 1 (L_1) current waveform with a peak-to-peak ripple of 0.5 A

Figures 6 & 7 shows the simulated inductor current waveforms i_{L1} & i_{L2} respectively under steady state operation (for 10 cycles). From fig. 6 it can be noted that the inductor L_1 peak to peak ripple approximately 0.5A. This value is exactly matches to the theoretical consideration of inductor L_1 design. From fig. 7 it can be noted that the inductor L_2 peak to peak ripple approximately 0.5A. This value is exactly matches to the theoretical consideration of inductor L_2 design. Finally, the simulated output waveforms are shown in the figs. 8 & 9 of the proposed converter. The DC output current can be given as 1.6667A theoretically. The simulated value is approximately 1.63A and is much closer to the theoretical value. Figure 9 represents the simulated DC output voltage with very low ripple ($< 0.5\%$ approximately). The simulated value is 118V, much closed to the theoretical value.

As mention above, the output power can be calculated as 192.34W for the 200W design and the voltage stresses of diode 1 voltage is 60V and d2 is 120V. Hence the efficiency is 96.13.

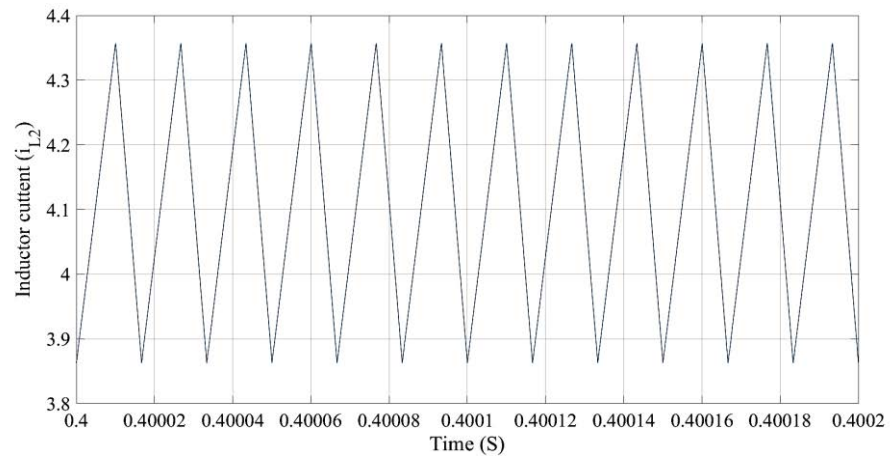


Figure 7 Inductor 2 (L_2) current waveform with a peak-to-peak ripple of 0.5 A

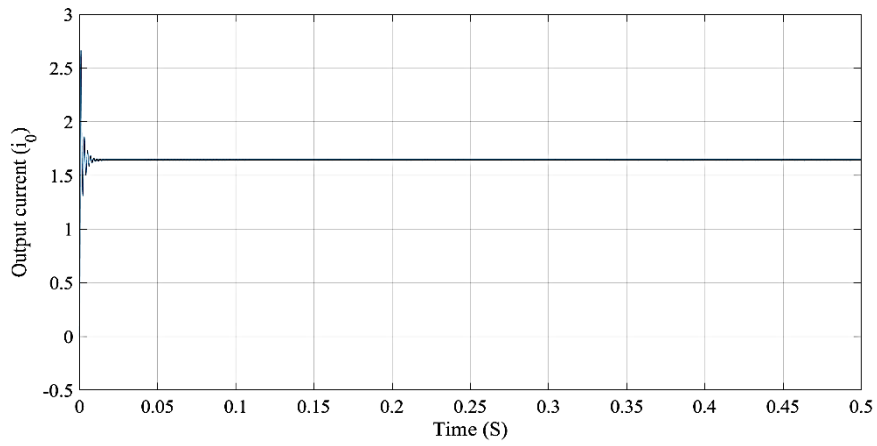


Figure 8. DC output current waveform of proposed topology

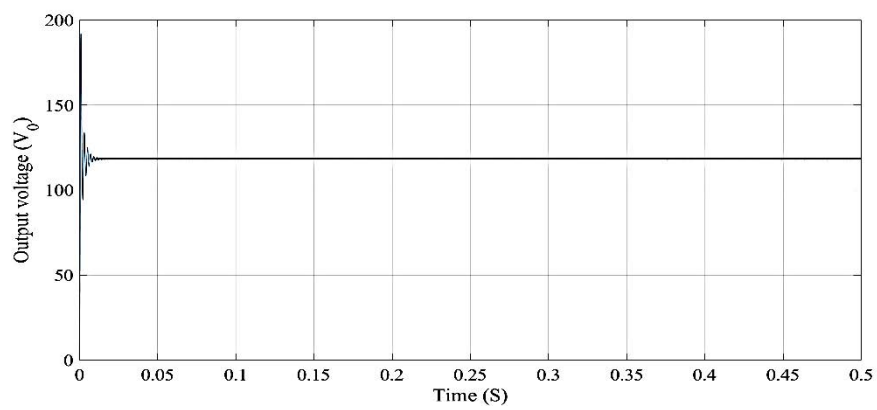


Figure 9. Output DC voltage waveform of proposed topology

4. CONCLUSION

A new TBC configuration was proposed for step-up applications with less voltage stress across the switch. Traditional SIBC required exactly the same number of components as SI boost circuit. When compared to a standard boost network and a SIBC, TBC's voltage gain was significantly higher. As compared to a standard converter, this converter used half as many diodes and experienced half the output voltage stress. As a result, active switches with low voltage ratings might be used in the TBC system. There was a discussion of the CCM mode's operation, including its voltage gain. Switches with lower voltage ratings have been shown to provide a larger voltage gain. Only diode D_a and switch S_b were used to link capacitance in Mode I of the proposed converter architecture to input supply in Mode II.

REFERENCES

- [1] B. Sri Revathi and M. Prabhakar, "Non isolated high gain DC-DC converter topologies for PV applications – a comprehensive review," *Renewable Sustain. Energy Rev.*, vol. 66, pp. 920–933, Dec. 2016.
- [2] M. S. Bhaskar, S. Padmanaban, and F. Blaabjerg, "A multistage DC-DC step-up self-balanced and magnetic component-free converter for photovoltaic applications: Hardware implementation," *Energies*, 10 (5), May 2017.
- [3] S. Padmanaban, M. S. Bhaskar, P. K. Maroti, F. Blaabjerg, and V. Fedák, "An original transformer and switched-capacitor (T & SC)-Based extension for DC-DC boost converter for high-voltage/low-current renewable energy applications: Hardware implementation of a new t & SC boost converter," *Energies*, vol. 11, no. 4, Apr. 2018, Art. no. 783.
- [4] R. Suryadevara and L. Parsa, "Full-bridge ZCS-converter-based high gain modular DC-DC converter for PV integration with medium-voltage DC grids," *IEEE Trans. Energy Convers.*, vol. 34 (1), pp. 302–312, Mar. 2019.
- [5] Y. Chen, Z. Lu, and R. Liang, "Analysis and design of a novel high-step-up DC/DC converter with coupled inductors," *IEEE Trans. Power Electron.*, vol. 33, no. 1, pp. 425–436, Jan. 2018.
- [6] R. Moradpour, H. Ardi, and A. Tavakoli, "Design and implementation of a new SEPIC-Based high step-up DC/DC converter for renewable energy applications," *IEEE Trans. Ind. Electron.*, 65 (2), pp. 1290–1297, Feb. 2018.
- [7] S. Lee and H. Do, "Quadratic boost DC-DC converter with high voltage gain and reduced voltage stresses," *IEEE Trans. Power Electron.*, 34 (3), pp. 2397–2404, Mar. 2019.
- [8] Nagi reddy. B, Sahithi Priya. Kosika, Manish Patel. Gaddam, jagadhishwar. Banoth, Ashok. Banoth, Srikanth goud. B, "Analysis of positive output buck boost topology with extended conversion ratio", *Journal of Energy Systems*, 6(1), pp. 62–83, 2022.

Control Techniques for Bipolar Bidirectional Converter for Interfacing Renewable Energy Storage System to DC Micro-grid

Srikanth Nunavath¹, Patil Mounica¹

¹Department of EEE, Vardhaman College of Engineering, Hyderabad, India.
nsrikanth5406@gmail.com, mounica.p@vardhaman.org

Abstract

Electric vehicles have become more popular as they help in reducing pollution and require no gasoline in comparison to other automobiles. As a result, it is essential to develop fast-charging terminals for electrical vehicles (EV) where terminals are operated through dc microgrids. This will help us to alleviate concerns about power quality and increase the efficiency. This work proposes the model predictive control (MPC) and Proportional-integral (PI) techniques to control a bidirectional Buck-Boost converter that is utilized to exchange power between a dc-microgrid and energy storehouse devices. This presented system comprises 2 solar panels with attached converters, storehouse systems, dc loads, and ports for Electric Vehicle charging, and a converter for AC utilities. By controlling the gating of proposed converter by PI and MPC control techniques, the flow of power between battery and microgrid is controlled. Using MATLAB, a bipolar DC microgrid under different climatic conditions and for various loads is simulated and examined voltage unbalance issues.

Keywords. Three-level bidirectional converter, PI controller, MPC technique, Energy storehouse, three-level DC microgrid, Voltage regulation, NPC inverter, State of charge, Buck-Boost converters.

1. INTRODUCTION

A Microgrid is a simple system for transferring power among storage units and loads; A DC microgrid has good efficiency compared to AC microgrid. Ac grids have higher losses such as power factor losses; power density is low, reactive power losses, and poor efficiency. We picked dc microgrids for enhanced performance due because of these losses and complexities in AC. While in bipolar microgrid, the linkage between distributed generation units (DGU) and dc load is versatile. In terms of sharing loads, bipolar microgrid possesses superior control and versatility [1,2] as well as improved voltage profile and Balance. Unstable grid voltage, power issues are the most common issues encountered during load disturbances and power generation variation. bipolar converters or Voltage balancers are better alternative for these issues. There is more literature on voltage equality [7] and fewer papers on voltage balancing by using three-level Boost mode. [5] describes a bidirectional converter controlling strategy for balancing voltage of the bipolar boost converter. [6] explains how to use a neutral point (NPC) converter to manage an EV charging port utilizing voltage balancing approach. [3] shows the MPC

controlling technique for a wind farm's bipolar converter combined with addition of an NPC inverter. In order to obtain high gain for bipolar DC grids, this study suggests a non-isolated three level converter with an overlapped switching capacitor appropriate for both less & more power applications [9]. MPC is to be a powerful, quick, and effective control strategy for the best power translation. The power produced from the PV system is transmitted to dc microgrid by using boost converter [10]. The bipolar bidirectional converter connects the energy storage devices to the microgrid, furthermore loads connected to a dc microgrid. Additionally, this system can reduce imbalance losses while maintaining good voltage profile. bipolar bidirectional converter is controlled, based on the battery's state of charge (SoC).

2. CIRCUIT DESCRIPTION

2.1. Bidirectional converter

There are two modes to operate the three-level bidirectional converter i.e., Boost mode and Buck modes of operation. In buck mode, switch3 (S3) and switch2 (S2) will operate simultaneously and switch1 (S1) and switch4 (4) will be used to make the operation in Boost mode. The equations for the calculation of the three-level bidirectional converter are given below equation 1 & 2.

Switching equations are derived by monitoring the four modes of operations in buck mode as well as Boost mode. In boost mode, the power will transfer to the microgrid from the Battery to balance the voltage at capacitor1 by diodes 1 and 4 in conducting position and the voltage is controlled at the capacitors. The battery becomes discharged. In a similar way the voltage across the capacitor is get charged by doing the operation of diodes 2 and 3 and it will control the voltage across the capacitor2.

$$V_{dc} = V_{cap2} * (1 - S_3) + V_{cap1} * (1 - S_2) \quad (1)$$

Switches 1 & 4 will be in the ON position and the battery will gain power by taking the voltage from load capacitor1 to give or transfer the power to the microgrid when it needs more power. To process for discharging the load capacitor1, switch1 should be in on position. Similarly, battery will also take the power from capacitor2 by making switch 4 ON.

$$V_{dc} = V_{cap1} * S_1 + V_{cap2} * S_4 \quad (2)$$

2.2. Energy Storage System

Renewable energy is always varying the generating power depending on nature and environmental conditions. In a solar plant, the power is high when the sunlight maximum and power generation is low when the sunlight minimum. So, it is necessary to store the power and supply it to the consumers according to their needs. In this study, we are using the Li-ion battery to store the generated power from the PV. The battery is designed with the specification of 120V, 25A in Simulink. So, it can store the power when generating power is high and supply it to the consumers when the generated power is low. The battery is designed with the minimum capacity to store half of the power from the grid. The equation for the design of the battery is analysed from [8] and the modelling is done in MATLAB.

3. THREE LEVEL CONVERTER MODELLING

3.1 Review of the Boost Mode

After examining the different stages of Boost mode, KVL and KCL are used to buck and boost modes, with direct voltage (Vdc) serving as the input signal, capacitor voltages (Vcap1, Vcap2), and inductor currents (I_ind) as state variables. The following matrix representation of the set of equations makes it simple to understand.

$$\begin{bmatrix} \frac{dI_{ind}}{dt} \\ \frac{dV_{cap1}}{dt} \\ \frac{dV_{cap2}}{dt} \end{bmatrix} = \begin{bmatrix} \frac{-R}{L_{ind}} & \frac{-1+S2}{L_{ind}} & \frac{-1+S3}{L_{ind}} \\ \frac{1-S2}{Cap1} & \frac{-1}{R1*Cap1} & 0 \\ \frac{1-S3}{Cap2} & 0 & \frac{-1}{R2*Cap2} \end{bmatrix} * \begin{bmatrix} I_{ind} \\ V_{cap1} \\ V_{cap2} \end{bmatrix} + \begin{bmatrix} \frac{1}{L_{ind}} & 0 & 0 \end{bmatrix} * \begin{bmatrix} V_{dc} \\ 0 \\ 0 \end{bmatrix} \quad (3)$$

3.2 Analysis of Buck Operating Mode

A buck converter's four operational modes are examined for the given case, and the state-space equation is completed in the mathematical form shown below.

$$\begin{bmatrix} \frac{dI_{ind}}{dt} \\ \frac{dV_{cap2}}{dt} \\ \frac{dV_{cap1}}{dt} \end{bmatrix} = \begin{bmatrix} \frac{-R}{L_{ind}} & \frac{S1}{L_{ind}} & \frac{S4}{L_{ind}} \\ \frac{-S1}{Cap1} & \frac{1}{R1*Cap1} & 0 \\ \frac{-S4}{Cap2} & 0 & \frac{1}{R2*Cap2} \end{bmatrix} * \begin{bmatrix} I_{ind} \\ V_{cap1} \\ V_{cap2} \end{bmatrix} + \begin{bmatrix} \frac{-1}{L_{ind}} & 0 & 0 \end{bmatrix} * \begin{bmatrix} V_{dc} \\ 0 \\ 0 \end{bmatrix} \quad (4)$$

where Vcap1 and Vcap2 represent the voltage across the first and second capacitors, respectively. I_ind stands for inductor current, L_ind for load inductor, and Vdc for supply dc voltage. Figure 2 displays the bipolar bidirectional converter's voltage output.

3.3 Discrete Time Modelling

There are numerous ways to change a continuous-time model into a discrete-time model. The first technique is known as discretization by matrix transformation, and the equations needed to turn a continuous-time model into a discrete-time model for state-space analysis are provided by,

$$X = e^{AT} ; Y = (A-1) * (X-1) * B \quad (5)$$

$$Y = \int_0^{Ts} (1 + At) * Bt \quad (6)$$

$$X(n+1) = [X] * x(n) + Y * u(n) \quad (7)$$

Similar calculations are made using the Backward Euler's technique, which is the second way, for (n+1) intervals of current and voltage and specific types of data are anticipated using existing current and voltage values are displayed as follows for the nth sample moment in discrete-time model.

$$\begin{aligned}
I_{ind}(n+1) &= \left(1 - \frac{RT_s}{L}\right) * I_{ind}(n) + \frac{S1 * T_s}{L} * V_{cap1}(n) + \frac{S4 * T_s}{L} * V_{cap2}(n) - \frac{V_{dc}(n) * T_s}{L} \\
V_{cap1}(n+1) &= \left(\frac{-S1 * T_s}{Cap1}\right) * I_{ind}(n) + \left(1 + \frac{T_s}{R1 * Cap1}\right) * V_{cap1}(n) \\
V_{cap2}(n+1) &= \left(\frac{-S4 * T_s}{Cap2}\right) * I_{ind}(n) + \left(1 + \frac{T_s}{R2 * Cap2}\right) * V_{cap2}(n)
\end{aligned} \tag{8.a, b, c}$$

Calculations of sampling time for converter's Boost mode of operation could be made using the discrete-time model as follows,

$$\begin{aligned}
I_{ind}(n+1) &= \left(1 - \frac{RT_s}{L}\right) * I_{ind}(n) - \frac{(1-S2) * T_s}{L} * V_{cap1}(n) - \frac{(1-S3) * T_s}{L} * V_{cap2}(n) + \frac{V_{dc}(n) * T_s}{L} \\
V_{cap1}(n+1) &= \left(\frac{(1-S2) * T_s}{Cap1}\right) * I_{ind}(n) + \left(1 - \frac{T_s}{R1 * Cap1}\right) * V_{cap1}(n) \\
V_{cap2}(n+1) &= \left(\frac{(1-S3) * T_s}{Cap2}\right) * I_{ind}(n) + \left(1 + \frac{T_s}{R2 * Cap2}\right) * V_{cap2}(n)
\end{aligned} \tag{9.a, b, c}$$

4. CONTROL TECHNIQUES

4.1 PI Controller for Bipolar Converter

The bidirectional converter can be controlled using the PI controller in two different operating modes. The battery's SOC determines whether the battery is operating in buck mode or boost mode. The converter can operate in Boost mode if the SOC min is smaller than SOC and Buck mode if the SOC max is greater than SOC. The controller's primary goals are to recover produced power and balance capacitor voltage under various load circumstances. The issue will be detected when the reference point and grid voltage are compared by PI controllers. The error will be reduced in the current controller, which will then transmit information to the switches S2 and S4. The voltage throughout both capacitors is checked accordingly at the PI block, which then uses a PI controller to transmit switching sequence to the S1 and S3; the voltage is controlled at 300 volts and adjusted at 150 volts. When the charge status (SOC) meets all requirements, the valves S1, S2, S3, and S4 are turned on accordingly. It will shut off immediately if the SOC condition is not met.

4.2 MPC Controller for Bipolar Converter

The PI control technique is used to compute the voltage regulation. The charge status (SOC) is used to determine whether the battery situation is within acceptable bounds and to help in selecting the converter's operating modes. The model predictive control technique's objective is to maintain a steady voltage level during variations in load and manage the grid voltage to boost grid efficiency. It will investigate the difference between both the load demand (PL) and produced power (Pg) to decide whether to operate in buck mode or boost mode. If difference of powers is negative or $P_g < P_L$, the battery discharges and delivers energy to the grid while operating in the boost mode. The converter will select the Buck operating mode as well as the storage system will charge or retain from grid power if $P_g > P_L$ or difference in the two power is Positive. Figure 5 shows the MATLAB / Simulink environment used to create the model predictive control.

5. SIMULATION RESULTS

5.1 MATLAB Results of PI technique

By varying solar irradiation levels

The DC microgrid is powered by 2 PV panels, and maximum output power is drawn from the PV panels by using incremental conductance algorithm in the MPPT technique. The microgrid is connected with 900w DC-load, irradiation levels for PV1, PV2 are maintained at 500,600 W/m² and for this case $P_g=1100>P_L=900$. The needed load power is drawn out of DC microgrid, converter is operated in buck, and battery is charged. At $t=2$ sec, the illuminations are adjusted to 400, 300W/m² for PV1&PV2, Therefore, $P_g=700<P_L=900$. The Boost mode is activated, supplying the DC grid. At $t=4$ sec, illuminations are increased to 1800 W/m², so the $P_g=1800>P_L=900$, resulting battery is charging by activating buck mode. Figure 6 depicts the corresponding waveforms.

By varying Load conditions

Here by keeping a constant load at the grid, the irradiation levels of the PV1 & PV2 are changed to check the Battery status. Whenever the irradiation levels of PV panels are changed, the Storage system can adjust the power and gives constant required power to the load. By observing the Waveform from figure 1 of irradiation levels, initially, 500W/m² at PV1 and 600W/m² are given to the PV2. After $t=2$ s the irradiation levels of PV1 are changed to 400W/m² and PV2 is changed to 300W/m². At $t=4$ s again the irradiation levels of PV1 are set to 1000W/m² and irradiation levels of PV2 are set at 800W/m² and continuously keep on changing the irradiation levels them to check the battery status and to maintain the constant power at load.

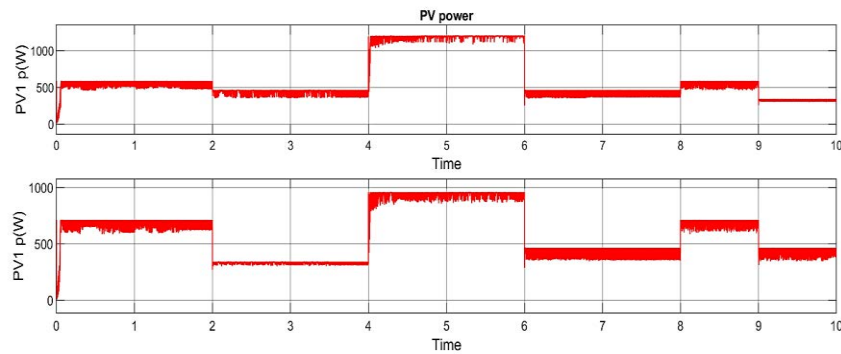


Figure 1. change in irradiation levels of PV1 and PV2

The load is kept constant at 900W and by changing the irradiation levels of the Solar panels, the required power is supplied from the PV panels with a help of a storage system. Initially, 1100W of power is generated from the PV panels and 900W of power is given to load and the remaining power of 200W is stored in a battery. At this moment the Battery SOC is increased. The power exchange from the grid and storage system is done by a Bidirectional Buck-Boost converter. At $t=2$ s the generated power from both panels is 700W, here the generated power is less than the load power so the storage system will provide the remaining

200W of power. At this instant, the State of charge (SoC) is slightly decreased, and this process will continuously happen during the change in generated power by keeping the load constant.

At the time of State of charge increased, the Voltage of the battery also increased, and the battery current is negative. Whenever the SoC is starting decreasing, the battery voltage is decreased for 2 seconds and the battery current increases due to the SoC decreasing.

The waveform of Battery Power is the product of the current and voltage of the battery. By observing the waveform of battery SoC and power waveform, at the period of power is low at the Battery, the SoC is high and if the power is high, the SoC starts decreasing during the period of power increment

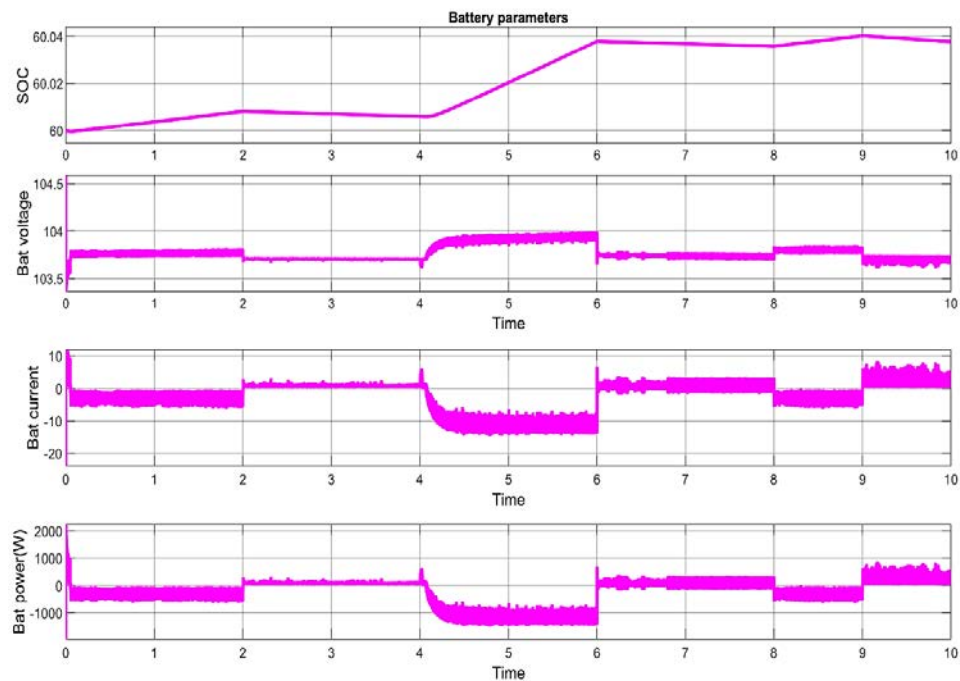


Figure 2. Waveforms of Battery parameters

Here the Load at the Grid is maintained constant to check the performance of a Bipolar Bidirectional converter and power exchange between the Grid and Energy storage system. We connected the two constant loads at 400W.

The voltage of each load is constant at 150V, and the Load current of each load is constant at 2.5A. By adding both loads the total required power to the load is maintained at 900W shown in the waveform figure 2.

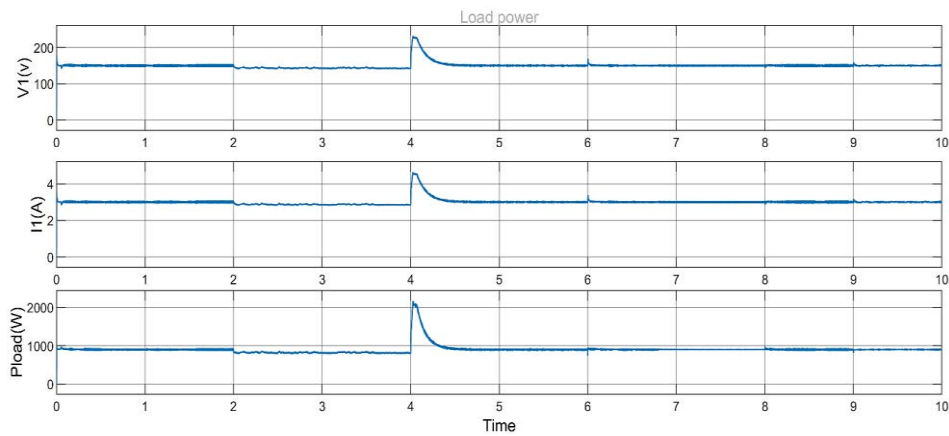


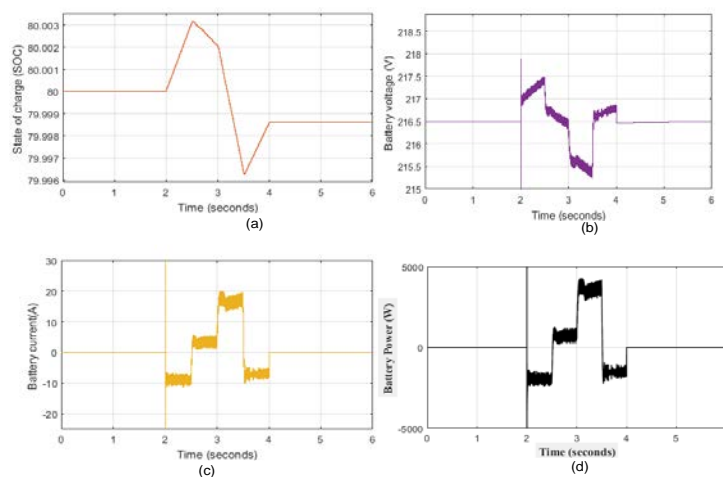
Figure 3. Load waveforms

5.2 MATLAB results of MPC technique

By varying irradiation

In this, the illumination rates are altered while maintaining a steady load. Each DC grid pole is interconnected to a continuous load of 650W, and the maximum load linked to the grid is 1300W. The voltage at grid is seen when the PV1 and PV2 irradiation levels are adjusted to 600 W/m^2 and 400 W/m^2 , respectively. This results in produced power of 1020W and demand power of 1300W. ($P_g < P_L$).

The boost mode is activated and 280W of electricity from the storage system is sent to the grid network. At $t=2\text{s}$, the PV1 and PV2 have respective irradiation levels of 1200 and 800 W/m^2 , as well as the produced energy is 1890W, that is greater than the load demand ($P_g > P_L$). The battery should charge with 620W at this moment since the converter is operating in buck mode. When additional power is needed by the load, the storage system can provide to the grid. This process will continue, and power will be adjusted between the load demand and produced power.



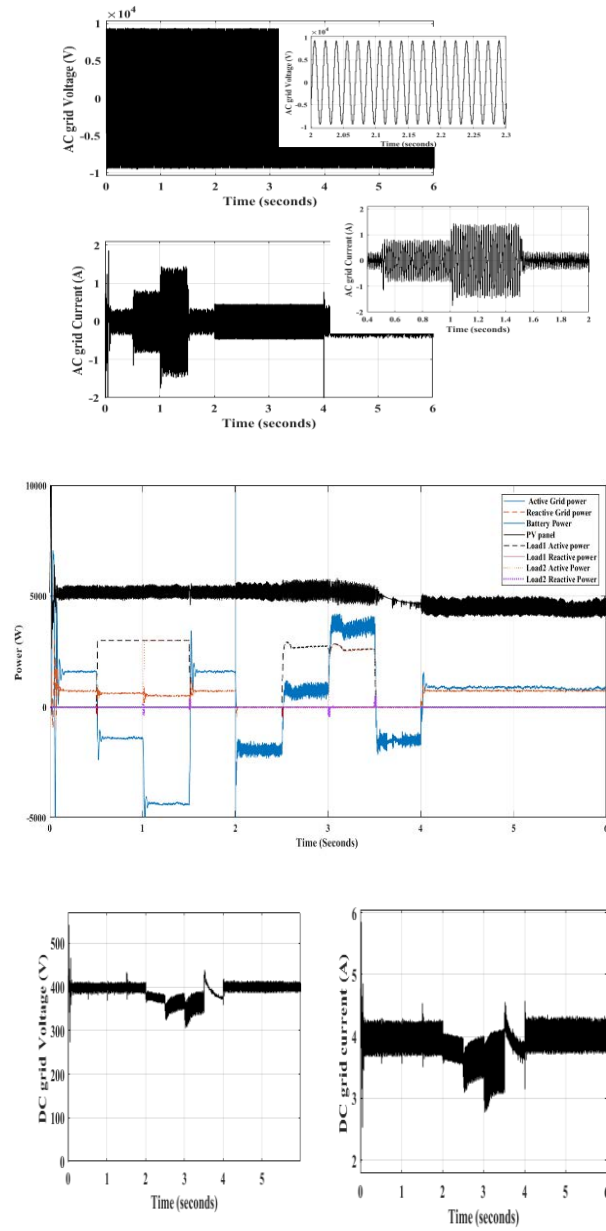


Fig. 4. (A). Battery specifications, (B). Voltage & current of AC grid, (C). Voltage & current of DC grid, (D). power curves

By changing the load

Both PV1&PV2 photovoltaic panels are receive 500 W/m^2 and 600 W/m^2 of irradiation, accordingly, are kept at particular irradiation levels. we adjust the load to get a different converter operation. The DC grid is initially loaded with 350W and 450W of power. The P_g is currently 1050 W greater than the 800 W of PL currently put to the grid. At this instant the battery will charge with 250W. The total load is adjusted to 1800W ($P_g < PL$) at time $t=2s$, the converter will work in boost mode, and the battery will supply the final 750W of electricity to microgrid to balance the load demand. The MPC technique can regulate the voltage at the Grid network as seen in waveforms, and whole bipolar DC grid voltage is controlled at 300V, much as PI technique. In comparison to PI technique, the MPC technique responds more quickly to changes in load.

6. CONCLUSION

In MATLAB, the developed scheme of the bipolar bidirectional converter aiding a DC-microgrid is constructed. At various load conditions, various irradiation levels the results of simulation are analysed. load imbalances are introduced in the DC microgrid by varying loads connected to the microgrid while maintaining the balance of load capacitors C1, C2. The DC grid regulates a total voltage of 300V, and balanced voltages at capacitor's are +150v, -150v. The problem of grid's unbalanced voltage is reduced utilising PI and MPC control strategies, and the DC microgrid's efficiency is improved. DC grid voltage is converted to AC voltage for AC loads by using an NPC converter, which balances active power in AC loads.

PI controller does have some disadvantages, such as a slower response time than Model Predictive Control method and has more ripples in output waveform. Model predictive control operation overcomes the issues and demonstrates this is a far more efficient and productive control mechanism in terms of power conversion than that of PI control scheme.

REFERENCES

- [1] H. C. Chen, and J. Y. Liao, "Modified interleaved current sensor less control for three-level boost PFC converter with considering voltage imbalance and zero-crossing current distortion," *IEEE Trans. Ind. Electron.*, vol. 62, no. 11, pp. 6896–6904, Nov. 2015.
- [2] Mounica, Patil & Sandepudi, Srinivasa. (2021). Bipolar Bidirectional DC-DC Converter for Medium and High Voltage DC Micro grids. 1-5.
- [3] F. Wang, Z. Lei, X. Xu and X. Shu, "Topology Deduction and Analysis of Voltage Balancers for DC Microgrid," in *IEEE Journal of Emerging and Selected Topics in Power Electronics*, vol. 5, no. 2, pp. 672-680, June 2017.
- [4] V. Yaramasu and W. Bin, "Predictive control of a three-level boost converter and an NPC inverter for high-power PMSG-based medium voltage wind energy conversion systems," *IEEE Trans. Power Electron.*, vol. 29, no. 10, pp. 5308–5322, Oct. 2014.

- [5] H. Kakigano, Y. Miura, and T. Ise, "Low-voltage bipolar-type dc microgrid for super high-quality distribution, " *IEEE Trans. Power Electron.*, vol. 25, no.12, pp. 3066–3075, 2010.
- [6] R. M. Cuzner, A. R. Bendre, P. J. Faill, and B. Semenov, "Implementation of a non-isolated three level dc/dc converter suitable for high power systems," in *Proc. 42nd IEEE IAS Annu. Meeting, 2007*, pp. 2001–2008.
- [7] L. Tan, Bin Wu, Venkata Yaramasu, Sebastian Rivera, and Xiao qiang Guo, "Effective Voltage Balance Control for Bipolar-DC-Bus-Fed EV Charging Station with Three-Level DC–DC Fast Charger," *IEEE Trans. Ind. Electr.*, vol. 63, no. 7, pp 4031-4041, July 2016
- [8] X. Zhang, C. Gong, and Z. Yao, "Three-Level DC Converter for Balancing DC 800-V Voltage," in *IEEE Trans. on Power Electronics*, vol. 30, no. 7, pp. 3499-3507, July 2015.
- [9] V. F. Pires, D. Foito, A. Cordeiro and A. J. Pires, "A Bidirectional DC-DC Converter to Interlink Unipolar and Bipolar DC Microgrids," 2021 9th International Conference on Smart Grid (icSmartGrid), 2021, pp. 37-42, doi: 10.1109/icSmartGrid52357.2021.9551209.
- [10] Tremblay O, Dessaint L-A, Dekkiche A-I (2007) A generic battery model for the dynamic simulation of hybrid electric vehicles. In: *Proceedings of 2007 IEEE vehicle power and propulsion conference*, pp 284–289
- [11] Patil Mounica & S Srinivasa Rao (2021), "Bipolar Bidirectional DC-DC Converter for Bi-polar DC Micro-grids with Energy Storage Systems", *International Journal of Electronics*, 2021.
- [12] Nisha KS and Dattatraya N Gaonkar "Predictive Control of Three Level Bidirectional Converter in Bipolar DC Microgrid for EV Charging Stations" *IEEE PESGRE 2020*.

A Neuro-Fuzzy Method for Forecasting Electricity Consumption in the Agricultural Sector for India

S. Saravanan¹, Devineni Gireesh Kumar^{1*}, Sainadh Singh Kshatri¹,
Nagineeni Venkata Sireesha², R. Muneeswar¹, K. Vijaya Bhaskar Reddy¹

¹Department of Electrical and Electronics Engineering, B V Raju Institute of Technology, Narsapur, Telangana, India.

²Department of Information Technology, Institute of Aeronautical Engineering, Dundigal, Hyderabad.

Email: gireesh218@gmail.com

Abstract

The forecasting of electrical energy consumption (EEC) plays a key role in the planning, scheduling, and operation of the power system. Consequently, accurate and reliable prediction of electrical energy consumption is important and electrical energy is also very relevant for developing and developed countries. As the economy of these countries grow in the positive direction, their electric energy consumption increases rapidly. In this research study, ANFIS technique is applied to predict the long-term agriculture sector (AS) EEC in India. The empirical data inputs identified in this study are population, per capita GDP and permanent crop land (% of land area) and the AS-EEC is the predicted output variable. The time span considered for the historical data used in this study are between 1970 and 2021. The available 46 years data are randomly divided into two categories, such as 80% of data is used to train the network and the remaining 20% is used to assess network accuracy. Based on the percentage error calculation, the constructed model shows the very good predicting performance. According to the predicted results by the proposed model, the AS-EEC in the following years 2025 and 2030 will reach 223.465 Tera Watt hour (TWh) and 255.023 TWh respectively.

Keywords. Electrical energy consumption; India; agriculture sector; ANFIS.

1. INTRODUCTION

Electrical energy consumption forecasting (EEC) plays an essential role in planning, scheduling, distribution and power system operation. In general, EEC is linked with the growth of economy and the human population. Recent two to three decades the development of the electrical and electronics industry in the developed and developing country, the EEC is increasing significantly due to the reason behind that, almost in all the field, majority of the work doing with the help of electrical energy and also increasing the human population. Predicting electricity demand has become a very important task for electricity utilities in order to support GDP growth in a positive trend and meet the demand for electricity continuously in the coming years [1]. Because of India's economic growth, energy demand has increased by an average of 3.6% per year over the past three decades. In this contest, a good forecasting method is essential for exact investment planning for new

power generating stations and their types, providing additional/upgrading the transmission and distribution lines and installation/upgrading of the new transformers. The installed capacity of India in the year March 2021 was 382.1 Giga Watts, among that two third of the electricity is produced with the help of the fossil fuels and the remaining one third produced from nonrenewable energy sources.

In India, AS-EC is the third biggest sector of the electric energy consumption. In the year 2015, AS of India consumed 18.36% of electrical energy. Figure 2 shows that the AS-EC has increased exponentially from the year 1947 to 2021. It has increased from 90.292 TWh in 2005 to 214.97 TWh in the year 2021. The growth rate of AS-EC was around 10.59% for the year 2013-14 over 2014-15 and the EEC of AS was reached 17.89 %, which is highest in the year 2015-16 among all countries. Therefore, the forecasting of AS-EEC is essential. The primary objective of this research study is to provide an AS-EEC forecast model taking into account India's population input factors, per capita GDP and permanent cropland (percentage of land area).

For the last four decades, the forecasting of electric energy consumption/demand is a research area of widespread current attentiveness among the researchers. Since 1980, much research was conducted on the conventional methods and the applications of soft computing techniques [2]. Vincenzo Bianco analyzed the EEC prediction in Italy using regression analysis. They used a historical data between 1970 and 2007.

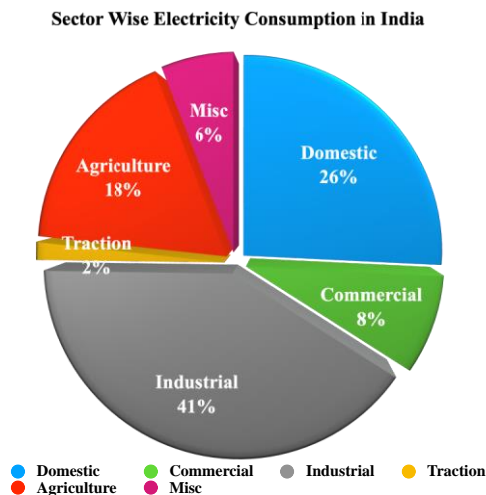


Figure 1. Sector wise electricity consumption in India as on 31 March 2021.

K. Panklib *et. al* [1] predicted Thailand's electricity consumption using multiple linear regression and Artificial Neural Network. It is used GDP, population, average ambient temperature and peak demand for electrical power input variables and stated that the output estimates of an ANN model were more reliable than the regression model. S. Saravanan *et.al* [3] predicted the demand for electricity in India using the Fuzzy logic method and compared the results with the 18th power survey report. They reported that the forecasted results are nearer to the actual value with minimum error. Suhono and Sarjiya [4] used the long-range alternate energy planning

system to estimate the demand for electricity in the household and non-household industries. De Vita et al. [5] studied energy demand in Namibia for the time period between 1980 and 2002.

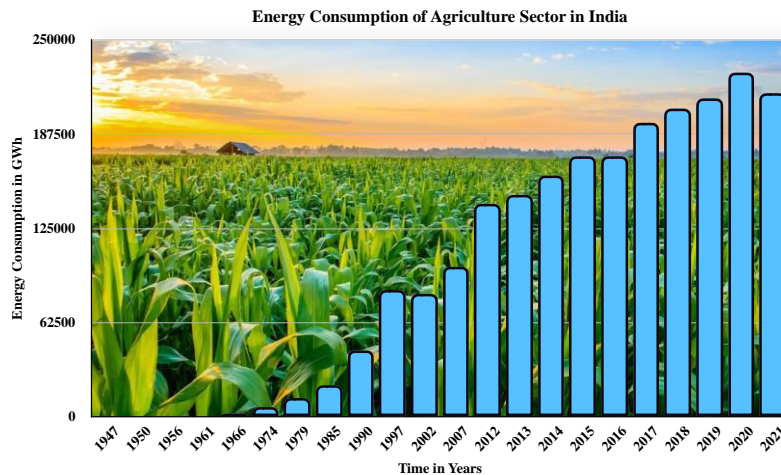


Figure 2. AS-EC between the year 1947 and 2021

They reported that the energy consumption going in negative direction to changes in price of energy and the air temperature and going in positive directions to changes in GDP. P. D. Sreekanth et al used for feed-forward neural network and ANFIS methods for predicting the ground water level in Maheshwaram. They concluded that the both models provided the better accuracy. Elham Pourazarm and Arusha Cooray studied that, residential sector EEC in Iran and also find the correlation between the output variables and its determinants. They estimated that the electricity price was negligible and that the profit elasticity was lower than the level, and that the EEC residential market would rise at an annual rate of 80% by 2020. Kavaklioglu used support vector regression approach for forecasting of EEC in Turkey considered the input variables population, imports, exports and Gross National Product.

2. ARTIFICIAL NEURO FUZZY INFERENCE SYSTEMS

ANFIS is one of the Fuzzy Inference Systems (FIS) most commonly used. Roger Jang proposed in 1993 that ANFIS could correlate the relationship between the data input variables and the output variable(s) using a combination of multilayer feed forward network and FIS. ANN is capable to learn from the experience and generalized the model to produce the significant solutions. Fuzzy logic provides the thinking and reasoning capability. ANFIS can overcome the disadvantages of fuzzy logic and neural network. In fuzzy logic, identify the correct membership function, if-then rules and also poor generalization capability. For neural networks, problem to determine the size and function of the neural network and to establish the learning parameters. The ANFIS is the combination of the FL and the ANN and the preservation of the two strengths, the MF and, if so, the ANN determines and optimizes the laws of the fuzzy structures. A learning procedure has two steps: 1) The input data sets / parameters are propagated and the optimum resulting data is calculated using iterative method, while the training set, assuming the data sets are initially to be defined. 2)

The patterns are circulated again; back propagation is used to alter the initially assumed data during this time, while the resulting data sets remain fixed. Then this process is iterated in [5].

To present the architecture of an ANFIS model, a FIS with three input variables, two rules, and one output variable is considered. ANFIS accepts the input parameters such as population, per capita GDP and permanent crop land (% of land area) in the format.

- The input parameters are given to the ANFIS.
- The network implements the forward pass, i.e., AS-EEC is computed.
- Next input parameters are given continuously to the network and the computing process until the input / output parameters of the network are trained.

3. PERFORMANCE MEASURE AND TESTING

With the following performance criterion, the reliability of a qualified network can be measured: (i) Root Mean Square Error (RMSE).

$$\text{RMSE} = \sqrt{\frac{\sum_{i=0}^n (A_i - P_i)}{n}} \quad (1)$$

and (ii) MAPE or Mean Bias Error

$$\text{MAPE} = \left(\frac{1}{n} \sum_{i=0}^n \left| \frac{(A_i - P_i)}{A_i} \right| \right) \times 100 \quad (2)$$

Where, P_i , A_i are the expected and real data values for example i , and ' n ' is the total data set used for analysis. Lesser the value of MAPE and RMSE indicate that more accuracy in the prediction.

4. RESULTS AND DISCUSSION

The identified input parameters used for this proposed model are population, per capita GDP and permanent crop land (% of land area) and AS-EEC is the predicted output variable. ANFIS modelling includes various parameter choices such as membership functions (MFs), types and MFs numbers relevant to each input parameter, selecting the output of the model being created. Further studies were performed in this research study in order to obtain the best results. The following seven different MFs are considered and the number of MFs varies from 2, 2, 2 to 4, 4, 4 and Table 1 shows the best results for each MF.

- a) Built-in MF consisting of a two-sigmoid MF product ('psigmf')
- b) Generalized bell MF ('gbellmf'),
- c) Gaussian mixture of MF ('gauss2mf'),
- d) Gaussian curve integrated in MF ('gaussmf'),
- e) Built-in trapezoidal MF ('trapmf'),
- f) Built-in MF consisting of two sigmoidal MF gap ('dsigmf')
- g) Triangular MF ('trimf') and
- h) Pie-shaped built-in MF ('pimf').

Table 1: Best results with different number MFs and their types

Types of MFs	No. used in each MFs	MAPE	Types of MFs	No. used in each MFs	MAPE
Psigmf	2,3,4	1.308	Trapmf	3,3,4	0.95
Gbellmf	3,4,3	1.292	Dsigmf	2,3,4	1.308
Gauss2mf	2,4,3	1.422	Trimf	3,4,4	1.29
Gaussmf	4,4,2	1.148	Pimf	3,4,4	1.145

From Table 1, it is examined that the ‘Trapmf’ MF with the numbers used in each MFs are 3, 3, 4 is establish to have a good accuracy in terms of MAPE with 0.95. Table 2 displays the other parameters and their values for the proposed implementation of the ANFIS model.

Table 2: Parameters for the ANFIS model and their values

Parameters	Numbers
Fuzzy rules	36
Epochs	100
Nodes	98
Linear parameters	144
Parameters that are not linear	40
Total parameter number	184
Training pairs of data	41
Testing pairs of data	09

The results for the proposed model are given in the Table 3 and it contains the actual and predicted AS EEC values (TWh), error variation, average MAPE and average RMSE.

Table 3: Comparison between actual and predicted AS-EEC

Year	Actual (TWh)	Predicted (TWh)	Error variation	MAPE	RMSE
1994	79.301	79.3256	-0.031	0.031	0.0006
1980	14.489	14.46923	0.136	0.136	0.0003
1991	58.557	58.54065	0.028	0.028	0.0002
1974	7.763	7.610207	1.968	1.968	0.0233
1992	63.328	64.41742	-1.720	1.72	1.1868
2013	152.744	157.0614	-2.826	2.827	18.639
2021	214.97	216.453	-1.483	1.483	1.1584
Average				1.0031	2.4693

The actual value of AS-EEC in 1985 was 23.42 TWh from the findings in Table 2, and the same was 152.744 TWh in 2013. The AS-EEC was estimated using the proposed ANFIS model is 23.475 TWh for the year 1985, and 157.0614 TWh for the year 2013. The error deviations in the range of -2.826 to 1.596, according to the results obtained.

5. FUTURE PREDICTION

To predict the AS-EEC, the input parameters (population, per capita GDP and permanent crop land (% of land area)) should be examined and should be predicted first and the predict the future years from the year 2023 to 2030. Using the predicted input parameters, an AS-EEC has been predicted using developed ANFIS model. The predicted results are given in Table 4.

Table 4: Predicted values of input parameters and output parameter

Year	Population (Million)	Per capita GDP (INR)	Permanent Crop land (% of land area)	AS_EC (TWh)
2023	1791.531	118984.275	5.023	212.016
2024	1863.192	123743.646	5.108	217.639
2025	1937.720	128693.391	5.195	223.465
2026	2015.228	133841.127	5.283	229.484
2027	2095.838	139194.772	5.373	235.722
2028	2179.671	144762.563	5.464	242.167
2029	2266.858	150553.066	5.557	248.844
2030	2357.532	158234.270	5.764	255.023

6. CONCLUSION

The prediction of AS-EEC is the most important in developing the sustainable energy policies. In this research study, an application of ANFIS, model was designed to map three parameters as inputs and AS-EEC is the predicted output variable. The proposed ANIFS model has very good predicting capability with MAPE of 0.95%. It can be summarized based on the findings that the implementation of the ANFIS model can be used as a useful tool for predicting the AS-EEC. The found results showed that the application of the ANFIS model is reliable and apt for indeterminate data because it composed the futures of fuzzy logic and ANN. The estimated AS-EEC may reach 223.465 TWh and 255.023 for the years 2025 and 2030. The predicted results are useful to give a new way to the power system planners and power producers.

REFERENCES

- [1] K. Panklib, et.al., "Electricity consumption forecasting in Thailand using an artificial neural network and multiple linear regression", *Energy Sources, Part B: Economics, Planning, and Policy* vol. 10, No. 4, pp. 427-434, 2015.
- [2] S. Saravanan, et.al., "Modeling and Prediction of India's Electricity Demand using Fuzzy Logic", *IEEE International Conference on Circuit, Power and Computing Technologies*, pp. 93-96, 2014.
- [3] Suhono and Sarjiya, "Long-term Electricity Demand Forecasting of Sumatera System Based on Electricity Consumption Intensity and Indonesia Population Projection 2010–2035", *Energy Procedia*, vol. 68, pp. 455-462, 2015.
- [4] P. D. Sreekanth, et.al., "Comparison of FFNN and ANFIS models for estimating groundwater level", *Environmental Earth Sciences*, vol. 62, pp. 1301-1310, 2011.
- [5] G. De-Vita, K. Endresen, L. C. Hunt, "An empirical analysis of electricity demand in Namibia", *Energy Policy*, vol. 34, pp. 3447 – 3463, 2006.

Fuzzy Logic based Switched Reluctance Motor for EV

Mohammed Mateen¹, S. Saravanan¹, D. Gireesh Kumar¹, K. Vijaya Bhaskar Reddy¹,
K. Mahesh¹, P. Chandrababu¹

¹Department of EEE, B V Raju Institute of Technology, Narsapur, Telangana, India
Email: mohammedmateen234@gmail.com

Abstract

Fuzzy logic control (FLC) can be used to mitigate the current ripple of electric vehicle (EV) switching reluctance motors. The main goal of this paper is to maintain a motor current value that fluctuates as little as possible while using SRM control with FLC. Depending on the speed of the motor, the PI controller is used to produce the reference current signals. For the controller's responsiveness in fault scenarios, the nonlinear model of the 10/8 SRM with symmetrical converter and C-code controller is applied during the simulation. FLC outperforms more traditional systems like hysteresis current control, according to studies of SRM current control under various fault scenarios.

Keywords. Fuzzy Logic Control, Electric Vehicle, Switched Reluctance motor

1. INTRODUCTION

A streamlined representation of the set of rules served as a model for the creation of computer systems based on fuzzy logic controllers. The most important components of a physical system may be observed through testing or modelling. A few of the technical fields where FLCs are used are dynamic modelling and signal processing [1,2]. Power electronics have employed FLC to control high-performance drives, manage power converters, and locate and identify electrical machine faults [3]. They are able to perform their duties despite the commotion. This technology has been used in hybrid electric cars, aviation starter/generators, washers and dryers, and vehicles over the past 20 years. The remarkable torque-to-weight ratio, straightforward structure, high reliability, and inexpensive price of SRMs are a few factors that contribute to this [1]. Only a few of the topologies supported by SRM are 6/4, 8/6, and 10/8. A nonlinear relationship between the magnetic characteristics of the SRM, phase current, and rotor position serves as the foundation for the controller model. Because the magnetic field is dynamic, it is challenging to develop a mathematical model of it [4]. In controller design and evaluation analysis, linear models have been used to streamline the procedure [5]. The present research focuses on the fuzzy controller of SRM. In order to determine how well the fuzzy controller (FLC) enforces an ideal current profile, controls speeds around a nominal operating point by mapping incremental changes to the reference current (output), and minimises speed errors, it must be compared to a

conventional control system as a method of evaluation (and speed changes). The effectiveness of the suggested control method is shown using simulated data [6]–[7]. Unlike traditional AC and DC electric motors, SRMs offer the design with a machine that lacks a steady state, exhibits high localised saturation, and necessitates a novel power-electronic converter [8]. The SRM is the most cost-effective electrical machine to manufacture [9]. When designing an SRM, it is possible to minimize the thermal load by carefully selecting the various sources of loss [10]. Grid Interconnection of PV system Using Symmetric and Asymmetric MLI Topology and SHE Controlled CHB 7-Level Inverter with Unequal DC Sources using MPSO Algorithm [11]-[12].

2. FLC BASED SPEED CONTROLLER

This FLC relies heavily on the programming language's If-else statement and does not involve any kind of mathematical model. As a result, not only is it easier to execute a very complicated solution, but it is also simpler to analyze the offered solution. The diagram below demonstrates FLC's internal structure. It mainly contains 3 parts i.e., fuzzification, rule- based system and defuzzification.

2.1. Fuzzification

Simplistic definitions to an ever-expanding database: It is possible to map the membership intensity of a subcategory to a specific value, such as (x) (x) . In order to flush a toilet, there are a number of steps. Experiments with the variables to see what happens. Computers change the range of each input variable and then transfer the new range into the matching discourse universe. Input data is transformed into language variables that may be used as fluorescence sets labels.

2.2. Knowledge Base

Fuzzy MFs as input and output variables are based on definitions and control rules that govern when, how, and why to utilize them. A database and a set of language rules are part of the framework. The database serves as a resource for language control and pointless data processing. The basic rule structure uses a collection of language rules to establish control goals and controls for domain experts.

2.3. Defuzzification

Defuzzification is the preferred strategy for numerical values that are influenced by the language in which they are expressed. This inquiry used the centre method. Uses a mapping scale to convert input value ranges into sets of output variable names. A fluctuating control operation may be distinguished from one that is non-fluffy using this method.

The error signal is computed as,

$$e(t)=x_i(t)-x_f(t) \quad (1)$$

Calculation of error change is as follows:

$$E(s) = X_i(s) - X_f(s) \quad (2)$$

The length of the service cycle might either shorten or lengthen as a dependent variable. Table-1 shows the controller's 49 rules. Figures 1 and 2 of the input and output demonstrate seven separate membership functions.

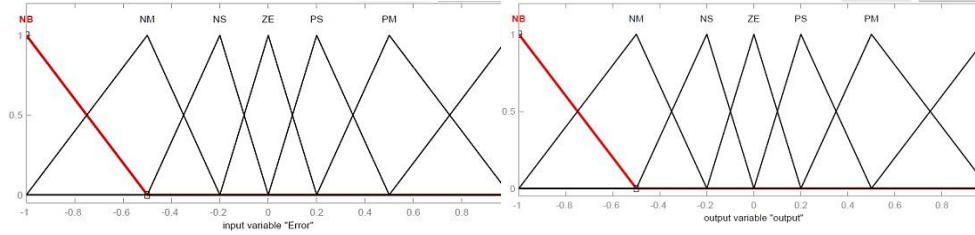


Fig. 1. Input error (Fuzzy set)

Fig. 2. Output delta PWM (Fuzzy set)

3. MODELLING OF ELECTRIC VEHICLE

Creating a new class of electric vehicles from the ground up. An electric vehicle's dynamics can be predicted using its total tractive force. The 'Tracy effort' refers to the total amount of work necessary to move a vehicle.

- Rolling resistance force, $F_{rr} = \mu_{rr} \times m \times g$ (3)

Where, μ_{rr} is signifies the rolling resistance, m is the weight of vehicle & g is gravity.

- Aerodynamic drag, $F_{ad} = \frac{1}{2} \times \rho \times A \times C_d \times V^2$ (4)

Where, ρ = air density, A = front area, V = velocity & C_d = drag coefficient

- Hill climbing force, $F_{hc} = m \times g \times \sin(\psi)$ (5)

Where, ψ is slope inclination

- Linear acceleration force, $F_{la} = m \times a$ (6)

- Pointed acceleration power, $F_{\phi a} = I \times G_{ratio}^2 \times a / (\eta_g \times r^2)$ (7)

Where r is radius of tire, I is motor inertia, G_{ratio} is transmission system gear ratio, and η_g is efficiency of gear. The switching reluctance motor specifications in Table 1 and their dynamics characteristics in Table 2 are provided to represent electric cars. The 48V/200Ah lithium-ion battery pack is available.

Table-1 Motor Specifications

Sl. No	Vehicle model parameter	Values
1	Payload	830 kg
2	Gross wt-m	965 kg
3	Width(w) and Height mm	132.4 × 151cm
4	Frontal Area-A	1.53 m ²

Table-2 Dynamic Constraints of SRM

Sl. No	SRM parameter	Values
1	Model (generic)	10/8
2	Stator resistance	0.05 Ω
3	Stator inductance (L)	970 H
4	Friction (Nm-s)	0.005 Nm-s
5	Inertia (kg-m ²)	0.0082 kg-

5	Coefficient (μ_{rr})	0.005
6	drag coefficient (Cd)	0.6
7	Transmission coefficient (η_g)	0.95
8	Gear ratio	16
9	Gravity acceleration	9.81 m/s ²

		m ²
6	Unaligned (L)	0.00067 H
7	Aligned L	0.0235 H
8	Saturated L	0.00015 H
9	Maximum current	400 A
10	Max. flux linkage	0.486 Wb

4. SIMULATION RESULTS

Figure 2 shows an SRM-powered electric vehicle with fuzzy controller modelled in Simulink Standard State. There is an SRM drive and a battery included in this schematic. The controller has two control loops: one for current and the other for speed. The controller uses the difference between the reference speed and the actual speed to create a reference current. Consistent current is maintained in the designated phase by the current controller.

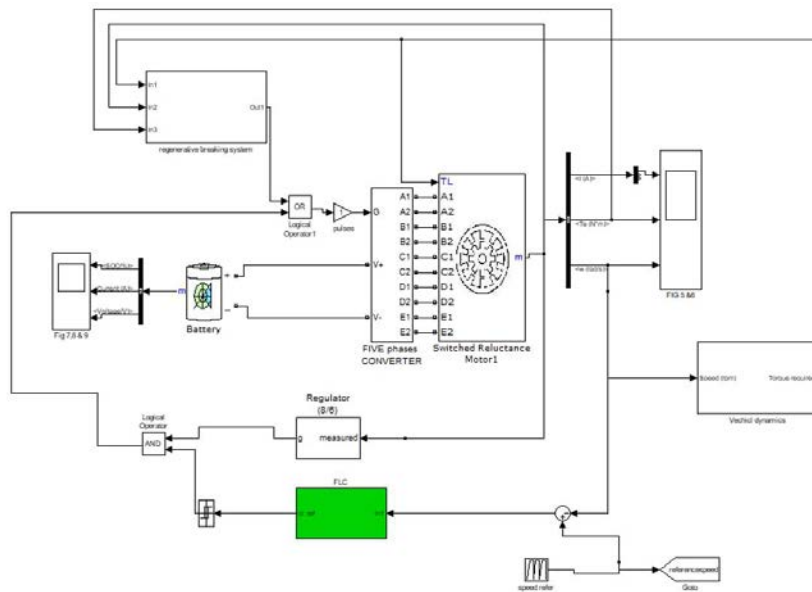


Fig. 2. Simulink model of SRM based electric vehicle with a fuzzy controller

5. FAULT INVESTIGATION

Electric drive systems must be reliable, and simulation, modelling, and fault analysis are essential tools in this process. It's because the SRM drive's components can fail in practice. Because of this, the electric car driven by SRM is examined in various fault scenarios in this research. Several elements are taken into consideration, such as:

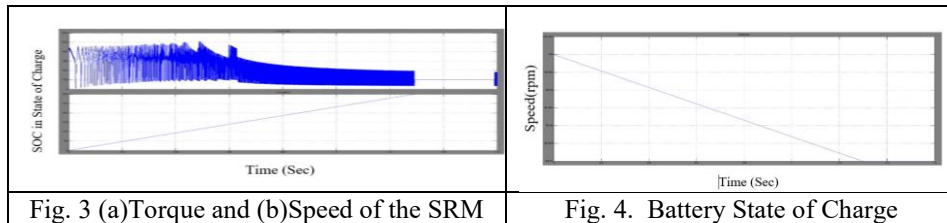
5.1. Inaccessible stage circumstances

In open circuit, the phase is separated, and the HRC fuse blows to isolate the faulty component, so that condition is taken into consideration.

The current situation may be summed up as follows:

- | | |
|---|-----------------------------|
| a) short circuit fault of converter switch, | b) Single Phase OC fault |
| c) Two phase Open circuit fault | d) Single phase SC fault |
| e) Two phase SC fault | e) Line to line short fault |

The figure 3 and 4 represents the torque, speed characteristics with respect to time under the consideration with Converter switch short circuit fault conditions.



5.2. Impact of up and down climbing

Regenerative braking effects may be seen during down-climbing experiments. An investigation of the methodology used to calculate torque ripple Subtract the greatest and lowest output torque numbers from each other to calculate torque ripple. [10]. To find the solution, formulas are used as,

$$\% T_{avg} = (T_{max} - T_{min}) / T_{max} \quad (8)$$

where, T_{max} = Maximum torque, T_{min} = Minimum torque, T_{avg} = Average torque.

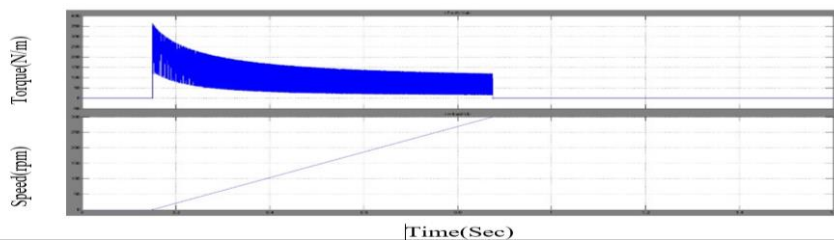


Fig. 5. (a) Current (b) Torque and (c) Speed of the SRM

The figure 5 shows that Current, Torque and Speed of the SRM with respect to time under the Up climbing at a slope of $\Theta = 20^\circ$

6. CONCLUSION

For use with the SRM drive, this research involves building a speed controller based on FLC. The FLC is suitable for a stable and simple-to-tune controller and controlling of SRM non-linear systems for EV applications in systems with a high degree of nonlinearity. Researchers are looking into FLC controller and have found it to be very helpful for a variety of problems. Both transient and steady-state control can be accomplished with the suggested fuzzy logic controller very well. This control strategy is the most suitable one for real-time use in EV applications because of its simplicity, robustness, and adaptability.

REFERENCES

- [1] K. S. Narendra, K. Parthasarathy, "Identification and control of dynamical system using neural networks", IEEE Trans on Neural Networks, vol.1 March 1990, pp,4-27.
- [2] F. Fillipetti, G. Franceschimin, L. Tassion, "Neural Network aided on line diagnostics of induction motor rotor faults", IEEE Trans on Industrial Application. Vol 3 June 1995, pp 852-889.
- [3] D. S. Reay. T.C Green and B.W. Williams, "Neural Network used for torque ripple minimization for SRM", EPE, Briton, Sep 1993, pp 1-5.
- [4] P. Vijayraghavan and R. Krishnan, "Front-End Buck Converter Topology for SRM drives-Design & Control", Proceedings of International IEEE Conference, 3 Feb 2003, pp. 3013-3018.
- [5] C. Muniraj and R. Jeyabharth, "High performance direct torque control for switched Reluctance Motor", Proceedings of International conference on ICSCI-2007, vol.2 Hyderabad, 13 Jan 2007, pp. 13-16.
- [6] C. Muniraj and S. Chandrasekar, "Fuzzy logic control and Faults Analysis of 6/4 Switched Reluctance Motor", Proceedings of international conference on modeling and simulation, CIT India, 27-29, Aug 2007, pp.909-915.
- [7] Krishnan, R., "Switched Reluctance Motor Drives: Modelling, Simulation, Analysis, Design, and Applications", CRC Press, 2001.
- [8] Shyam S. Ramamurthy and Juan Carlos Balda "Sizing a Switched Reluctance Motor for Electric Vehicles" IEEE Transaction on industrial electronics, vol. 37.
- [9] V S Prasadarao K and V Joshi Manohar, "Grid Interconnection of PV system Using Symmetric and Asymmetric MLI Topology "International Journal of Power Electronics and Drive System (IJPEDS) Vol. 9, No. 4, December 2018, pp. 1616~1623.
- [10] Joshi Manohar, V Lakshmi Devi and Adinaryana "SHE Controlled CHB 7-Level Inverter with Unequal DC Sources using MPSO Algorithm" proceedings of IEEE International Conference on System, Computation, Automation and Networking (ICSCA), pp 1-6, 2018.

Power Sharing Strategy Based on Inverted Droop Controlled Microgrid

Prabaakaran K¹, Senthil Kumar R², Srividhya R³, Praveen G⁴, Dinesh Kumar R⁵,
Sanjai T P⁶

¹Department of Electrical and Electronics Engineering, Easwari Engineering College, Chennai, India,

^{2,4,5,6}Department of Electrical and Electronics Engineering, Vel Tech High Tech Dr. Rangarajan Dr. Sakunthala Engineering College, Chennai, India

³Department of Electronics and Communication Engineering, Vel Tech Rangarajan Dr. Sagunthala R & D Institute of Science and Technology, Chennai, India.

Email: prabaakaran031@gmail.com

Abstract

To guarantee framework soundness in islanded activity, nearby control of Distributed Energy Resources (DER) in microgrids commonly utilizes the hang calculation. Voltage Control Mode (VCM) and Current Control Mode (CCM) inverters get customary and switch hang control, individually (CCM). Conventional P-F and Q-V hang attributes are delicate to drive coupling in low-voltage microgrids, which can prompt shaky working circumstances because of burden dependence on voltage and recurrence. Subsequently, modified hang, a P-V and Q-F reversed hang highlight, is utilized in recreations and trial tests to show its handiness for stable and decoupled guideline of islanded LV microgrids. Neighbourhood sustainable power sources and enormous burdens in power circulation organizations, for example, the developing number of electric charging stations, cause various difficulties that straightforwardly affect the electrical lattice's unwavering quality. The microgrid concept with proposed droop produces sharing of power ranging between 87% of base load under each DER, which divides the grid into small sub-grids that maintain power and energy balance, is one attempt to address these difficulties. A microgrid is isolated from the principal matrix and works freely with miniature sources and loads, it is supposed to be in islanded mode.

Keywords. Microgrid, inverted droop, power sharing, distributed generation.

1. INTRODUCTION

The concept of inverted droop control is being considered as a viable solution to these issues. The inverted droop, which is the time integral of the voltage, is written as a function of the reactive power based on this concept [1]. Furthermore,

the inverted angular difference is given as a function of active power. There are no sophisticated transformations or PI regulator adjustment required in this method [2]. Furthermore, similar to direct torque control and direct power control, the switching signals are created via the direct flux control methodology [3]. The proliferation of that rising number that tiny generator connected to renewable sources has characterized the growth of distribution networks; these generators, due to the variability of their power generation, can present challenges in the functioning of distribution networks [4]. Adoption of new structures and innovative control systems can overcome technical limitations to a large-scale deployment that distributed energy resources (DER) [5]. Microgrids, which are depicted as a low-voltage dissemination network with generators, load, and energy stockpiling frameworks coupled to the circulation network at a solitary point, are building up momentum [6]. They are frequently connected to the DGs network, although they can be planned to run independently on the case of a main grid outage.

2. LITERATURE REVIEW

A microgrid can be connected to or turned off from the primary framework, and it is expected to guarantee power adjusting among neighbourhood loads and supplies on a nonstop premise. Besides, in light of the fact that various power units are connected to same microgrid, power sharing value is essential. The flow project researches an island working of a microgrid with various sources, like battery stockpiling frameworks, and imparting capacity to various burdens, for example, electric vehicle chargers, a circumstance that is appropriate for a city matrix. A nearby control arrangement is portrayed and demonstrated by mathematical and trial discoveries for a steady working of the microgrid in wording both of force equilibrium and power sharing.

The requirement for concurrent creation from circulated generators (DGs) to convey the heap expected by customers has developed as the need might arise in microgrids (MGs) have expanded. Since the DGs should purchase interest in all the while, they stand up to various specialized and monetary issues, including keeping away from DG over-burdening and keeping up with network solidness when feeder impedance differs. This work depicts a way for redesigning the hang regulator utilizing a sliding mode approach, permitting DGs to set up an adequate responsive power share without botch even in progressively convoluted MGs. At last, the prevalence, straightforwardness, and effectiveness of the third request sliding mode control (SMC) not entirely settled by looking at the controlling boundaries of the proposed philosophy with current procedures. The overall design of a data center can be classified in 4 categories Tier I-IV each one presenting advantages and disadvantages related to power consumption and availability. In most cases availability and safety issues yield to redundant N+1, N+2 or 2N data center designs and this has a serious effect on power consumption. According to that, data center has the following main units

3. SYSTEM DESCRIPTION

While tending to the previously mentioned issues, the microgrid control framework should be fit for guaranteeing the microgrid steady and savvy activity. Miniature matrices enjoy the benefit of having the option to work in both framework associated and independent modes, with a consistent change between them. For every method of activity, a few control systems might be laid out, thus a fast-landing recognition technique is basic for changing the control procedure properly. The strategy incorporates a lattice shaping converter that is liable for matrix age and slave converters that add to framework steadiness (working in network support). The procedure is like the expert slave approach, in which a solitary unit makes slave references. However, no correspondences have framed in this model, hang bends have been built to hand-off the microgrid power requests by means of AC transport flagging. The matrix framing converter conveys the quick burden's transient power and makes the microgrid voltage in view of inward references (V_n and n). The framework shaping converter changes the delivered voltage and recurrence by following a hang bend (P , V , Q) contingent upon its immediate result dynamic and receptive power. Flagging matrix support converters is empowered by changes in microgrid voltage abundance and recurrence. Framework support converters change dynamic and responsive power in light of network voltage and recurrence estimations (V , P , Q hangs). The result of the converters is directed; hence, the chose hang highlight depends on that the low voltage line impedance.

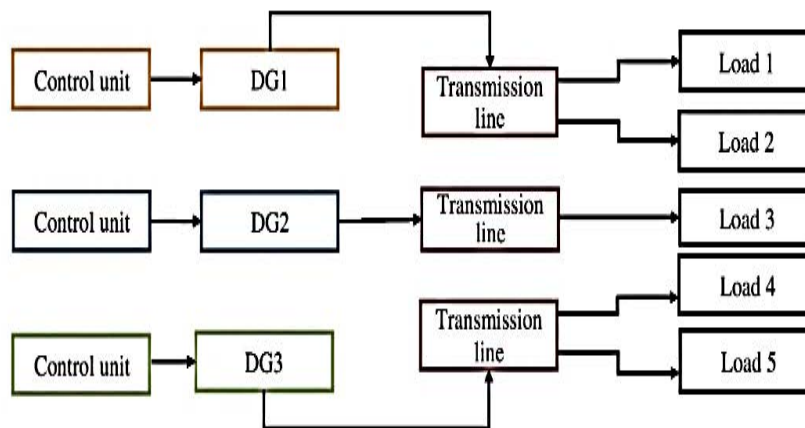


Figure 1. Block diagram of proposed system

The above block diagram has contained three control unit and DGs with some transmissions line and finally we have the five different types of loads are using in our proposed system. By doing like that the change in load can get our efficiency by our proposed inverted droop method.

4. RESULTS AND DISCUSSION

To discuss and validate the proposed inverted droop controller under different testing load conditions are performed. Simulation study in the Matlab/Simulink software environment is used to test the suggested control approach. The suggested control approach is applied to an islanded microgrid with very resistive line impedances. For this new proposed inverted droop, we are taking five different loads with that they provide satisfied results to the proposed system. The following ratings of loads are $5.8e3+0.2e3$, $5.8e3+0.2e3$, $2.3e3+0.3e3$, $6.3e3+1.0e3$ and $5.83e+0.2e3$. Illustrates the output frequency and simulation results of active power sharing across DG's units.

For this, three distinct sorts of loads and separated them into different time, with a constant voltage of 320 volts. The different situations for THD values are tested to achieve low harmonic distortion. The newly suggested system has shown positive outcomes when compared to previous findings. The system has been given a high level of efficiency, thanks to the new way. From here, it is continued on to values that it can see in greater detail in the image below for each scenario. It provides us with extra information to study and comprehend THD results. The obtained THD% value of 0.57% is for our newly proposed inverted droop.

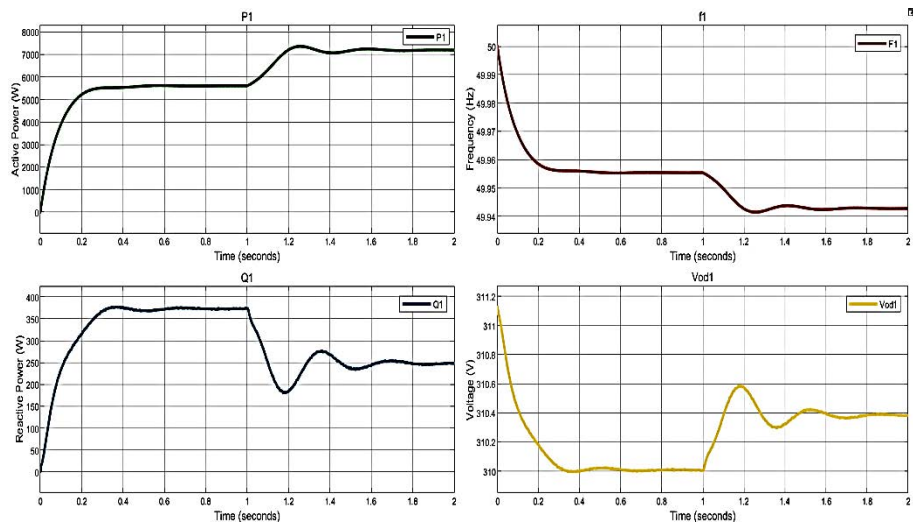


Figure 2 DGs 1 of a. Active Power, b. Reactive Power, c. Frequency, d. voltage

In fig.2. the active power was initially was at zero and it was reaching at the 5.8kW and maintaining constant till one second. After one second, we are changing different load of active power reaching 7kw and it stabilizes at 1.8 sec. Fig 2.b. reactive power the load was initially at zero the load was reaching 400kVAR at the time interval of 0.6 sec. since the active power is inversely proportionally to Reactive power. After reaching the maximum again it's varying because changing

in load its reaching 180VAR at the time interval of 1.2 sec. In frequency fig 2.c it's starting at the maximum level since we cannot maintain frequency at stable for a long time because the load is running.

At the level on 50Hz the time interval it will be the initial stage. And it's reduced at the time interval of 0.2 sec. And it gets stabilizes till at the time interval of 1sec. And again, sometime interval again its going down and the time interval of that is after 1 sec the frequency will be the 49.95Hz. Now it is observed about the voltage fig 2.d at the starting the voltage will be 311V at the time interval was 0.01 sec and its reaching at the voltage. 310V at the at the 0.4 sec again by varying the load again the voltage was increasing linearly at the 310.6V at the time interval of 1.2 sec and after some time again the voltage will vary after that the voltage will be constant. And this will the total output of DGs 1 of Active power, Reactive power, Frequency and Voltage.

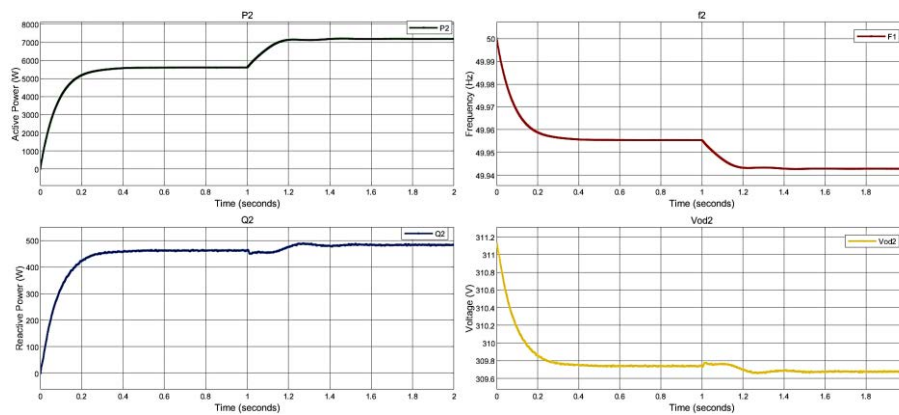


Figure 3 DGs 2 of a. Active Power, b. Reactive Power, c. Frequency, d. voltage

In the Distributed Generator 2 the active power is start by 1 kW in 0.01 sec later it gets settled down to 5.3 kW up to 1.0 sec. Later, occurrence of change in load condition in order to verify the nature of droop control. The change of load happens about 1.0 sec to 2.0 sec. The incremental of load happens by 5% of incremental of base load range. It shows that, the droop control provides the sufficient active and reactive power balancing to the variable load. The active power attains to 7.3 kW which is shown in fig. 3.a.

Fig 3.b discusses about the system frequency at various loading conditions. It is clearly observed that the system frequency is maintained within the desire limits. The variation of system frequency ranging from 50 to 49.92 Hz. It meets out the IEEE standards of frequency limitations. In fig 3.c. the reactive power of DG2 is addressed. The essential of reactive power support to the grid system, it helps to maintain the main grid under stable operating condition. The proposed droop control helps to enhance and maintain the reactive power within the desire limits. It can be observed that, it gets vary from 0.6kVAR to 0.97kVAR with the duration about 0.01 sec to 2 sec. It also supports during load change at 1.0 sec. It also helps to eliminate

the power quality issues like sag, swell, interrupt and unbalancing conditions. The droop control helps to regulate the voltage under stable conditions during the transient conditions starts from 1.0 sec due to change of load. It is clearly states that the grid voltage is regulated properly using droop control.

5. CONCLUSION

The output impedance of inverters has been proposed to increase power quality, and the droop controller for enhancement of parallel operation of inverters implemented in this paper. The inverter stability analysis equipped with large and small signal has been investigated. The major goal of this paper is to look into how a micro grid operates under different loads. When operating on an island, however, become deeply involved in dynamic simulation. When it comes to dynamic modelling, control settings for droop and reverse droop proportionately with multiple modes of DG units within converter capability and it has the ability to provide the power sharing between 87 % to 93 % of base load in DG's and also capable to compensate harmonics within 1.27% of THD. The power sharing impact of reverse droop selection the parameters are examined. Finally, modelling results reveal the validation of the research.

REFERENCES

1. S. Vijay, N. Parth, S. Doolla and M. C. Chandorkar, "An Adaptive Virtual Impedance Control for Improving Power Sharing Among Inverters in Islanded AC Microgrids," in *IEEE Transactions on Smart Grid*, vol. 12, no. 4, pp. 2991-3003, July 2021
2. P. Kandasamy et.al., Deep CNN–LSTM-Based DSTATCOM for Power Quality Enhancement in Microgrid, *Journal of Circuits, Systems and Computers*, vol 31,10, pp.1-38, 2022.
3. Natesan, S. Ajithan, S. Mani, and P. Kandhasamy, "Applicability of Droop Regulation Technique in Microgrid - A Survey", *Eng. J.*, vol. 18, no. 3, pp. 23-36, Jul. 2014.
4. Chen, T.; Abdel-Rahim, O.; Peng, F.; Wang, H. An improved finite control set-MPC-based power sharing control strategy for islanded AC microgrids. *IEEE Access* 2020, 8, 52676–52686.
5. Zhang, Q.-Q.; Wai, R.-J. Robust Power Sharing and Voltage Stabilization Control Structure via Sliding-Mode Technique in Islanded Micro-Grid. *Energies* 2021, 14, 883.
6. K. Chandrasekaran et.al., Deep learning and reinforcement learning approach on microgrid, *Int. Trans. On Elec. Energy systems*. vol.30. 10, pp. 1-19, 2020.

Implementation of Leader Follower Approach in Quadcopter

¹Pandiyarajan.R, ²Chandravadhana, ³Vivek. T, ⁴Agnishwar Jayaprakash

^{1,2,3} Department of Mechanical Engineering, Agni College of Technology-OMR, Thalambur, Chennai-600130 Tamilnadu, India.

⁴Garuda Aerospace, OMR Chennai-600130, Tamil Nadu, India.

Email: pandiyarajan8@gmail.com

Abstract

Modern concepts and technology have the potential to address many of the problems we confront on a daily basis and in our professions. In order to demonstrate the advantages of using the control strategy (Leader-Follower) through drones and their comprehensive application-oriented functioning, the project "Implementation of Leader Follower Approach in Quadcopter" has been detailed in this article. Building and using a quadcopter has been shown to be feasible for "Autonomous flight without aid of ground pilot" as the electronic age has progressed. The topic of formation control of numerous quadcopters, which has uses in the entertainment, medical, and defence industries, has been developed in this part. Additionally, "lift-up technologies" utilise it. which today are completed with the assistance of cranes and other tools. Due to the introduction of several cutting-edge technologies, including as GPS, Bluetooth, and other new-age sensors, the design of drones is much more trustworthy and amazing by incorporating both hardware and software requirements. This project's primary objective is to enhance drone capabilities by utilising low-cost electronics and a single drone to implement the Leader-Follower strategy using GPS interfaced with Arduino, as has been extensively discussed. A variety of theoretical principles, notably those relating to mathematical modelling based on control system and dynamics, served as the foundation for the drone's design and testing.

Keywords. Leader-Follower approach, Autonomous Flying, GPS, Arduino.

1. INTRODUCTION

Future drone applications will heavily rely on the field of drone formation control. The use of artificial intelligence and machine learning technologies to control drones in formation will completely alter the tech industry. This motivated many tech experts in the field of aerial vehicle control to conduct additional study on how to get a large number of drones to cooperate in order to carry out a specified operation. Between drones Quadcopters have a number of benefits, including excellent reliability, low cost, and tiny size. The copters are capable of performing a variety of difficult jobs, such as search and rescue missions, risk and hidden zone

inspections, aerial mapping, and military uses. In any application, using many quadcopters that can interact with one another and cooperate to achieve a task more effectively than using a single quadcopter.

A formation of multiple quadcopters, as opposed to a single quadcopter, increases room for carrying sensors and other components, provides a greater cargo capacity and surveillance range, and as a result, can accomplish more difficult and time-consuming jobs more effectively. In formation control of quadcopters, there are different kinds types of approaches which are currently in use. Some of those approaches are 1) Leader-Follower, 2) Virtual Structure, and 3) Behavior-based. Among these approaches Leader-Follower approach is considered to be the less complex one in which one of the quadcopters is assigned to be a leader and other quadcopters will be assigned as a follower. The followers are programmed in such a way that it orients and navigates to the position of leader with a predefined offset.

This paper discusses about the possibility of making an autonomous quadcopter which follows its leader (remote GPS device or predefined waypoints) based on the instructions given by the programmed microcontroller which calculates the navigation vector using the “Haversine Formula” and the “Forward Azimuth Formula” based on the location and orientation data collected from the GPS receiver and compass respectively.

1.1. PROJECT’S MAIN IDEA

This project is aimed at implementing Leader-Follower approach in quadcopter by making it fly autonomously without using any remote controller. To achieve this, we have used a microcontroller interfaced with GPS and compass which is programmed in such a way that it mimics the function of remote controller by controlling the drone autonomously by providing input commands to the Flight controller on board the quadcopter.

2. PROPOSED SYSTEM

Calculating the drone's distance from the leader's waypoint and its orientation in relation to the leader's location is important if you want the drone to follow the leader's waypoint on its own. The Haversine Formula, which derives circle lengths between two places on a sphere from their longitudes and latitudes, was used to determine the distance to the target. The heading was determined using the forward azimuth formula. The leader's GPS position, the drone's coordinate acquired from the GPS receiver, and the drone's heading in relation to North obtained from the digital compass may all be used to determine both parameters. In order to approach the leader's location with a certain offset, the quadcopter's microcontroller (Arduino UNO) continuously recalculates the navigation vector and utilises the obtained distance and direction to regulate the input commands of the flight controller onboard.

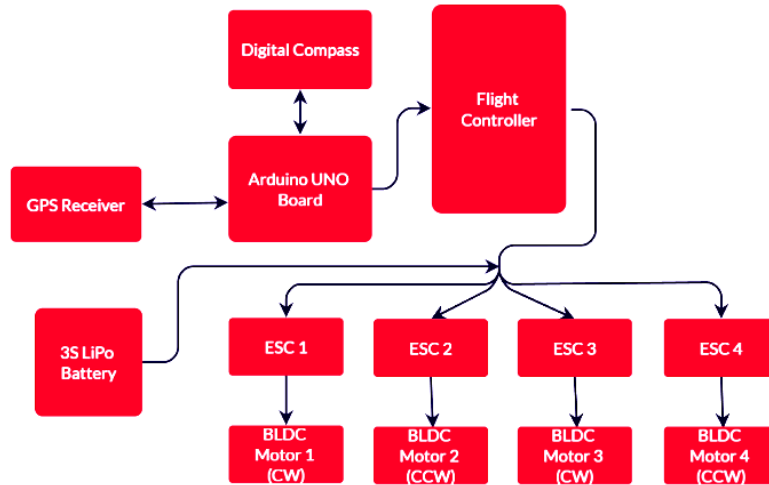


Figure 1. Block diagram of the project work

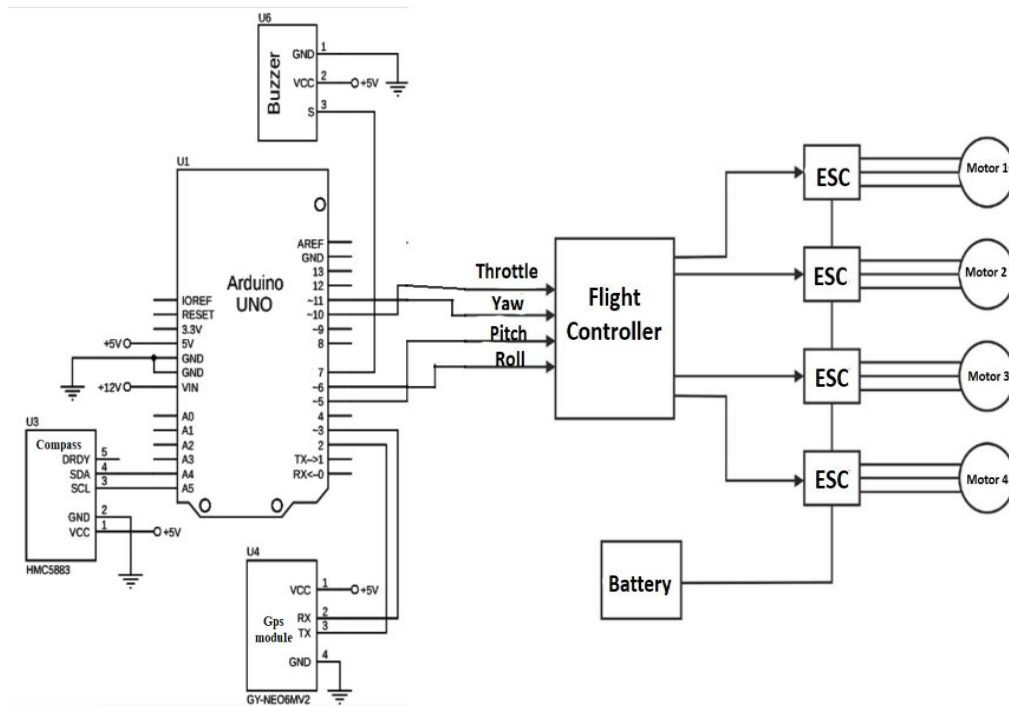


Figure 2 Circuit diagram of the project

We have utilised an Arduino UNO board as the primary controller to accomplish our goal. We selected Arduino since it is simple to use and has a vast array of libraries. As a result, connecting numerous sensors to an Arduino UNO becomes simpler. The U-blox NEO-6M GPS module is the GPS receiver we

selected for the job. It reaches the maximum degree of sensitivity and can track up to 22 satellites on 50 channels. The GY-271 module, which is based on the Honeywell HMC5883L microprocessor, houses the digital compass. Both are inexpensive modules that use Arduino libraries that are easily accessible. The HMC5883L utilises the I2C serial protocol, whereas the U-blox NEO-6M uses the UART serial communication interface.

We utilised an 11.1v, 2,200 mA-hour 3S (LiPo) Lithium-Polymer battery to power the four ESCs (Electronic Speed Controllers), which in turn provide power to the Arduino UNO, GPS module, digital compass, and flight controller. The block diagram and circuit diagram for the suggested system are shown, respectively, in Figures 1 and 2.

3. METHODOLOGY

A flow diagram of the algorithm the quadcopter uses to follow its leader is shown in Figure 3.

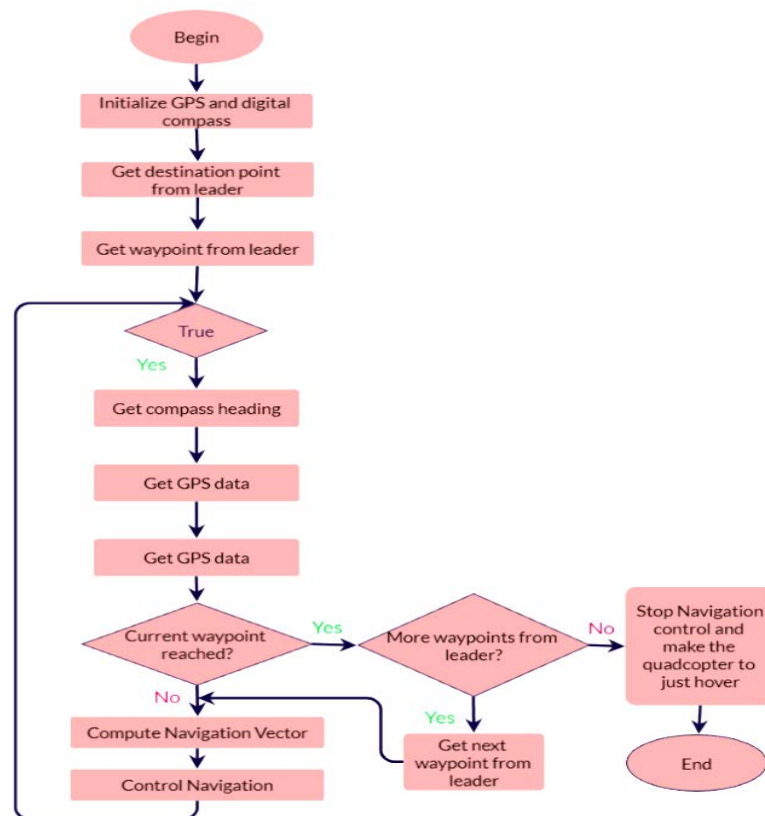


Figure 3: Flow diagram describing the algorithm

As already noted, we utilised the Forward Azimuth Formula to determine the leader's orientation with regard to magnetic North and the Haversine Formula to get the distance to the leader's position. The algorithm will proceed to pitch the quadcopter forward by regulating inputs of the flight controller if the distance between the leader and the follower exceeds a specified distance tolerance error (1m). Additionally, the algorithm will yaw the quadcopter until its face is pointing in the direction of the objective if the heading angle of the quadcopter with respect to the leader is outside of a specified heading tolerance error (plus or minus 5 degrees). If another waypoint is located, the algorithm will continue to fly the quadcopter until it reaches the leader's location; otherwise, it will hover at a certain height. Because more distance and direction errors are introduced into the system with each movement, the Arduino must repeatedly calculate the navigation vector and regulate its motion.

3.1. NAVIGATION VECTOR CALCULATION

The definition of the Navigation vector (distance and direction) is illustrated visually in Figure 4. The leader's coordinates, the quadcopter's coordinates, and the quadcopter's direction in relation to magnetic North are used to calculate these two components. The mistakes that we will next attempt to minimise with our control method are heading and distance. The quadcopter's distance error can be decreased by applying a linear velocity via a PWM signal from the Arduino UNO board to the PITCH input pin in the flight controller, and the angle error can be reduced by applying a pertinent angular velocity via a PWM signal from the Arduino UNO board to the YAW input pin in the flight controller. We may get the distance error "d" using the Haversine Formula, and we can determine the azimuth (waypoint angle) using the Forward Azimuth Formula to determine the heading error.

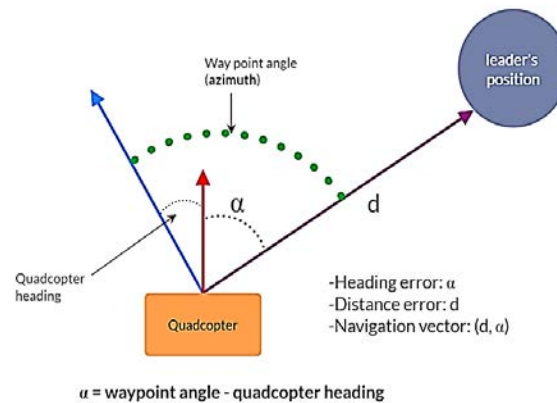


Figure 4: Computation of navigational vectors

To determine the separation between two places on the surface of the Earth, one can use the Haversine formula, which is a general formula in spherical trigonometry. We need the coordinates (Latitudes and Longitudes) of two places on the surface of the Earth in order to compute their separation. Equations 1 and 2

provide, respectively, the generic Haversine formula and the trigonometric identity of the Haversine function. Equations 3, 4, and 5 make up the algorithm's logic and are a breakdown of the general equations.

$$\text{hav}(d/r) = \text{hav}(\varphi_2 - \varphi_1) + \cos(\varphi_1) * \cos(\varphi_2) * \text{hav}(\lambda_2 - \lambda_1) \rightarrow 1$$

$$\text{hav}(\theta) = \sin^2(\theta/2) = (1 - \cos(\theta))/2 \rightarrow 2$$

$$a = \sin^2(\Delta\varphi/2) + \cos(\varphi_1) * \cos(\varphi_2) * \sin^2(\Delta\lambda/2) \rightarrow 3$$

$$c = 2 * \arctan 2(\sqrt{a}, \sqrt{1-a}) \rightarrow 4$$

$$d = r * c \rightarrow 5$$

where, φ_1 = follower's latitude, φ_2 = leader's latitude, λ_1 = follower's longitude,

λ_2 = leader's longitude, d = arc (distance), r = Earth's Radius,

$$\Delta\varphi = \varphi_2 - \varphi_1,$$

$$\Delta\lambda = \lambda_2 - \lambda_1.$$

A direction line, which is defined by two locations on the surface of the Earth, and a North base line or meridian are the two points from which the azimuth is measured. We may determine the actual azimuth by using true North as a point of reference. The matching "magnetic azimuth" is obtained by taking the magnetic North. Therefore, we can determine the angle between the line connecting the quadcopter's location to the North and the line connecting the quadcopter to the leader's position using the azimuth formula. Equation 6 illustrates the azimuth formula, which calls for the coordinate values for the leader and follower.

$$\theta = \arctan^2(\sin \Delta\lambda * \cos \varphi_2, \cos \varphi_1 * \sin \varphi_2 - \sin \varphi_1 * \sin \varphi_2 * \cos \Delta\lambda) \rightarrow 6$$

where, φ_1 = follower's latitude, φ_2 = leader's latitude, θ = waypoint or azimuth

$$\Delta\lambda = \lambda_1 - \lambda_2$$

The heading error (α), which is just the difference between the azimuth and the follower's heading with regard to North as determined by the digital compass, may be calculated once the azimuth or waypoint angle has been determined.

$$\text{Heading error } (\alpha) = \text{waypoint angle } (\theta) - \text{quadcopter's heading}$$

3.2. NAVIGATION CONTROL

The quadcopter navigation control algorithm is made straightforward. Initially, the quadcopter's heading error is minimised by giving the flight controller in the quadcopter a YAW command to the right if the angle error is positive or to the left if the error is negative. We have established a tolerance range of plus or minus 5 degrees because it is challenging to decrease the inaccuracy precisely to zero. The distance inaccuracy is decreased by instructing the forward PITCH operation to the quadcopter's flight controller using an Arduino UNO once the follower has been positioned at the proper angle. However, this process tends to

make the angle error bigger, whether it's positive or negative. This happens as a result of tolerance problems that affect both the sensor modules and outside disturbances. Therefore, until the follower reaches the leader's position, we must continuously repeat over the computation of a new navigation vector and the minimising of both errors.

4. CONCLUSION

The paper mainly focuses on the effective way to make a quadcopter follow its leader autonomously using a pre programmed microcontroller (Arduino UNO) which processes the data from sensor modules (GPS module and digital compass) and makes an effective decision to reach the leaders location. Here the leader's location can be provided to the Arduino board either by pre defining it in the algorithm or can be transmitted wirelessly with the help of Bluetooth or Wi-Fi module. By implementing this approach in several number of drones where one drone acts as a leader and others as follower then a more complex formations of drones can be achieved which can contribute in completion of tasks without much human interference in wide variety of applications. Figure 5 and 6 shows the pictures of the follower drone that we have made using kk flight controller.



Figure 5: Flying quadcopter using kk flight controller



Figure 6: Top view of our quadcopter

REFERENCES

- [1] Xuan-Mung N, Hong SK. Robust adaptive formation control of quadcopters based on a leader-follower approach. *International Journal of Advanced Robotic Systems*. 2019;16 (4).
- [2] Pebrianti, Dwi et al. "Leader Follower of Quadrotor Micro Aerial Vehicle." *Journal of Telecommunication, Electronic and Computer Engineering* 10 (2018): 67-73.
- [3] Falin Wu, Jiemin Chen and Yuan Liang (2016) "Leader-Follower Formation control for Quadrotors", *IOP Conference Series: Materials Science and*

Engineering, Volume 187, 2016 Second International Conference on Mechanical and Aeronautical Engineering (ICMAE 2016) 28–30 December 2016, Hong Kong

- [4] Lee, K.U.; Choi, Y.H.; Park, J.B. Backstepping Based Formation Control of Quadrotors with the State Transformation Technique. *Appl. Sci.* 2017, 7, 1170.
- [5] Rifqi Rafifandi, Dea Lana Asri, Estiyanti Ekawati and Eko Mursito Budi (2019) “Leader- Follower formation control of two quadrotor UAVs”, *SN Applied Sciences*, 2019, vol 1:539.
- [6] Zain Anwar Ali, Amber Israr, Eman H. Alkhamash, and Myriam Hadjouni (2021) “Leader-Follower Formation Control of Multi-UAVs via an Adaptive Hybrid Controller”, *Complexity publications*, 2021.
- [7] Michael James Compobasso (2017) “Leader-Follower Trajectory Generation and Tracking for Quadrotor Swarms”, A thesis submitted to the Department of Physical Sciences and the committee on graduate studies, 2017.
- [8] K. Nonami, F. Kendoul, S. Suzuki, W. Wang, D. Nakazawa (2010) “Autonomous flying robots-Unmanned aerial vehicles and micro aerial vehicles”, Springer

A low-cost IoT-based system for monitoring the health of individual soldiers and tracking their real-time whereabouts in combat zones

A.S.S. Murugan¹, R. Harshavardhan¹, N. Karupiah² and P. Manoj Kumar³

¹Department of EEE, CVR College of Engineering, Mangalpalli, RR District, Telangana.

²Department of EEE, Vardhaman College of Engineering, Kacharam, Hyderabad, Telangana.

³Department of EEE, Bannari Amman Institute of Technology, Sathyamangalam, Tamilnadu.

Email: assm17174@gmail.com

Abstract

The security of the soldiers is said to play a significant role in the security system of the country today because it is dependent on the enemy's fight. It is extremely impossible for the army base station to be aware of the location and health state of every soldier as soon as one more soldier cross into the enemy lines. Numerous tools are available to monitor a soldier's physical well-being and ensure their safety. The suggested system employs GPS to track the soldier's direction in terms of latitude and longitude values to make finding direction simple. The suggested technology, which uses GPS to track the soldier's whereabouts and health state, can be mounted on their body. The IoT will be used to provide this information to the control panel. The system that is being suggested consists of tiny transmission modules, sensors, and wearable physiological equipment. As a result, it is feasible to establish a low-cost mechanism to preserve priceless human life on the battlefield with the use of the proposed equipment. Using GPS (Global Positioning System) and GSM (Global System for Mobile) in its design, this device provides a wireless platform for monitoring the soldier's body temperature and heart rate while also tracking their whereabouts. Thus, every troop can easily share their health status with the nearby ground station during combat.

Keywords. Navigation system, GPS System, GSM module, Mobile Health Monitoring, Global security system.

1. INTRODUCTION

In India, the Army, Navy, and Air Force are responsible for maintaining and monitoring national security. Soldiers who give their lives in service to their country play a significant and crucial role. A lot of people are worried about the soldier's safety. A lack of communication tends to result in dead civilians as they approach

enemy territory, so it is imperative that the army base station is aware of both the whereabouts and health status of every soldier. Because there was inadequate medical support and communication between the men on the battlefield and the authorities at the army base stations, India has already lost a significant number of soldiers in combat. Supporting the armed forces is essential. Launching this initiative is necessary in order to reveal the soldiers' health status and provide for their needs when they are in terrible straits on the battlefield [1]. Everyone must be concerned about the soldiers' safety, so a new monitoring system has been developed to track the soldiers' health and provide immediate medical attention as soon as possible.

One physiological signal that is monitored by the geolocation-based heart rate monitoring system is heart rate, which is measured on board or by a wearable heart rate sensor. This methodology makes use of the resources offered by mobile technology. The created mobile application enables consultation with health experts and provides alert messages via notification [2].

A wireless combined vital sign technology that can assess both heart rate as well as oxygen levels has been demonstrated [3]. navigation system to track the whereabouts of soldiers and track their health metrics. The AT89C51 microcontroller was employed to capture vital signs, which were then communicated to the main unit over GSM [4]. Another wireless system with a health monitoring system has been designed using a Fiber Bragg Grating (FBG) sensor and the Zigbee network [5]. The idea of putting GPS [6–8] into practise has been handled as a GPS-based tracking system that is made up of open-source software, cheap hardware, and a remarkably easy user interface via a web application using Google Earth software. It is suggested to use a smart watch-based fitness surveillance device [9] that provides information on heart rate, blood pressure, and the ECG. A communication interface is created using Bluetooth.

The objective of this project is to create trustworthy, non-interference health status indicators that are cheap, low power-consumption, and reliable. It is also used to find the location of the soldier.

The soldier's current location will be provided via the GPS tracker, which will help locate the soldier and get medical assistance to him as quickly as possible. Using the GSM modem built into the gadget, if a soldier is hurt, nearby medical centres or the central node will receive an SMS to call the emergency services. GPS is used to track troops, and GSM is used to enable network connectivity.

2. HARDWARE COMPONENTS

2.1. ARDUINO Nano

The Arduino Nano is, as its name implies, a small, feature-rich, and breadboard-friendly microcontroller board. The Nano board has dimensions ranging from 4.5 cm to 1.8 cm and weighs approximately 7 grammes (L to B). Like the

Arduino UNO [10], the Nano comes equipped with an ATmega 328P microprocessor [11].



Figure 1(a). Arduino Nano



(b) GPS Module

The UNO board is offered in PDIP (Plastic Dual-In-line Package) form with 30 pins, while Nano is offered in PQFP (Plastic Quad Flat Pack) form with 32 pins. This is the primary distinction between both. While the Arduino UNO has six ADC ports, the Arduino Nano has eight, which are served by the extra two pins. In contrast to other Arduino boards, the Nano board only contains a mini-USB connection for power. Both serial monitoring and programming are done using this port.

- Operating Voltage: 5V
- Flash memory: 32 KB (ATmega328P) of which 0.5 KB is used by the bootloader
- Clock frequency: 16 MHz

2.2. *GPS Module*

It is a navigation system that is based in space and delivers precise location and time information in all weather conditions. Anybody with a GPS receiver can publicly access the global positioning system (GPS), which will be administered by a US business. It has thirty or more GPS satellites in ordinary earth orbit (2000 - 3500 km), and a dozen satellites will work together to form what is known as a satellite network. It is mostly utilized in various applications related to surveying and navigation. The orbital period of the GPS satellites is 12 hours, and they fly in a sphere at a height of 20,200 kilometres. They are made up of at least six satellites that can be seen from anywhere on the planet, and their orbital planes are centred on Earth.

2.3. *Wi-Fi module ESP8266EX*

The ESP8266 is a low-cost system on a chip (SOC) Wi-Fi microchip made by Espressif with integrated TCP/IP network communication and microcontroller characteristics. A Wi-Fi-based microchip with a 9600 baud rate capable of serial communication is the ESP 01 chip. The Wi-Fi module's self-contained soc, which is integrated with the TCP/IP protocol, allows access to any microcontroller on its Wi-Fi network. An AT command set was initially programmed into ESP01. It can be connected to any sensor because of the large storage capacity and on-board processing it possesses

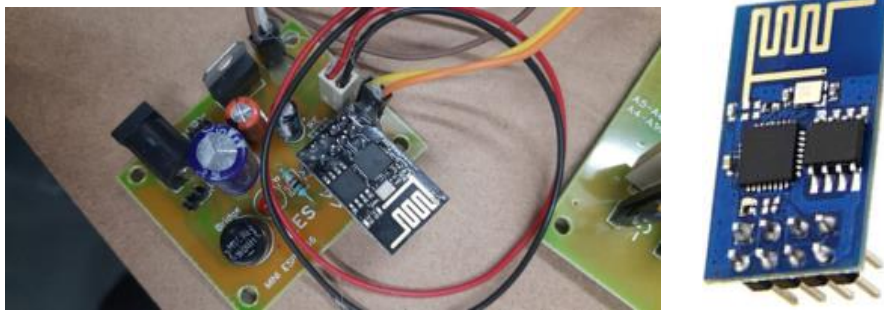


Figure 2. Wi-Fi Module

2.4. *Heartbeat Sensor*

The term "sensor" refers to a device that generates a signal corresponding to the quality being measured. The physical parameter being monitored by the sensor is converted into an electrically measurable signal by the sensor. A sensor is frequently used in conjunction with other electronics, although it can also be a mechanical sensor. There are huge sensors available for a variety of purposes. A biomedical sensing device is employed in this study. Heartbeat sensors operate based on a change in optical power; as light is absorbed while travelling through the blood, its optical power changes according to the rate at which the heart beats.



Figure 3(a) Heartbeat Sensor (b) Temperature Sensor (c) Display unit

Light-emitting diodes [12] and photodiodes are used in the heartbeat sensor. Whenever the heart is beating, the heartbeats will fluctuate, resulting in changes in blood circulation throughout a variety of body parts. This also happens when tissue lights up due to light from an LED. Plasma would absorb a portion of the illuminating light, with the photo diode capturing the leftover light reflected. Brightness has always been related to Jersey heart rate, and the quantity of light absorbed corresponds to the volume of blood in the tissue.

2.5. *Temperature and humidity sensor (DHT11)*

The DHT11 digital temperature [13] and humidity sensor is a hybrid instrument with a standardized digital signal output for both temperature and relative humidity. The device offers exceptional long-term stability and high dependability thanks to the application of temperature and humidity sensing technologies as well as a dedicated digital module collection.

- 3.5 V to 5.5 V voltage range
- 3 mA measuring current 60 μ A standby current
- Serial data output
- from 0°C to 50°C in the temperature range.
- Both temperature and humidity are 16-bit measurements.
- 1°C and 1% precision

3. PROPOSED SCHEME

This model includes body sensor networks, including temperature and heartbeat detectors. The health vitals of soldiers are monitored using these devices. The heartbeat sensor measures the troops' pulse rate in beats per minute (BPM), while the sensor module (DHT11) keeps track of the temperature of the person and their immediate surroundings. The model's pictorial depiction is demonstrated in figure 4.

A situation is deemed urgent if there is any difference between the detected data and the established threshold. The node is upgraded to include a GPS receiver in addition to the body sensor networks to track and locate the soldier. To report his whereabouts using a GPS module in an emergency, the soldier might hit the panic button. The micro controller processes and records all the data coming in from the sensors, and then sends it to the next node, the squadron leader's node, which then sends it to the control room via a wifi module built into the system. The experimental setup for the suggested system is shown in Figure 5.

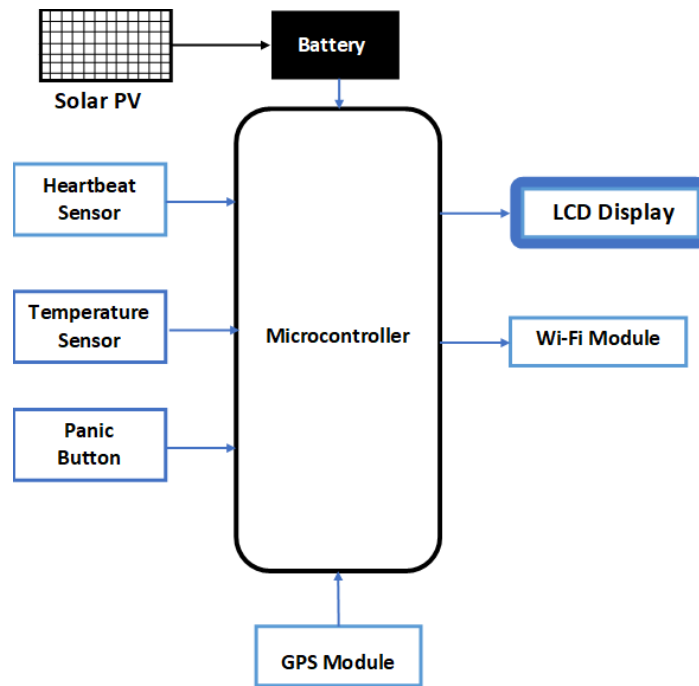


Figure 4. Proposed system block diagram

4. WORKING MODEL

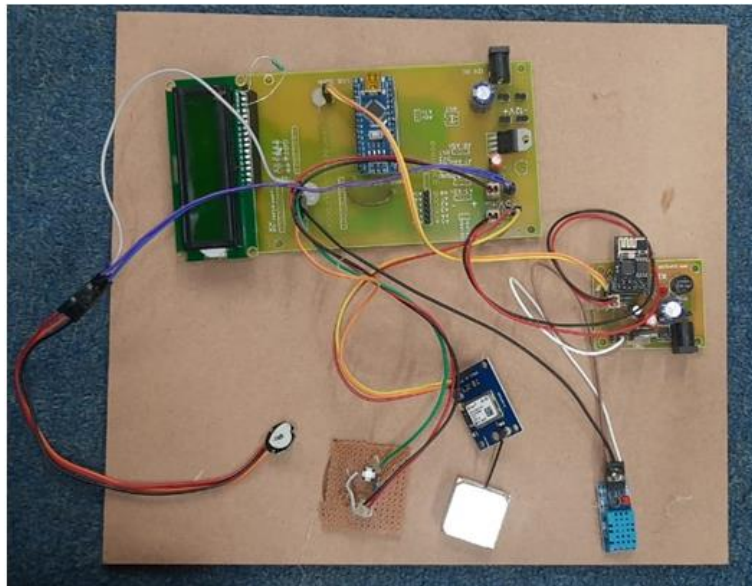


Figure 5. Experimental setup of the proposed system

The fitness of the trooper as determined by his pulse and body temperature is essentially our scheme's biggest priority. When a warrior is shot and knocked out, or if he loses consciousness for any other reason, his pulse progressively tends to rise or drop. In an emergency, a soldier may press the panic button to use a GPS module to transmit his whereabouts. All the information, along with the geolocation, was gathered by the microcontroller and sent to the closest ground station. The different tracking parameters of the soldier are relayed via a Wi-Fi unit, allowing the central server to access the trooper's present position via IOT. This information will be kept on the web and can be retrieved from the command centre as needed. Based on these details, the authorities can take fast action by sending out a health care team, an emergency response team, or any other support group to assist.

The module exclusively uses inexpensive, low-power semiconductors. Only simpler components were employed in this module, making it simple for soldiers to transport it to the battlefield. Several accessories can be fitted inside the soldier's jacket. The entire arrangement is powered by a solar-powered electric battery. Soldiers, those taking part in special expeditions, or individuals on specific assignments will benefit from this service.

5. CONCLUSION AND FUTURE SCOPE

The study describes a low-cost Arduino-based prototype system for tracking and monitoring the soldiers' health conditions. Biomedical sensors provide each soldier's heart rate, body temperature, and ambient data to the command post. This technique may assist in solving the problem of soldiers going missing in combat by accurately locating missing soldiers who are in critical condition.

To enhance the system's performance, new designs and sophisticated technologies may be used. Additionally, by utilising AI/ML algorithms, we could predict which soldiers will need medical assistance soon. Additionally, it could predict whether a sensor or component would need to be replaced or maintained. Other enhancements that can be made include the use of modern security protocols and techniques on the wireless RF modules, which will increase the security and dependability of the entire process of transmitting and receiving sensor data.

REFERENCES

- [1] S. Shelar, N. Patil, M. Jain, S. Chaudhari, S. Hande, 'Soldier Tracking and Health Monitoring Systems', *Int. Journal of Soft Computing and Artificial Intelligence*, Vol. 3, Issue. 1, May-2015.
- [2] E. O. Tartan and C. Ciflikli, 'An android application for geolocation-based health monitoring, consultancy and alarm system', 2018 42nd IEEE International conference on computer software and applications, pp.341-344, 2018.
- [3] P. B. Crilly, E. T. Arakawa, D. L. Hedden, and T. L. Ferrell, 'An Integrated Pulse Oximeter System for Telemedicine Applications', *Proc. of the IEEE Inst. and Meas. Conference*, Ottawa, Canada, Vol. 1, pp. 102- 104, May 1997.

- [4] A. V. Armarkar, D. J. Punekar, M. V. Kapse, S. Kumari, J. A. Shelk, 'Soldier Health and Position Tracking System', Int. Jour. of Eng. Sci. and Computing, March 2017.
- [5] H. Kim, J. Do and J. Park, 'Wireless Structural Health Monitoring System Using ZigBee Network and FBG Sensor', Int. Journal of Security and Its Appli., Vol. 7, No. 3, May 2013.
- [6] N. Chadil, A. Russameesawang, P. Keeratiwintakorn, 'Real Time Tracking Management System using GPS, GPRS and Google Earth," Proc. of the 5th ECTI-CON, Thailand, pp. 393-396, 2008.
- [7] P. Kumar, G. Rasika, V. Patil, S. Bobade, 'Health Monitoring and Tracking of Soldier Using GPS', Int. Jour. of Res. in Advent Tech., vol. 2, no.4, pp. 291-294, Apr. 2014.
- [8] S. Nikam, S. Patil, P. Powar, V. S. Bendre, 'GPS Based Soldier Tracking and Health Indication System', Int. Journal of Advanced Research in Electrical, Electronics and Instrumentation Engineering Vol. 2, Issue 3, March 2013.
- [9] Y. Gu, J. Shen, and Y. Chen, 'poster abstract: know you better: a smart watch-based health monitoring system', 2019 IEEE/ACM int. con. on connected health: applications, systems, and engineering technologies (CHASE), pp.7-8, 2019.
- [10] J. Patil, S. Chougule, S. Duke, M.U. Phutane, 'Soldier Health and Position Tracking System Using GPS and GSM Modem,' Int. Journal of Innovative Research in Electrical, Electronics, Instrumentation and Control Engineering, Vol. 10, Issue 4, April 2022.
- [11] S. Kodam, N. Bharath goud, B. Ramachandran, 'A review on smart wearable devices for soldier safety during battlefield using WSN technology', Materials Today: Proceedings, 2020.
- [12] S. Shelar, N. Patil, M. Jain, S. Chaudhari, S. Hande, 'Soldier Tracking and Health Monitoring Systems', Int. Journal of Soft Computing and Artificial Intelligence, Vol. 3, Issue 1, 2015.
- [13] J. Bhargav, M. Panchasara, A. Zanzarukiya, R. Parekh, 'Realtime Wireless Embedded Electronics for Soldier Security,' IEEE 2020 Int. Con. on Electronics, Computing and Communication Technologies (CONECCT) - Bangalore, India, 2020.

Improved load frequency control of 2-area power system using nature inspired algorithm

Pasalapudi Sai Pavan Kumar¹, Idamakanti kasireddy², DSNM Rao³, Ch. Phani Kumar⁴

^{1,2,4} Department of EEE, Vishnu Institute of Technology, Bhimavaram.

³Department of EEE, Gokaraju Rangaraju Institute of Engineering & Technology, Hyderabad.

Email: 20pa1d6002@vishnu.edu.in

Abstract

Automatic generation control is required in power systems to satisfy customer load requirements without disturbing the power quality with voltage and frequency swings. Any sudden load perturbations will cause a mismatch of power between generation and demand. Small disturbances can be self-managed by the synchronous generators. But the large disturbances may lead to an unstable system. In this case, speed governors come into action which is primary speed control. But the decline in frequency still exists from the nominal value. Therefore, to ensure the power quality, Automatic generation control is needed. The goal of Automatic generation control (AGC) is to hold system frequency at or very close to a specified nominal value with intelligent controllers (PID) which is a secondary speed control using frequency sensors.

Most of the methods used for automatic generation control are optimization control methods. The main goal is to improve the generation controller performance index by choosing a good optimal control algorithm so that we will get minimized change in frequency in a faster time. In this paper, we study & utilize some of the nature-inspired optimization algorithms to better regulate the automated production of linked power systems by using PID controllers. We compare these results of two area-connected thermal power systems with each algorithm and try to reduce the minimum frequency change mainly to get better settling time characteristics.

Keywords: Automatic Generation Control (AGC), Particle Swarm Optimization (PSO), Differential Evolution (DE), Artificial Neural Networks (ANN).

1. INTRODUCTION

One of the primary goals of the power system is to fulfil customer load requirements while satisfying important system constraints, such as voltage and frequency fluctuations that could create instability and, under more extreme circumstances, grid failures. Due to the rising need for electricity, power systems are now run as complex, interconnected systems. Three categories such as generation, transmission, and distribution are used to categorize the entire process. The role of the power system's components is to ensure steady operation, supply reliability, and quality. It is described as Automatic generation control (AGC). [1] In the interconnected power system, AGC's main objectives are to maintain each control area's frequency at a constant value and to set the tie-line power flows within a given tolerance range. We can adapt the real power outputs of the control area generators to the changing load requirements. It is also known as Load frequency control (LFC).

Tie-lines link each of the interconnected control areas. The overall generation capacity should be balanced with the total load requirement and losses for linked power networks to function reliably. The linearized model, which is the best scenario, is used by the majority of ideal techniques. [2, 3] The frequency of particular control regions and linked power exchange are the two relevant variables. A load frequency controller such as a proportional, integral, or PID is included in each control region to monitor the system frequency and linked power exchange. Area control error (ACE) is a combination of these two factors. Both the frequency of specific regions and the linked power exchange is maintained within the nominal values for the system to operate steadily. This issue is referred to as AGC or LFC. [4, 5]. A variety of control techniques have been created to enhance the functionality of interconnected power systems. Similar to this, a variety of creative techniques have been applied to enhance the system's dynamic performance.

In order to accomplish effective automatic generation control, controllers can be employed in conjunction with a variety of optimization techniques, including genetic algorithms, differential evolution algorithms, artificial neural networks, particle swarm optimization algorithms, etc. Thus, AGC is so needed in current power systems. The test systems used in this paper are explained in the next section.

2. TEST SYSTEM OF POWER SYSTEM MODEL

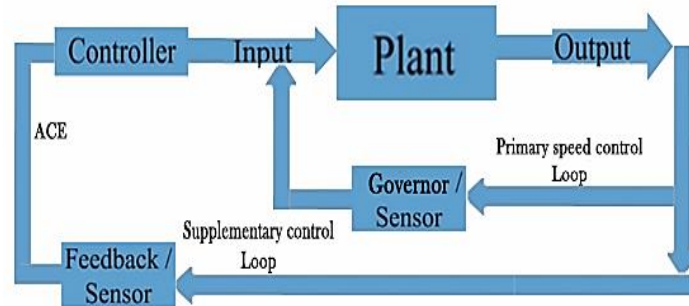


Figure 1. Test system

In Fig. 1, the feedback input to the load frequency controller is taken from area control error (ACE) for the improvisation of transient response characteristics of a supplementary control loop.

3. NATURE INSPIRED ALGORITHMS

Nature Inspired algorithms fall under the category of meta-heuristics that incorporate randomness in the variables. [6] The development of these algorithms was inspired by natural phenomena, including Bacteria, [7] African bees, colony optimization, strawberry plants, [8, 9], etc.

As we are having so many nature-inspired algorithms we use Differential Evolution (DE), Artificial Neural Network (ANN), and Particle Swarm Optimisation (PSO) algorithms for the study purpose that are employed in this paper.

3.1. Differential Evolution (DE)

A population-based optimization approach is called the Differential Evolution algorithm (DE) [10, 11]. It functions with two populations that are represented by an older and a younger generation. A quick explanation of the optimization procedure is below:

- a) Initialization: In this step initialize all the DE parameters required in the range interval [Lb, Ub] and create target vectors X was given as:

$$X = Lb + (Ub - Lb) * r \quad (1)$$

Where r = random matrix of order (1, d), d = no of input variables

- b) Mutation: In this step, three parent vectors (X_1, X_2, X_3) are chosen for mutation from previously initialized target vectors and are used to create the child vector. The weighted difference between the two vectors is added to the other vector to produce a child vector which is also known as donor vector V . It is given as:

$$V = X1 + f * (X2 - X3) \quad (2)$$

Where f is a constant within the range (0, 2)

- c) Crossover: In this step, the crossover of initially developed target vectors X and donor vector V are compared with probability range k for the creation of trial vector U . The trial vector U is later updated with the elements of the target vector or donor vector. It is given as:

$$U = X*(1-k) + V*k \quad (3)$$

Where, k is a constant of probability range {0,1}

- d) Selection: In this step, the target vectors X are compared with trial vectors U and later updated with selected new best values of fitness function (ITAE). Now a new population is created due to the altering of target vectors X which are fed again for the mutation process. The cycle continues for the best tolerable optimized value and evolves for every generation.

3.1.1. Test system of two area power system model using DE algorithm

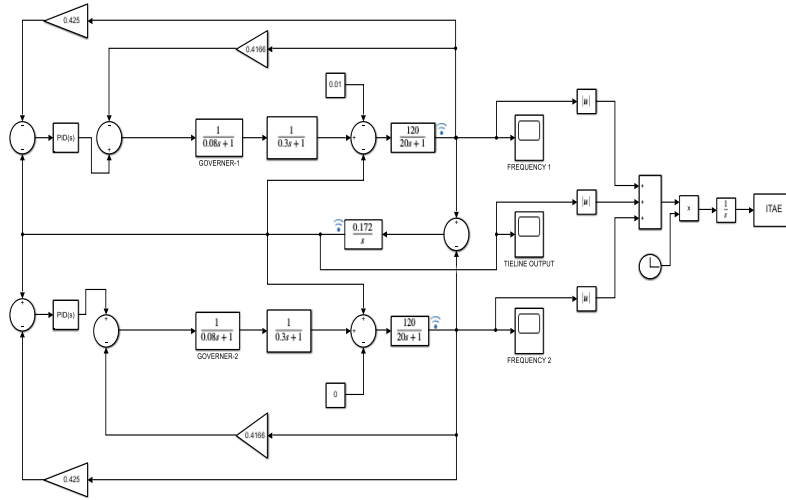
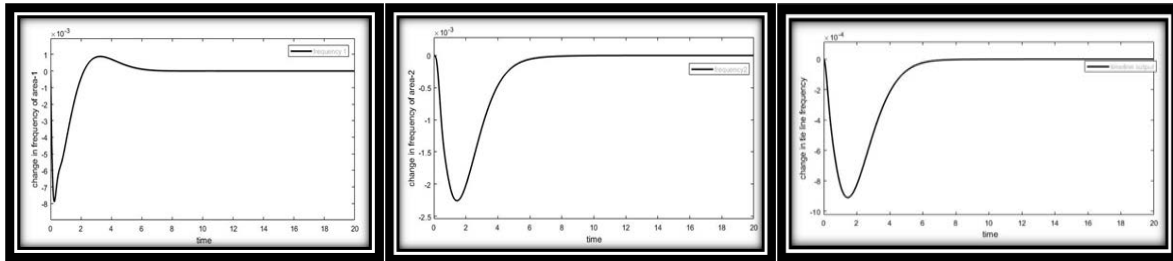


Figure 2. Modelling of test system simulation under one percent variation in area-1

Figure 2 shows the modelling of a load frequency control for test system. The specification values of every block in the system are taken from the base paper mentioned in [12].

3.1.2 Comparison of output results for change in frequency



(a). Area-1 frequency variation (b). Area-2 frequency variation (c). Tie-line frequency variation

Figure 3. (a), (b), (c) Characteristics of Test system

The sub-figures mentioned in Fig 3 give the characteristics of change in frequencies in both areas and tie lines of test system. The output frequency characteristics are obtained for the same values of DE optimized PID controllers in both the areas of power system for one percent variation in area-1 and output is given as: $k_p=1.500$, $k_i=1.960$, $k_d=1.092$, $f_{min}=0.0281$ for best settling time.

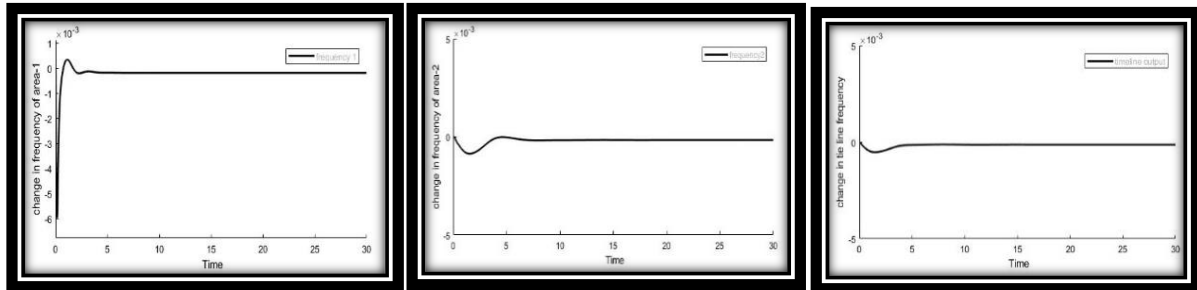
3.2. Artificial Neural Networks (ANN)

The best control commands are determined using an artificial neural network. [13] Even nonlinearities can be applied to it. While starting, the system settings are not necessary. Even if inputs to the system are momentarily lost or faults are introduced, it can still operate. The controller keeps working in the event of any breakdown, minimizing the requirement for decision-making support software. Initially make the outputs and inputs initialized. Initialize the weight values and the values of bases using functions like tansig, trainlm, logsig, etc. Following the initialization of the maximum number of training epochs, the results are displayed at every iteration with the error training. Once the system has successfully trained, you may begin the process of concluding it by generating a trained simulation system.

3.2.1 Test system of two area power system model using ANN algorithm

Figure 2 shows the modelling of a load frequency control for test system. The specification values of every block in the system are taken from the base paper mentioned in [12]. Only the controller in area-1 is trained by using ANN algorithm.

3.2.3 Comparison of output results in a change in frequency



(a). Area-1 frequency variation (b). Area-2 frequency variation (c). Tie-line frequency variation

Figure 4. (a), (b), (c) Characteristics of Test system

The sub-figures mentioned in Fig 4 gives the characteristics of change in frequencies in both areas and tie lines of test system. For training of ANN controller initially we had done extensive simulation and the values for gain are taken as $k_p=1.400$, $k_i=1.600$, $k_d=1.400$ for getting the input and output data. The output frequency characteristics are obtained for same values of ANN trained controller in area-1 and PID controller trained by extensive simulation in area-2 of power system for one percent variation in area-1. The drawback is that despite the load disruption, area-2 response still exhibits some inaccuracy with best settling time compared to DE algorithm.

The figure 5 (a) is the ANN trained controller obtained as output and figure 5 (b) gives the inside view of ANN controller which contains input layer, output layer and hidden layers. The output trained ANN controller is given below:

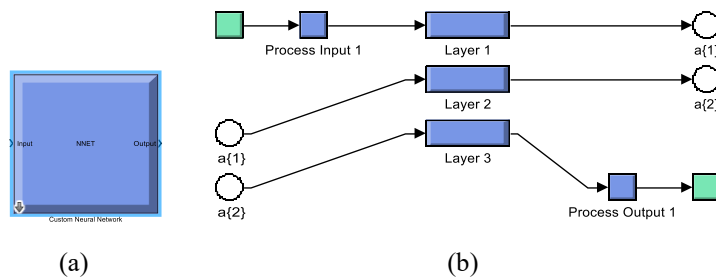


Figure 5. (a) ANN trained controller and (b) ANN trained neural network structure

3.3. Particle Swarm Optimization (PSO)

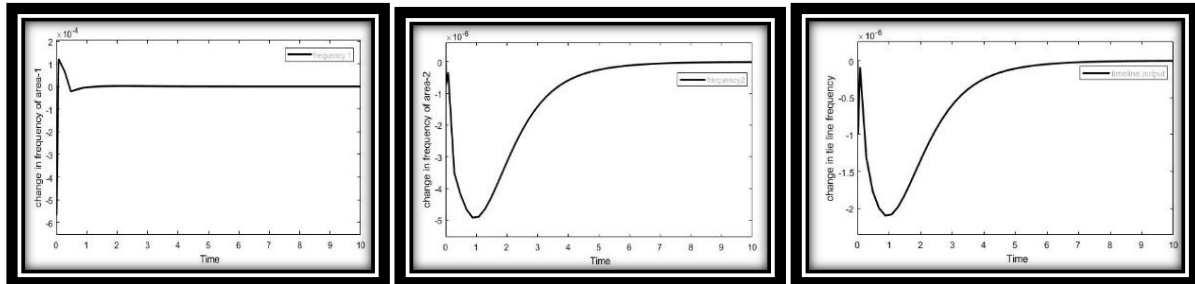
For optimization issues, Kennedy and Eberhart developed the PSO algorithm [14]. It is one of the algorithms that draw inspiration from nature and is based on a simulation of the flock's behaviour of birds. It is mostly population-based and has gained popularity as a global optimizer, especially for issues where the decision variables are actual numbers. Since it simply requires the objective function for optimization, it differs from other optimization techniques. The main points of Particle swarm optimization are given as:

- Each particle in particle swarm optimization has an associated position, velocity, fitness value.
- Each particle keeps track of the particle best Fitness value and particle best Fitness position (Pbest).
- A record of global best Fitness position and global best Fitness value is maintained (Gbest)

3.3.1 Test system of two area power system model using PSO algorithm

Figure 2 shows the modelling of a load frequency control for test system. The specification values of every block in the system are taken from the base paper mentioned in [12]. Only the controller is optimized by using the particle swarm optimization algorithm.

3.3.2 Comparison of output results in a change in frequency



(a). Area-1 frequency variation (b). Area-2 frequency variation (c). Tie-line frequency variation
Figure 6. (a), (b), (c) Characteristics of Test system

The sub-figures mentioned in Fig 11 gives the characteristics of change in frequencies in both areas and tie lines of test system-1 and test system-2. The output frequency characteristics are improved for test system-2 as compared to the original test system-1 for same values of PSO optimized PID controllers in both areas of power system for one percent variation in area-1. Here we use Rosenbrock solver settings while simulation at a tolerance of $1e+6$ and for optimisation. The values of k_p , k_i , k_d are $1.0e+03 * 0.8918$, 1.0000 , 0.2838 for best settling time.

4. CONCLUSION

In ANN optimized Algorithm, by comparative analysis, the output frequency characteristics are improved compared to DE for the same values of ANN trained controller in area-1 and PID controller trained by extensive simulation in area-2 of power system for 1% step change in area-1. But the disadvantage is that we can still see some error in the area-2 response which is not having the load disturbance. Even though it gives better settling time compared to DE-optimized results.

In PSO optimized Algorithm, by comparative analysis, the output frequency characteristics are improved compared to ANN for the same values of PSO optimized PID controllers in both the areas of the power system for 1% step change disturbance in area-1. Here we use Rosenbrock solver settings while simulation at a tolerance of $1e+6$ for optimization.

Thus, by comparing all these algorithms, Particle swarm optimization (PSO) provides better optimization results when comparing all these techniques of two area-interconnected power systems, and the Test system-2 improves network performance when compared to the Test system-1 with the least settling time of change in frequency.

REFERENCES

- [1] K. P. S. Parmar, S. Majhi and D. P. Kothari, "Automatic generation control of an interconnected hydrothermal power system," 2010 Annual IEEE India Conference (INDICON), 2010, pp. 1-5, doi: 10.1109/INDICON.2010.5712663.
- [2] Idamakanti Kasireddy, A. W. Nasir, R. Shashi Kumar Reddy, and Veeraiah, "Determination of stable zones of LFC for a power system considering communication delay", AIP Conference Proceedings 2418, 040014 (2022) <https://doi.org/10.1063/5.0081986>
- [3] Bhoopal, N., Rao, D.S.M., Sireesha, N.V., Kasireddy, I., Gatla, R.K., Kumar, D.G. (2022). Modelling and performance evaluation of 18w PEM fuel cell considering H2 pressure variations. Journal of New Materials for Electrochemical Systems, Vol. 25, No. 1, pp. 1-6. <https://doi.org/10.14447/jnmes.v25i1.a01>

- [4] Ahamed, T.P.I., Rao, P.S.N., Sastry, P.S., 2002. A reinforcement learning approach to automatic generation control. *Electr. Power Syst. Res.* 63 (1), 9–26.
- [5] Arora, K., Kumar, A., Kamboj, V.K. (2019). Automatic Generation Control and Load Frequency Control: A Comprehensive Review. In: Mishra, S., Sood, Y., Tomar, A. (eds) *Applications of Computing, Automation and Wireless Systems in Electrical Engineering. Lecture Notes in Electrical Engineering*, vol 553. Springer, Singapore. https://doi.org/10.1007/978-981-13-6772-4_39.
- [6] Xin-She Yang, Nature-inspired optimization algorithms: Challenges and open problems, *journal of Computational Science*, Article 101104, (2020). <https://doi.org/10.1016/j.jocs.2020.10110>
- [7] Ali, E.S., Abd-Elazim, S.M., 2011. Bacteria foraging optimization algorithm based load frequency controller for interconnected power system. *Int. J. Electr. Power Energy Syst.* 33 (3), 633–638.
- [8] Gupta, N.K., Kasireddy, I., Singh, A.K. (2022). Design of PID Controller Using Strawberry Algorithm for Load Frequency Control of Multi-area Interconnected Power System with and Without Non-linearity. In: Kumar, J., Tripathy, M., Jena, P. (eds) *Control Applications in Modern Power Systems. Lecture Notes in Electrical Engineering*, vol 870. Springer, Singapore. https://doi.org/10.1007/978-981-19-0193-5_13.
- [9] Merrikh-Bayat, Farshad. "A Numerical Optimization Algorithm Inspired by the Strawberry Plant." *ArXiv abs/1407.7399* (2014).
- [10] Banaja Mohanty, Sidhartha Panda, P.K. Hota, Differential evolution algorithm based automatic generation control for interconnected power systems with non-linearity, *Alexandria Engineering Journal*, Volume 53, Issue 3, 2014, Pages 537-552, ISSN 1110-0168. <https://doi.org/10.1016/j.aej.2014.06.006>.
- [11] M. A. Zamee, K. K. Islam, A. Ahmed and K. R. Zafreen, "Differential evolution algorithm based load frequency control in a two-area conventional and renewable energy based nonlinear power system," 2016 4th International Conference on the Development in the in Renewable Energy Technology (ICDRET), 2016, pp. 1-6, doi: 10.1109/ICDRET.2016.7421476.
- [12] Çelik E (2020) Improved stochastic fractal search algorithm and modified cost function for automatic generation control of interconnected electric power systems. *Eng Appl Artif Intell* 88:103407
- [13] Load frequency control: a generalized neural network approach. (1999). *Fuel and Energy Abstracts*, 40(6), 392. doi:10.1016/s0140-6701(99)98929-4
- [14] Ghosal, S.P., 2004. Optimization of PID gains by particle swarm optimization in fuzzy based automatic generation control. *Electr. Power Syst. Res.* 72 (3), 203–212

Analysis and Simulation of Fuel Cell Powered Integrated Converter with Single Active Switch

*¹C. V. Vijay Kumar, ¹T. Sanjana, ¹B. Nagi Reddy

¹ Department of EEE, Vignana Bharathi Institute of Technology, Hyderabad, India
*Email: cvvijay93@gmail.com

Abstract

Cascaded boost and Lou converters will serve as the foundation for this project's integrated converter, which will be driven by fuel cells and have a single active switch. The fact that the suggested converter is capable of delivering high levels of efficiency as well as voltage gains qualifies it for use in applications involving fuel cells. This converter offers a number of benefits, including a higher voltage gain ratio with no deployment of a transformer, improved efficiency, continued flow of input current, and the use of a single power switch. These benefits are derived from the fact that the converter only uses a single switch. The mode of continuous conduction is going to be investigated. Under steady-state conditions, the performance of the proposed DC-DC converter is analyzed and assessed. This performance is tested using the MATLAB to validate the proposed converter's capabilities in steady-state circumstances.

Keywords. DC-DC converter, fuel cell, high voltage gain, single switch integrated converter, continuous input current.

1. INTRODUCTION

The two basic categories of DC-DC topologies are isolated and non-isolated systems. Independent of the high value of the duty cycle, the turn ratio of the coils in the isolated topologies plays a crucial part in the rise in voltage gain. Sensitive loads are shielded from input source failures by the isolation that the high-frequency transformer's presence creates. The disadvantages of including a magnetic core include its increased bulk, weight, cost, and loss, notwithstanding the benefits described above. Additionally, the discontinuity in the input current and the presence of leaking inductors point to the need for snubber circuits, which raises the complexity and number of circuit components in the circuit. Therefore, when there is little justification for using an isolated circuit, it makes sense to use a non-isolated topology. The buck-boost and boost converters, which are among the classic non-isolated configurations and include buck-boost, buck, and boost converters, may step increase the input source's voltage level. The primary drawbacks of buck-boost converters include the discontinuous input and output currents and the output voltage's negative polarity. Because of this, the buck-boost converter experiences a pass-through rather than a step-up [1-3]. The input voltage gain can be increased by

using a typical boost converter. Theoretically, more orders of voltage gain can be attained by boosting the duty cycle and its proximity to unity. The conduction time of the diode approaches zero as the duty cycle gets closer to unity, which complicates the diode's reverse recovery time [4].

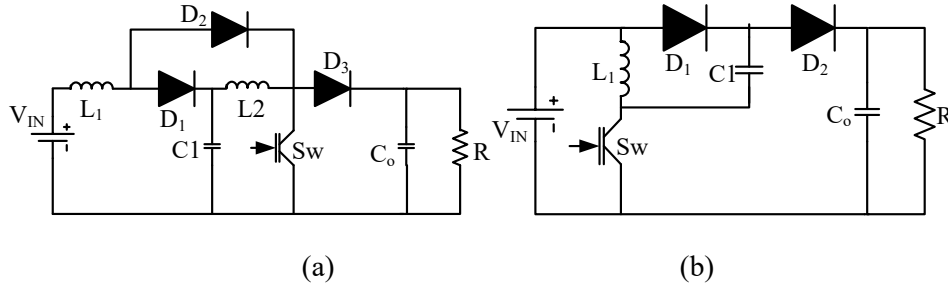


Figure 1. (a) Boosting topology, and (b) Luo circuit.

The aforementioned ideas provide the grounds for the birth of novel DC-DC converter topologies. The cascade of the boost converter is one of the provided structures and is shown in Figure 1a. Its topology, which was created by connecting two boost topologies, consisted of a switch and three diodes, as is clear [5]. When the duty-cycle gets closer to one in order to get more voltage gain, the number of parts can go up, which can have a big effect on efficiency. Figure 1b shows a Luo converter, which is another high step-up topology. The input current has a greater current ripple as compared to the boost topology, which raises the input DC-link capacitor's value. The diode is turned on because of the current created when the first capacitor and the source of power are connected in parallel. Additionally, a current ripple of this kind might shorten the capacitor's lifespan, which has an impact on the whole topology's longevity. Quadratic buck-boost topologies are introduced in [6]. The indicated converters of [6] had intermittent input currents; there were many inductors, and the voltage & current stress on the switching devices was substantial. The second sort of quadratic converter that has been recommended for fuel cell applications are the converters presented in [6]. A greater duty cycle value is necessary to obtain a significant voltage gain.

In this study, a cascaded boost and a Luo converter-based architecture are given. In contrast to the recommended converters [6], the developed converter's boost topology implementation in the first stage. Additionally, the suggested converters, and Luo converters are successful in solving the excessive current ripple of the input current. In the recommended topologies of [4-6], different amounts of inductor current travel through the input source. The voltage and current stresses on semiconductor components in the converter have decreased to a low, reachable value that is lower than unity [7-9]. As a result, the operating point has increased by more than 90%, and the planned topology's efficiency has reached high values.

2. PROPOSED INTEGRATED TOPOLOGY

Figure 2 illustrates the suggested topology's circuit diagram. The circuit first half employs the boost topology, results in a constant input current, which is the primary factor contributing to the developed converter's viability for usage in renewable energy applications. In the continuous conduction mode, the given architecture provides two operation modes (CCM). For analyzing, it is assumed that the converter is in steady-state. The first and third diodes are triggered in the first operating mode as a result the switch begins to conduct. The inductors are magnetised and have positive voltages at this time. Due to their respective negative currents, the converter's first and output capacitors have been discharged, while its second capacitor has been charged as a result of its positive current.

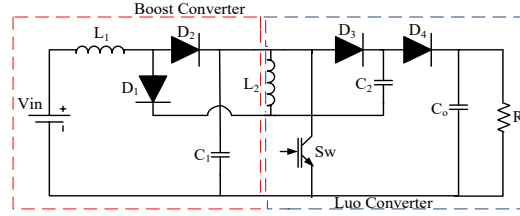


Figure 2. The proposed configuration.

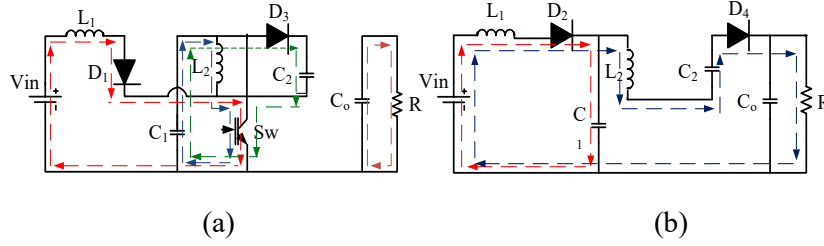


Figure 3. (a) Equivalent circuit of ON mode; (b) Equivalent circuit of OFF mode.

The 2nd and 4th diodes, however, begin to pass the current. In this mode, a negative voltage is given to the inductors. The inductors have therefore become demagnetized. The first and output capacitor currents have turned positive and are now beginning to charge. The equations at the inductors and capacitors are:

$$L_1 \frac{di_{L1}}{dt} = v_{in}D + (v_{in} - v_{c1})(1 - D) \quad (1)$$

$$L_2 \frac{di_{L2}}{dt} = v_{c1}D + (2v_{c1} - v_0)(1 - D) \quad (2)$$

$$C_1 \frac{dv_{C1}}{dt} = -(i_{L1} + i_{c2})D + (i_{L1} - i_{L2})(1 - D) \quad (3)$$

$$C_2 \frac{dv_{C2}}{dt} = i_{c2}D - i_{L2}(1 - D) \quad (4)$$

3. DEVICE STRESSES

The voltage second balance is used to compute the inductor voltage and the current second balance is used to calculate the capacitor current. They can be given as:

$$V_{c1} = \frac{V_{in}}{1 - D} \quad (5)$$

$$V_{c2} = \frac{V_{in}}{1 - D} \quad (6)$$

$$V_{c0} = \frac{(2 - D)V_{in}}{(1 - D)^2} \quad (7)$$

$$I_{L1} = \frac{(2 - D)}{(1 - D)} I_o \quad (8)$$

$$I_{L2} = \frac{1}{1 - D} I_o \quad (9)$$

Voltage/current stress on semiconductors is expressed using relationships such as duty cycle, input voltage, and output current. The difference between the highest and minimum inductor currents may be used to calculate the ripple inductor current. The difference between the highest and minimum capacitor voltages may also be used to compute the ripple in the capacitor voltage.

$$I_{D2} = \frac{(2 - D)I_o}{1 - D} \quad (10)$$

$$I_{D3} = I_{D4} = I_o \quad (11)$$

$$V_{S1} = V_{D3} = V_{D4} = \frac{V_{in}}{(1 - D)^2} \quad (12)$$

$$V_{D2} = \frac{V_{in}}{1 - D} \quad (13)$$

4. RESULTS & DISCUSSION

The projected converter is designed for an output power of 500W, with an output voltage of 200V. With the input voltage of 20V, the required output voltage with a gain of 10, can be produced at a duty ratio of 63%. To reduce the converter size, it is advisable to take higher switching frequencies (fs), however for the proposed simulation and design 50 kHz frequency is considered. With the considerable current and voltage ripples on the inductors and capacitors respectively, the energy component values are calculated and are observed in table 1. Figure 4 represents the input DC voltage waveform plotted using MATLAB simulation. A 20V DC input voltage is considered as the output of fuel cell to design the proposed converter.

Table 1 Simulation component values

S. No	Components	Step up mode
01)	Input Voltage (V_{in})	20 V
02)	Output Voltage (V_o)	200 V
03)	Output Power (P_o)	500 W
04)	Switching Frequency (F_s)	50 KHz
05)	Output Load R	80 ohms
06)	$M(D)=V_o/V_{in}$	10
07)	Duty cycle D	0.63
08)	$L_1(\Delta=1A)$	63 μH
09)	$L_2(\Delta=2A)$	340.54 μH
10)	$C_1(\Delta=2V)$	42.57 μF
11)	$C_2(\Delta=2V)$	25 μF
12)	$C_3(\Delta=5V)$	504 μF

The simulated voltage waveform of capacitor 1 (C_1) is shown in fig. 5. From the previous discussion, the capacitor (C_1) discharges the energy when the active switches are turned on, and charges when the switch is turned off. This phenomenon can be observed in the fig. 5, with a considerable peak ripple of 2V. Similarly, the simulated voltage waveform of capacitor 2 (C_2) is shown in fig. 6.

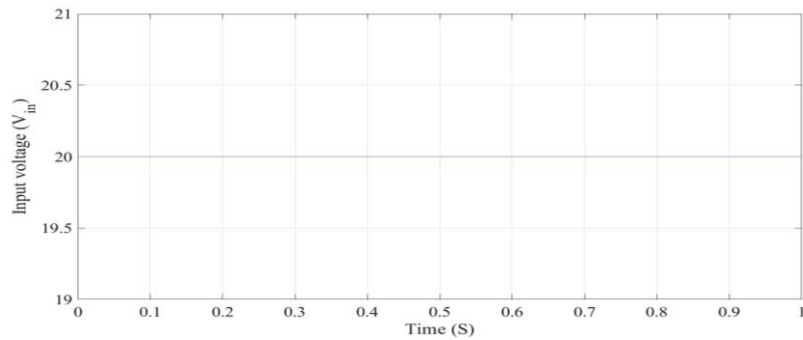


Figure 4. Simulated waveform of the input DC voltage

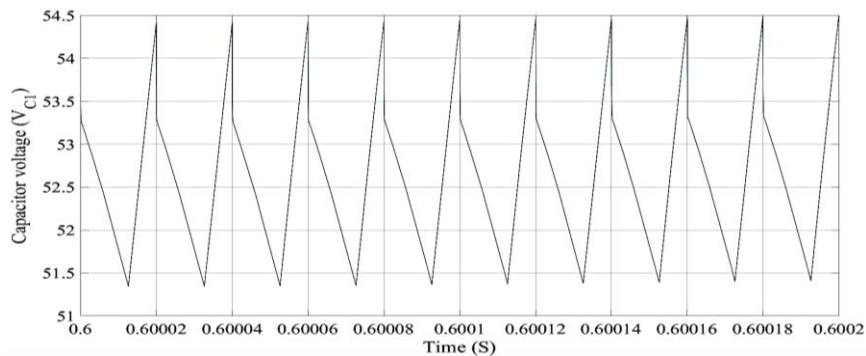


Figure 5. Simulated waveform of the capacitor 1 voltage with a peak ripple of 2V

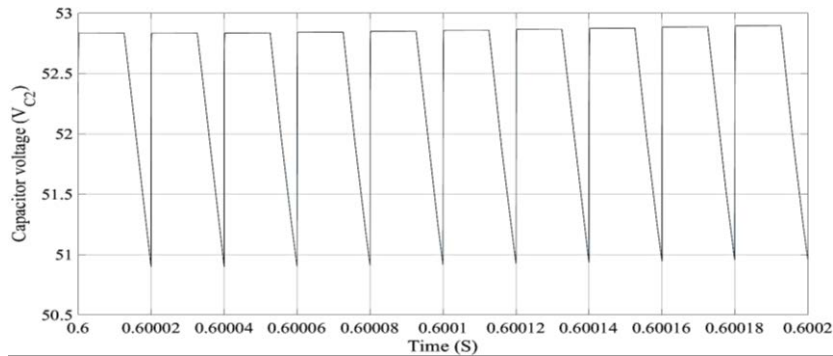


Figure 6. Simulated waveform of the capacitor 2 voltage with a peak ripple of 2V

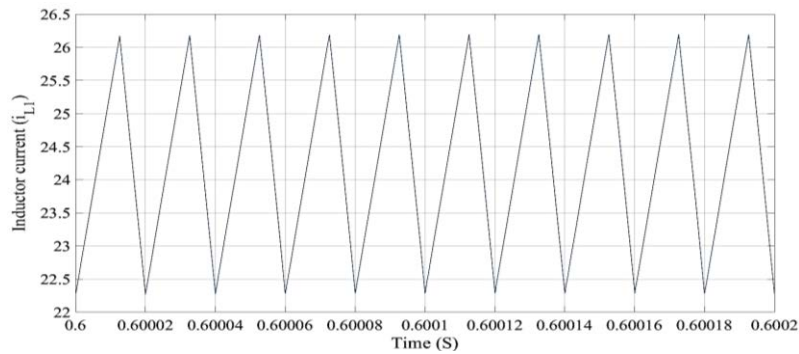


Figure 7. Inductor 1 (L_1) current waveform with a peak-to-peak ripple of 4 A

From the operation of the converter, the capacitor 2 (C_2) charges its energy when the active switches are turned on, and discharges when the switch is turned off. This phenomenon can be observed in the fig. 6, with a considerable peak ripple of 2V. Figures 7&8 shows the simulated inductor current waveforms i_{L1} & i_{L2} respectively under steady state operation (for 10 cycles). From fig. 7 it can be noted that the inductor L_1 peak to peak ripple is approximately 4A. This value is exactly matches to the theoretical consideration of inductor L_1 design.

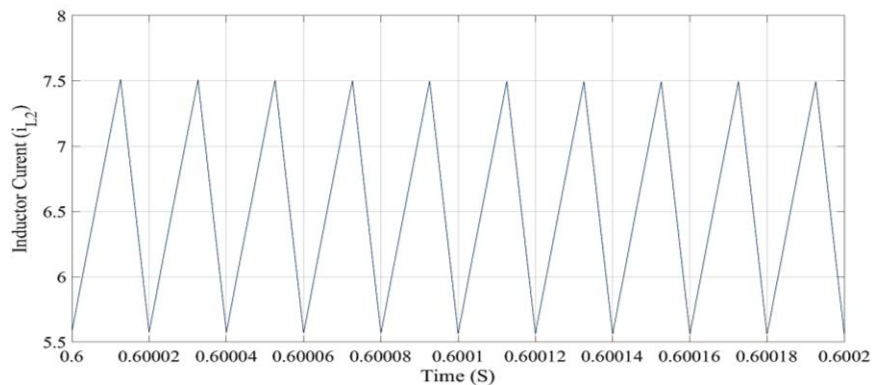


Figure 8. Inductor 2 (L_2) current waveform with a peak-to-peak ripple of 2 A

From fig. 8 it can be noted that the inductor L_2 peak to peak ripple is approximately 2A which exactly matches to the theoretical consideration of inductor L_2 . Figure 9 shows the simulated output current waveform with negligible ripple. The simulated value is approximately 2.42A and is much closed to the computed theoretical value. Figure 10 represents the simulated DC output voltage waveform with very low ripple (<0.5% approximately). The simulated value is approximately 194V and is much closed to the computed theoretical value.

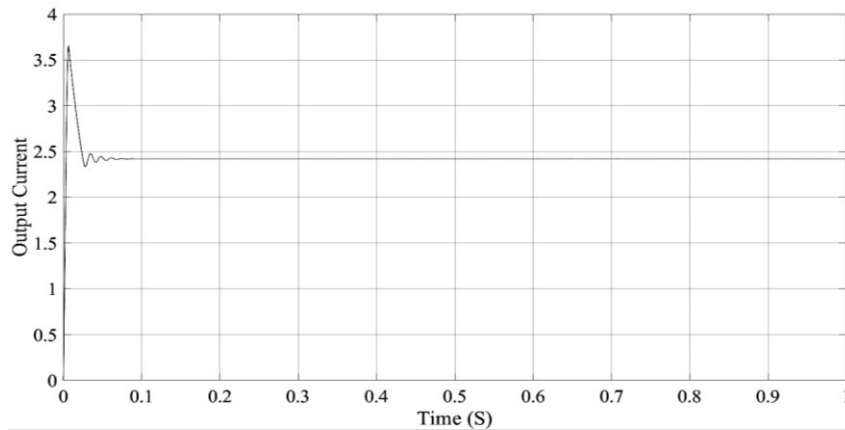


Figure 9. DC output current waveform of proposed topology

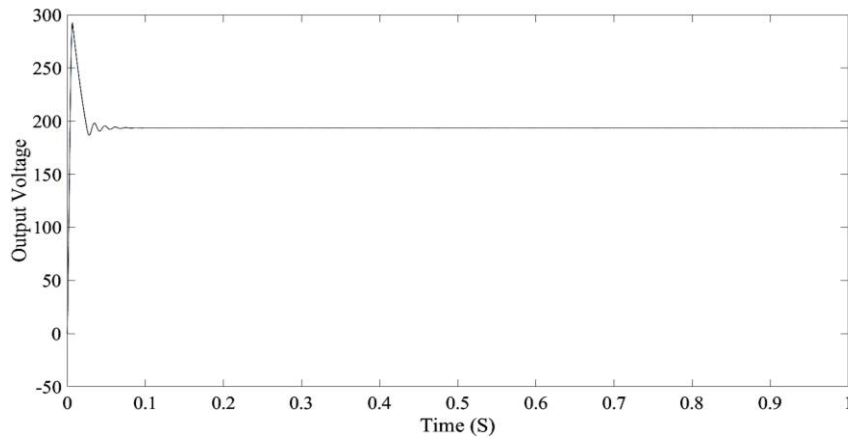


Figure 10. Output DC voltage waveform of proposed topology

5. CONCLUSION

In the paper, the formation of a step-up configuration was facilitated by the cascading of boost and Luo converters. It owns a variety of advantageous qualities, such as a high voltage conversion ratio without the requirement for transformers, high efficiency, stability in the input current, and the utilization of just one power switch. The configurations of the circuits, their operating principles, and how they

function in the mode of continuous conduction have been given. Simulation and analysis of performance are carried out by making use of theoretical values.

REFERENCES

- [1] Miao. S, Wang. F, Ma, X. “a new transformer less buck-boost converter with positive output voltage”, *IEEE Trans. Ind. Electron.*, 63, 2965–2975, 2016.
- [2] E. Salari, M. Banaei and A. Ajami, "Analysis of switched inductor three-level DC/DC converter", *Journal of Operation and Automation in Power Engineering*, vol. 6, no. 1, pp. 126-134, 2018.
- [3] Gopi, R.R, Sreejith. S, “Converter topologies in photovoltaic applications—A review”, *Renew. Sustain. Energy Rev*, 94, 1–14, 2018.
- [4] Nagi reddy. B, Sahithi Priya. Kosika, Manish patel. Gadam, jagadhishwar. Banoth, Ashok. Banoth, Srikanth goud. B, “Analysis of positive output buck-boost topology with extended conversion ratio”, *Journal of Energy Systems*, 6(1), pp. 62–83, 2022.
- [5] A. Tavassoli, B. Allahverdinejad, N. Rashidirad and M. Hamzeh, "Performance analysis of series SPOs in a droop-controlled DC microgrid", *2017 Smart Grid Conference (SGC)*, pp. 1-6, 2017.
- [6] Rosas-Caro. J.C, Valdez-Resendiz. J.E, Mayo-Maldonado. J.C, Alejo-Reyes. A, Valderrabano-Gonzalez. A, “Quadratic buck–boost converter with positive output voltage and minimum ripple point design”, *IET Power Electron.*, 11, 1306–1313, 2018.
- [7] V. Jagan, J. Kotturu and S. Das, "Enhanced-Boost Quasi-Z-Source Inverters with Two-Switched Impedance Networks," in *IEEE Transactions on Industrial Electronics*, vol. 64, no. 9, pp. 6885-6897, Sept. 2017, doi: 10.1109/TIE.2017.2688964.
- [8] A. Y. V. B. N. S. Naidu, S. Srinivas, V. Jagan and V. Sharma C., "Modified High Boost Quasi Z-Source Inverter with an Active Switched Network," *2020 IEEE Students Conference on Engineering & Systems (SCES)*, 2020, pp. 1-6, doi: 10.1109/SCES50439.2020.9236732.
- [9] Nagi Reddy, B., Chandra Sekhar, O., Ramamoorthy, M. “Analysis and implementation of single-stage buck-boost-buck converter for battery charging applications *Journal of Advanced Research in Dynamical and Control Systems*, 2018, 10(4), pp. 446–457.

Power Optimization Scheme in Electric Vehicle Using Induction Motor Based FOPID Control Strategy

B. Akhil Raj¹, Devineni Gireesh Kumar¹, Nagineni Venkata Sireesha^{2*},

S. Saravanan¹, DSNM RAO³, R. Muneeshwar¹, Ranjith Kumar Gatla⁴

¹Department of EEE, B V Raju Institute of Technology, Narsapur, Medak, Telangana, India

²Department of Information Technology, Institute of Aeronautical Engineering, Telangana, India.

³Department of EEE, Gokaraju Rangaraju Institute of Engineering & Technology, Telangana, India.

⁴Department of EEE, Institute of Aeronautical Engineering, Dundigal, Telangana, India.

Email: gireesh218@gmail.com

Abstract

The increased use of fossil fuel cars nowadays has increased the amount of CO₂ in the atmosphere. Electric vehicles (EVs) provide a way to lessen negative consequences. Despite the fact that induction engines are often used for exercising, synchronous engines are more frequently used in electric cars (EVs). Since electric vehicle (EV) battery storage capacity is limited, energy efficiency is critical. When employed in EV applications at less than full capacity, these vehicles face the risk of poor performance and more energy consumption than is really necessary to keep them operating. PID controllers, FUZZY Logic Controllers (FLC), and Fractional Order PID(FOPID). controllers are used in induction cars to overcome these issues. The feedback loops on the PID and FUZZY controllers are more varied, and thus need more time to relay error indicators back to the input so that errors may be fixed. Therefore, it was suggested in this project that FOPID techniques be employed to improve the induction motor's overall performance. To save more electricity, FOPID might change the initial modern amplitude. The suggested version's performance was evaluated using the MATLAB/SIMULINK tool.

Keywords. Electric Vehicle (EV), Induction Motor, PID, Fuzzy Logic Controller (FLC), Fractional Order PID(FOPID).

1. INTRODUCTION

As fossil fuel consumption has increased, CO₂ levels in the atmosphere have risen, particularly in the last few decades. Worldwide carbon dioxide emission reduction efforts are urgently needed to address climate change and increasing sea levels. Increasing the efficiency of automobiles is essential due to the fact that transportation accounts for over 20% of total carbon dioxide emissions [1]. The environmental benefits of electric cars (EVs) outweigh the drawbacks of gasoline-powered vehicles, as well as their quieter operation and reduced reliance on foreign oil. The efficiency and cost of a driving system are heavily influenced by the electrical equipment that power it. Even if a car is classified as an electric or a hybrid, it will not run without electric powertrain. There are two types of synchronous motors that can power electric vehicles: induction motors and synchronous motors (IMs). Propulsion for the EV-motor, according to [2], should include high torque density to deliver suitable driving force during start-up, ascending and accelerating; high efficiency to increase the driving distance; and flow regulation to widen the static power speed range. For electric vehicles (EVs), traction drives like the IM are becoming increasingly popular because of

their great durability, low cost, and low maintenance needs. As a result of higher losses, EV applications have a poorer machine efficiency. Low energy density, increased weight, longer charging times, and longer battery life [5] are the major obstacles to the widespread use of these vehicles in transportation. Energy efficiency must be maximized in order for an EV to work correctly [6]. It is typical practice for industrial drives to use proportional integral derivative (PID) controls because of their efficacy and ease of implementation. The most frequent type of controller in current control loops is the PID controller, which is widely utilized in industrial settings. For example, a shift in working conditions might cause significant performance loss [7]. [8] For example, a fuzzy logic controller (FLC) is an intelligent control method that can improve performance because it is difficult to accurately express the precise analytical model of a managed system. Several strategy principles are simplified by the usage of language tags in the FLC framework. As a result, other examples have employed another technique to manage EV energy demand. FLC is a model-free approach, hence a mathematical model of the system under control is not required. Adaptive FLC system controllers are needed if we are to improve EV traction in areas where there are fixed defects. Other FLC trends to consider include low steady-state error, low overshoot, and a rapid rise time. As a result, the fundamental goal of contemporary design methods is to reduce steady-state losses. Typical induction machines designed for high stability efficiency may suffer from significant and excessive current peak losses during transit with variable flow linkages. In light of the EV's traction motor drive cycle's dynamic character, the focus of this research is on the losses of transient machines. In the literature, a variety of control schemes have been presented for electric vehicle applications. Among the most common linear control methods are sliding mode control [11] and field-oriented control [12]. A technique called the "golden section" is used to reduce secondary winding harmonic losses by employing a model reference adaptive system with an optimized base power scheme. Use speed error change as an input to build frequency by employing an adaptive quadratic interpolation and slip control (SC) based on fuzzy controllers with nine rules [14].

2. PROPOSED SYSTEM DESCRIPTION

The most prevalent kind of AC is a three-phase model. The gearbox and differential link the wheel hub to the gearbox and differential. Additionally, it has a DC/AC power converter and its own management system in addition to a chemical-based energy storage battery.

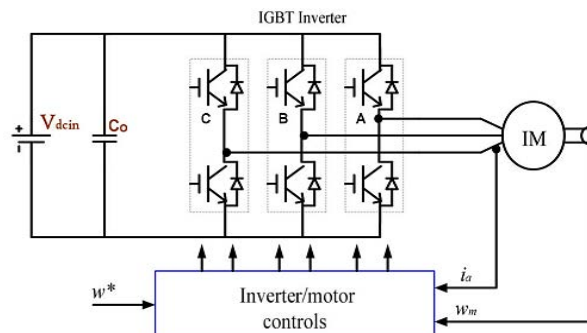


Figure. 1 Schematic representation of an induction motor-powered electric car drive system.

Figure 1 depicts the three major parts of a battery-powered vehicle's electric motor system, which is generally only one electrical unit. Finally, the electric automobile uses a three-phase frequency and voltage control system to power it. The accelerator and brake pedals are linked to this system. A phase-locked loop and the DQZ conversion formulas are used to achieve the goal of synchronizing the utility current regulator. The phase currents' coordinates are shifted to fit within a d-q frame in order to convert a-b-c coordinates to d-q coordinates. Conversions for the d-q components can be summarized as follows: A three-phase electric machine is shown in Figure 1 as a means of generating power. The differential gear ratios on the left and right wheels enable for high-speed electric motor shaft adjustment at low speeds. When a DC battery supply is converted into three-phase AC voltage, the inverter regulates it. Component losses must be taken into consideration when calculating the power consumption of an electric car not linked to the grid. Our ultimate goal is to develop electric vehicle (EV) controllers that are as efficient as feasible. To compensate for the controller's lack of adaptability, flexibility, and power, FLC techniques for EV applications can be used.

3. CONTROL STRATEGY

As a general-purpose feedback control loop, PID controllers are commonly used in industrial control systems. When there is a disparity between a consistency process variable and the intended set point, the PID controller generates and executes corrective actions to correct it. PID controllers employ time constants that are both integral (K_i) and derivative (K_d) (K_d). These three variables make up the PID controller algorithm. The quantity of recent mistakes, the pace at which errors change, and the Integral all have an effect on error response. These three actions may be directed by the use of control devices such as a control valve or a heating element. Figure 2 depicts closed-loop control systems using a PID controller.

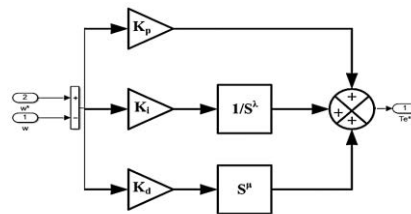


Figure. 2 A closed-loop process control system based on FOPID controllers.

4. SIMULATION RESULTS

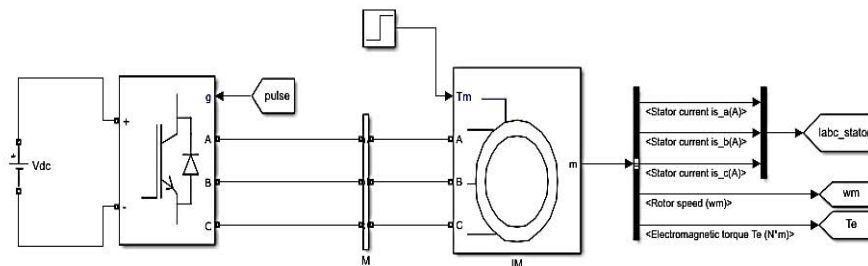


Figure.3 MATLAB/SIMULINK circuit diagram of the system

A) EXISITNG RESULTS

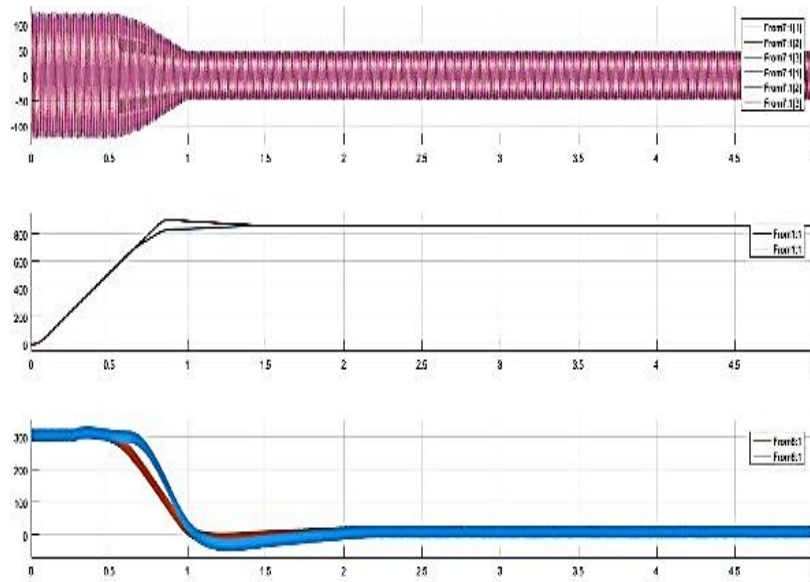


Figure.4 (a) 3-phase stator currents of PID and FLC models (b) Rotor speed of PID (red) and FLC (blue) When N_{ref} 859 rpm (c) Torque response of PID (red) and FLC (blue)

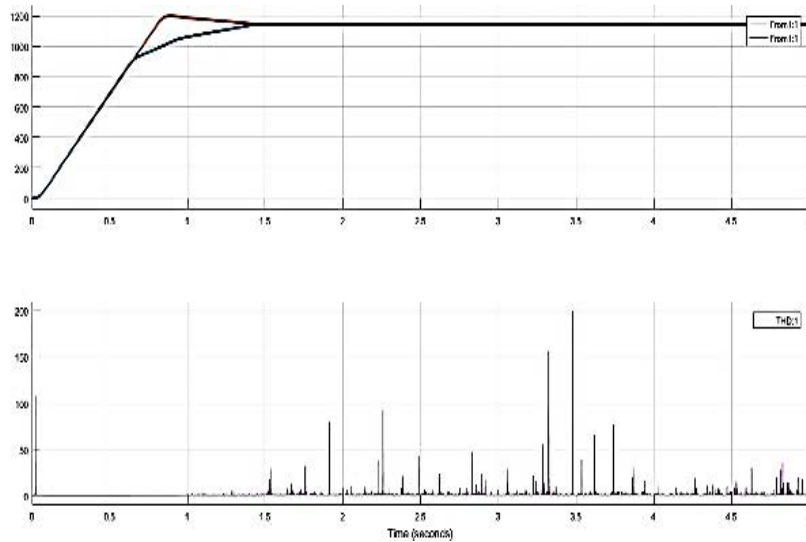


Figure.5 (a) Rotor speed comparison for PID (red) and FLC (blue) When N_{ref} 1145rpm (b) Harmonic speed waveform

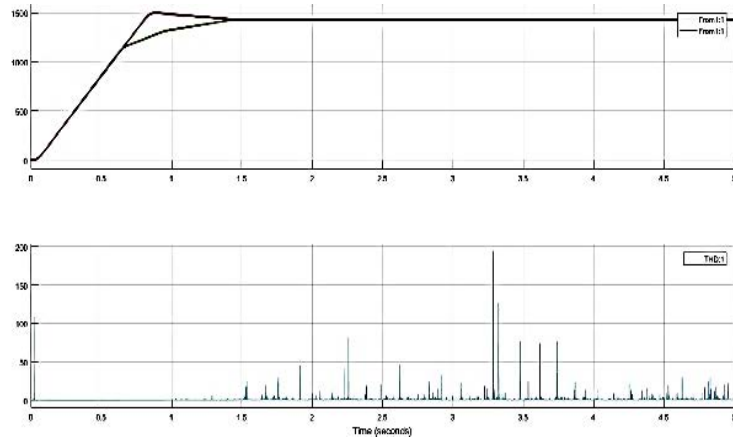


Figure.6 Rotor speed comparison for PID (red) and FLC (blue) When N_{ref} 1432 rpm
(b) Harmonic speed waveform

B) EXTENSION RESULTS

Various PID, FLC, and FOPID simulations were done to control the IM speed. Figures 4, 5, and 6 show the results of testing the control unit using a constant load torque. For multistep speed input, FOPID provides faster rise and fall times than PID. FLC outperformed FOPID when compared to PID. Three-phase IM, on the other hand, benefited from FOPID's more precise and quick response, as well as the absence of overshoot or steady-state error. Simulated EV applications were utilized to test the effects of PID, FLC, and FOPID on the speed of the internal combustion engine (IM). The simulations took into account a variety of operational variables, such as the reference speed and the applied load. PID, FLC, and FOPID performance was compared.

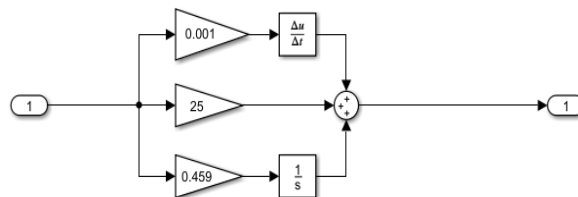


Figure.7 Subsystem of FOPID controller

Table 1. Comparison of the multistep speed response capabilities of FOPID, FLC and PID

Reference speed, rpm	Rise time, s			Settling time, s		
	FOPID	FLC	PI	FOPID	FLC	PI
1432	0.821	0.731	0.681	1.890	1.982	2.584
1145	0.745	0.630	0.543	1.825	1.910	2.679
859	0.601	0.547	0.402	1.712	1.868	2.419

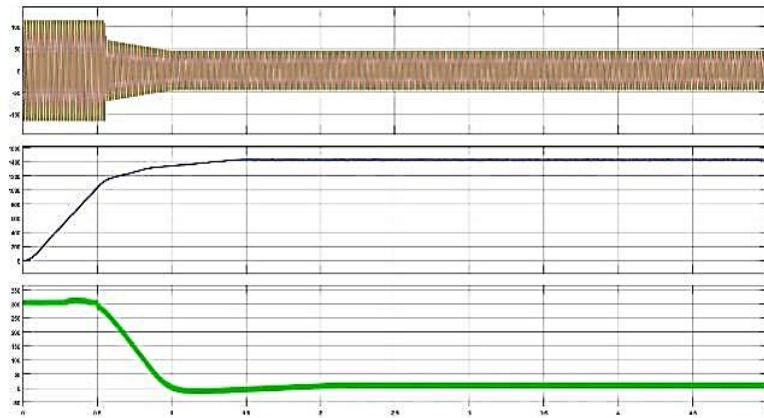


Figure.8 (a) 3-phase stator currents of PID and FLC models (b) Rotor speed of PID (red) and FLC (blue) When N_{ref} 1432 rpm (c) Torque response of PID (red) and FLC (blue)

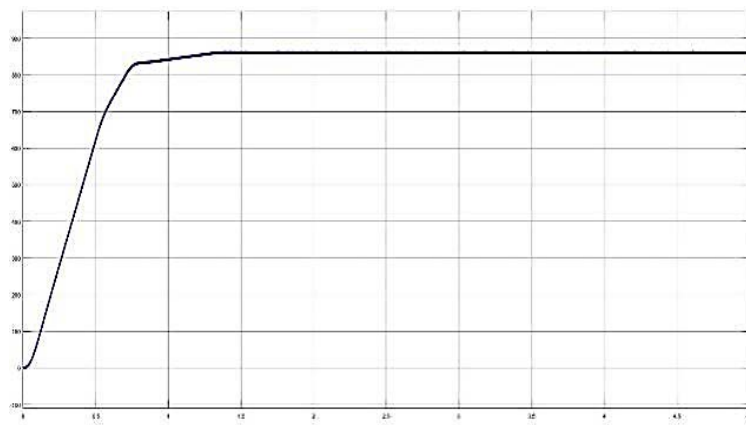


Figure.9 Rotor speed when N_{ref} is 859 rpm by using FOPID controller

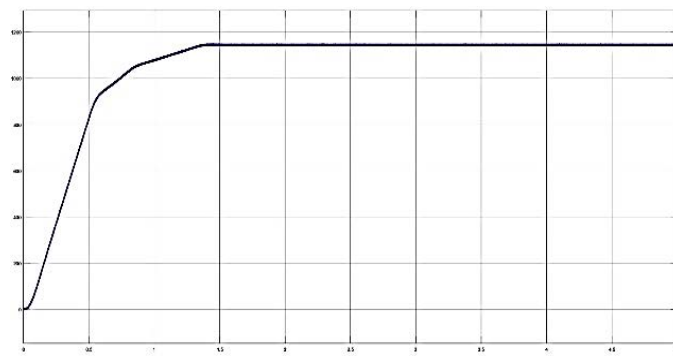


Figure.10 Rotor speed when N_{ref} is 1145 rpm by using FOPID controller

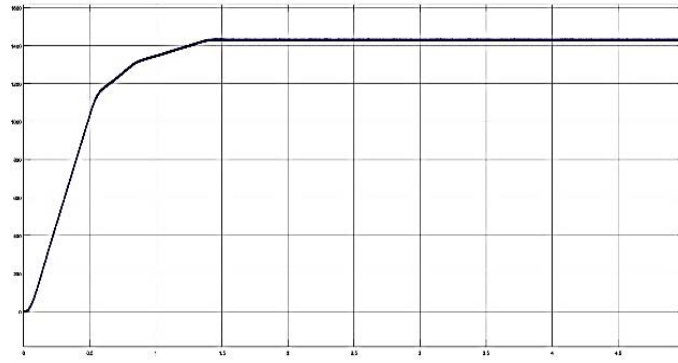


Figure.11 Rotor speed when N_{ref} is 1432 rpm by using FOPID controller

5. CONCLUSION

By employing FOPID at the beginning of the charging process, more energy may be conserved. When an error is detected, the FOPID controller acts swiftly to construct an equal controller term for use outside of the FOPID controller loop. A 50-horsepower electric car was simulated in this experiment. It's being studied if peak overshoot and steady-state inaccuracy may be used as indications. Researchers' findings reveal that despite the decreased amplitude, the suggested system's phase current has more loss components (less overall amplitude). In the steady condition, the average loss amplitudes of real torque diminish. Maintaining a constant torque optimizes performance. The suggested FOPID controller system outperformed traditional PID controllers and even fuzzier ones in terms of stability and performance.

REFERENCES

1. Sato, E.: 'Permanent magnet synchronous motor drives for hybrid electric vehicles', *IEEJ Trans. Electr. Electron. Eng.*, 2007, 2, (2), pp. 162–168.
2. Agency, I.E.: 'Global EV outlook 2016: beyond one million electric cars' (OECD Publishing).
3. Sayed, K.: 'Zero-voltage soft-switching DC-DC converter-based charger for LV battery in hybrid electric vehicles', *IET Power Electron.*, 2019, 12, (13), pp. 3389–3396.
4. Gomez, J.C., Morcos, M.M.: 'Impact of EV battery chargers on the power quality of distribution systems', *IEEE Power Eng. Rev.*, 2002, 22, (10), pp. 63–63.
5. Rasha Kassem, Khairy Sayed, Ahmed Kassem and Ramadan Mostafa, "Power optimisation scheme of induction motor using FLC for electric vehicle", *E-First on 21st July 2020 IET Electr. Syst. Transp*, vol. 10, no. 3, pp. 301-309, 2020.
6. Adriana Tintelecan, Anca Constantinescu Dobra and Claudia Mari, "LCA Indicators in Electric Vehicles Environmental Impact Assessment", *Icpe solar park Bucuresti Romania*, pp. 3-4, October 2019.
7. Saqib Jamshed Rind, Mohsin Jamil and Anas Amjad, *Electric Motors and Speed Sensorless Control for Electric and Hybrid Electric Vehicles: A Review*, IEEE, 2018.

8. Swagat Pati, Manas Patnaik and Abinash Panda, "Comparative Performance Analysis of Fuzzy PI PD and PID Controllers used in a Scalar Controlled Induction Motor Drive", 2014 International Conference on Circuit Power and Computing Technologies [ICCPCT].
9. Rasha Kassem, Khairy Sayed, Ahmed Kassem and Ramadan Mostafa, "Energy Efficient Control Scheme of Induction Motor Based EV", 21st International Middle East Power Systems Conference (MEPCON).
10. Basil H. Jasim and Adel M. Dakhil, New pi and pid tuning rules using simple analytical procedure.
11. Juan Moreno, Miguel Cipolla, Juan Peracaula and Paulo J. da Costa Branco, Fuzzy logic-based Improvements in Efficiency Optimization of Induction Motor Drives.
12. Ali M. Eltamaly, A. I. Alolah and Basem M. Badr, Fuzzy Controller for Three Phases Induction Motor Drives.
13. S. Patil Mayuri and S. S. Dhamal, "A Detailed Motor Selection for Electric Vehicle Traction System", IEEE Xplore Part Number: CFP19OSV-ART.
14. Zonggen Yi and Peter H. Bauer, Sensitivity Analysis of Environmental Factors for Electric Vehicles Energy Consumption, IEEE, 2015.

Design of IoT based real time Geofencing Model for the realization of high security system

Shuvendra Kumar Tripathy¹, Kaliprasanna Swain², Gopinath Palai²

¹Department of EEE, Trident Academy of Technology, Odisha, India.

²Department of EEE, Gandhi Institute for Technological Advancement, Bhubaneswar, Odisha, India

E-mail: shuvendra12478@gmail.com, gpalai28@gmail.com

Abstract

Using LBS (Position Based Service) and GPS (Global Positioning System) location sensors, which allow the information of the Geofencing region to be properly located, security will be maintained by creating virtual boundaries of a certain zone. In this study, an effort is made to keep track of the items' whereabouts and to be able to sound an alert when they leave the Geofence zone. The true position of the object and its final destination, along with the precise borders it entered or left, were revealed by the results. This method can be used in classrooms to set virtual limits for students and in prisons to implement inmate security proposals.

Keywords: Mobile APP, Raspberry Pi 3, Ublox, IoT, virtual boundaries.

1. INTRODUCTION

A technique called geofencing is primarily used to gather data and disseminate information inside a given geographic area. In mobile APPs, geofencing is a form of GPS tracking mechanism. It is a technique that enables the automatic detection and execution of pre-planned activities when a user device is present in a certain Geofenced region. The Google Android Geofencing platform has always been supported by this technology. This technique combines information from the cellular network, GPS, and IP addresses based. GPS is quite precise and can be used in Geofencing to determine the user's location.

2. LITERATURE SURVEY

Geofencing is the cutting-edge technology present ubiquitously in the world. In the organization employs a large number of people, making it impossible to track everyone's attendance using RFID and thumbprint technology. It will require lots of time., for this a geo-fenced mobile application is develop for the company's staff [1] Application Kit that aids people in preventing the spread of

COVID-19 This groundbreaking tool stops the spread of the coronavirus by combining geofencing and machine learning. The second feature is a powerful tracking system that monitors everyone who interacts with the user by using Geofencing technology [2-3].

Ankle trackers powered by Arduino that use a GUI-based application to build geofencing and track people inside of quarantined homes. Within a geofence, a virtual boundary that is circular in shape, the ankle tracker serves as the trigger that is being monitored. With the use of Geofencing-based applications, a user in a smart city can discover the best services or shops nearby by using data from the GPS in his mobile service. [4]. The finest example of a geofencing scenario in a dairy farm is receiving feedback from wearable sensors like heat, drinking, and feeding from the cow. Farmers can simply obtain data about each cow from each place using IoT-based SMS technology, such as position, milk production, health, etc. [5].

Geofencing for a certain region is required to approach close to the target in a precise manner for unmanned aerial vehicles utilizing GIS-based technology to locate objects on the side of the road. where Geofencing for a certain area is required to allow an unmanned vehicle to approach an object in close proximity and precisely [6]. Geofencing can be used to alert the naval officer when a ship approaches a specific underwater catastrophe region or to inform drivers on a highway about the construction of the road's operating condition when they enter that Geofencing-based area in their car [7]. Finding a sea border is a challenging undertaking in the water. Using Geofencing technology, it is feasible to send alerts to fishermen when they cross an offensive border into another country [8]. In the event of child safety, wearable sensors such as temperature and pulse can provide information regarding the child's status as well as location, which can also be tracked by GPS, and alerts can be sent using GSM technology [9].

A virtual barrier, such as Geofencing, can be used to regulate access to public spaces where smoking and drinking are prohibited. These sensors can detect intoxicated individuals and provide alert messages about the location [10]. If the peripheral of jail is trotted with a virtual boundary utilizing Geofencing method, without utilizing CCTV camera modules, then if any inmate tries to cross jail boundary, the jailer will receive an escape alert message [11].

If a vehicle is being tracked, the owner must configure the geofencing graphical region in the mobile app so that, should the vehicle depart from the geofencing physical boundary for whatever reason, the owner will receive an SMS alert [12]. By measuring the precise distances between buildings, trees, and other obstacles, a drone would be provided a safe region in which to move [13].

3. GEOFENCING TECHNIQUES

This method allows for pre-programmed tracking of portable objects entering or leaving a Geofenced area. When distinct mobile devices enter or leave the limit, warnings are generated. The Geofence's shape can either be square or more amorphous, like a complicated polygon. At actuality, the Geofence is shaped like a circle, with the eye point in the centre. Given that it only requires two boundaries—the precise spot and an estimated range—this method is the simplest way to implement geofencing. The computation determines the distance between the circle's perimeter and centre.

4. METHODOLOGY OF THE PROPOSED SYSTEM

A wearable physical sensor for gathering data from school students will transmit data to the next door and then be transferred to a data base station through the internet. The information is sent from the base station to the cloud, where it is analyzed using a variety of methods and strategies. The Google Map API and the Google Places API are two examples of how the Google API is used with mobile clients. Figures 1 and 2 display the proposed system's block diagram and hardware implementation. There are three modules in the complete framework.

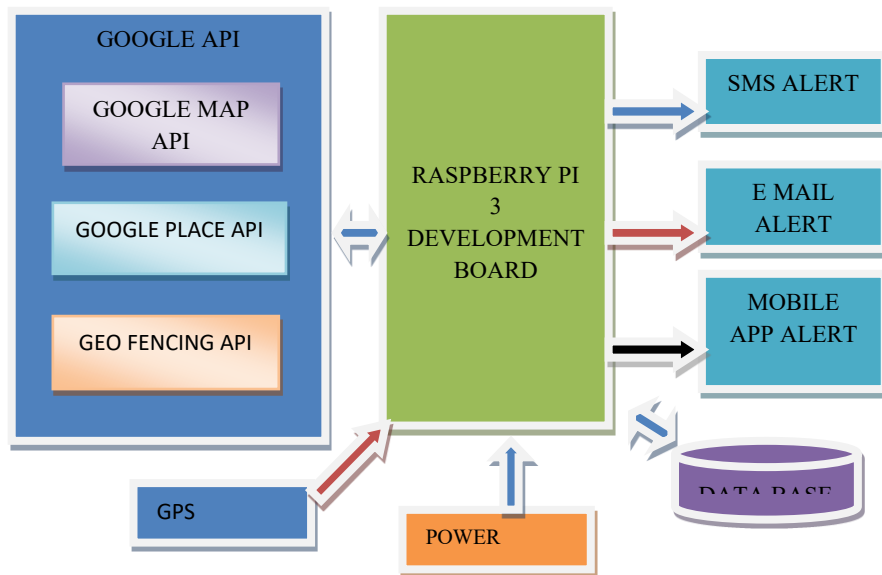


Fig. 1 Block Diagram Geofencing System using IoT

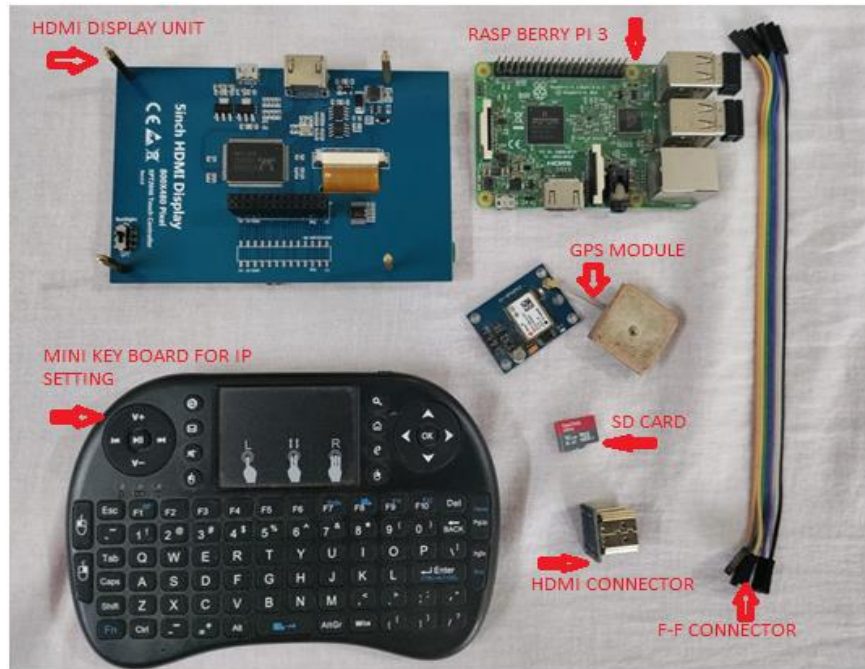


Fig. 2 Hardware Implementation of IoT Based Geo-Fencing System

5. GEOFENCE NODE SETTINGS IN NODE RED

Geofence app must be successfully installed on a phone so that it may operate server-side. It comprises both mobile and laptop operations, such as continuous tracking of when a device enters or exits a geofence, such as a school fence. Node RED collects the data when we leave the location, translates it into human language, and then sends the SMS alert. It will only need to be set up once for every OS-operated device.

Every position reported into mosquito protocol for NodeRED includes a coordinate like longitude and latitude along with the device's tracker id thanks to a Geofence put up on the server side. This process offers pre-programmed inspection of mobile objects travelling through or inside a Geofenced area. The Raspberry Pi, GPS, micro-SD card and U BLOX and make up the module.

The proposed system is being developed using a number of different pieces of software, including NOOBS OS, mobile applications, PHP, the MQTT Protocol, Python language, and Node RED technologies. The flowchart in Figure 3 provides an explanation of the Geofencing system's architecture.

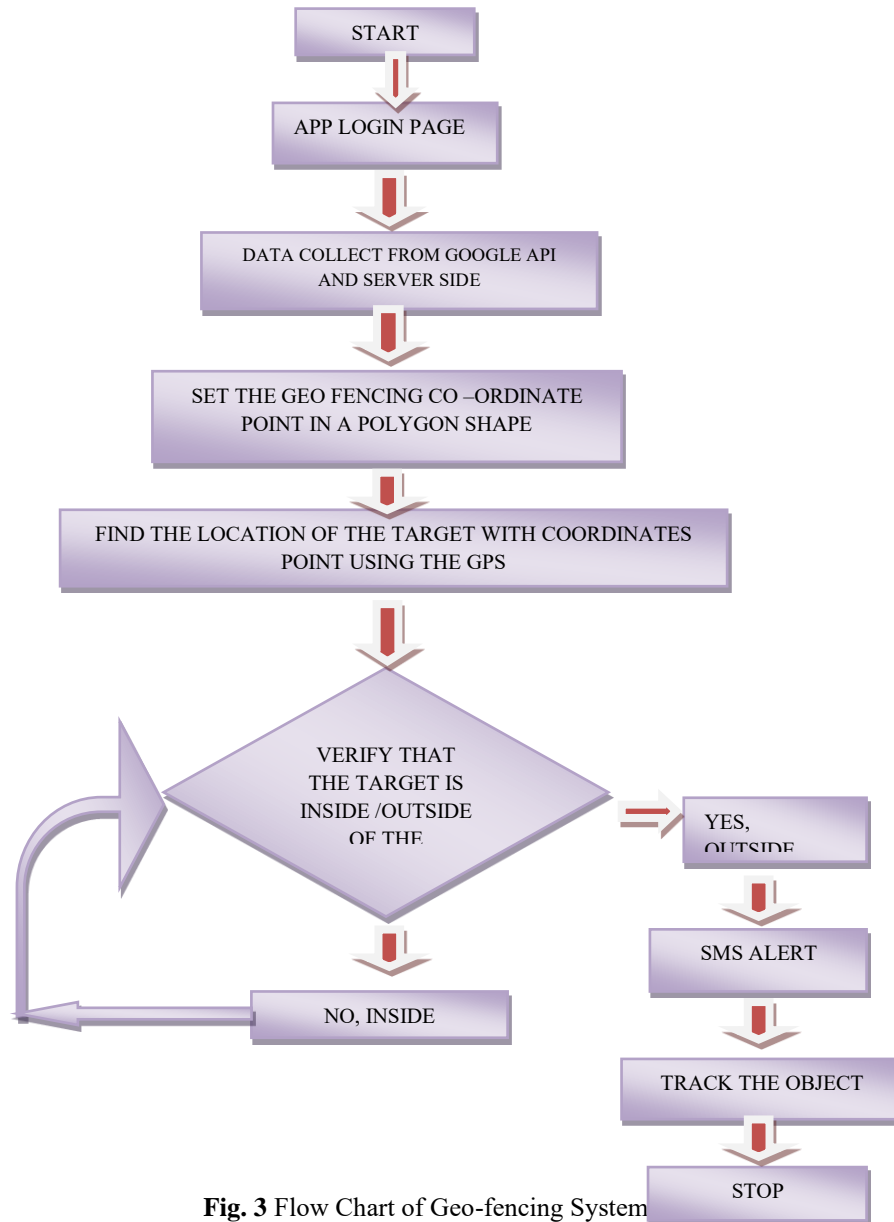


Fig. 3 Flow Chart of Geo-fencing System

6. RESULTS AND DISCUSSION

Any youngster, student, or anybody else can use this concept to check entering or exiting through Geofence borders for security reasons. It can be used in many different places, such as parking lots, jails for criminals, animal habitats, etc. A user can examine and monitor the person by connecting the IP address

192.168.201.34 with the port number 1880 in the Geofencing track in system. By supplying the specific latitude and longitude of that Geofencing position, which are given in IP (192.168.201.34), based on a user's Geofencing tracking in the Google Map VNC viewer, they can also receive a message alert if that person is beyond the virtual Geofence the user has set up.

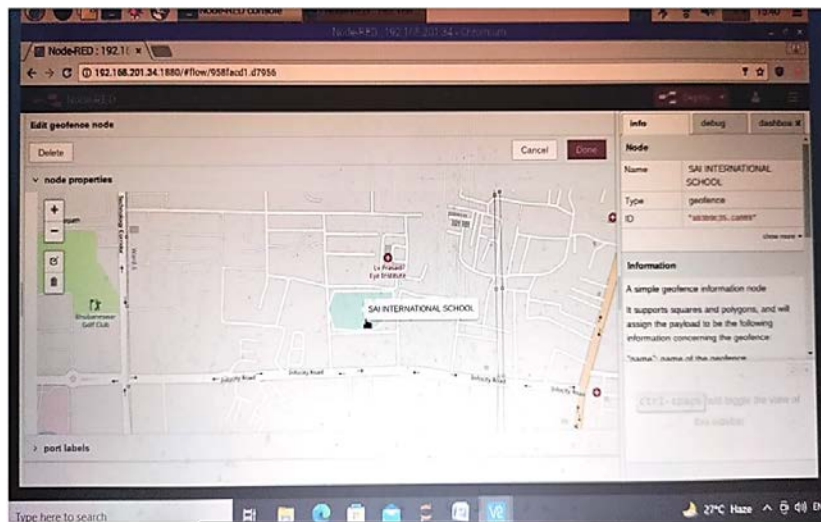


Fig. 4 The user using the remote sharing viewer in Google Maps displayed a geofencing map around a SAI INTERNATIONAL SCHOOL at IP (192.168.201.34)

7. CONCLUSION

In this paper, an appropriate model is put forth that can be used to control Geofencing at schools. This model demonstrated the best results of maximum security by limiting student movement when they entered or left the virtual boundary area that was created by the user, in this case the user's parents. It can safeguard the criminal screen next to the school.

REFERENCES

1. R. Shinde, A. Nilose and P. Chandankhede, "Design and Development of Geofencing Based Attendance System for Mobile Application," 2022 10th International Conference on Emerging Trends in Engineering and Technology - Signal and Information Processing (ICETET-SIP-22), 2022, pp. 1-6.
2. D. Koshti, S. Kamoji, K. Cheruthurthy, S. P. Shahi and M. Mishra, "A Detection, Tracking and Alerting System for Covid-19 using Geo-Fencing and Machine Learning," 2021 5th International Conference on Intelligent Computing and Control Systems (ICICCS), 2021, pp. 1499-1506.

3. J. C. Dela Cruz, A. H. Ballado, C. V. P. Constantino and K. I. B. Lee, "Implementation of Geofencing for Monitoring People under Home Quarantine," 2021 5th International Conference on Electrical, Telecommunication and Computer Engineering (ELTICOM), 2021, pp. 78-83.
4. Emil R. Kaburuan, Alkaton Sutikno, Elko Priatama, Nilo Legowo. (2020). Application of Location-Based Service and Geofencing in Event Request. *International Journal of Advanced Science and Technology*, 29(04), 3930-3937.
5. Muhammad Osama Akbar, Muhammad Saad Shahbaz khan, Muhammad Jamshaid Ali, Azfar Hussain, Ghazia Qaiser, Maruf Pasha, Urooj Pasha, Malik Saad Missen, and Nadeem Akhtar, "IoT for Development of Smart Dairy Farming", *Journal of Food Quality, Hindawi, Volume 2020*, pages 8.
6. M. Maiouak and T. Taleb, "Dynamic Maps for Automated Driving and UAV Geofencing," in *IEEE Wireless Communications*, vol. 26, no. 4, pp. 54-59, August 2019.
7. Anish Deshpande, Abhishek Shingte, Ashutosh Dwivedi "GEOFENCING FOR DISASTER MANAGEMENT SYSTEM", *International Journal of Emerging Technologies and Innovative Research*, Vol.6, Issue 5, page no.21-24, May 2019.
8. M.B. Mukesh Krishnan, D. Saveetha, A. Arokiaraj Jovith, P. Rajasekar, "Fisherman Navigation and Safety System", *International Journal of Innovative Technology and Exploring Engineering*, Volume-8 Issue-12, October 2019.
9. N. Senthamilarasi, N. Divya Bharathi, D. Ezhilarasi and R.B. Sangavi, "Child Safety Monitoring System Based on IoT", *Journal of Physics: Conference Series*, Volume 1362, International Conference on Physics and Photonics Processes in Nano Sciences 20–22 June 2019, Eluru, India.
10. Wray TB, Pérez AE, Celio MA, Carr DJ, Adia AC, Monti PM. Exploring the Use of Smartphone Geofencing to Study Characteristics of Alcohol Drinking Locations in High-Risk Gay and Bisexual Men. *Alcohol Clin Exp Res*. 2019 May;43(5):900-906.
11. J. Cynthia, C. Bharathi Priya, Nageswara Guptha M, "IoT based Prisoner Escape Alert and Prevention system", *International Journal of Pure and Applied Mathematics*, Volume 120 No. 6 2018, 11543-11554.
12. D. Suganthi, S. Paul Raj John, Shamil J.S, Dhruva G. Patel, "Vehicle Tracking with Geo Fencing on Android Platform", *International Journal of Engineering Science and Computing*, April 2018, 16992 – 16995.
13. Dasu, Tamraparni Kanza, Yaron Srivastava, Divesh. (2018). Geofences in the Sky: Herding Drones with Blockchains and 5G. 26th ACM SIGSPATIAL International Conference on Advances in Geographic Information Systems (ACM SIGSPATIAL 2018), At Seattle, WA, USA.

Design and study of a double – boost non-isolated converter with continuous input current

¹A. Gopalakrushna, ²G. Priyanka

^{1,2}Department of EEE, Vignana Bharathi Institute of Technology, Hyderabad, India
Email: agopalakrushna@gmail.com, gpriyanka4598@gmail.com

Abstract

Environmental pollution is becoming worse, and the energy issue is getting worse. New electric vehicles (NEVs), on the other hand, are drawing steadily greater attention. DC – DC converters are therefore necessary in electric vehicle applications to obtain high voltage gain and improved power regulation. Therefore, investigation on high voltage gain DC – DC configurations is quite crucial. The study on double-boost DC – DC configuration with continuous input current and high gain is proposed in this project. The suggested converter also enhances efficiency while resolving switching stress and output voltage ripple issues. With fewer parts, a straightforward design, and the aforementioned benefits, the double boost converter will be a serious rival to existing high gain converters. Utilizing the MATLAB/SIMULINK software, a simulation design was created to demonstrate the viability of the suggested converter. To demonstrate the performance's robustness and functioning capacity, it is also evaluated under various duty ratios.

Keywords. Double-boost, continuous input current, non-isolated, dc – dc configuration.

1. INTRODUCTION

New energy vehicles, sometimes referred to as NEVs, are garnering an increasing amount of interest as ecological contamination and the energy emergency continue to worsen. Ultra-gain DC-DC topologies may be split into several separate categories, each of which is defined by the topologies that they utilize and the applications that they are meant to fulfil. Ultra-gain DC-DC topologies can be found in a variety of different applications. Depending on whether or not a transformer is used in the design, they can either be nonisolated DC-DC configurations or isolated DC-DC configurations [1]. These converters fall into one of two categories. A nonisolated DC-DC converter provides a number of benefits, some of which include a high-power density, an uncomplicated design, and an easy-to-understand and straightforward control. Because of the transformer, the isolated converter suffers

from a variety of drawbacks, the most significant of which are its substantial bulk, its small power density, and its straightforward magnetic flux saturation. Because of these drawbacks, the implementation of isolated structures in electric vehicle (EV) applications can be restricted. So, nonisolated DC-DC configurations are recommended for the overhead applications to get the most power density and efficiency [2].

The vast majority of hybrid topologies in research on the topology of nonisolated DC-DC configurations use expansions of fundamental chopper circuits. These topologies are used because they are the most efficient. Cascaded topologies, topologies that are based on Z-source & quasi-Z-source, switched capacitor and switched inductor configurations are some examples of these types of topologies. There is a DC-DC converter with a high voltage gain that was derived from a Zeta converter. Even though there is only one primary switch in the design, utilizing a switching mode that has a low resistance can assist in decreasing switching loss in addition to voltage stress. This is because low resistance allows for a smoother transition between states. In [3], high voltage gain, a non-coupled inductor, SEPIC-based DC-DC converter was demonstrated to the audience. This converter eliminates the need for an extra clamping circuit and reduces the amount of conductive loss that occurs as a result of its utilization of a switch that possesses lower levels of conductive resistance. This converter has several benefits, some of which include an output voltage that is in-phase, high efficiency, a high voltage gain, a stable input current, and reduced voltage stress. Other advantages include the same. A DC - DC converter with a large voltage gain is described. This converter combines the most useful aspects of a cuk converter and a secondary boost into a single piece of equipment for your convenience. This converter needs just one switch in order to accomplish the goals of having a high step-up ratio, having streamlined control, and having common ground on both the input and output sides.

In the research described in reference number [4], a voltage multiplier converter was developed that made use of switched capacitors. This specific boost converter has a boost ratio that is twice as high as that of regular boost topologies, yet the voltage stress that it exerts on capacitors and diodes is only half as severe as the stress that is caused by the typical boost converters. Another issue is that there is a mismatch between the data that is being input and the data that is being produced. Cascade design may be utilized in a variety of applications, including fuel cells. The first stage of this design is made up of two boost converters that are staggered in different directions. The second step of this architecture is a three-level boost converter. Both the interleaved structure and the three-level design have the potential to lessen the ripple in the input current. However, only the three-level architecture can minimize switching loss and increase converter efficiency. It is feasible to enjoy both of these benefits at the same time. This is despite the fact that the voltage gain has not changed. An input that is made up of four parallel

connections between inductors is included in a DC/DC converter that has four phases that interleave with each other. This helps to smooth out the waveforms. As a consequence, the total value of the ripple effect is diminished. Particle swarm optimization is an example of an optimization strategy. The system is optimized by the use of a particle swarm with this method. The results of the studies show that the suggested method of control is better in terms of both how well it works and how well it can be tracked and changed [5].

Particle swarm optimization and artificial physical optimization are used in the research work to achieve the goals of vector decoupling and parameter tweaking in the context of an electric car charging system. These goals were successfully attained. Validation of a system that uses tools that include hardware in the loop can be accomplished by using a boost converter that is of the standard bidirectional kind. The results of the experiment back up the idea that the suggested method is both reliable and effective. This strategy is proposed as a possible solution. The objective of this strategy is to modify the electric grid in such a way that it makes use of alternative and renewable forms of energy in order to facilitate the rapid recharging of electric cars. In the publication [6], the authors recommend the use of an endless series input boost converter that possesses a high fault tolerance for scenarios that involve vehicle-to-aid communication. The outcomes of a series of experiments that compared the performance. The results of this study were achieved through a process of experimental comparison.

In conclusion, hybrid topologies are formed by employing fundamental DC-DC converters, which are then paired with switched inductors or switched capacitors [7,8]. In addition, hybrid topologies can also use switched resistors. Although this may combine the benefits of numerous distinct topologies, the negatives of each of the various topologies that it combines are still very important. This is the case even though Z-source converters have the potential to significantly increase the voltage gain. This paper is organised into four sections, Section II describes about the propose converter circuit configuration and its analysis in the CCM mode. In Section III the simulation block diagram and results are given a detailed discussion is done. Finally, conclusions are made in section IV.

2. DOUBLE-BOOST CONFIGURATION

Figure 1 depicts the proposed double-boost configuration. The configuration is comprised of 3 diodes D1, D2, & D3, 2 power switches Q1 & Q2, 2 inductors L1 & L2, and a capacitor that acts as an output filter. Q1 & Q2 are the power switches. If the inductors L1 & L2 are the identical, then the enduring diodes and MOSFET switches will have the same characteristics. Figures 2 and 3 illustrate the two distinct ways in which the converter can perform its job.

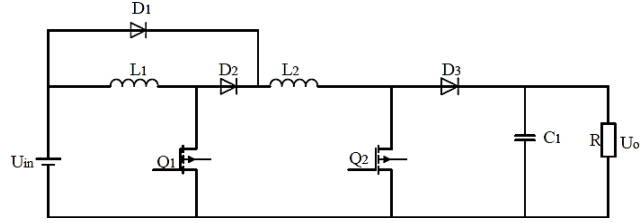


Figure 1. Double-boost circuit configuration

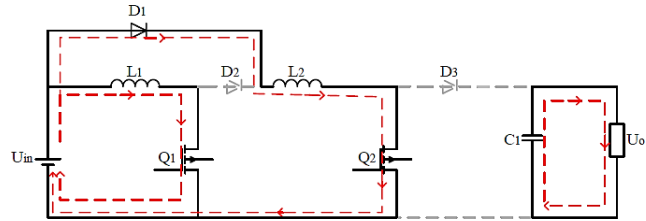


Figure 2 Switch ON equivalent circuit

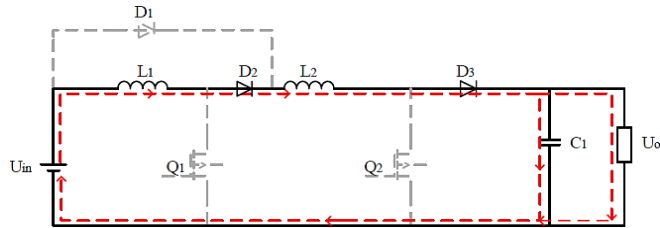


Figure 3. Switch OFF equivalent circuit

In the ON period, the power supply charges the inductors L1 and L2, and the inductors charges the energy; the C1 capacitor transfers the energy to the resistance. Indicating that the converter is in the ON state is the simultaneous activation of switches Q1 and Q2. Figure 2 depicts the operating mode that will be utilized by the proposed converter. During this time, the diode D1 is active while the diodes D2 and D3 are active with the voltage in the opposite direction. The first loop is produced when the input power U_{in} begins to charge the inductor L1, which does so by way of the switch Q1. The input power U_{in} is responsible for charging the inductor L2 via the switch Q2. The load gets power from the output capacitor C1. The equation (1) below demonstrates the amount of energy.

$$W_L = U_{in} I_L D T_s \quad (1)$$

In this equation, W_L stands for the amount of energy that is taken in by the inductor during the time that the switch is turned on. In the OFF state of the analogous circuit, when both switches Q1 and Q2 are closed, energy from the input power supply flows via L1 and L2 inductors and charges capacitor C1. Figure 3 displays the converter's active mode. In this mode, the reverse voltage causes diodes

D2 and D3 to switch off, while it causes diode D1 to turn on. The input energy supply U_{in} & the L1 and L2 inductors are joined in series with one another in order to give power to the resistance plus charges the filter capacitor C1. The amount of energy may be seen in equation 2.

$$W'_L = \left(\frac{U_o - U_{in}}{2} \right) \times I_L \times (1 - D) \times T_S \quad (2)$$

where W_L' is the amount of energy that is created by the inductor during the time that the switch is turned off and $1-D$ is the amount of time that the switch is turned on. The law of energy conservation may be used to derive the below equation, which can be constructed as Equation based on the rule (3).

$$W_L = W_L' \quad (3)$$

In accordance with Equations (1) through (3), the voltage conversion ratio $G(D)$ of the given topology may be calculated in Equation (4).

$$G_D = \frac{1 + D}{1 - D} \quad (4)$$

3. SIMULATION RESULTS

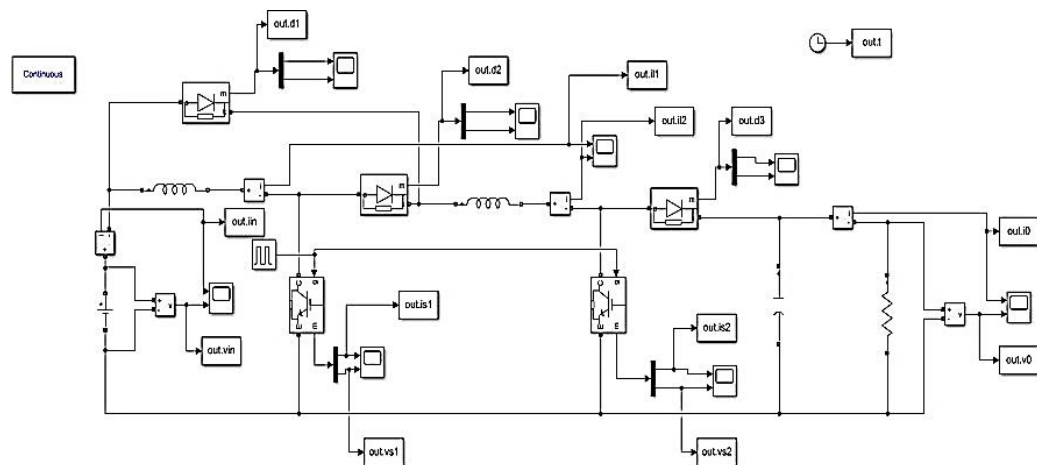


Figure 4. Simulation model of Double Boost DC-DC Configuration

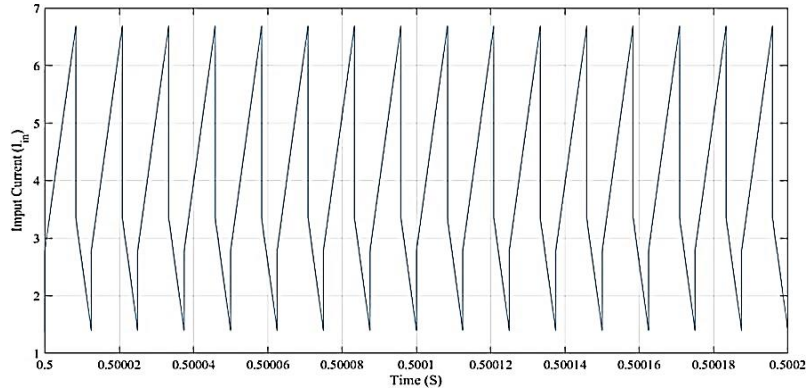


Figure 5. Simulation waveform of input current

A simulation platform, depicted in Fig. 4, was developed to validate its performance. The projected converter is designed for an output power of 200W, with an output voltage of 250V. With the input voltage of 50V, the required output can be produced at a duty ratio of 66.67%. The load is calculated as 312.5Ω . For the simulation 80 kHz frequency is considered. The waveform shown in the fig 5 represents the change in input with respect to time. As the input current is continuous with an allowable ripple. Figure 6 represents the input DC voltage waveform plotted using MATLAB simulation. A 50V DC input voltage is considered as the input to design the proposed converter which can be observed in fig. 6. The output power and voltage are considered randomly for the design.

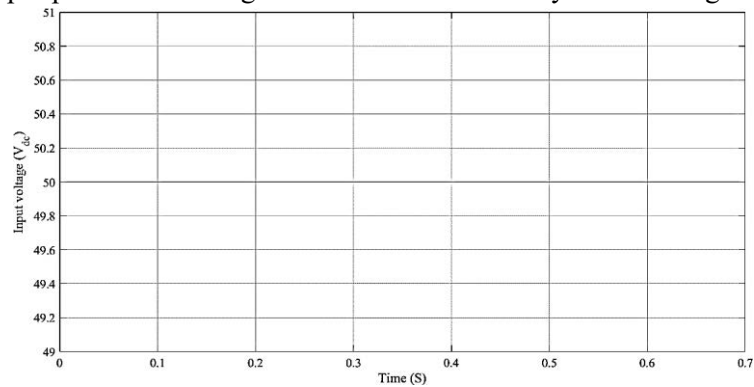


Figure 6. Simulated waveform of input voltage

The simulated output waveforms are shown in the figs. 7 & 8 of the proposed integrated converter. For a 200 W power, the integrated converter is designed with an output voltage of 250V. A load of 312.5Ω resistance is used at the output and hence the DC output current can be given as 0.8A theoretically.

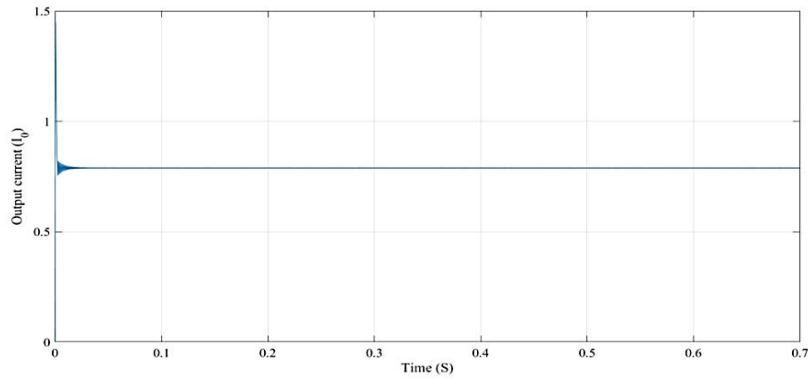


Figure 7. Simulation waveform of output current

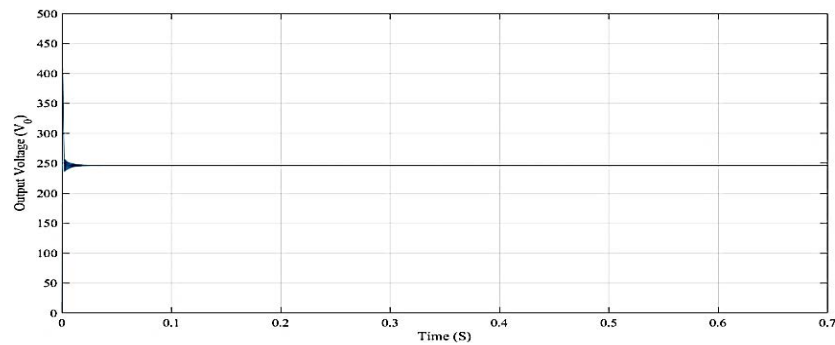


Figure 8. Simulation waveform of output voltage

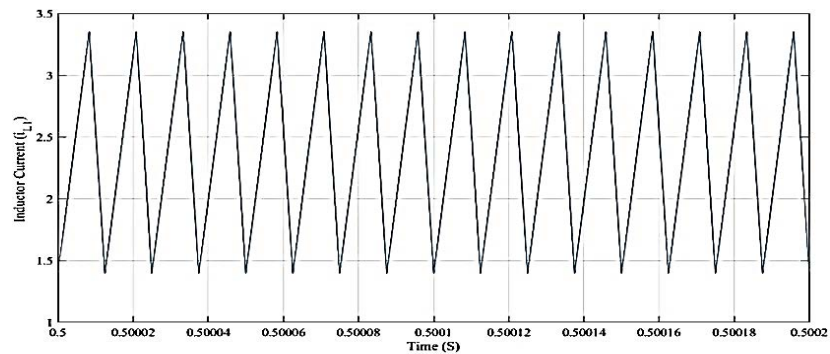


Figure 9. Simulation waveform of inductor current I_{L1} .

Figure 7 shows the simulated output current waveform with negligible ripple. The simulated value is approximately 0.75A and is much closed to the computed theoretical value. Figure 8 represents the simulated DC output voltage waveform with very low ripple (<0.5% approximately). The simulated value is

approximately 247V and is much closed to the computed theoretical value. Figures 9 & 10 shows the simulated inductor current waveforms i_{L1} & i_{L2} respectively (for 16 cycles). From fig. 9 it can be noted that the inductor L_1 peak to peak ripple approximately 2A. This value is exactly matches to the theoretical consideration of inductor L_1 design. From fig. 10 it can be noted that the inductor L_2 peak to peak ripple approximately 2A. This value is exactly matches to the theoretical consideration of inductor L_2 design. For various duty ratios the proposed converter shows better performances with an efficiency greater than 90.

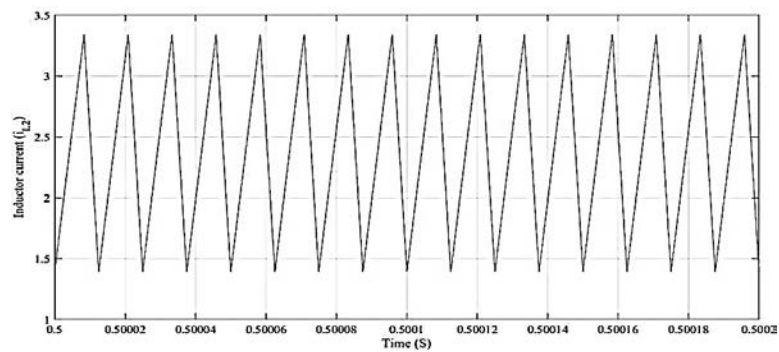


Figure 10. Simulation waveform of inductor current I_{L2}

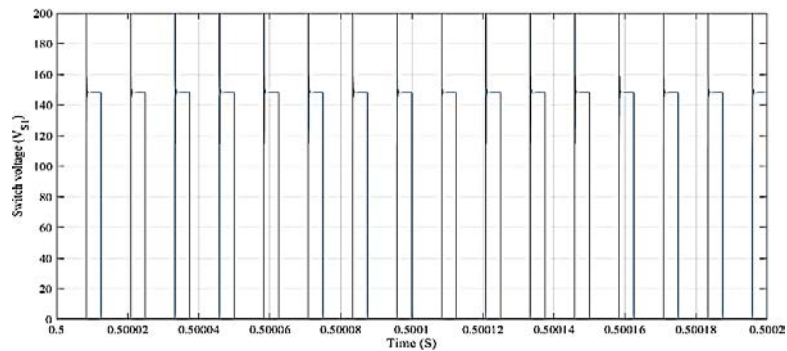


Figure 11. Plot of Switch voltage V_{s1}

The simulation waveform of switch voltage V_{s1} is shown in fig. 11, during the time interval of 0.5002s. The waveform shows the switch voltage at 150V, with respect to time. The simulation waveform of switch current I_{s1} is shown in fig 4.12, during the time interval of 0.5002s. The waveform shows the switch current at 3.4 amps with respect to time.

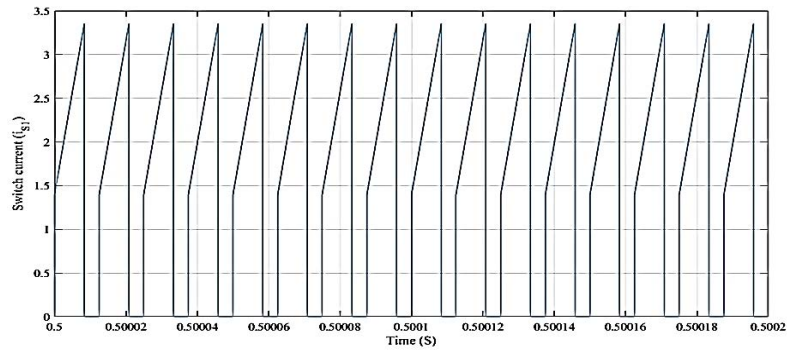


Figure 12. Plot of Switch current I_{s1}

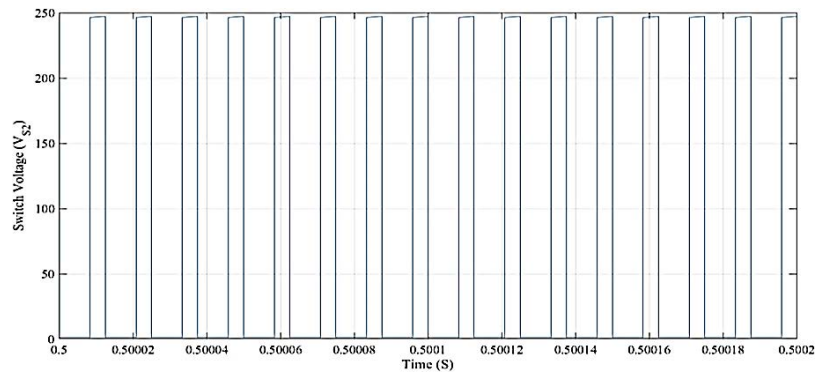


Figure 13. Plot of Switch voltage V_{s2}

The simulation waveform of switch voltage V_{s2} is shown in fig.13, during the time interval of 0.50002s. The waveform shows the switch voltage at 245V, with respect to the time. The simulation waveform of switch current I_{s2} is shown in fig.14, during the time interval of 0.50002s. The waveform shows the switch current at 3.3 amps with respect to the time.

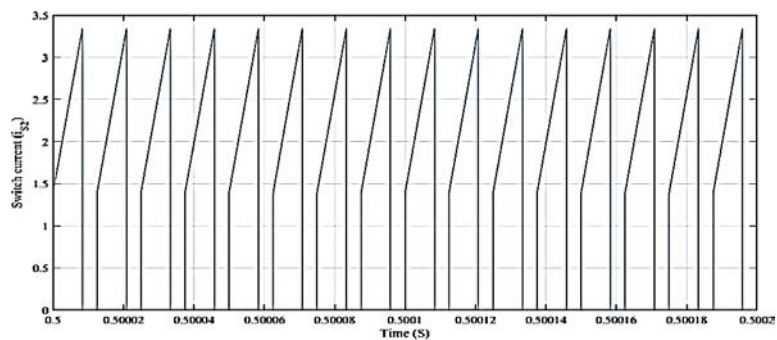


Figure 14. Plot of Switch current I_{s2}

4. CONCLUSION

From an investigation into the working principle of the proposed converter, as well as its modelling, the results of proposed DC-DC converters, which are frequently utilized in electric vehicles, one can derive the following conclusions:

1. When compared to standard boost configurations the converter that was presented offers a number of advantages, particularly in terms of the voltage gain, the device stress, and the number of components.
2. It may quicken the return of the output voltage to stability when there is a sudden change in the load and the input voltage.
3. Under a wide range of conditions, the double converter that was recommended provides glaring benefits in terms of both the real voltage conversion ratio and the efficiency of the system.
4. In addition, in contrast to the usual boost configuration, the double-boost network that was suggested has a lower ripple in output voltage.

REFERENCES

1. Ali, A.; Hossein, A.; Amir, F. A novel high step-up DC/DC converter based on integrating coupled inductor and switched-capacitor techniques for renewable energy applications. *IEEE Trans. Power Electron.* 30, 4255–4263, 2015.
2. Nagi reddy. B, Sahithi Priya. Kosika, Manish patel. Gadam, jagadhishwar. Banoth, Ashok. Banoth, Srikanth goud. B, “Analysis of positive output buck-boost topology with extended conversion ratio”, *Journal of Energy Systems*, 6(1), pp. 62–83, 2022.
3. Arab, A.S, Shokrollahi, M.J. A novel high voltage gain noncoupled inductor SEPIC converter, *IEEE Trans. Ind Electron*, 66, 7099–7108, 2019
4. Yun, Z.; Lei, Z.; Mark, S.; Ping, W. Single-Switch, Wide Voltage-Gain Range, Boost DC–DC Converter for Fuel Cell Vehicles. *IEEE Trans. Veh. Technol.* 2018, 67, 134–145.
5. Vinnikov, D.; Roasto, I.; Strzelecki, R.; Adamowicz, M. Step-Up DC/DC Converters with Cascaded Quasi-Z-Source Network. *IEEE Trans. Ind. Electron.* 2012, 59, 3727–3736.
6. Rodríguez Licea, M.A. Fault Tolerant Boost Converter with Multiple Serial Inputs and Output Voltage Regulation for Vehicle-to-Aid Services. *Energies*, 13, 1694, 2020.
7. Nagi Reddy, B., Pandian, A., Chandra Sekhar, O., Ramamoorthy, M. “Performance and dynamic analysis of single switch AC-DC buck-boost buck converter” *International Journal of Innovative Technology and Exploring Engineering*, 2019, 8(4), pp. 307–313.
8. Nagi Reddy, B., Chandra Sekhar, O., Ramamoorthy, M. “Analysis and implementation of single-stage buck-boost-buck converter for battery charging applications *Journal of Advanced Research in Dynamical and Control Systems*, 2018, 10(4), pp. 446–457.

Enhancing Smart Farming Techniques by Applying Prediction Techniques through IoT and Machine Learning

Rudraraju Vandana¹, SV Vaishnavi², G. Surya Prabhav³, R. Karthikeyan⁴

^{1,2,3,4}Department of CSE(AI&ML), Vardhaman College of Engineering, Hyderabad, Telangana.

Email: vandanaraju30@gmail.com, svaishnavisunchu@gmail.com, suryaprabhav23122002@gmail.com, karthikeyan231977@gmail.com

Abstract

One of the key drivers of the Indian economy is the agricultural industry. Due to the growing population, there is a constant growth in the demand for food production. This proposed work is a farm management system that uses information and technology to identify and analyse field variability through the use of crop production techniques. In order to simplify farming, machine learning and big data technologies have arisen. The results are obtained using techniques for data mining and data analysis. To increase yield, it is possible to forecast the ideal crop for a certain location and piece of land using IoT and machine learning algorithms. The economy of many developing nations is heavily dependent on agriculture. India still employs traditional agricultural methods despite being one of the world's top producers of diverse foods in large quantities. Farmers struggle to meet the increased expectations for high-quality food production in addition to dealing with the changing weather conditions. In order to produce high-quality crops, farmers actually need to be conscious of the shifting climatic circumstances. Smart agriculture powered by IoT and machine learning would assist farmers with crop and fertiliser suggestions in addition to real-time crop monitoring. This paper's main goal is to propose an Internet of Things (IoT)-based Smart Agriculture system that would give farmers advice based on a variety of variables, including soil type, region, crop kind, and rainfall. The system would also concentrate on recommending fertilisers to farmers based on elements like the soil's amounts of nitrogen, phosphorus, and potassium. The four problem statements covered in this essay are yield prediction, price prediction, soil health, and crop disease. So that it can be analysed and offer us approximative results, the useful information about the region, crop type, rainfall, soil type, etc. is provided.

Keywords. Crop Prediction, Price Prediction, Soil health status, Disease detection, Internet of Things, Machine Learning.

1. INTRODUCTION

Agriculture is already starting to benefit significantly from machine learning (ML), which will increase its effectiveness and efficiency. In order to produce agricultural products more effectively, precision agriculture relies on the collection, processing, and analysis of data. With the aid of cutting-edge technology, data can be gathered on a contemporary farm. Agricultural ML is intended to gather particular data and employ particular algorithms to ascertain

anticipated results. It has the ability to sort through a lot of data.

The Internet of Things (IoT) is utilized in smart farming to monitor the fields. It is employed for agricultural monitoring, climate condition monitoring, and other purposes. It helps in data collection. It raises standards while lowering dangers. Farmers can access current weather information, which aids in decision-making.

It requires manual monitoring.

- Insufficient production.
- Diseases of the crop may spread easily.
- The life of top soil is killed.
- Cannot predict the yield at all.
- Weather conditions cannot be predicted.

According to Gartner, Inc., there will be 4.9 billion linked items used in 2015, an increase of 30% over 2014, and there will be 25 billion used between now and 2020. The Internet of Things (IoT) has become a powerful driver for enterprise change in all sectors of the economy and society.

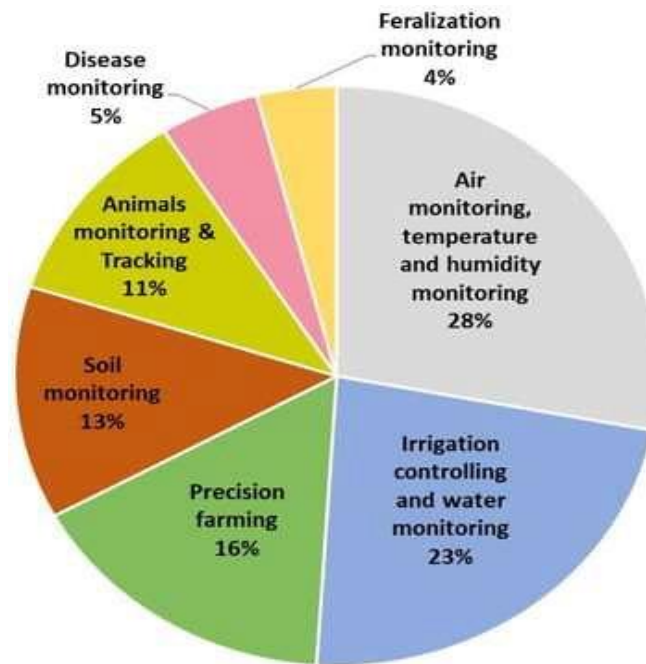


Fig.1 Issues of Traditional Systems in Agriculture [4]

Four problem statements from our project are addressed by the suggested work. As follows:

1) Yield prediction:

Before harvesting, a job called yield prediction is carried out to estimate the yield that will be obtained. It takes a long time to complete. By using information on rainfall, crop type, geography, soil type, etc., our website makes it simpler to anticipate this yield. Using the Random Forest method, it analyses and forecasts the result.

2) Price Prediction:

Before deciding whether to farm a certain crop kind, an evaluation of the price is made. The price that farmers will eventually be paid for their crop is unknown. By analysing historical data, our website provides assistance with this price projection.

3) Prediction of Soil Health:

Knowing which crop to plant depends greatly on the health of the soil and the amount of nutrients present in it. Poor soil health has negative consequences on the crop. Our website provides the crop's N, P, and K values, making it much simpler to anticipate the soil's health. Farmers can choose which crop to cultivate based on those N-P-k levels.

4) Disease Detection

The greatest threat to the crop is crop diseases. It is exceedingly challenging to detect these disorders early. The development of these illnesses threatens to have severe effects on farmers who rely on these robust crops. Simply by categorizing photographs of the leaves of a certain crop, our website aids in the diagnosis of the illness and the provision of a remedy.

2. RELATED WORK

Numerous initiatives have been taken to stop crop loss brought on by illnesses. Integrated pest management (IPM) strategies have replaced historical methods of applying insecticides widely over the past ten years [2] (Ehler, 2006). Whatever the method, the first step in effective illness management is accurate disease identification when it first manifests. The computer power, high-resolution displays, and broad built-in accessory sets of smartphones in particular, including their high-definition HD cameras, provide very innovative techniques to assisting in the identification of diseases. By 2020, it is predicted that there will be between 5 and 6 billion smartphones worldwide. Mobile broadband penetration reached 47% in 2015, a 12-fold growth from 2007, and by the end of that year, 69 percent of the world's population had access to it [3] (ITU, 2015). When HD cameras, high-performance CPUs, and widespread smartphone use are coupled, it creates a situation where, if technically possible, disease diagnosis based on automatic picture identification can be made available on a never-before-seen scale. Here, we use 54,306 photos of 14 crop species with 26 illnesses (or healthy) made publicly available by the Plant Village project to show the technical viability of a deep learning strategy [4] (Hughes and Salath, 2015).

The proposed work, which we found in the previous research papers is that everyone uses climatic factors like rainfall, sunlight and agricultural factors like soil type, nutrients possessed by the soil [5] (Nitrogen, Potassium, etc.) but the problem is we need to gather the data and then a third party does this prediction and then it is explained to the farmer and this takes a lot of effort for the farmer and he doesn't understand the science behind these factors. To make it simple and

which can be directly used by the farmer this paper uses simple factors like which state and district is the farmer from, which crop and in what season [6-7] (as in Kharif, Rabi, etc.). In India, there are more than a hundred crops planted around the whole country. These crops are categorized for better understanding and visualization. The data for this research has been acquired from the Indian Government Repository [1]. The data consists of attributes – State, District, Crop, Season, Year, Area and Production with around 2.5 Lakh observations.

3. NOVEL MACHINE LEARNING BASED PREDICTION TECHNIQUE FOR SMART FARMING

In this paper, proposed method is about designing a website for making farming much better and effective. It deals with the 4 problem statements i.e., yield prediction, price prediction, soil health status and disease detection. The inputs are given to the website. The website classifies the data and gives the output with the help of Machine Learning algorithms Random Forest and Support Vector Machine it is shown in the figure2. Crop yield is the quantity of agricultural production harvested from a given area of land. Usually used for grains and cereals, the measurement is expressed in tones or pounds per acre. Amount of harvest per area is a measurement used by agricultural producers. On the basis of the crop's collected weight, the extrapolation for the entire farm is subsequently completed. Start-ups, governmental organizations, and academic institutions are leveraging Landsat and satellite imagery for data-driven decision-making since crop production prediction is a key use case in spatial data science. Predictive algorithms are developed with the aid of satellite picture data.

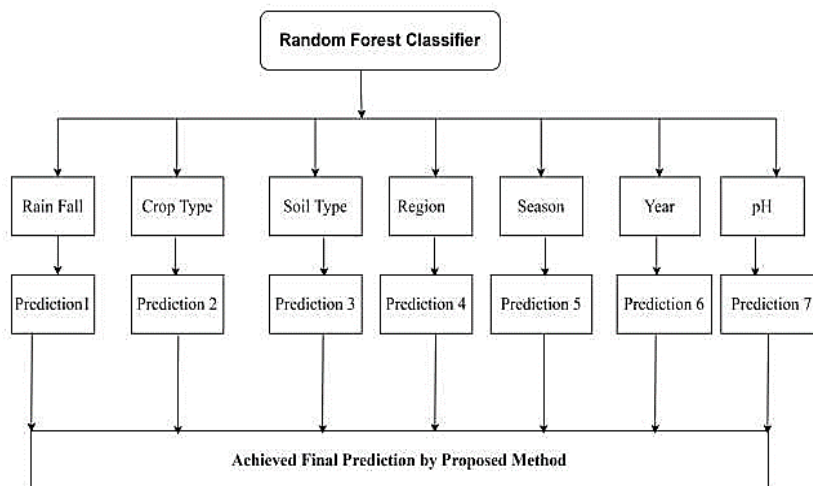


Fig.2 Architecture for different prediction

Prediction of Crop Yield Using AI and ML

Some of the reasons for the decreased rate of agricultural production include the climate and its unpredictability. Thus, accurate weather forecasting is crucial for better crop management. Other sectors that are connected to agriculture include

the sugar industry, which is dependent on sugarcane farmers.

Therefore, agricultural production prediction using machine learning or AI also aids them in organising their business' logistics. As a result, there are many ways that AI and related IoT devices are used in agriculture.

Let's examine the advantages of crop yield prediction using AI/ML.

- Crop monitoring for better production
- Resource and field mapping
- Remote monitoring of farm regions and
- Predictive analytics for data-driven decision-making

Weather predictions

When it comes to forecasting crop yields, there are many different factors. Studying weather information, satellite images, soil conditions, and potential pest attacks are a few of these. These factors come together to provide a comprehensive picture of the ideal window of time for crop production. To deal with any unforeseen issues, there are additional what-if scenarios and alternate action plans.

Therefore, crop output forecasting is crucial to the global food production system. Making informed decisions is made feasible with greater data at hand. The information on crop yield forecast is also helpful to government organizations so they can plan for the security of the nation's food supply.

- **Yield prediction:** We give inputs of crop, state, season, year, area and rainfall. It predicts the yield in Quintal.
- **Price prediction:** We give the inputs of state, crop and year. It predicts the price.
- **Soil Health prediction:** Inputs of crop, temperature, humidity, rainfall and pH are given. It gives optimal N- P-K values of the soil.
- **Disease detection:** We give the images of the leaves. It detects the disease and gives the cure.

Prediction of Soil Health

The basic goal of soil management in farming is to increase crop productivity by enhancing and maintaining dynamic soil characteristics. Particularly in emerging nations like India, population pressure, land constraints, and the deterioration of traditional soil management techniques have resulted in a decline in soil fertility. Crop health is a crucial element in the high productivity agricultural methods used today.

Crop Disease Prediction

Plant disease is characterised as a condition of localised or systemic aberrant physiological functioning of a plant as a result of ongoing, protracted "irritation" brought on by organisms (infectious or biotic disease agents). Insects and parasitic plants, as well as harmful organisms like fungi, bacteria, viruses, and protozoa, are the principal causes of infectious plant illnesses.

4. CONCLUSION AND FUTURE ENHANCEMENTS

One of the key industries in our nation's economic development is the agricultural industry. The issues with traditional farming techniques are eliminated by this strategy, which also improves and simplifies farming. The suggested approach uses ML techniques to enhance crop planning decisions utilising IoT and ML algorithms based on various metrics. Utilizing it is pretty simple. It gathers the data, examines it, and makes predictions. The farmers can make better decisions thanks to this system. It provides the output promptly. It lessens the issue of manual and ongoing farm monitoring. Farmers can greatly benefit from it by boosting their output, effectiveness, and crop quality.

The future of urban farming must take into account a variety of elements, including the changing climate, natural disasters, community resilience, and socioeconomic aspects of farming, in addition to the projected trend of declining agricultural supplies. An indoor vertically scalable climate-controlled structure that integrates renewable energy, biodiversity, and resource management could be the face of farming in the future. This structure would also eliminate waste by turning waste into resources in a circular economy.

REFERENCES

- [1] International Telecommunication Union (ITU), report on Climate Change, Oct. 2008.
- [2] G. Koutitas, P. Demestichas, 'A review of energy efficiency in telecommunication networks', Proc. In Telecomm. Forum (TELFOR), pp. 1-4, Serbia, Nov., 2009.
- [3] Gartner Report, Financial Times, 2007.
- [4] I. Cerutti, L. Valcarenghi, P. Castoldi, 'Designing power-efficient WDM ring networks', ICST Int. Conf. on Networks for Grid Applications., Athens, 2009.
- [5] W. Vereecken, et. al., 'Energy Efficiency in thin client solutions', ICST Int. Conf. on Networks for Grid Applications., Athens, 2009.
- [6] J. Haas, T. Pierce, E. Schutter, 'Data center design guide', whitepaper, the greengrid, 2009.
- [7] Intel, 'Turning challenges into opportunities in the data center', White Paper,

IOT BASED RENEWABLE ENERGY MONITORING SYSTEM

¹Yarava Venkata Suresh, ²Hari Shankar Jain

^{1,2}Department of EEE, Vardhaman College of Engineering, Hyderabad, India
Email: sureshyarava340@gmail.com, jhshankar@gmail.com

Abstract

Due to the increasing dependence on renewable energy and related systems it is important to closely monitor and identify the governing parameters for efficiency with respect to environmental circumstances (temperature, irradiation. etc.). To maximise energy production, it is crucial to conduct in-depth analysis with an emphasis on the properties of photovoltaic devices. In-order to obtain the parameters like Power, Energy and Efficiency basic parameters are required such as voltage, current and system specific (inverters and converters) parameters like losses and efficiency. Manually, using analog measuring devices to measure voltage and current calculating and making a note of it and plotting a graph is an arduous and time-consuming task. So, to overcome this trying to develop an IOT enabled device which does all the above-mentioned work and makes the work easier permits monitoring the performance characteristics on mobile application with no extra work to be done by us. Using this device and inbuilt algorithms can introduce and keep a track of other related parameters like; power output, charge conditions, used power, temperature, irradiation, wind speed variation etc. The results can be readily printed using blue tooth from mobile/ transferred to other mediums. This whole process of sending the data after processing takes place on internet, thus no extra medium is required and only one thing that is to be ensured is that availability of Continuous power supply for the base monitoring station/ micro-controller. The system shall be developed in two parts: base monitoring and relaying and mobile application.

Keywords. renewable energy, Internet of Things, Monitoring, micro controller, photovoltaic device.

1. INTRODUCTION

Renewable energy is the energy that is collected from the renewable resources or in other words energy collected from a source which is not exhausted when used. However, the amount of energy available per unit of time is limited. The

major types of renewable energy are solar energy, wind energy, hydro energy, biomass energy and geothermal energy [1]. So, humans are very dependent on these type of energies and related systems it is important to closely monitor the consumption and usage of these type of energies [2]. To monitor and optimize energy production, detail investigation should be carried out with an emphasis on photovoltaic device properties. So manually using analog measuring devices to measure voltage and current calculating them making note of them takes a bit lot of time. So, a IOT enabled device is developed in this project to do all above work and permits monitoring the performance characteristics. This project helps to monitor them through mobile application and values get updated in a excel sheet time to time. Monitoring them can be done from anywhere in the world by connecting to internet. IOT (Internet of Things) refers to the interconnection via internet of computing devices embedded in everyday objects, enabling them to send and receive data. In other way IOT enables the objects to be sensed, while also controlling it remotely, which enables better interaction of physical world to the computers. This would improve the accuracy, efficiency with limited human intervention. THINGS in IOT include HARDWARE + SOFTWARE + SERVICE. IOT is not just about getting devices connected.

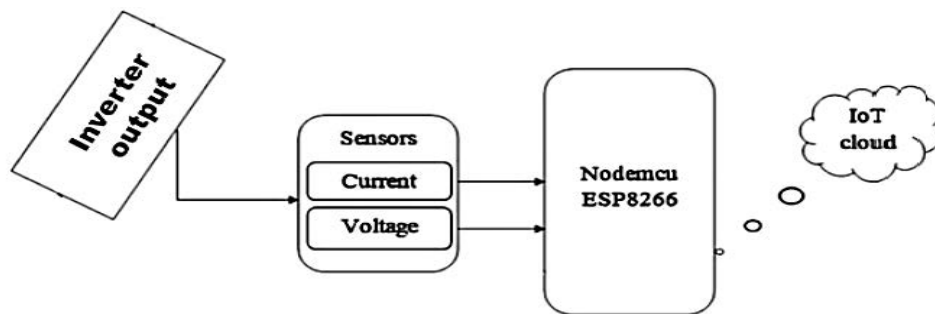


Figure 1. Block Diagram

IoT is not just about getting devices connected. It is more about exchange of meaningful information from one device to another to get another meaningful accomplishment. IOT is not one technology, but it is a collection of technologies and domain knowledge and hence interpretation matters a lot, otherwise there are going to be a lot of misconceptions.[3] Apart from renewable energy monitoring there is also a need of a solution which can monitor and manage the existing source of energy present. This solution will closely monitor energy consumption of the home residents and help in reducing the energy cost and energy losses.[3] Electricity, like water and food, is a need in today's world. We urgently require Electricity powers heating, lighting, refrigeration, public transportation, and all household appliances. The use of energy is increasing daily, but the availability of energy is decreasing. As a result of the constant decrease, various alternative energy sources are used to meet power needs and produce power. Non-renewable sources

are used in the other approach. One method employs renewable resources, while the other uses non-renewable resources. Non-renewable resources include solar, wind, and tidal energy. As a result, solar and wind energy are frequently referred to as a long-term power source. As a result, an IoT-based renewable energy monitoring system is being proposed to address the need for performance monitoring.

2. METHODOLOGY

First thing that needs to be done is, calibrating the voltage sensor. Here calibration of voltage means positioning the pin available on the sensor to provide an accurate sine-wave output.

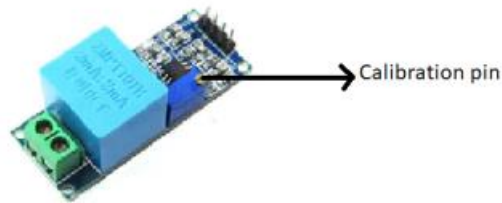


Figure 2. Voltage sensor

Calibrating the module by its Potentiometer (Calibration pin), you wire the module, plug the Arduino and upload the code onto Arduino and do not forget to place the measuring probes to the power socket and you already know the voltage over. By running the code and positioning the pin available on the sensor it leads to the accurate sine wave output which is required here.

The next step is to connect to google spread sheet by means of esp32 module. Firstly, create a new spread sheet in google drive and note the id of that sheet and then using this id we would make request to add rows into google spread sheet we need to add a json file in the extension part of google spread sheet.

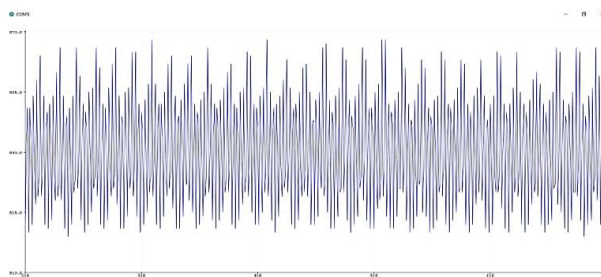


Figure 3. Calibrated module sine wave output

Here while connecting to Arduino IoT cloud, we need to first setup the device Esp32 At the end of setup you will be asked to enter a name for the board and then after entering, you will be provided with device id and secret Key. And it

is to be noted that secret key cannot be recovered after noting them done you need to click on continue. And you make your own thing and then a dashboard for it and enter the coding part for it and then by entering the Wi-Fi details and security key which is already available after device setup. And you will be also asked for device network name and password on which this device gets connected and will be available for us to monitor the data.

While calculating current flow through the sensor we must know the maximum rating up-to which the sensor can measure. If it is a 5A current sensor, then it has different magnitude of voltage at the output for 1A of current flow through the sensor. The output voltage for different rated current sensors is provided by the manufacturer itself. For example, a 30A current sensor (ACS712 Hall effect Sensor) would result in 66mv/A.

After calculating the values of current, voltage and power these values are updated on the mobile application through the help of Arduino IOT cloud which is connected to the mobile application and updated on the google spreadsheet which is connected to our Arduino. These are the two sources of applications to monitor on our mobile. In this project a relay is added to provide time delay function and to use it as a switching power source whenever needed.

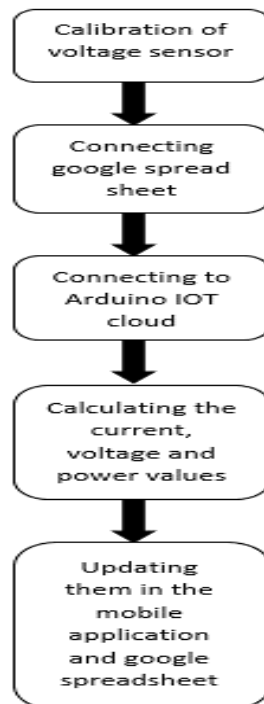


Figure 4. Methodology used

3. RESULTS

According to the algorithm energy source that is being used is monitored in two different ways and this is achieved through IOT. The two different ways are

- Monitoring the readings on google spread sheet.

Timestamp	Purpose	Power	Voltage	Current
February 11, 2	Major	7.68	244.92	0.03
February 11, 2	Major	7.68	260.44	0.03
February 11, 2	Major	7.68	255.97	0.03
February 11, 2	Major	7.68	245.01	0.03
February 11, 2	Major	7.68	249.81	0.03
February 11, 2	Major	7.68	243.99	0.03
February 11, 2	Major	7.68	254.74	0.03
February 11, 2	Major	7.68	256.76	0.03
February 11, 2	Major	7.68	243.77	0.03
February 11, 2	Major	7.68	255.15	0.03
February 11, 2	Major	7.68	255.7	0.03
February 11, 2	Major	7.68	252.93	0.03
February 11, 2	Major	7.68	250.53	0.03
February 11, 2	Major	7.68	252.9	0.03
February 11, 2	Major	7.68	253.62	0.03
February 11, 2	Major	7.68	252.93	0.03

Figure 5. Readings in Google spread Sheet

- Monitoring the readings on Mobile application.

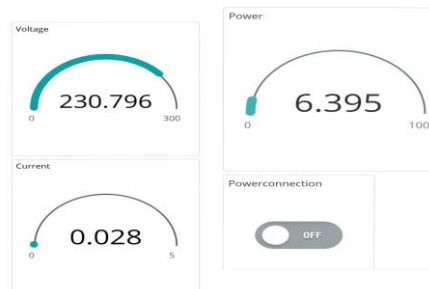


Figure 6. Readings in Mobile application

4. DISCUSSION

Economic considerations are one of the key reasons businesses and governments are investigating IoT's potential for energy efficiency. Everyone in the supply chain benefits from improved spending and investment control, waste reduction, and real-time power usage monitoring thanks to smart metres and data-driven predictions. To comply with new standards aimed at reducing emissions, the energy sector has experienced considerable changes. Companies are gradually incorporating IoT energy consumption and management software and other solutions into their operations in order to decrease their carbon footprint — optimise resource use, measure and analyse environmental impact, and establish long-term plans targeted at net-zero targets.

Companies utilise IoT not only to employ analytics tools to assess how effectively companies are complying with existing environmental standards, but also to manage energy in their everyday operations. Modern SaaS platforms include analytics capabilities that demonstrate if clients are eligible for incentives and industry certifications.

Professionals in this industry, both downstream and upstream, recognise that a shift to green energy is unavoidable and are taking steps to incorporate clean energy strategies into their operations. By utilising energy monitoring sensors, performance, and power consumption data, utilities, for instance, can better understand how to maximise the use of renewables in their services and execute energy conservation efforts.

5. CONCLUSION

The IoT based Renewable Energy Monitoring System has been designed and implemented satisfactorily. The presence of each module has been carefully reasoned out of place adding to the optimal running of the unit. This Energy Monitoring System is designed to provide an easy way to monitor the amount of energy being generated at every instant of time.

Because of the growing reliance on renewable energy and related systems, it is critical to keep a careful eye on and establish the governing parameters for efficiency in relation to environmental circumstances. In order to optimise energy output, extensive study, focused on the features of photovoltaic devices, is critical. Manually measuring voltage and current with analogue measuring instruments, calculating and recording the data, and displaying a graph is a tedious and time-consuming operation.

So, to address this, we are aiming to design an IoT-enabled gadget that accomplishes all the above and makes the job easier by allowing us to monitor performance parameters on a mobile application without having to do any extra effort. The only thing that must be ensured is that the base monitoring station has a continuous power supply.

REFERENCES

1. Srinivasan, K Rajendran, Vimala Devi. (2019). Solar Energy Monitoring System by IoT. (2019).
2. L. Zhao, Y. Zhou, I. Matsuo, S. K. Korkua and W. Lee, "The Design of a Holistic IoT-Based Monitoring System for a Wind Turbine," 2019 IEEE/IAS 55th Industrial and Commercial Power Systems Technical Conference (ICPS), 2019, pp. 1-7,
3. Srivastava, Prakhar Bajaj, Mohit Rana, Ankur. (2018). IOT based controlling of hybrid energy system using ESP8266. 1-5. 10.1109/ETECHNXT.2018.8385294

Finger Print Based Intelligent Locker System

Senthil Kumar R^{1*}, Prabaakaran K³, Mohammed Ovaiz A², Suguna R¹,
Shanmugapriya M¹ and Naresh Kumar S¹

¹Department of Electrical and Electronics Engineering, Vel Tech High Tech Dr. Rangarajan Dr. Sakunthala Engineering College, Chennai, India.

²Department of Electronics and communications Engineering, Vel Tech High Tech Dr. Rangarajan Dr. Sakunthala Engineering College, Chennai, India.

³Department of Electrical and Electronics Engineering, Easwari Engineering College, Chennai, India

Email: rskumar.eee@gmail.com, prabaakaran031@gmail.com, ovaiz.eee@gmail.com

Abstract

The notion behind this article is to develop a prototype which assures fully automated highly secured locker system for the user in commercial centers such as malls, airport, tourist spots, hospitals, education institutions, railway station etc. System assigned to manage an array of lockers which are locked with digital solenoid locks, interaction between user and system is established with key pad and LCD display. Access to the lockers is secured with the deployment of finger print sensor to authorize it. System is fully automated with Arduino controller to avoid manual labour for monitoring and fee collection, RFID based prepaid card are provided to do initial registration and auto detection of fee collection. For validation, system is tested in real time by considering a locker system with (two* three) array of lockers that is six lockers, in that three slots were left vacant for user and user is availing the slot for three hours at a tariff of 20 rupees per hour. The total time for new registration completes in 115 seconds which is comparatively less time compared to existing automatic locker system. System offers simple cost effective, fully automated and highly secured locker system for commercial centers; hence system will be fruitful for both the users as well as service providers.

Keywords. RFID, Arduino, finger print Sensor, locker system, automatic, prepaid card.

1. INTRODUCTION

It seems to be hectic tasks for people wonder with their luggage's in their travel. Hence it is necessary to provide a storage space for them to accommodate

their belongings safely. Not only for the traveller, even its required in places such as such as malls, tourist spot, education institutions, medical centres etc. it will greatly reduce burden of the people in carrying their belongings all the way they are roaming, this eases their work.

At the same time storage space can't be provided at free cost, in this world where even virtual cloud storages are in rent. But this process will require manual monitoring for allotment of lockers and payment collection. As manual labour seems to be more expensive, hence it is indispensable to automate the complete process.

In this process, concern priorities on the security aspect in accessing the locker and simple user friendly to the users. In the point of storage space provider, the system to has to be economical and fully automated.

2. LITERATURE REVIEW

The concern of the article [1,6] was to assure the security in accessing the lockers, for this it has adopted face recognition technique for providing the required security, which seems to offers less degree of accuracy compared to finger print authorization. There were practical difficulties in revealing their facial details removing the mask in this COVID-19 pandemic situation. Moreover, it hasn't concentrated on fee collection.

Article [2,7] was deployed in rural area for logistic purpose, here process seems to be one way the, logistic will be placed by the service provider in one common point in rural area, reducing the delivery man work, the consignment details and secret code will be reaches the customer via mobile applications, here again security level and it cannot be used in other locations where user have to store their belongings.

System [3,8] was developed keep students as the end user in education institution where they can store their material instead carry daily to institution, system was developed with IoT and Bluetooth platform which offers a remote-control operation via mobile applications, again system was developed for a single specific user (students), under this condition payment collection was not mandatory in many institutions, so it hasn't focused on fee collection from the user.

Article's [4,9] concern was only with assuring the at most security to the locker, it is provided with alert system if any one tries to open the lock in unauthorized manner, it will activate the alter system and it is provided with a camera to take stills of person who is mishandling the system, again this system also haven't designed for fee calculation and collection.

Paper [5,10] disclose the complete survey on smart locker, it has covered various technology used in designing a smart locker system, it also display the different applications where smart locker can be employed as it was portrait in figure

2.1. The finds its utility in wide applications such as health, education, commerce, banking, condominium etc.

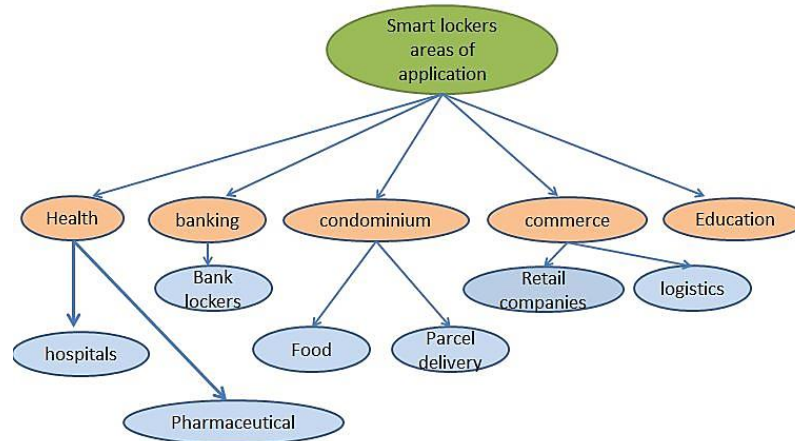


Figure. 2.1. Utilites of smart lockers.

All the above author's concern was to develop system keeping end user in mind and to offer them secured and user-friendly system. But system should have to be of mutual benefit to user as well as storage space provider. Hence it becomes indispensable to develop a system of high security, cost effective, fully automatic in monitoring and fee collection.

Few existing system deployed in various different applications are showcased in figure 2.2



Figure 2.2 a. Pharma collect b. lockers in hospital c. laundry lockers

3. PROPOSED METHODOLOGY

Figure 3.1 showcase the pictorial representation of the system what proposed it house finger print sensor to provide high degree authorization to the user, key pad act as tool to simplify the interaction between user and system. System holds an array of (2*3) solenoid digital lockers which open and close the individual locker units, controller interact with user via LCD display, it displays the necessary details to user and instruct the process to followed to move on to next stage.

Batteries are provided to power the controller and solenoid lockers; Arduino Uno controller is being used to manage the entire process in and payment collection. RFID scanner and RFID prepaid cards are provided for each locker separately and are used for registration process and auto fee payment.

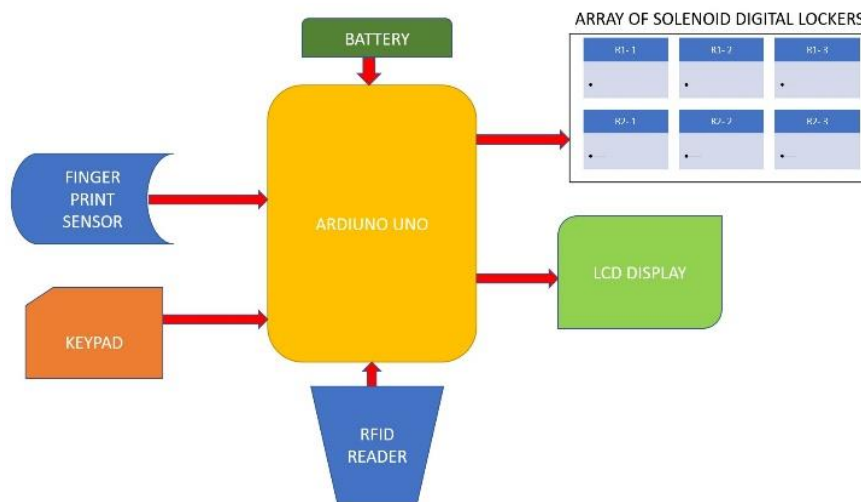


Figure 3.1. Pictorial representation of Proposed Methodology

The Figure 3.2 display the pictorial process flow image, the process house two parallel process of new registration and process involved with existing user for accessing the locker. Once the user pressed the enter key in the keypad, first query will be posted new registration if user enter “YES” then new registration process will be initiated, if user enter “NO” then another process to access the locker will be initiated.

If new registration is initiated by the user, then user will be asked to scan the prepaid RFID card, when details are stored, tariff will be displayed via LCD display. If user accepts the tariff through key pad, available slots (lockers) will be displayed to user, so that they can select number lockers as per their requirement. Once slot is selected by the user, user will be asked to scan their finger print, finger print data will be mapped with the slot selected and if registration is completed it will move on to next level.

Controller will actuate particular solenoid lock to open the locker, in case if “NO” was feed by the user at initialization it will process another parallel process for existing user. User will be asked to scan the finger print for authorization, if authorization was successful, it will retrieve details mapped with particular finger print and calculate the fee to be collected based the duration of hiring. After manipulation fee detail will be displayed to the user. Next user will be asked to scan the RFID prepaid card to initiate the payment process, in this process respective fee will be auto detected from the prepaid card and once the fee collection was

successful, it will display payment successful thankyou with that this process complete.

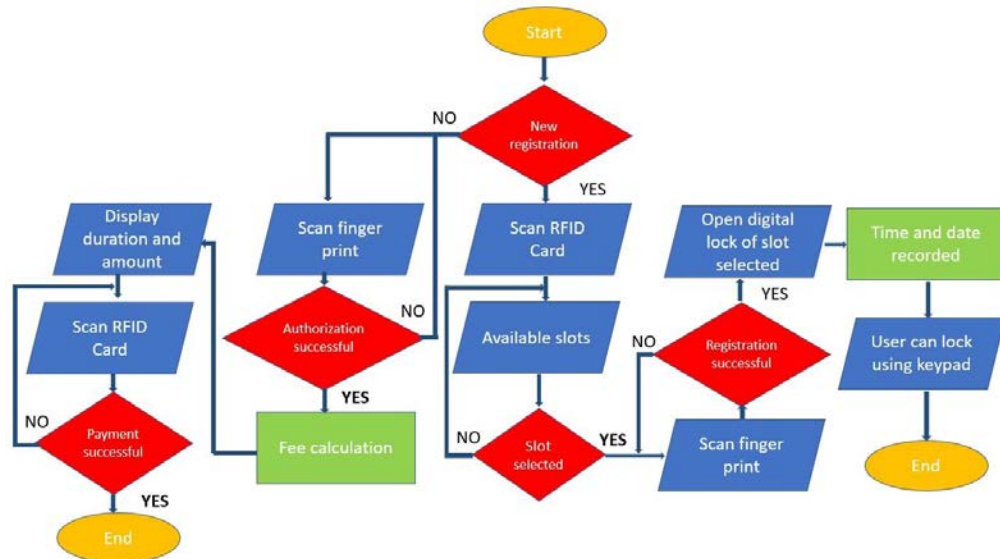


Figure 3.2. Process flow chart of Proposed Methodology

Figure 3.3 - the hardware interface displays clearly specific pin which are initialized as input-ports and output –ports, nearly seven pins are set as output ports, among which six pins are deployed for controlling the six solenoid locks, one pin is assigned for LCD display through which controller interact with user.

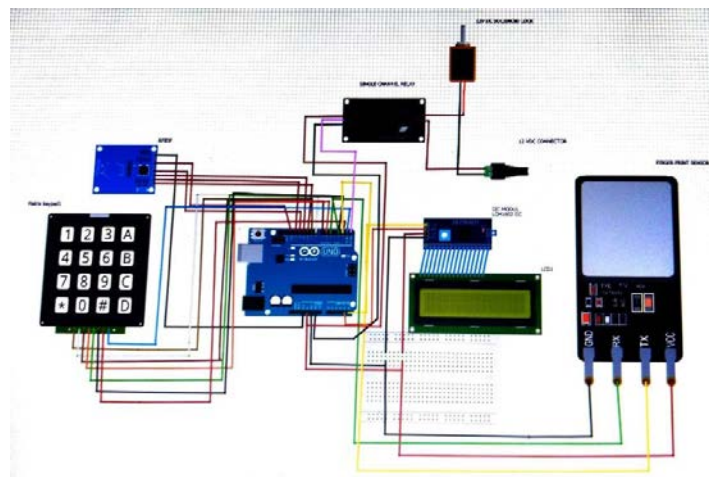






Figure 3.3. Hardware circuit interface

Three pins are configured as input-ports, among them one pin was assigned for keypad, via which user interact with the controller. One pin is configured for finger print sensor, through which finger print details are feed to the controllers. One pin is assigned for RFID reader which is used for initial registration and for fee collection. Power supply for controller is given at Vcc and Gnd of controller. Along with that power supply from battery has to be provided to solenoid lockers.

4. RESULTS AND DISCUSSION

For validation, system is tested in real time by considering three slots are vacant for user and user availing the slot for three hours at a tariff of 20 rupees per hour. Table 1 showcase the details displayed as per process flow in LCD display and its corresponding inferences

Table 1: Outcomes and its inferences.

LCD Display	Inference
	After user feed as new registration via keypad system initiate the registration process by asking to scan the RFID card, details of card will be recorded future processes.
	Once the RFID card are registered tariff details will be displayed here, we have considered twenty rupees in Indian currency is charged for 1 hour and was fixed as the minimum base value to avail the lockers. Also based the duration of availing the locker the fee will be calculated.
	Next to tariff display if user accepts to pay via keypad available slots will be displayed, so that user can select the locker he wants via key pad.
	Once locker is selected finger print of user is registered with that particular locker, finger print offers unique authorization for user, thereby ensures the high security to the user and increase the reliability of the system.



If the finger print is feed via sensor got successfully registered with that particular selected locker, in LCD display following statement will be displayed “FINGER PRINT REG SUCESSFUL”



If fee amount to be collected from the user if he select the option “NO” for new registration at the time starting, this process is initiated for user who have already registered and kept his belongings in the locker assign to user, it will first ask to enter the locker details, then it will ask for finger print authorization, if authorization was successful then it will ask to scan the RFID card.



Once prepaid RFID card is scanned then based on the fee calculated, amount will be auto detected from the card. If the fee collection was successful then it will be displayed as “PAYMENT SUCCESS THANKYOU” entire process complete with this.

5. CONCLUSION

The System is validated to function in a secured way for a locker system with (two* three) array of lockers that is six lockers. Total new registration completes in 115 secs which is comparatively less time compared to existing automatic locker system. System seems to be user friendly in selecting lockers and payment processes. From the point of component selection and process involved system is economical, system also eliminate manual labour in managing the locker system and collection of payment.

REFERENCES

1. Niaz Mostakima et. at. ‘Smart Lockers: IoT based Intelligent Lockers with Password Protections and Face Detection Approaches’, I.J. Wireless and Microwave Technologies, Hong Kong, May, pp-1-10, 2019.
2. T. Gundu, "Smart Locker System Acceptance for Rural Last-Mile Delivery," 2020 2nd International Multidisciplinary Information Technology and Engineering Conference (IMITEC), 2020, pp. 1-7.
3. H. F. Alqahtani et al., "Automated Smart Locker for College," 2020 3rd International Conference on Computer Applications & Information Security (ICCAIS), 2020, pp. 1-6.

4. Naik, Rasika and Agarwala, Sanchit and Raisinghani, Siddanth and Satam, Swapnil and Sawant, Shubham, Smart and Secure Locker System (April 8, 2020). Proceedings of the 3rd International Conference on Advances in Science & Technology (ICAST) 2020.
5. Alícia F. S. Luís, Gonçalo M. C. Martins, João M. L. P. Caldeira, Vasco N. G. J. Soares, "Smart Lockers: Approaches, Challenges and Opportunities", International Journal of Engineering and Advanced Technology (IJEAT), Volume-11, Issue-3, February 2022.
6. Shital P. Chavan, Sweety K. Sapkal, Tejaswini G. pagare, Gauri S. Shimpi, "SMART LOCKER SYSTEM USING BIOMETRICS AUTHENTICATION", International Journal of Innovative Research in Technology, vol. 4, no. 12, 2022, pp. 486-489.
7. Athang Bachhav, Omkar Gaikwad, Aditya Pawar, Pranav Changond, "Smart Locker", International Journal of Creative Research Thoughts, vol. 10, no. 3, 2022, pp. 250-257.
8. Akash A Phalak et.al., "An Iot based Smart Locker using BLE Technology", International Journal of Engineering Research & Technology, pp-274-276, 2019.
9. J. Sa-ngiampak et al., "Locker Swarm: An IoT-based Smart Locker System with Access Sharing," 2019 IEEE International Smart Cities Conference (ISC2), 2019, pp. 587-592.
10. Devi et.al., "Cloud Computing based Intelligent Bank Locker System", Journal of Physics, India, pp. 1-9, 2022.

Fully Automated Sun Drying System for Food Grains

**Senthil Kumar R^{1*}, Harshavardhan Naidu S², Suguna R¹, Raghunandhan R¹,
Poovendan V¹ and Sri Sai Vatsan R¹**

¹Department of Electrical and Electronics Engineering, Vel Tech High Tech Dr. Rangarajan Dr. Sakunthala Engineering College, Chennai, India.

²Department of Electronics and communications Engineering, Vel Tech High Tech Dr. Rangarajan Dr. Sakunthala Engineering College, Chennai, India.

Email: rskumar.eee@gmail.com, sapineniharsha@gmail.com, sugunamesh2429@gmail.com, raghunandhan30062001@gmail.com, poovendhanvenkat@gmail.com, jayshriramesh23@gmail.com

Abstract

The article was coined on objective of developing a fully automated sun drying system for various food grains. Hence food waste due to human error and manual monitoring can be reduced. Sun drying duration and temperature differs for various food grains, so it is necessary to adapt suitable drying duration for different grains, instead of having a common pre-set value. As the sun drying duration and temperature of grains have great impact on texture of grains which in turn are the deciding factors of quality grade of final product of grains. Another big issue is sun drying process is grains get wet due to unexpected rain which will delay the process or spoil the grains, creating huge loss. Hence a system is developed with Arduino and sensors to cover the grains immediately if rain is detected, monitor the temperature and drying duration. For validating the outcomes of the system, wheat grains are taken for study; system threshold values are set accordingly. System is tested for four objectives; they are in case of rain, if temperature exceeds permissible value, if drying period exceed the required period and under normal condition. On the whole system seems to be user friendly in changing the pre-set value which varies for different grains.

Keywords. Rain Sensor, Food Grains, Sun Drying, Arduino UNO, Temperature sensor, Automatic Protection.

1. INTRODUCTION

In 2017, according to New Delhi, around 57676 tons of food grains are wasted in the past five years, where the grains have got damaged, which were become useless, for the human consumption. Such a huge amount of food grains

could be able to feed around 1.15 crore people for a month. In the last few days, thousands of tonnes of wheat got spoiled and wasted due to unexpected rain, in Ambala. Apart from that, wheat which was brought to the grain market, got wet and spoiled. The agencies faced a huge loss, and are struggling to provide cover to farmers to protect food grains from getting wet.

In 2016, the wastage of food grains has increased from 12 percent to 14 percent. Which is a huge difference and huge amount. The heavy down pour of rain has created a huge problem and burden to the farmers, where the farmers are forced to work in a heavily pouring rain, to remove and cover the grains from getting wet. It is not possible for the farmers, of anyone to collect the food grains from heavy rain in a matter of seconds. The farmers have faced a huge loss in many places of India, where the prediction of rainfall is unexpected.

Table 1: Drying temperature and duration for various grains

Grains	Temperature in Celsius	Duration hours
Maize	41.1 - 58.9	2.6
Wheat	35 - 40	2
Millets	50 – 60	0.40
Paddy	55 – 60	2
Rice	25.8 - 29.27	2
Beans	40-54	10
Cow peas	70	7
Copra	53	1

2. LITERATURE REVIEW

People are struggling when unexpected rain comes during cloth drying in the direct sun. So here is the simple and best invention of fully automated system for cloth drying under direct sun. The humidity sensors are used to monitor the humidity. It will detect the rainfall, by measuring the humidity. To measure and detect the average sun rays, PV sensors are used. AC motors are used for movement of cloths from one location to another location, with the help of microcontroller, when there is an unexpected rain. This automated system, is cheap, will reduce human effort [1-3].

The design of rain detector alarm consists of a switching unit, microcontroller, power supply and buzzer. Even if there is a smallest drop, the rain sensor can be able to sense the rain drop which is falling on the rain sensor. The power supply consists of 9V battery. IC has three modes called bi-mode, Mono

stable mode, A-stable mode. As this IC is A-stable mode, there is no stable level of output. The buzzer is used for alarm, which indicate the user, in the form of sound when there is an unexpected rain fall. Double sided copper board are used in the construction of rain sensor. The rain sensor works as a switching device, when there is rain fall which causes the transistors present in the circuit to turn ON. So, this project makes the user, the simplest project, which reduces the time and made the job done quickly before heavy rain come [4].

In India, cricket is one of the most popular games in the world. But the problem is that, the cricket match gets delayed or get cancelled due to unexpected rainfall. To overcome such a problem, rain detector with alarm with automatic roofing system are used for Cricket Stadiums. The auto roof covers the entire stadium. The setup consists of Arduino UNO, servo motor, LED, Buzzer, GSM, and rain sensor. When there is a rainfall, the rain sensor activates and give signal to Arduino uno and GSM, which will turn on the buzzer to make sound and the LED to indicate, and the servo motor will automatically close the roof, which will prevent the Cricket Stadium from rainfall. When the rainfall stops, the roof will automatically open. And hence all the messages are sent to our respective smartphone [5].

Floods are caused due to heavy rainfall. Therefore, some tools and systems are used to monitor the rainfall. The Arduino uno is interfaced with temperature sensor, humidity sensor, and rain sensor to monitor the weather conditions. The whole setup will provide warnings and reports on the rainfall level, which is very useful for minimizing the amount of flood before the rainfall. We can make some arrangements, before the rainfall, which reduces the flood. Analog data signal from Arduino uno are sent to fuzzy interface. Using fuzzy algorithm, the data are processed. The device provides estimate of weather, to remain rain level detection [6].

3. PROPOSED METHODOLOGY

Figure 3.1 display the block diagram of the proposed system, it consists of Arduino Uno, rain sensor, temperature sensor, LCD display, keypad, driver circuit, motor and screen. Humidity sensor are used as the rain detector which is deployed for detecting the rain, temperature sensor is employed to monitor the temperature at which grain are dried under sun, as it is important to maintain the texture of grains, Arduino controller plays the role of brain in the system, as it is receives the input values and holds all preset value, with what it provides the control action as per the preset program. Keypad is provided to make system user friendly in varying the preset value as the grains considered for drying.

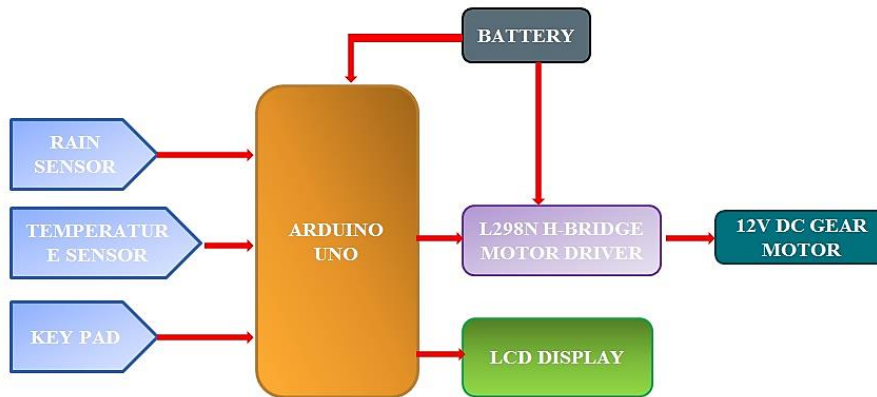


Figure 3.1. Pictorial representation of Proposed Methodology

The Figure 3.2 show case the process followed in the introduced system, as the Arduino controller has to process three parallel operations as the objective of the work demands monitoring of humidity, temperature and duration of drying. Humidity sensor continuously monitor the whether there is any rain fall or not. In case of rain fall sensor intimate the controller and controller will initiate the drive circuit to unwound the screen and entire grains will be covered.

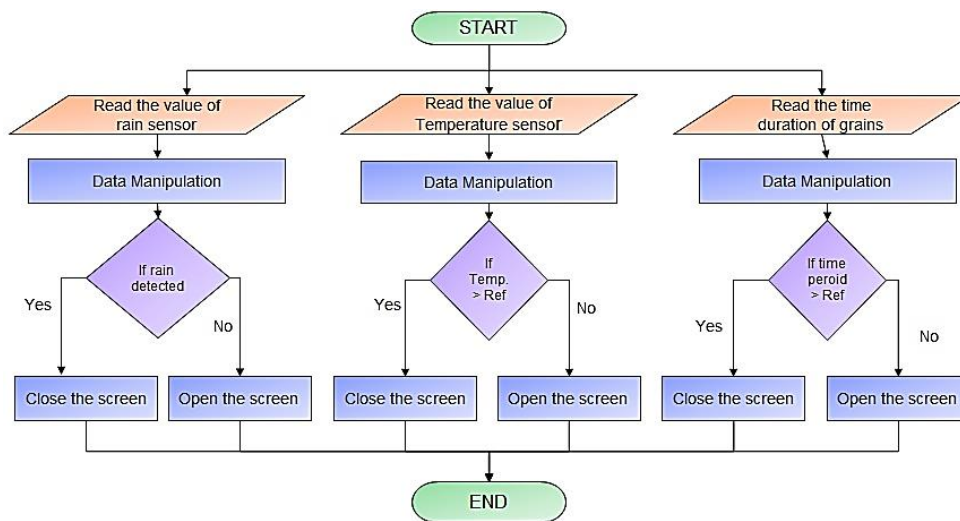


Figure 3.2. Process flow chart of Proposed Methodology

Another task which as to be processed in parallel are constantly monitoring the temperature of grains under sun drying as it is very important in maintain the texture in which grains are required in the market. Incase if temperature exceed the preset temperature value of any particular grain, then controller will unwound the

screen to cover the grains there by it will won't allow the temperature to exceed beyond the preset value of that particular grain.

The next objective which has to be monitored in parallel are duration for what the grains has to be dried under sun, for that controller will have the complete track record of duration for what the grains are dried under sun, which is very crucial deciding factor of the quality of the grains.

In case if duration of sun drying exceed the pre-set value controller will unwound the screen to coverup the entire grains which will maintain the expose time of the grain within the pre-set value.

Figure 3 display the hardware interface of proposed system hardware consist of input element as temperature sensor, humidity sensor and keypad. Temperature sensor continuously monitor the temperature of grains drying under the sun, humidity sensor will detect the rain. Key pad provides a flexibility to user to modify the threshold level based on grains dried under sun.

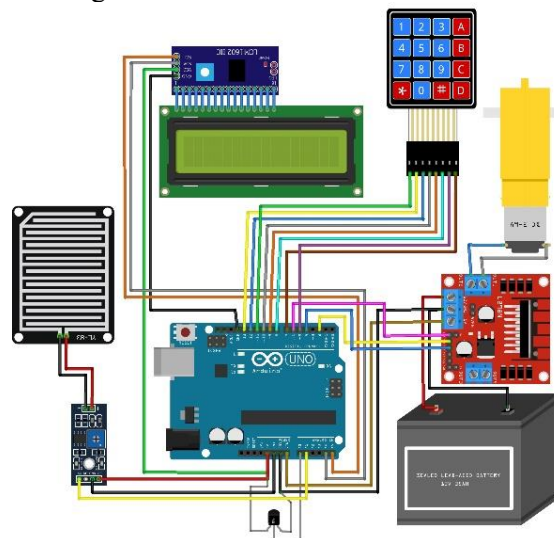


Figure 3.3. Hardware circuit interface

Here Arduino Uno is employed to control the entire system. Based on the condition as per the input what received controller provides the control signal to driver system which covers the grains with screen and all actions will be displayed in LCD display [7-9].

4. RESULTS AND DISCUSSION

For validation wheat grains taken for study and reference as threshold for system are set accordingly, figure 4.1 display the plot for a day of monitoring the temperature and rain while drying the wheat grain, drying period was restricted between morning 8:00 Am to evening 5:00 Pm with an overall time period of 8 hour a day, rest hours screen remains covered.

Here blue colour marks indicates that temperature is within the permissible level, while red colour marks the point where temperature crossed permissible level hence system automatically covers the grains with screen to avoid direct insolation of sun ray on grains. While the yellow colour marks are the point when sensor had detected rain, during this occasion also system automatically covers the grain. There by grains are protected from being get wet.

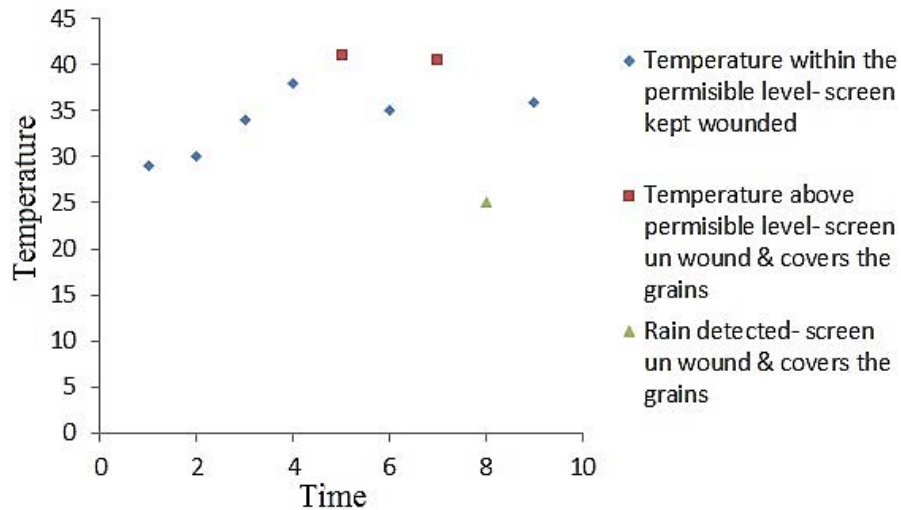



Figure 4.1. A day graph of sun drying

Table 2 show case the inference of the outcomes as per the conditions observed in the process of drying the wheat grains, all the four cases of study as per the objectives were evaluated. How the system reacted to following case are given in the table 2, first case under no rain and permissible temperature, second case if rain detected, third case if temperature exceed permissible temperature and fourth case if drying period exceed the required drying period.

Table 2: Outcomes and its inferences

LCD Display	Inference
	LCD shows that, the rain sensor has still not detected any rain, so it shows “NO Rain”. Hence when there is no rain drop on the rain sensor, the resistance value of the rain sensor is not less than the set value of resistance in the Arduino Uno code, the LCD display shows “NO Rain” screen remains uncovered allowing the grains to dry under sun.

A rectangular LCD display with a black border and a green background. The text "Rain Detected..." is displayed in a black, monospaced font.

LCD shows that, the rain sensor has detected rain, so the LCD display shows “Rain Detected”. Hence when the rain drops fall on the rain sensor, the resistance value of the rain sensor is less than the set value of resistance in the Arduino Uno code, the LCD display shows “Rain Detected” immediately screen unwound and cover the entire grains protecting the grains from being get wet.

A rectangular LCD display with a black border and a green background. The text "Preset time Complete" is displayed in a black, monospaced font.

LCD shows that, the time duration of the particular food grains, that we have kept for sun drying has completed. The time duration of particular food grains and specific allowable temperature is monitored. Once the drying duration completed screen unwound and cover the entire grain.

A rectangular LCD display with a black border and a green background. The text "TEMP. Exceed Present value" is displayed in a black, monospaced font.

LCD displays the temperature at which the food grains are drying under sun. If it exceeds the temperature value set to the particular food grains, then the screen closes, which stops sun drying. At the same time, the LCD display shows that “temperature exceed present value”. As the temperature at which various grain to be dried differs, it becomes indispensable to monitor the temperature closely.

5. CONCLUSION

The reaction time of the proposed system is around 2 micro seconds to detect the rain hence it is able to protect the grains from rain, before it is being getting wet by rain which seems to be fruitful in reducing the drying time and preventing grains from getting spoiled. For validating the outcomes of the system, wheat grains are taken for study; system threshold values are set accordingly. System is tested for four objectives; they are in case of rain, if temperature exceeds permissible value, if drying period exceed the required period and under normal condition. The study was carried over a day in monitoring the temperature and rain while drying the wheat grain, drying period was restricted between morning 8:00 Am to evening 5:00 Pm with an overall time period of 8 hour a day, rest hours screen remains covered, due to dew conditions. System proves to be most cost-effective solution to automate the drying process which demands constant manual monitoring. As the system is provided with additional features such as temperature and duration of drying monitoring helps in retaining the texture in which they are required to get the premium quality. System is also user friendly in varying the preset value as per various grains.

REFERENCES

- [1] Senthil Kumar R et al. "Novel Fully Automated Microcontroller Controlled Cloth Drying System Under Direct Sun", Indian Journal of Science and Technology, India, Nov, pp. 1-4, 2016.
- [2] Prabhakar Hegde, et al., "Automatic Protection of Clothes from Rain", International Journal of Advanced Research in Computer and Communication Engineering. India, Vol. 5, Issue 4, April 2016.
- [3] Manasa K, et. al., "Automatic Cloth Retriever System", International Research Journal of Engineering and Technology. India, Vol. 03, Mar 2016.
- [4] Anushka et al. "Design of Rain Sensor Alarm System", International Journals of advance in Science Eng and Tech, India, Jan., pp. 22-25, 2018.
- [5] Vishalini et al., "Rain Detectors with Alarms", Internationals Advanced Research Journals in Science', Engg and Tech, India, July, PP 86-89, 2021.
- [6] Ahmad Yusuf, et al. "Rain Detection Systems for estimate weather level using Mamdani Fuzzy inferences systems", Internationals Conferences on Information and Communications Tech, India, May, pp.848-854, 2018.
- [7] I. Wahyudi, et al., "Rainfall Prediction in Tenger Region Indonesia using Tsukamoto Fuzzy Inference System", International Conference on Information Technology, India, Nov, pp. 1-6, 2016.
- [8] A. Kaur, et al., "Comparison of fuzzy logic and Neuro fuzzy algorithms for air Conditioning system", International Journal of Soft Computing and Engineering (IJSCE), India, May, pp. 1-6, 2013.
- [9] S. Banik, et al., "Forecasting Bangladeshi monsoon rainfall using neural network and genetic algorithm approaches", International Technology Management Review, India, April, pp. 1-18, 2009.

Performance Assessment of SMA Based MPPT Controller for PV System Considering Random PSC

A Suresh Kumar¹, V Usha Reddy²

¹Department of Electrical & Electronics Engineering, G Pullaiah College of Engineering and Technology, Kurnool, India.

²Department of Electrical & Electronics Engineering, SVU College of Engineering, Tirupati, India.

Email: 12madhuryaas@gmail.com

Abstract

Renewable energy sources such as solar photovoltaics are numerous, making them an ideal alternative to conventional energy sources. Due to their natural and environment-friendly properties, they are also more efficient than conventional energy sources. One of the most critical factors that can affect the efficiency of a PV system is the PV power extraction due to the Partial shaded conditions. Although the performance of a PV system is generally improved by implementing a maximum power point tracking technique, this technique is not ideal for every type of system. The classical methods are usually preferred due to the only peak in the P-V curve. However, when it comes to the multiple peaks of the P-V curve, the conventional methods are not able to achieve the optimal performance. Hence in this paper a novel Slime Mould algorithm (SMA) is proposed and its effectiveness is evaluated in comparison with Particle swarm optimization algorithm. The proposed algorithm is implemented on a test case of 200 W PV system of 5 X 5 size with S-P and T-T configurations. Parameters such as PV mismatch losses, fill factor efficiency are evaluated. Proposed SMA MPPT algorithms exhibits the superior performance in comparison with PSO MPPT algorithm.

Keywords. SMA, PSO, PSC, MPPT, S-P, T-T.

1. INTRODUCTION

Today, solar power is widely used in the world due to its high efficiency and cost-effectiveness. It is regarded as a promising renewable energy source. Compared with other sources such as fossil fuels and oil, it is very clean and has an abundance of environmental friendliness [1]-[3]. Due to the increasing concerns about the power generation efficiency of PV systems under different shading conditions, the need for more effective PV configurations has been increasing.

Hence in this paper optimal MPPT control technique is implemented considering the configurations under random PSC [4].

A novel Slime Mould algorithm is proposed and its effectiveness is evaluated in comparison with Particle swarm optimization algorithm. The proposed algorithm is implemented on a test case of 200 W PV system of 5 X 5 size. Parameters such as PV mismatch losses, fill factor are evaluated. Proposed SMA MPPT algorithms exhibits the superior performance in comparison with PSO MPPT algorithm [5].

2. SLIME MOULD ALGORITHM

The concept of the slime mould algorithm is based on the oscillation style of the mould in nature. It takes into account the various feedbacks generated by the mould's propagation wave and generates a dynamic structure that can be used to improve the efficiency of the system. The SMA approach is illustrated in Fig. 1. Mathematical model is illustrated in Fig. 2. [6]

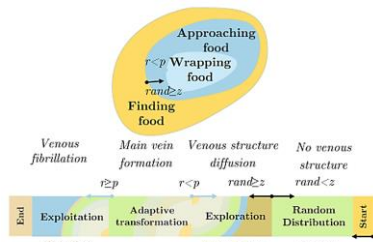


Fig. 1 SMA Approach

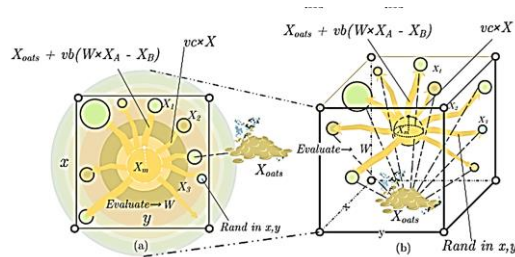


Fig. 2 Mathematical Model

3. PROPOSED SYSTEM

In this paper SMA optimal MPPT control technique is implemented considering S-P and T-T configurations under random PSC. A test case of 54 cell, 200 W PV system with 5 X 5 configuration is considered as shown in Fig. 3.

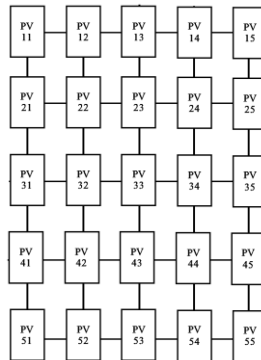


Fig. 3 Test Case Configuration

4. RESULTS AND DISCUSSION

In this paper the proposed algorithm is implemented on a test case of 200 W PV system of 5 X 5 size with S-P and T-T configurations. Parameters such as PV mismatch losses, fill factor efficiency are evaluated under the following cases.

- Performance Assessment Considering PSO Algorithm
- Performance Assessment Considering SMA Algorithm

4.1. Performance Assessment Considering PSO Algorithm

In this case PSO algorithm is implemented on a test case of 200 W PV system with 5 X 5 S-P and T-T configuration under random PSC condition. In the random PSC condition, the solar irradiance varies from 200 W/m² to 1000 W/m² at 25°C temperature. Parameters such as PV mismatch losses, fill factor and efficiency are evaluated.

1. Series Parallel (S-P) Configuration

In this case the PSO algorithm is implemented on S-P configuration. Under PSO algorithm, the Max. voltage is 111.100 V, Max current is 35.312 A, Max Power is 3923.163 W. The O. C. voltage is 162.047 V, S. C. current is 41.101 A. The evaluation parameters are tabulated in Table 1.

Table 1. Performance evaluation with S-P Configuration

Type	Fill Factor (%)	PV Mismatch Losses (%)	Efficiency (%)
Conventional MPPT	58.886	27.676	11.086
PSO MPPT	58.904	27.546	11.098

From the above evaluation table, it is clear that PSO MPPT exhibits the best performance than the conventional MPPT controller.

2. Triple Tie (T-T) Configuration

In this case the PSO algorithm is implemented on S-P configuration. The Max. voltage is 143.305 V, Max current is 31.399 A, Max Power is 4499.634 W. The O. C. voltage is 162.512 V, S. C. current is 41.101 A. The evaluation parameters are tabulated in Table 2.

Table 2. Performance evaluation with T-T Configuration

Type	Fill Factor (%)	PV Mismatch Losses (%)	Efficiency (%)
Conventional MPPT	67.460	11.429	12.703
PSO MPPT	67.366	11.206	12.728

From the above evaluation table, it is clear that PSO MPPT exhibits the best performance than the conventional MPPT controller.

4.2. Performance Assessment Considering SMA Algorithm

In this case SMA algorithm is implemented on a test case of 200 W PV system with 5 X 5 S-P and T-T configuration under random PSC condition. In the random PSC condition, the solar irradiance varies from 200 W/m² to 1000 W/m² at 25°C temperature. Parameters such as PV mismatch losses, fill factor and efficiency are evaluated.

1. Series Parallel (S-P) Configuration.

In this case the SMA algorithm is implemented on S-P configuration. Under the SMA algorithm, the Max. voltage is 112.320 V, Max current is 36.706 A, Max Power is 4122.818 W. The O. C. voltage is 163.010 V, S. C. current is 43.980 A. The evaluation parameters are tabulated in Table 1.

Table 1. Performance evaluation with S-P Configuration

Type	Fill Factor (%)	PV Mismatch Losses (%)	Efficiency (%)
Conventional MPPT	58.886	27.676	11.086
SMA MPPT	57.508	21.370	11.662

From the above evaluation table, it is clear that SMA MPPT exhibits the best performance than the conventional MPPT controller.

2. Triple Tie (T-T) Configuration

In this case the PSO algorithm is implemented on S-P configuration. The Max. voltage is 144.121 V, Max current is 32.411 A, Max Power is 4671.106 W. The O. C. voltage is 163.121 V, S. C. current is 44.012 A. The evaluation parameters are tabulated in Table 2.

Table 2. Performance evaluation with T-T Configuration

Type	Fill Factor (%)	PV Mismatch Losses (%)	Efficiency (%)
Conventional MPPT	67.460	11.429	12.703
SMA MPPT	65.064	7.123	13.213

From the above evaluation table, it is clear that SMA MPPT exhibits the best performance than the conventional MPPT controller.

5. PERFORMANCE COMPARISON

In this paper the proposed algorithm is implemented on a test case of 200 W PV system of 5 X 5 size with S-P and T-T configurations. Parameters such as PV mismatch losses, fill factor efficiency are evaluated under S-P and T-T configurations. Comparison analysis under S-P Configuration is illustrated in Fig. 3.

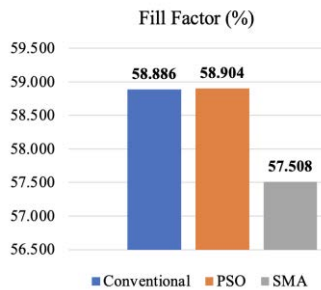


Fig. 3 (a) Comparison of Fill Factor

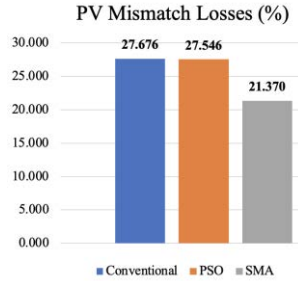


Fig. 3 (b) Comparison of PV Mismatch Losses

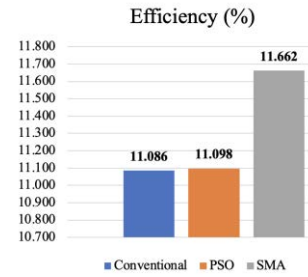


Fig. 3 (c) Comparison of Efficiency (%)

In the S-P Configuration Fill Factor is reduced, PV mismatch losses are minimized and the Efficiency is improved. Comparison analysis under S-P Configuration is illustrated in Fig. 4.

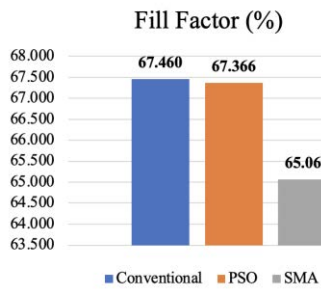


Fig. 4 (a) Comparison of Fill Factor

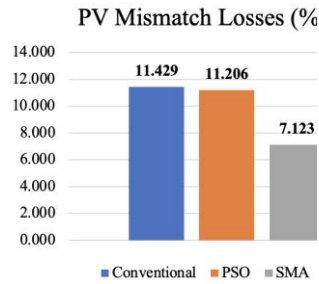


Fig. 4 (b) Comparison of PV Mismatch Losses

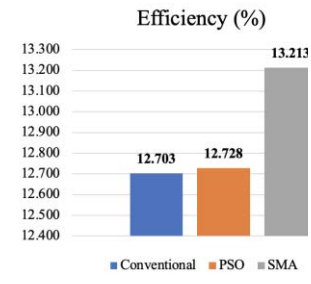


Fig. 4 (c) Comparison of Efficiency (%)

In the T-T Configuration Fill Factor is reduced, PV mismatch losses are minimized and the Efficiency is improved. Hence in all the cases the proposed algorithm exhibits the superior performance

6. CONCLUSION

In this paper a novel Slime Mould algorithm (SMA) is proposed and its effectiveness is evaluated in comparison with Particle swarm optimization algorithm. The proposed algorithm is implemented on a test case of 200 W PV system of 5 X 5 size with S-P and T-T configurations. Detailed literature review is presented. SMA algorithm approach is presented. Parameters such as PV mismatch losses, fill factor efficiency are evaluated considering conventional, PSO and

Proposed SMA algorithm. Proposed SMA MPPT algorithms exhibits the superior performance in comparison with PSO MPPT algorithm. In S-P configuration Fill Factor is reduced from 58.886 % to 57.508 %, PV mismatch losses are minimized from 27.676 % to 21.370 % and the Efficiency is improved from 11.086 % to 11.662. Similarly in T-T configuration Fill Factor is reduced from 67.460 % to 65.064 %, PV mismatch losses are minimized from 11.429 % to 7.123 % and the Efficiency is improved from 12.703 % to 13.213.

REFERENCES

- [1] A. A. S. Mohamed, A. Berzoy and O. A. Mohammed, "Design and Hardware Implementation of FL-MPPT Control of PV Systems Based on GA and Small-Signal Analysis," in *IEEE Transactions on Sustainable Energy*, vol. 8, no. 1, pp. 279-290, Jan. 2017.
- [2] C. Wei, Z. Zhang, W. Qiao and L. Qu, "An Adaptive Network-Based Reinforcement Learning Method for MPPT Control of PMSG Wind Energy Conversion Systems," in *IEEE Transactions on Power Electronics*, vol. 31, no. 11, pp. 7837-7848, Nov. 2016.
- [3] C. González-Castaño, C. Restrepo, S. Kouro and J. Rodriguez, "MPPT Algorithm Based on Artificial Bee Colony for PV System," in *IEEE Access*, vol. 9, pp. 43121-43133, 2021.
- [4] C. -Y. Tang, H. -J. Wu, C. -Y. Liao and H. -H. Wu, "An Optimal Frequency-Modulated Hybrid MPPT Algorithm for the LLC Resonant Converter in PV Power Applications," in *IEEE Transactions on Power Electronics*, vol. 37, no. 1, pp. 944-954, Jan. 2022.
- [5] H. H. H. Mousa, A. -R. Youssef, I. Hamdan, M. Ahamed and E. E. M. Mohamed, "Performance Assessment of Robust P&O Algorithm Using Optimal Hypothetical Position of Generator Speed," in *IEEE Access*, vol. 9, pp. 30469-30485, 2021.
- [6] S. Mouassa, A. Althobaiti, F. Jurado and S. S. M. Ghoneim, "Novel Design of Slim Mould Optimizer for the Solution of Optimal Power Flow Problems Incorporating Intermittent Sources: A Case Study of Algerian Electricity Grid," in *IEEE Access*, vol. 10, pp. 22646-22661, 2022.

Power Improvement of Uneven Irradiance Photovoltaic System Using Snake Ladder Pattern Array Reconfiguration

P. Keerti¹, B. Praveen Kumar¹

¹Department of EEE, Vardhaman College of Engineering, Hyderabad, TS 501218, India

Email: praveenbala038@gmail.com

Abstract

The working of solar photovoltaic (PV) system is disturbed due to changeable event of irradiance. Due to that, occurrence of mismatch losses happens and in turn reduces the power production of good PV panels in it. The aim of this work in this article is to extract the utmost power from each of the solar PV panel in the array by decreasing the losses because of mismatch. An innovative array reconfiguration method is projected in this article, which is the snake ladder pattern in the row/column formation. Each of the PV row/column is formation with different PV panels from the rows/column of the expected array reconfiguration. This developed project allows the PV system to function with lowest number of losses due to mismatch by uneven irradiance in the PV array. The production analysis is been checked and verified in the simulation of a 6×6 PV system in MATLAB. The developed array reconfiguration is around 39% more capable than the existing series-parallel connection and as well as superior than the TCT and sudoku puzzle pattern methods.

Keywords. Solar PV, maximum efficiency, reconfiguration, snake and ladder.

1. INTRODUCTION

In some years, the reduction of fossil sources directs to the process of non-conventional energy resources. Solar PV systems are the best power source between other non-conventional resources because of its advantages [1]. Various conservation parameters are inducing the drop of PV's organized conversion efficiency. Among those parameters, uneven irradiance is one of the most important one in dropping the PV efficiency. The conservative algorithms are united with soft computing methods like artificial-intelligence (AI), neural network (NN), Fuzzy Logic Control (FLC), and so on along with it. Though, during the uneven irradiance, the PV systems function with many local maximum power points (LMPP) and the maximum power point tracking (MPPT) algorithm unable to get the peak MPP (PMPP) amongst numerous LMPPs [2]. The drop in production power is based on the array connection and irradiance that happened in it. The series (Se) array

connection method has drawbacks on the uneven irradiance. Altered array reconfiguration techniques had been created such as series-parallel (Se-P), bridge-linked (BL), honey-comb (HC), and sudoku-puzzle pattern (SPP) by the researchers to bound the effects of uneven irradiance [3]. The electrical array reconfiguration (EAR) schemes were proposed for the PV array in [4]. This EAR scheme reshuffles the PV panel's inter-connection by using the switches like IGBTs and MOSFETs to produce more power even with the same uneven irradiance. A controller which will be controlling these switches according to the shading in the PV panels [5]. Except in the big PV power plants, the model of EAR is difficult to implement, because of this requirement of many controllers, switches, and sensors [6]. This article introduces a snake-ladder (SL) reconfiguration method with the enhancement ability of uneven irradiance dispersion. The faction of the dice is the fundamental ideas at the back this EAR scheme. The developed SL EAR is given with all necessary constraints. Many parameters are defined in the constraints, which satisfy the all supposition given in the snake-ladder pattern array reconfiguration. This developed SL EAR scheme has been tested in 6×6 PV arrays in MATLAB. The improved enhancement of the developed snake-ladder pattern array reconfiguration has been validated with different levels of irradiances and compared with various EAR scheme.

This article ordered as given: the mathematical model of PV panel is given in Section 2 and the developed snake-ladder EAR is discussed in Section 3 along with results and validation using 6x6 PV array. Section 4 provides the suggestions and the merits of the developed method are given as conclusion.

2. MATHEMATICAL MODEL OF PV PANEL

A PV cell's equivalent circuit is shown in Figure 2.1 and it is prepared using a current-source (I_{ph}) connected to a shunt-resistance (R_{sh}). Similarly, n numbers of PV cells are connected in Se-P manner to develop a PV panel. The equation of the PV panel is given in the form of current,

$$I_m = I_{ph} - I_{sat} \left[\exp\left(\frac{V_m + I_m R_s}{(nKT/q)}\right) - 1 \right] - \frac{V_m + I_m R_s}{R_{sh}} \quad (2.1)$$

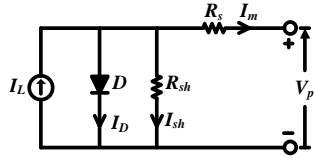


Figure 2.1. Equivalent circuit of solar cell

where, I_m is the extreme producing current, V_m is the extreme producing voltage, I_{ph} is photoelectric-current, saturation-current is given by I_{sat} Boltzmann's constant is K ,

series resistance (R_s), shunt resistance (R_{sh}), and temperature of PV panel is given by T .

3. DEVELOPED ARRAY CONFIGURATION

The planned electrical array reconfiguration (EAR) is executed with the help of the snake-ladder (SL) arrangement. This method will be selecting the PV panels from the old PV system with the optimized dissimilar PV system. A 6×6 PV array is taken in which all rows should have six number of PV panels. In the existing technique, the initial rows panels are P11, P12, P13, P14, P15, and P16, in the planned reconfiguration, the initial row have panels of all the rows like in the existing technique.

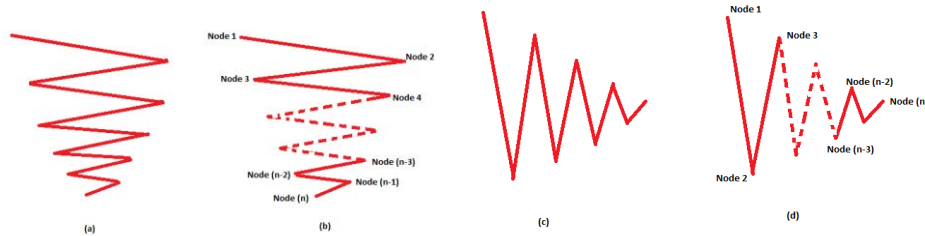


Figure 3.2. (a) horizontal snake ladder formation (b) horizontal node formation (c) vertical snake ladder formation (d) vertical node formation

The normal snake ladder formation and the node establishment from are given in the Figure 3.1. The snake-ladder formation can be developed into two ways like horizontal snake ladder (SL_H) and vertical snake ladder (SL_V) pattern. The horizontal snake ladder formation of array and the node establishment are depicted in Figure 3.1 (a) and (b). Similarly, the vertical array formation of array and the node establishment are depicted in Figure 3.1 (c) and (d).

The formulation of the planned electrical array reconfiguration is shown in Figure 3.2. These are represented for the horizontal SL EAR and vertical SL EAR. In both of those, a classification is created depends on the column count. The PV system having the even count in columns as well as an odd count in columns have different equations. Row development for the horizontal snake ladder in an odd count in columns begins with $(1)(i)$ and closes at $(n)(i+((n+1)/2))$. Similarly, in the horizontal snake ladder with an even count in columns, the row development begins with $(1)(i)$ and closes at $(n)(i+((n+2)/2))$. In parallel, row creation to the vertical snake ladder with an odd count in columns begins with $(i)(1)$ and closes at $(i+((n+1)/2)) (n)$. Similarly, in the vertical snake ladder with an even count in columns, the row development begins with $(i)(1)$ and closes at $(i+((n+2)/2)) (n)$. The planned snake ladder electrical array reconfiguration is applicable to any size of rows and columns of PV system. Every row is developed just by interchanging the values of i and n . The count of i stand for the total count of rows, its formation of

the initial row, the count of i is 1, similarly for the 2nd row, the count of i is 2 and so on. To the $m \times n$ PV system, the count of i begins with 1 to the last count of row m .

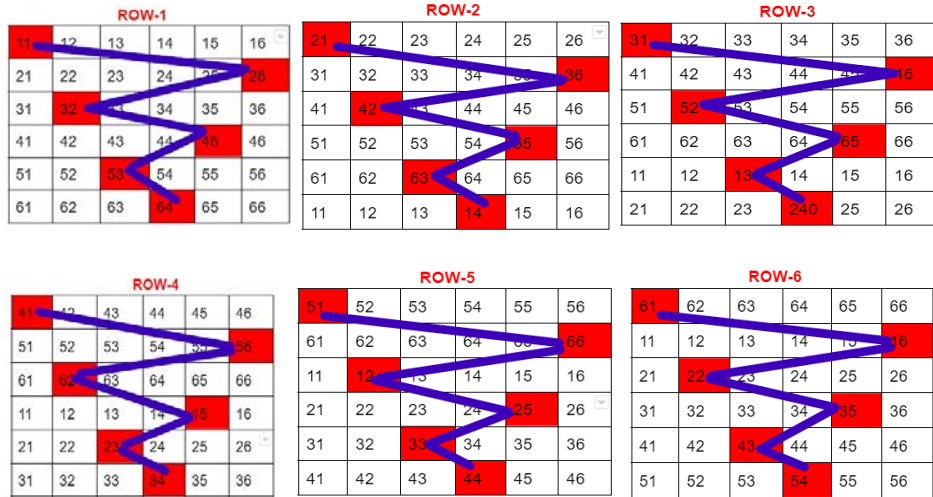


Figure 3.2. Row formation of horizontal snake ladder array formation

Consider this example, in the 6×6 PV system, row have 6 counts at the maximum. So, the initial row, i is 1, and 2nd row, the count of i is 2, and it go on till the 6th row. In horizontal SL formation, the row presents the outcome like P_{11} , P_{26} , P_{32} , P_{45} , P_{53} , P_{64} , the formation begins from the initial row and closes in 6th row. Except the 2nd row formation, it begins at second row and closes in first row and similarly in the 3rd row creation, it begins with third and closes in second row. It continues till the sixth-row creation, in that it begins in sixth row and closes in the fifth row.

Table 3.1. Node formation of the initial row for vertical snake ladder

Real Positions of PV panels	Expression	Location of PV panels in developed PV connection
P11	$= (1)(i)$	P11
P12	$= (2)(i+(n-1))$	P25
P13	$= (3)(i+1)$	P32
P14	$= (4)(i+(n-2))$	P44
P15	$= (5)(i+2)$	P53
P16	$= (6)(i+(n-3))$	P63

To the row development of initial row $I=1$ and $n = 6$

Equally the SL_H and SL_V reconfigurations are created in the 6×6 PV system. The results of developed and existing array reconfigurations were compared and explained. The power production of the developed and existing array reconfigurations is given in the Table 3.3. The power production and, efficiency during uneven irradiation conditions of Se-P, TCT, sudoku based reconfiguration,

horizontal snake ladder array reconfiguration (SL_H), and vertical snake ladder array reconfiguration (SL_V) were shown in the output results in Figure 3.3.

Table 3.2. Node formation of the initial row for horizontal snake ladder

Real Positions of PV panels	Expression	Location of PV panels in developed PV connection
P11	$= (i)(1)$	P11
P12	$= (i+(n-1))(2)$	P62
P13	$= (i+1)(3)$	P23
P14	$= (i+(n-2))(4)$	P54
P15	$= (i+2)(5)$	P35
P16	$= (i+(n-3))(6)$	P46

To the row development of initial row $i=1$ and $n=6$

Table 3.3. Comparison of power outputs

Sl. No	Topology	Efficiency η (%)
1.	Se-P	26.7%
2.	TCT	54.2%
3.	Sudoku	62.2%
4.	L-Shape [7]	60.7%
5.	Spiral-Pattern [8]	63.1%
6.	SL_H	67.8%
7.	SL_V	68.9%

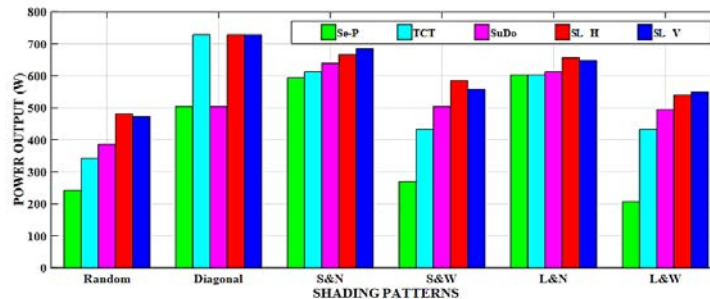


Figure 3.3. Power output comparison chart

For random irradiance, SL_H technique produces 6.70A of I_{sc} and 501W of P_m , similarly SL_V technique produces 6.65A of I_{sc} and 469W of P_m . The developed SL_H and SL_V are improved than existing techniques of Se-P, TCT, and sudoku patterns. During these uneven irradiances, the power productions from existing techniques are 234W, 324W, 368W respectively from Se-P, TCT, and sudoku patterns. The developed SL_H organization produces power with the effectiveness of 58.9% with the 66% of offered irradiance. Likewise, the developed SL_V reconfiguration produces power with the effectiveness of 59.1% with the 66% of offered irradiance. Another pattern such as Se-P, TCT, and sudoku has the

effectiveness of 41.1%, 43.0%, and 58.8% respectively. The developed SL_H and SL_V have good P-V and I-V curves than the existing reconfiguration. The effectiveness of the developed scheme is compared to L-shape reconfiguration [7] and spiral-pattern reconfiguration [8] methods. The two articles were about the array reconfigurations for reducing the divergence losses similar to the developed technique. The comparisons of power outcome results are given in Table 3.3. and Figure 3.3.

4. CONCLUSION

In this article, a new electrical array reconfiguration technique of solar PV system is developed based on the snake-ladder movement. The snake-ladder formation can be developed into two ways like horizontal snake ladder (SL_H) and vertical snake ladder (SL_V) pattern. The developed SL_H and SL_V were validated in the MATLAB software. These SL_H and SL_V reconfigurations were validated with different 6 types of possible variable irradiance. The results of the developed technique are compared with the existing array reconfigurations. The existing techniques are performing fine in few irradiance levels and performing bad in few irradiance levels. But the developed SL_H and SL_V array reconfiguration are performing well in all levels of irradiances. The performance of the PV system in different irradiances levels were improved using the developed SL_H and SL_V array reconfigurations.

REFERENCES

- [1] Christabel, S.C., et al., "Couple matching best generation algorithm for partially shaded photovoltaic systems", J. Electr. Eng, 2016, 16.
- [2] Srinivasan, A., et al., "Mitigation of mismatch losses in solar PV system – Two-step reconfiguration approach". Sol. Energy, 2020, 206, 640–654.
- [3] Prince Winston, D et al., "Performance improvement of solar PV array topologies during various partial shading conditions", Sol. Energy, 2020, 196, 228–242.
- [4] Palpandian, M, et al., "A New Ken-Ken Puzzle Pattern Based Reconfiguration Technique for Maximum Power Extraction in Partial Shaded Solar PV Array." IEEE Access 9 (2021): 65824-65837.
- [5] Nazeri, M, et al., "Firefly Algorithm-Based Photovoltaic Array Reconfiguration for Maximum Power Extraction during Mismatch Conditions." Sustainability 13, no. 6 (2021): 3206.
- [6] B. P. Kumar et al., "Performance Enhancement of Partial Shaded Photovoltaic System With the Novel Screw Pattern Array Configuration Scheme," in IEEE Access, vol. 10, pp. 1731-1744, 2022.
- [7] A. Srinivasan et al., "L-Shape Propagated Array Configuration With Dynamic Reconfiguration Algorithm for Enhancing Energy Conversion Rate of Partial Shaded Photovoltaic Systems," in IEEE Access, vol. 9, pp. 97661-97674, 2021.
- [8] S. K. Cherukuri et al., "Power Enhancement in Partial Shaded Photovoltaic System Using Spiral Pattern Array Configuration Scheme," in IEEE Access, vol. 9, pp. 123103-123116, 2021, doi: 10.1109/ACCESS.2021.3109248.

Android Based Campus Solution (AICS) for Department Management

¹Geerthik. S, ²Ranganathan. L, ³Anand. T, ⁴Sajitha. L. P

¹Department of Information Technology, Agni College of Technology, Chennai, India, geerthiks@gmail.com

²Department of Mechanical Engineering, Agni College of Technology, Chennai, India, ranganathan1975@gmail.com

³Department of Mechanical & Automation Engineering Agni College of Technology Chennai, anand.tvel@gmail.com

⁴Department of Computer Science and Business Systems, R.M.K Engineering College, Chennai, l.p.sajitha@gmail.com

Abstract

Android Based Campus Solution for Department Management is an app that helps manage and monitor the progress of students in a college or university. It can be used to track the performance of departments and to identify areas for improvement. The app can also be used to communicate with students and staff. The app allows departments to create and store student records, as well as track and manage student attendance, grades, and other data. The app is designed to work with the college's existing database, making it easy for departments to keep track of their student's data. The app is also integrated with Firebase, making it easy for departments to push updates and information to their students. The app also enables the management of departmental data, such as departmental budgets and staff. Additionally, the app can also help manage communication between departments.

Keywords. College Android App, Department App, Student data management, Education Management System, Information Retrieval

1. INTRODUCTION

A fast dissemination of information is essential considering the technological advancement and time. This is because there are now more advantages to automatic machines than there were in the past. This means that a lot of the work that was done by humans is now done by machines. These days, there is a need for machines that can do the work of humans in educational settings, like schools and colleges [1][2]. Students can consolidate their files and information thanks to advancements in computer technology that leverage the databases and apps in their information systems. An key part of this procedure involves Android. It results in the development of fresh methods for handling conventional transactional systems. The advancements in computer technology allow students to

consolidate their files and information by using databases and the information system's utility. Android is crucial to the processing of traditional transactional systems and contributes to its innovation [3][4]. The paper is discussing how technology has changed the way information is disseminated, and how this has changed the way educational institution function. It cites the example of the Department of Management at a school, which has switched from paper-based systems to mobile computing [5]. This has made it easier for students to access information and stay up-to-date on announcements and events. The essay concludes by discussing how the Android-based app "Act" has helped to resolve some of the issues associated with these changes.

With the increasing use of smartphones in recent years, many colleges and universities are now turning to Android-based solutions to help manage their departments and students [6]. Android apps offer a number of advantages over traditional desktop-based solutions, including the ability to manage student data on the go, keep track of departmental events and deadlines, and connect with other students and faculty members. The Android-based Campus Solution for Department Management is a comprehensive app that helps college and university administrators to manage their departments more effectively. The app provides a central database for storing student data, which can be accessed by departmental staff from anywhere. The app also includes a number of features for managing departmental events and deadlines, and for connecting with other students and faculty members.

The Android-based Campus Solution for Department Management is an essential tool for any college or university administrator looking to improve the efficiency of their department. The app's central database and easy-to-use interface make it simple to keep track of student data, departmental events, and deadlines, and to connect with other students and faculty members. The purpose of this research is to create and implement an Android-based Campus Solution for Department Management. The Android app was developed using Java and the Firebase database. The app was designed to help manage student data and department data. The app was tested on a group of students and faculty. The results showed that the app was able to manage student data and department data. The app was also able to help manage the education system. An application that allows the management of college departments and student data is called Android Based Campus Solution for Department Management. It uses a MySQL database and was created with Android Studio and Firebase. The software enables the insertion and removal of students from departments as well as the establishment and deletion of departments, as well as the maintenance of student data.

2. EXISTING SOLUTION

There is no application for students to download their study material and notes of the previous semester. The students are instructed to get the copy of their certificate from the College management. Students need to get the letter from the

department to get the copy of the certificate [2][6]. It leads to wastage of time to the students [5][6]. All the updates and announcements are circulated through paper form; it may or may not reach the students. The details of the students are recorded in the paper form it may lead to the loss of record. By using the existing system all the processes of the department may take lots of time to complete. The existing system doesn't have any module to get details about the students (resume, certificates, marksheets) for placement purposes [7]. In the past the working model didn't have study materials for arrear students [8]. In the existing system it does not contain an inbuilt chat system to communicate with staff of the department. On other hand the system does not hold any certificates, marksheet for future use of the students.

3. PROPOSED SYSTEM

For this investigation, both primary and secondary data were employed. For primary data collection, interviews were conducted with the professors and department heads of different colleges. This helped in understanding the requirements of the app and the way it should be developed. For secondary data collection, various articles, journals and websites were referred to get an understanding of the existing education management system and the way Android apps are developed. Both qualitative and quantitative methodologies were used to assess the data that was gathered. Both the quantitative and qualitative data were examined using descriptive statistics and content analysis, respectively. The Android app was developed using the Android Studio IDE. Firebase was used as the database for the app. The proposed system will be developed using the Android SDK. The app will be developed using the Java programming language. The app will use the Firebase database for storing the data. The data will be stored in the form of JSON objects.

The department heads will be able to view the data, add new students and staff, and edit the data. The first step is to create the project in Android Studio and add the required dependencies. Then, the Firebase database is set up and the necessary fields are created. The next step is to create the activities required for the app. The login page, the home page, the add student page, the view student page, the edit student page, and the delete student page are all included in the activities. The login page will be used to verify the user's identity. To access the other activities, utilise the home page as a navigational tool. New students will be added to the database via the add student page. The view student page will be used to view the details of the students. The edit student page will be used to edit the details of the students. The delete student page will be used to delete the students from the database. The system will be tested by adding, editing and deleting the students from the database. The results will be verified by checking the database. The system would be secure, using the Data Encryption Standard (DES) algorithm to encrypt data. Students would be able to view their attendance, class timetable, and department announcements. Staff would be able to manage student details,

add/delete student information, and call students and parents. The proposed system will be developed using the Android SDK. The app will be developed using the Java programming language. The app will use the Firebase database for storing the data. The data will be stored in the form of JSON objects. The department heads will be able to view the data, add new students and staff, and edit the data. The results of the study showed that the Android app developed was helpful for the departments to manage the students' data and the education system in a better way. The app was easy to use and had all the required features.

3.1 Proposed System Architecture

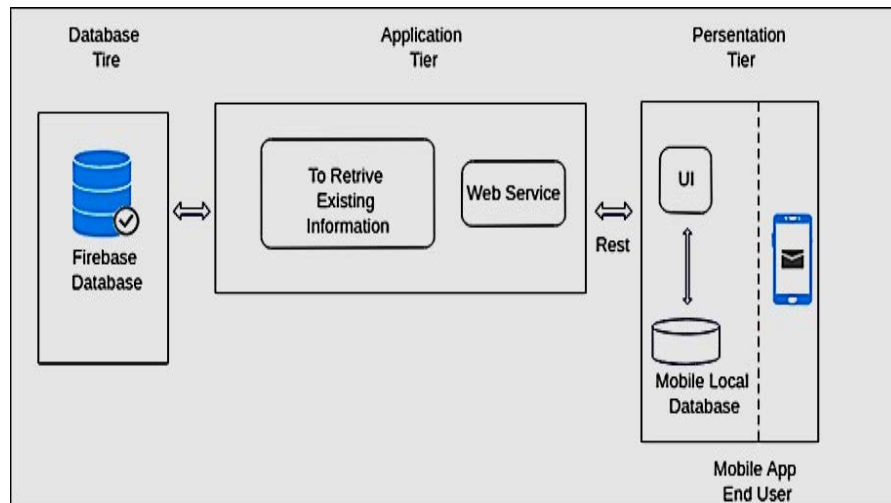


Fig 3.1. Proposed System Architecture

The architecture diagram in figure 3.1 represents the project module which is designed using hardware and software, which is useful for students.

3.2 Module Description

3.2.1 User Module

By giving an email address and password, we are authenticating users in this module. They will be directed to their screens if their email address and password are genuine. We use a distinctive email from an Android smartphone along with the information kept in the database to identify users. The system examines the status of that session and transfers control to the appropriate user-interface when they are matched up in the database.

3.2.2 Admin Module

By giving an email address and password, we are authenticating the HOD and employees in this module. They will be directed to their screens if their email address and password are genuine. The super admin of the system will create and update unique login credentials for each member of the departmental staff. The

admin homepage now has tools for taking attendance, uploading notes, the syllabus, and results, as well as sending notifications to students, which HOD or staff can access. The attendance recorded and uploaded outcomes of the students inside the module are also viewable by staff or HOD.

3.2.3 Login and Signup Module

The proposed work contains a login and signup screen for both the user and admin app. For user app users (Students) need to create an account by entering details like Register Number, Name, Academic Year, Department, Phone Number, Parents Phone Number, email all the data are stored in Firebase real time database. By using the login screen, the user (Student) is able to login to the app. For Admin app already login credentials for each individual staff created by the Super admin of the app.

3.2.4 Home Module

After successful login users and staff are redirected to the respected home page of the user and admin app. Both Apps which use the same Firebase database are interconnected. The Home page of the user will showcase the feature of the app (main features) and the admin app contains details of the department.

3.2.5 Time Table Module

The user of the app (Students) will be able to know their Academic Class Time Table within the app. The Time table of the academic year is uploaded by the Staff or admin from the admin app in the format of PDF. The PDF format is stored in Firebase Database & Firebase Storage as well. The Time Table for each Academic Semester will be uploaded separately.

3.2.6 Student Details Module

The main aim of the proposed system is to make the student details record in paperless mode. The admin or staff is able to view the details of each individual student of the department. These details of the students are uploaded by students while creating an account in the app and stored in firebase real-time database. In the student details module, the staff is able to call the student within the app and parents as well. These details are also helpful for placement purposes.

3.2.7 Attendance Module

Students' attendance can be taken by teaching staff at the beginning of the day, or throughout that time. The admin app's staff generates and sends QR codes, and the user has an attendance module with a scanner. When a student scans the attendance QR code, the information is saved in the Firebase database along with the user's location and time stamp. Users with college geolocation are only able to scan QR codes; otherwise, the system won't recognise the student's attendance for the specified day. He or she is not permitted to take attendance at any other time.

3.2.8 Announcement Module

The primary aim of the proposed system is for students to know the current updates, news and announcements of the department within the app via the Notification. By using the Firebase Push Notification, the feature is possible. When the Admin or staff update the announcement or news from the admin app it will be stored in Firebase real-time database and send it to the Firebase Push Notification. It will send the notification to the user of the app (students). By this feature all the activities of the department are known by each individual student of the department.

3.2.9 Notice Board Module

The main aim of this module is for students to know the daily updates of the department within the app. When the Admin or staff update the daily data or news of the department like placement updates, events updates and achievement of the students from the admin app it will be stored in Firebase real-time database. Both the user and admin app use the same Firebase database; the stored data is reflected in the notice board module in the user app. By this feature, daily activities of the department are known by each individual student of the department.

3.2.10 Notes and Syllabus Module

The main aim of this module is for students to get the syllabus and study material within the app. When the Admin or staff update the syllabus and Notes for each semester of the academic year from the admin app, it will be stored in Firebase real-time database and Firebase storage. Both the user and admin app use the same Firebase database; the stored data is reflected in the Notes and syllabus module in the user app. Users are able to search by subject code to get the Notes or Study material for all the semester within the app. It will be more helpful to students to get the study materials for the arrear examination. Students are able to view and download the Syllabus and notes.

4. TAL RESULT

The Results of the Proposed System will be displayed shown in figure 4.1 - 4.9 and it will be tested with the android version of ANDROID 8 / ANDROID 9 / ANDROID 10 and ANDROID 11. The proposed system is compared in various android platforms and it performs better in the latest versions compared with the previous versions. The information retrieval speed is higher in ANDROID 11 compared with ANDROID 10. The request rate and error rate per client is also better in the updated versions.



Fig 4.1. Login Module



Fig 4.2. Signup Module



Fig 4.3. Home Module



Fig 4.4. Explore Module



Fig 4.5. Admin Home Module

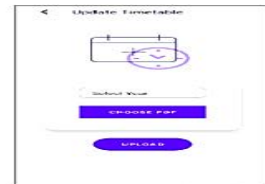


Fig 4.6. Admin Time Table

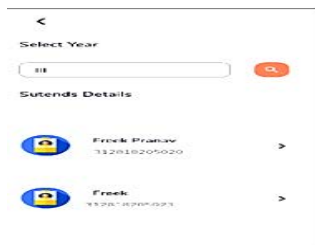


Fig 4.7. Student Details Module



Fig 4.8. Student Contact Details



Fig 4.9. Student Parents Details

5. CONCLUSION

The Android-Based Campus Solution for Department Management is a great tool for managing student data. It is flexible and has a lot of features that make it a great choice for managing student data. It helps in the easy and efficient management of student data and departmental information. The use of Firebase as the database for this system makes it very convenient to use. The Android-based Campus Management System is a great tool for managing college. The app is very user-friendly and is very helpful for managing education systems. It is easy to use and has numerous features that make it very useful for college administrators. The app is also very affordable, which makes it a great option for colleges and departments that are on a budget. Overall, the Android Based Campus Solution for Department Management is a great choice for managing student data. The proposed system is an Android application for managing departments in a college. The app will be used by the department heads to manage the students and staff in their department.

REFERENCES

- [1] Dhiman, R., & Basral, A. (2019, March). A New Android Application (Breeze) for College Management System. In 2019 3rd International Conference on Computing Methodologies and Communication (ICCMC) (pp. 1-3). IEEE.
- [2] Malhotra, R., Kumar, D., & Gupta, D. P. (2020). An android application for campus information system. *Procedia Computer Science*, 172, 863-868.
- [3] Mhalgi, S., Marne, P., Kulkarni, M., Kapure, S., & Shekapure, S. (2019). Cloud based android app for college canteen management system. *IJRAR*, 6(1), 969-972.
- [4] Kumar, M. A., Srinivas, C. M., Reddy, K. V. V., & Kumar, K. K. (2018, June). College Activity Management System. In 2018 Second International Conference on Intelligent Computing and Control Systems (ICICCS) (pp. 1-4). IEEE.
- [5] Lau, N., O'Daffer, A., Colt, S., Joyce, P., Palermo, T. M., McCauley, E., & Rosenberg, A. R. (2020). Android and iPhone mobile apps for psychosocial wellness and stress management: systematic search in app stores and literature review. *JMIR mHealth and uHealth*, 8(5), e17798.
- [6] Yu, J. (2019, August). Design of a lightweight autonomous learning system for the course of software testing based on android. In *Journal of Physics: Conference Series* (Vol. 1288, No. 1, p. 012051). IOP Publishing.
- [7] Gao, Zhigang et al. "A Student Attendance Management Method Based on Crowdsensing in Classroom Environment." *IEEE Access* 9 (2021): 31481-31492.
- [8] D. Mijić, O. Bjelica, J. Durutović and M. Ljubojević, "An Improved Version of Student Attendance Management System Based on RFID," 2019 18th International Symposium INFOTEH-JAHORINA (INFOTEH), 2019, pp. 1-5, doi: 10.1109/INFOTEH.2019.8717750.

Enhanced Machine Learning Technique for Multi-Stages Alzheimer's Disease Classification

S Bhavya Sri¹, S Keerthi², Md Hassan³, R. Karthikeyan⁴

^{1,2,3,4}Department of CSE (AI&ML), Vardhaman College of Engineering, Hyderabad, Telangana.

Email: bhavyasrisanka2603@gmail.com, keerthi.sirnam@gmail.com,
karthikhonda77@gmail.com

Abstract

Recently, there has been a lot of concern about Alzheimer's. Around 45 million people around the world are affected by this illness. Alzheimer's is a degenerative mental condition with no recognized early stages that typically affects elderly people. It took away people's capacity for thought, reading, and a wide range of other activities. The sickness is identified, but only at an advanced stage. Therefore, if the condition is identified earlier, its symptoms may be slowed. Neuroimaging methods including CT, MRI, PET, and EEG are also indicated for people who also experience additional symptoms like behavioural and psychological problems, as well as cognitive mental impairments like confusion and amnesia. Traditional procedures for diagnosing Alzheimer's disease (AD) are time-consuming, and learning and practising them requires a significant amount of effort. The major goal is to identify individuals who are showing early signs of Alzheimer's disease. So, we use CDR and SMMSE tests online before moving on to MRI or CT scans, and then follow them up with machine learning algorithms to evaluate the data along with test results. With the aid of these tests, it will be possible to identify Alzheimer's disease in its early stages. An ML framework can help resolve this issue by diagnosing the disorder. The outcomes and examination of numerous machine learning models aimed at dementia diagnosis are presented in this work. The most precise variables for Alzheimer's disease prediction have been discovered using a range of techniques, including Decision Tree, Random Forest, Support Vector Machine, and K Nearest Neighbour classifiers. Predictions for Alzheimer's disease are made using the Open Access Series of Imaging Studies (OASIS) data, and the effectiveness of ML models is evaluated using metrics including Precision, Recall, Accuracy, and F1-score. Despite the dataset's limited size, some important numbers are included. Two machine learning models were utilized to analyze the data. Following system development, findings demonstrate that SVM performs better than other models. Based on metrics, we can say that SVM gives the best results. The method is simple and can assist people in identifying dementia promptly.

Keywords. Stages in Alzheimer's disease, Support Vector Machine, Logistic Regression, Decision Tree Classifier, K-Nearest neighbour.

1. INTRODUCTION

Originally, Technology that imitates and exhibits "human" cognitive abilities connected to the human mind, such as "learning" and "problem-solving," is referred to as "artificial intelligence." Major AI researchers are increasingly describing AI in terms of reason and behaving rationally [1]. They reject this notion and do away with all restrictions on what constitutes intelligence.

TABLE-I ALZHEIMER STAGES AND SYMPTOMS

S.NO	STAGE OF ALZHEIMERS	SYMPTOMS INCLUDES
1	Early stage	<ul style="list-style-type: none"> ❖ Misplacing the items unknowingly ❖ Losing track of place and thing names ❖ Repeating themselves frequently, for as by repeatedly posing the same query becoming hesitant
2	Moderate stage	<ul style="list-style-type: none"> ❖ Confusion and disorientation are getting worse ❖ Impulsive, obsessive, or repeated behaviour ❖ Delusions (believing things that are untrue) ❖ Issues with language or speech (aphasia) ❖ Sleep disturbances ❖ Mood fluctuations that are regular or that cause you to feel angry, nervous, or frustrated ❖ Poor judgement and poor decision making
3	Advanced stage	<ul style="list-style-type: none"> ❖ Difficulty moving or changing positions without assistance ❖ Significant weight reduction ❖ Speech short-term and long-term memory gradually decline

Robots can display artificial intelligence (AI), which is intelligence, in contrast to the Animals, including humans, have innate intellect. The learning of intelligent agents, or any system that senses its environment and acts to increase its chances of success, is called artificial intelligence (AI). People are unable to interpret, assess, and make judgments using even a small percentage of the vast amount of data that exists in today's society [13]. To make such complex decisions, higher cognitively capable entities than humans are required.

A subfield of computer science and artificial intelligence (AI) called "machine learning" aims to mimic human learning by using data and algorithms to gradually increase a system's accuracy. This area of research focuses on comprehending and developing "learning" strategies, or methods that employ data to enhance performance on a certain set of tasks. Without being expressly instructed to do so, machine learning algorithms create a model from sample data, commonly referred to as training data, to generate predictions or judgments. Machine learning techniques are used in a variety of domains, such as speech recognition, email filtering, computer vision, and many more, when utilising standard algorithms is either impossible or impractical [3].

Support Vector Machine (SVM), one of the most popular supervised learning techniques, is applied to classification and regression problems.

2. ALZHEIMERS DISEASE AND STAGE PREDICTION

Alzheimer's sickness is a neurological disorder that causes mind atrophy and cell death, which impairs memory and cognitive function. Alzheimer's illness, the furthestmost prevalent type of dementia, impairs a person's capacity for independent living and is categorised by a stable decline in social, interactive, and cognitive skills. The main symbol of Alzheimer's illness is memory loss. one of the original signs is having trouble recalling previous conversations or events. As the condition worsens, memory issues get worse, and new symptoms start to show up. Alzheimer's disease-related brain modifications result in increasing problems with:

- Memory
- Reasoning and Thinking
- Making judgements and decisions
- Making similar plans and carrying them out
- Changes in personality and behaviour
- Maintained expertise

3. RELATED WORK

[1] In this study, the rapid shift clustering technique is used to partition the dataset into smaller groups in the embedded space. The experiments employing the recommended approaches show incredibly strong performance for clustering images into AD and normal ageing using the Clinical Dementia Rating (CDR) scale as a benchmark. [2] In this work, three biomarker modalities—MRI, FDG-PET, and CSF biomarkers—were integrated using a kernel combination approach with a 93% accuracy rate to distinguish between AD and healthy controls. [3] Outlined a novel method for automatically differentiating between older controls and based on a comprehensive classification of hippocampus shape parameters, patients with Alzheimer's disease (AD) or mild cognitive impairment (MCI). [4] This study proposes a fully automated system for categorising patients with Alzheimer's disease (AD) and elderly control participants based on diffusion tensor imaging (DTI) and anatomical magnetic resonance imaging (MRI).

[5] The proposed methodology is based on the 95% accurate selection of voxels that show Welch's t-test results over a specified threshold between the two groups, normal and Alzheimer images. Study [6] discusses how structural magnetic resonance imaging can be used to diagnose Alzheimer's disease by estimating the three-dimensional displacement field. The methods [7-9] employ conventional computer vision methods. [10] This study briefly describes the classification of Alzheimer's illness founded on the structural MR images using Neural networks whereas [11] study shows the results in classification between having Alzheimer's or not based on Convolutional Neural Networks. Approaches [12–13] use deep CNN to forecast the disease. [14] In this study, the disease is classified based on the automated MR images with the help of Deep learning model. [15] This approach describes the classification of the disease based on the Deep Learning based CNN approach on MR images. [16] Study helps to classify the type of disease with the help of Deep Learning algorithms. The results in classification between having Alzheimer's or not based on Convolutional Neural Networks.

4. ATTRIBUTES APPLIED IN CLASSIFICATION SYSTEM

4.1. *Socioeconomic Status (SES)*

The term "socioeconomic status" refers to a person or group's social standing or class. Utilizing a combination of work, money, and education is a common method of assessment. The analysis of socioeconomic statuses frequently uncovers differences in resource access as well as issues with privilege, power, and control.

4.2. *Total Intracranial Volume Assumed (TIVA)*

Total intracranial volume (TIV/ICV), which can serve as a stand-in for maximum premorbid brain capacity, is a vital covariate for volumetric assessments of the intelligence and different intelligence areas, predominantly in the learning of neurodegenerative illnesses. The gold-standard method for manually outlining brain images demands meticulous labour from knowledgeable operators.

4.3. *Standard Mini Mental State Examination (SMMSE)*

The Standard Mini-Mental State Inspection, often recognised as the Folstein test, is a 30-item survey that is widely applied in clinical and research contexts to evaluate intellectual impairment. In medicine and allied health, dementia screening is a common practise. It is a helpful instrument for recording a patient's response to therapy since it is also used to follow the progression of a person's cognitive changes over time and assess the severity and development of cognitive impairment.

4.4. *Clinical Dementia Rating (CDR)*

The CDR is calculated using a semi-structured interview with the subject and the caregiver (informant), as well as the clinician's clinical judgement. The CDR is determined by evaluating six different cognitive and behavioural domains on a scale of 0 to 5, including memory, orientation, judgement, and problem-solving, as well as community affairs, home and hobby performance, and personal care performance.

TABLE-II ALZHEIMER STAGES AND SYMPTOMS

	No dementia	Early Stage	Moderate Stage	Advanced stage	Maximum Score
SMMSE	24 - 30	19 - 24	10 - 19	0 - 9	30
CDR	0 – 0.5	0.5 - 1.0	1.0 - 2	3 - 5	5

4.5. *Normalised Whole Brain Volume (NWBV)*

Among the most well-researched techniques for calculating the progression of neurodegeneration in MS are measurements of changes in normalized brain volume and brain parenchymal fraction (BPF) across time.

5. IMPLEMENTATION

5.1 Logistic Regression

Logistic regression is one of the most well-liked machine learning methods that falls under supervised learning. A set of independent variables is used to predict the category dependent variable.

5.2 Decision Tree Classifier

Classification and regression issues can be resolved using the supervised learning technique known as a decision tree, however this approach is frequently preferred.

5.3 K Nearest Neighbours

K-Nearest Neighbour, which employs the supervised learning approach, is one of the simplest and most fundamental machine learning algorithms. A new data point is classified based on similarity, and all previously saved data is also stored.

6. RESULTS AND ANALYSIS

Accuracy is defined as the number of events that were accurately predicted. It falls under a specific label for classification. It is a frequently used presentation measuring criterion in a wide range of applications. It is the best production measurement criterion for datasets with an equal number of false positives and false negatives, or symmetric datasets. It is specified as:

True Positive=TP

False Positive=FP

True Negative=TN

False Negative=FN

$$\text{Accuracy} = (\text{TP} + \text{TN}) / (\text{TP} + \text{TN} + \text{FP} + \text{FN})$$

TABLE III ACCURACY COMPARISON

Algorithms used	Accuracy	F1 Score	Recall	Precision
K-Nearest Neighbour	87.33	85.46	84.74	86.33
Support Vector Machine	96.00	95.65	91.67	94.86
Decision Tree Classifier	93.33	92.96	94.44	97.06
Logistic Regression	94.67	94.29	91.67	97.06

7. CONCLUSION AND FUTURE ENHANCEMENT

There is a chance that disease detection will get more precise. It is possible to create multi-model frameworks to have a more precise detection system. The data that is widely used in the diagnosis of neurological illnesses is OASIS data. It will be helpful to have a framework for sifting through numerous data sources and extracting information that can be used to diagnose Alzheimer's. Our system will be more accurate if we combine these to more sources. We employ numerical data that is processed using machine learning algorithms in order to identify subjects with Alzheimer's disease and examine data relating to brain regions

affected by the disease. Compared to other techniques, Support Vector Machine performs much more accurately.

REFERENCES

- [1] Martin T. Hagan and Mohammad B. Menhaj, "Training feedforward networks with the Marquardt algorithm," *IEEE Transactions on Neural Networks*, vol. 5, no. 6, pp. 989-993, November 1994.
- [2] Zhang D, Wang Y, Zhou L, Yuan H, Shen D and the Alzheimer-s Disease Neuroimaging Initiative, "Multimodal classification of Alzheimer-s disease and mild cognitive impairment," *Neuro Image*, vol. 55, no. 3, pp. 856-867, April 2011.
- [3] Gerardin E, Chetelat G, Chupin M, Cuingnet R, Desgranges B, Kim HS, Niethammer M, Dubois B, Lehericy S, Garnero L, Eustache F, Colliot O and the Alzheimer-s Disease Neuroimaging Initiative, "Multidimensional classification of hippocampal shape features discriminates Alzheimer-s disease and mild cognitive impairment from normal aging," *Neuro Image*, vol. 47, no. 4, pp. 1476-1486, October 2009.
- [4] Chupin M, Gerardin E, Cuingnet R, Boutet C, Lemieux L, Lehericy S, Benali H, Garnero L, Colliot O and the Alzheimer-s Disease Neuroimaging Initiative, "Fully Automatic Hippocampus Segmentation and Classification in Alzheimer-s Disease and Mild Cognitive Impairment Applied on Data From ADNI," *Hippocampus*, vol. 19, no. 6, pp. 579-587, June 2009.
- [5] M. Lopez, J. Ramirez, J.M. Gorriz, D. Salas-Gonzalez, I. Alvarez, F. Segovia and C.G. Puntonet, "Automatic tool for Alzheimer-s disease diagnosis using PCA and Bayesian classification rules," *Electronics Letters*, vol. 45, no. 8, pp. 389-391, April 2009.
- [6] S. Wang, Y. Zhang, G. Liu, P. Phillips, T.-F. Yuan, Detection of Alzheimer's disease by three-dimensional displacement field estimation in structural magnetic resonance imaging, *J. Alzheimer's Dis.* 50 (1) (2016) 233–248.
- [7] Beheshti, Iman, Norihide Maikusa, Hiroshi Matsuda, Hasan Demirel, and Gholamreza Anbarjafari. "Histogram-Based Feature Extraction from Individual Gray Matter Similarity-Matrix for Alzheimer's Disease Classification." *Journal of Alzheimer's Disease* 55, no. 4 (2017): 1571-1582.
- [8] I. Beheshti, H. Demirel, H. Matsuda, Alzheimer's Disease Neuroimaging Initiative, et al., Classification of Alzheimer's disease and prediction of mild cognitive impairment-to-Alzheimer's conversion from structural magnetic resource imaging using feature ranking and a genetic algorithm, *Comput. Biol.Med.* 83 (2017) 109– 119.

Fuzzy Logic Controlled Hierarchical Power Management Scheme for A Solid-State Transformer (SST) Interfaced DC Micro Grid

Udutha Satheesh¹, B. Raja Gopal Reddy²

¹Department of EEE, Vardhaman College of Engineering, Hyderabad, Telangana, India
uduthasatheesh360@gmail.com

²Department of EEE, Vardhaman College of Engineering, Hyderabad, Telangana, India
b.rajagopalreddy@vardhaman.org

Abstract

The system integration of an advanced, integrated solid-state transformer (SST) micro-grid system is examined and, for the first time, used in this project. A power management strategy is required for this system in order to allow operating in islanding mode operation, SST-enabled operations, as well as the smooth switching between two modes. The recommended power management technique includes three levels of control: First control is for the local controller, second control for recovering the bus voltage of the dc micro grid, and third control for controlling battery state of charge.

This project delves into the proposed system design and control methodologies, as well as constructing a micro grid simulation to test the system's performance. All three regulating processes are controlled using the fuzzy logic technique in this project. For all three controlling operations in this project, the fuzzy logic control technique is applied. This project delves into the proposed system design and control methodologies, as well as constructing a micro grid simulation to test the system's performance. For all three controlling operations in this project, the fuzzy logic control technique is applied. This project delves into the proposed system design and control methodologies, as well as constructing a micro grid simulation to test the system's performance. All three of the above are controlled in this project using fuzzy logic control.

Keywords. Power management, fuzzy logic controller, solid state transformer (SST), Dc-microgrid.

1. INTRODUCTION

Distributed generation (DG) is becoming more and more popular as a result of the decade-long rapid advancement of renewable energy technology [1]. Offering a continuous and stable supply of energy is difficult since the output power of

distributed renewable resources (DRER) electricity depends on a number of uncontrollable natural elements, such as solar irradiance and wind speed.

Finding qualified DG electricity is a major problem for engineers, and micro grids seem to be a workable solution. The micro grid is composed of power electronic-based distributed renewable energy resources [DRER] and distributed energy storage devices [DESD], which can operate in island mode in rural regions and offer reliable and adaptable power to the conventional grid. Based on its architecture, micro grids fall into two kinds [2]. The a.c micro grid is the first, while the D.C micro grid is the second.

The dc micro grid does have the following benefits over the ac micro grid:

1. Hybrid systems that feed into a micro grid from a variety of power sources are simpler to build and may be expanded as needed.
2. They are more efficient since many power conversion steps are eliminated and filter requirements are reduced.
3. Renewable resources are easy to incorporate, particularly for Photovoltaic cell, fuel cell, battery, super capacitors, and so on.
4. They will be able to directly send power dc loads such as projectors, LEDs, and electric vehicles.

The present dc micro grid, on the other hand, can only connect to the distribution system via a big and bulky line frequency transformer and rectifier, which takes up too much space. Furthermore, grid support features such as harmonic filtering, VAR compensation and other grid support functions may not be available when passive transformer interfaces with the distribution system. A research focus is maintained on designing a much smaller and active grid interconnect to allow a more efficient dc micro grid system. The dc micro grid additionally encounters various issues in terms of power management, to name a few:

1. How to provide the loads or the utility with long-term and stable power.
2. How to regulate every element with in micro grid system intelligently; and
3. How to make the most of distributed renewable energy resources (DRER) and distributed energy storage system devices (DESD) in light of their character peculiarities.

• In this study, SST [3] is combined with a fuzzy logic controller to maintain a steady voltage profile and increase system stability.

To regulate the micro grid, a combination of multiple techniques has been devised. Artificial intelligence (AI) has also been used by certain researchers as a major or secondary tool to operate and manage micro grids. Fuzzy logic-based control is the most common application of all AI systems, notably among power system engineers

and the industrial electronics application industry. In many areas of science and engineering, fuzzy logic is a simple and useful tool rather than classical Boolean logic. The researchers favor a fuzzy logic-based control approach [4,5].

Because it has various advantages such as dependability, precision, simplicity, and ease of implementation. It is also utilized as a trustworthy tool for power system management, motor speed control, aeronautical control, power conversion control, and photovoltaic systems (PV) system, Maximum Power Point Tracking (MPPT) algorithm, among other things [6,7]. Particle swarm optimization (PSO) technique, multi-agent-based control, modified hill-climbing, fuzzy logic control, methods, and other current noteworthy research tactics in micro grid control include.

Using simulation and case studies, a fuzzy logic-based management and control system for a hybrid power system is devised and confirmed in this work [7,8].

The following are the major control objectives:

- To manage overall power generation in a micro grid while taking into account load variations.
- Managing the power needed for the storage system while taking into consideration both load changing and charge storing system.
- To avoid using diesel generators to power the storage system.
- To avoid the generators and storage system from supplying electricity when an external load is required.

2. SYSTEM DESCRIPTION

A 380V dc bus bar is enabled by the solid-state transformer (SST) in the Upcoming Renewable Electric Energy Delivery and Management System, essentially producing an SST enabled dc micro grid, as shown in Figure 1. The SST transports power between both the distribution network and the low-voltage dc system, allowing real power monitoring of the dc micro grid, which includes DRER, DESD, and loads (380 V). Dc/dc converters link these devices to a common 380 V bus. The SST-enabled dc micro grid, in comparison to the traditional transformers plus rectifier architecture, not only acts as an active grid interface, needing less size and space but it may also effectively supply reactive power, balance harmonic currents, and so on.

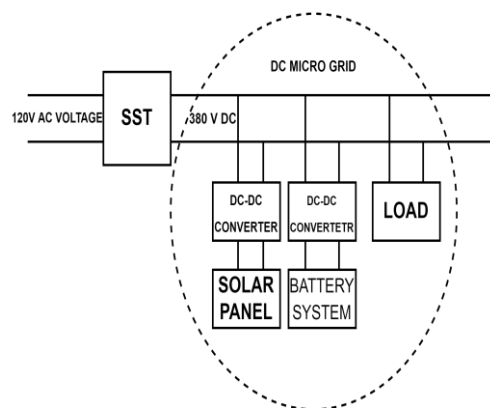


Figure 1. Block Diagram

It also serves as an interface to the distribution network for both ac and dc home grids. Whenever the dc micro grid goes offline from the SST in a system, the islanded mode is defined. The SST-enabled mode is defined because when the dc micro grid is interconnected to the SST. This study makes a significant contribution by demonstrating the simulation integration of SST with dc micro grid for the first time to illustrate the practicality of this innovative concept. A power control strategy is also required to ensure the efficient and optimum operation of the micro grid under various operating situations.

3. SST INTRODUCTION

It is also clear from the SST's design that it may be possible to obtain some additional potential features not available with regular transformers. First, solid-state semiconductor device and circuits, similar to Facts controllers, allows for both current and voltage regulation. This offers prospective benefits including power flow management, fault current limiting, voltage sag compensation, and other features that standard transformers cannot provide. The SST can thus improve the electricity distribution grid's stability and controllability. Second, voltage source converters linked to the SST's secondary terminal could easily support a regulated dc bus that could be attached to the dc micro grid, allowing the new micro-grid design to be implemented. The SST architecture used in this research is seen in Figure 2, with the front-end being a cascaded seven-level rectifier.

The floating dc links of the rectifier are connected to three dual active bridge (DAB) converters, with the secondary connected in parallel. As a result, a lower voltage bus is created. A lower voltage a.c terminal can be generated using a single-phase inverter. provide detailed details on this simulation and control mechanism.

4. SOLAR CELL

Sun-based cells, as their name implies, are designed to convert (at least a part of) available light into electrical energy. This is performed without using synthetic processes or moving parts. The sun-based cell, that is mostly constructed of PV wafers, produces power without using an electrolytic effect by directly converting the energy from the sun from sun-oriented illumination into the voltages and flows for load. The solar-powered cell is

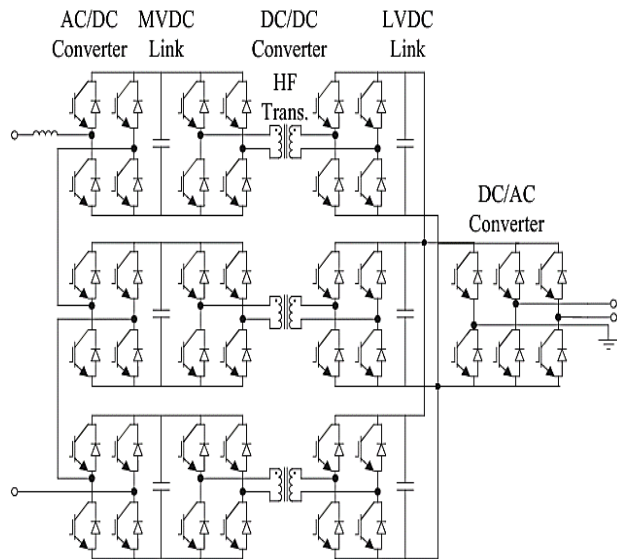


Figure 2. Topology of Presented SST

sometimes referred to as a PV cell because the electrical energy is obtained directly from the semiconductor's PN junction [9]. The similar circuit of a solar-powered cell is shown in Figure 3.

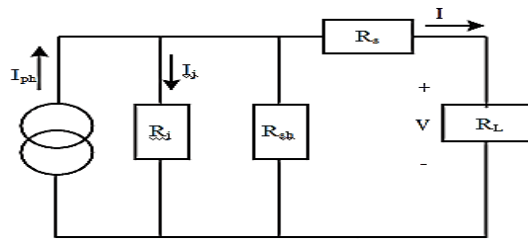


Figure 3. Equivalent Circuit of PV Array

The newest source the photo-voltaic current with in cell is controlled by I_{ph} , the nonlinear obstacle at the p-n junction is controlled by R_j , and the conventional series and shunt safeties are controlled by R_s and R_{sh} , respectively. Normally, R_{sh} has a very high value while R_s has a very low value. Therefore, in order to improve the research, both of them might be disregarded. Photovoltaic cells arranged in larger clusters are what make up PV modules. By joining devices in a series-equal mix, PV clusters can likewise be created. The numerical approach used to create the PV display handles the condition. Where n_s is just the number of series cells, n_p is the number of equal cells, q is the charge of an electrons, and K is the Boltzmann steady, I is the PV cluster producing current, V is the PV exhibit yield voltage, and n_s , n_p , and q are all numerical values. A_n , T , and I_{rs} all address the p-n intersection ideality factor, cell temperature, and invert immersion current, respectively.

5. FUZZY LOGIC CONTROLLER

Fuzzy logic is used successfully in a variety of control applications. Almost every item purchased has some form of fuzzy control. Controlling the temperature of the room with a forced-air system, anti-lock brakes in automobiles, clothes washers, traffic signal control, massive financial frameworks, and so on are just a few examples. A control device is a collection of real-world components that are used to alter the behavior of another real-world structure so that it exhibits the desired characteristics [10].

The following are among some of the reasons why fuzzy logic is used in charge frameworks.

- It's vital to fully know the concept and the objective rationale while using regular control. This makes it difficult to apply in some circumstances.
- By using fluffy logic for control, we can use human knowledge and experience to construct a regulator.
- The fantastic designing a control framework is the fuzzy control principles or IF-THEN standards. The significant segments of the FLC, as seen in the above image, are as follows:

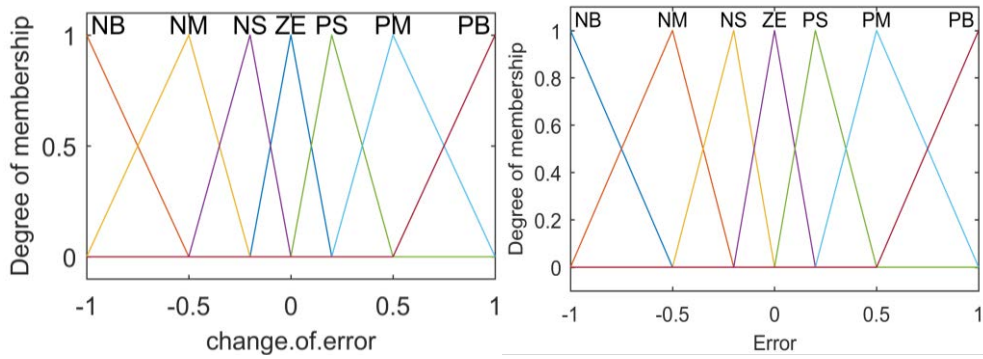


Figure 4: Membership Functions of Fuzzy Inputs

6. SIMULATION RESULTS

At initial stage the 120 v AC input voltage (as shown in Figure 5) is given to SST, SST converts the 120 v AC to 380 v DC at the final stage of the SST output, and the output is fed to the DC micro grid. The operation of the proposed system flows by taking input at SST from an AC source and processes the voltage through AC/DC converter and MVDC link, which undergoes different stages of operations and system tries to maintain a constant output voltage.

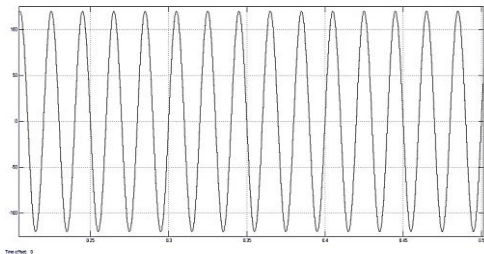


Figure 5. A.C Input Voltage

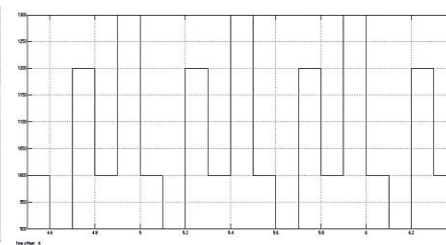


Figure 6. PV Panel Irradiance

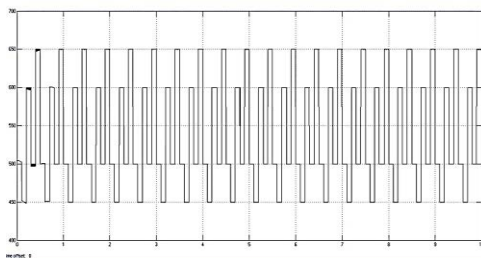


Figure 7. PV Panel Voltage

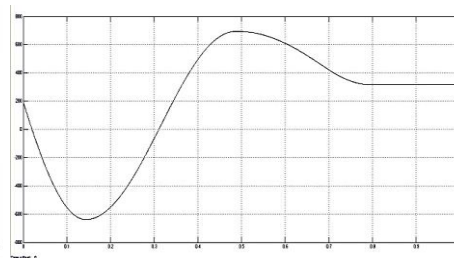


Figure 8. PV System Final Stage Output Voltage

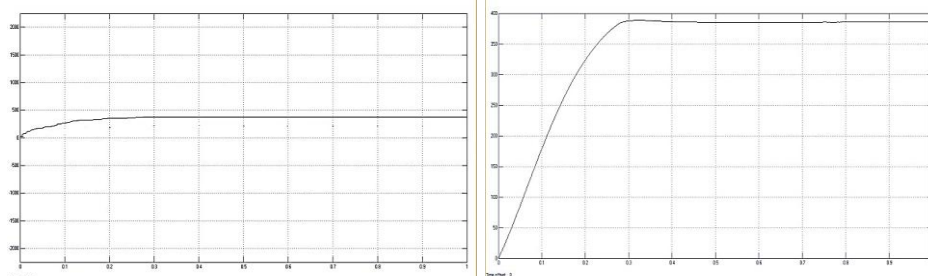


Figure 9. Battery System Output Voltage

Figure 10. D.C Micro Grid Voltage

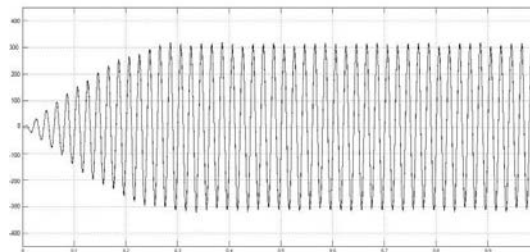


Figure 11. A.C Load Voltage Response

The fuzzy logic controller based on the errors in the system inputs , it generates the switching pulses for maintaining the constant output voltage at 380 v , the fuzzy controller also provides inputs to the battery and the PV system which do not have a constant output due to change in irradiance conditions(as shown in Figure 6) ,the switching inputs are given such that the both systems will maintain the output which will match the SST output(as shown in Figure 8,Figure 9), by maintaining all the voltages at a proper level, the micro grid will have a balanced voltage (as shown in Figure 10)to supply the loads, from Figure 11 we can observe that AC load connected to it have a consistent load voltage of 300 v.

7. CONCLUSION

In this study, a hybrid micro grid power regulation system based on fuzzy logic is developed. An active grid interface which is more compact and lightweight than previous micro grid architectures is used by the presented micro grid system to communicate with the distribution network. The proposed micro grid is really a significantly smaller system as a result. The dc micro grid can operate more reliably in islanding mode by employing primary control, and it can quickly switch between islanding operation mode and SST-enabled operating mode by using secondary control. The paper's main contribution is the incorporation of battery state - of - charge (SOC) inside tertiary control for battery storage management via regulated charging and discharge. To further verify that the system stays reliable, more PV panels will also be connected to the dc bus.

8. REFERENCES

- [1] F. Lei, "Typical Design and Simulation Experimental Study of DC Micro-grid Control System," 2018 China International Conference on Electricity Distribution (CICED), 2018, pp. 2320-2324, doi: 10.1109/CICED.2018.8592425.
- [2] H. H. H. De Silva, D. K. J. S. Jayamaha, N. W. A. Lidula. Review on design and control of solid-state transformer based microgrids[J]. AIMS Energy, 2019, 7(6): 901-923. doi: 10.3934/energy.2019.6.901.
- [3] X. She, A. Q. Huang, and X. J. Ni, "Current sensor less power balance strategy for dc/dc converters in a cascaded multilevel converter based solid-state transformer," IEEE. Trans. Power. Electron., vol. 29, no. 1, pp. 17–22, Jan. 2014.
- [4] A. AlKassem, M. Al Ahmadi and A. Draou, "Modeling and Simulation Analysis of a Hybrid PV-Wind Renewable Energy Sources for a Micro-Grid Application," 2021 9th International Conference on Smart Grid (icSmartGrid), 2021, pp. 103-106, doi: 10.1109/icSmartGrid52357.2021.9551215
- [5] J. M. Guerrero, M. Chandorkar, T. Lee, and P. Loh, "Advanced control architectures for intelligent micro grids—part I: Decentralized and hierarchical control," IEEE Trans. Ind. Electron., vol. 60, no. 4, pp. 1254–1262, May 2013
- [6] S. Tarannum and S. Jabin, "A comparative study on Fuzzy Logic and Intuitionistic Fuzzy Logic," 2018 International Conference on Advances in Computing, Communication Control and Networking (ICACCCN), 2018, pp. 1086-1090, doi: 10.1109/ICACCCN.2018.8748844
- [7] K. M. Sreedivya, P. A. Jeyanthi and D. Devaraj, "Fuzzy logic-based power system stabilizer for damping low frequency oscillations in power system," 2017 International Conference on Innovations in Electrical, Electronics, Instrumentation and Media Technology (ICEEIMT), 2017, pp. 201-205, doi: 10.1109/ICEEIMT.2017.8116835
- [8] D. Popescu, R. C. Dinu and C. Bratu, "Fuzzy control of cooling water pumps related to a power plant," 2017 International Conference on Electromechanical and Power Systems (SIELMEN), 2017, pp. 541-545,
- [9] Z. Chen, K. Wang, Z. Li and T. Zheng, "A review on control strategies of AC/DC micro grid," 2017 IEEE International Conference on Environment and Electrical Engineering and 2017 IEEE Industrial and Commercial Power Systems Europe (EEEIC / I&CPS Europe), 2017, pp. 1-6.
- [10] S. Shi, Y. Zhang, C. Fang, Y. Wang, A. Ni and Z. Fu, "Energy Management Mode of the Photovoltaic Power Station with Energy Storage Based on the Photovoltaic Power Prediction," 2019 6th International Conference on Systems and Informatics (ICSAI), 2019, pp. 319-324, doi: 10.1109/ICSAI48974.2019.9010143

Design and Implementation of a Low-Cost Fully Automated Solar-Powered Mower Vehicle

R. Harshvardhan¹, A. S. S. Murugan², D. Obulesu³ and N. Karuppiah⁴

^{1,2,3}Department of EEE, CVR College of Engineering, Mangalpalli, RR District, Telangana

⁴Department of EEE, Vardhaman College of Engineering, Kacharam, Hyderabad, Telangana

Email: 83.harsha@gmail.com, assm17174@gmail.com, dakkaobulesh@gmail.com, natarajankaruppiah@vardhaman.org

Abstract

This research concentrates on the hardware design of a photovoltaic grass cutter, which is used to cut various grasses for various uses. A solar panel with a battery system will provide the supply for the DC motor with cutting blades assembly. The paper focuses on using digital technology where a robot vehicle can cut the grass on a lawn, small farm, etc. The system will be totally automated. Obstacles in the path are detected with the help of an ultrasonic sensor. This structure uses four motors, two of which are used for grass cutting (high-speed DC motors) purposes, and the other two are utilized for vehicle movement. For power saving and automation purposes, the system is developed with a solar panel and battery.

Keywords. Solar pv panel, Mower vehicle, Ultrasonic sensor, Motor, Battery.

1. INTRODUCTION

In general, the wide grasslands in various places of institutions, green spaces, and nature reserves are maintained by garden labour with his hand and scissors. However, it is not uniform, and completing the assignment within the time limit is not a simple task and requires a significant amount of human work. The only viable answer is automation, which has decreased both time and labour requirements [1-2]. Today's globe is experiencing a shortage of electricity and all other quasi energy sources, and these resources could eventually run out [3]. Therefore, we focused on environmentally friendly renewable energy sources like the sun's electricity.

The photovoltaic-powered mowing robot is a completely automated machine that uses little energy and needs few workers to cut the grass [4-6]. It also identifies obstructions in the way and adjusts the movement direction accordingly. There is no need for human interaction.

If something gets in the way of the grass cutter, the proximity sensor detects it and sends a signal to the microcontroller to adjust the direction [7]. The sensors

function as an automated machine's eyes. A blade is attached to the automated equipment that cuts the grass swiftly and at a high RPM [8].

2. WORKING OF SOLAR MOWER VEHICLE

It is equipped with photovoltaic panels that are set up so that it is simple to take in the sun's intense solar radiation. Solar photovoltaic structures instantly transform light energy from the sun into electricity. Using a solar charger, this electrical energy is now stored in the battery. When the battery storage system is charging, the solar controller's sole role is to enhance the current generated by the solar photovoltaic system. Additionally, it unplugs the solar photovoltaic system from the battery energy storage device when it is completely packed and hooks up again whenever the pack is running short on electricity. Through connecting wires, the motor is connected to the battery. A 555 timer is used as part of the control circuit. A photo-electric proximity sensor is also included for obstacle avoidance. The 555 timer's pin-2 is triggered when an impediment is identified, causing the required delay. As a result, the relay activates and cuts the supply to the right-hand motor, causing the car to spin and continue moving. The blades are powered by a high-speed motor that is connected directly to the battery.

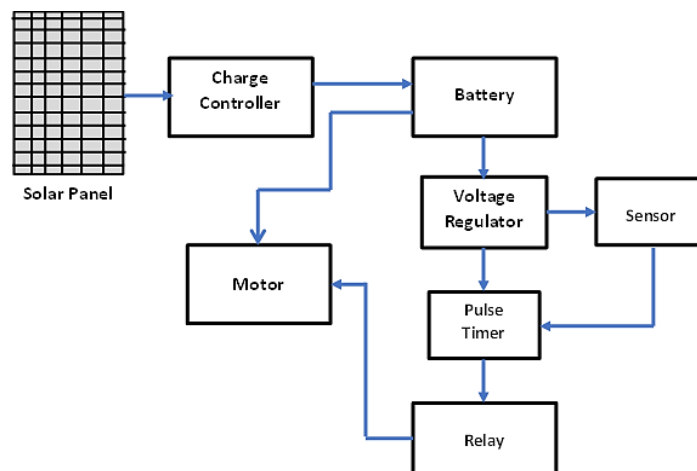


Figure 1. Schematic representation of the suggested system

3. HARDWARE PARTS

3.1. Solar PV Panel

Sun photovoltaic cells are energy-converting devices that convert solar light into electricity in a solar panel [9-11]. A PV system with a 5-watt power output and voltages of 21.6 volts at no load and 17 volts at full load. A charge controller, which regulates the voltage and current of the battery's charging, links the photovoltaic panels to the battery.

Solar Panel Specifications

- Rated Power (P_{max}) : 5W
- Electric potential in open circuit (E_{oc}) : 21.6V
- Current during short circuit condition (I_{sc}) : 0.33A
- Specified Potential (V_{mp}) : 17.0V
- Specified Current (I_{mp}) : 0.30A
- Power Tolerance : $\pm 3\%$
- Specifications are at STC : 1000W/m²
- Insolation AM 1.5, Cell Temp 25°C

3.2. *Charge Controllers for Solar Panel*

The power charge manager, also referred to as a battery charger, is situated somewhere in between the battery bank, the equipment, and the applications [12]. Regulators used in solar applications should be connected in series to minimize overcharge and over discharge by monitoring the voltage of the battery. Gadgets are linked and disconnected using switches, which can be solid state or electromagnetic types of relays.

It is never a good idea to connect solar chargers in series. The switch opens the charging circuit when the battery's voltage exceeds the high voltage disconnect (HVD) or cut-off break point, preserving the battery against overheating. By cutting the load, the low voltage disconnect (LVD) prevents the battery from being overcharged. The PV panels can be automatically unplugged by sophisticated controllers to prevent the battery from being discharged at night. Additionally, to increase the storage battery's lifespan, they can periodically discharge it by employing a process known as the pulse width modulation (PWM) technique. The PV panel charger features three LED displays. As soon as the battery packs receive a solar charge, the first LED flashes. The very next light turns on when the battery performance of the device is low. The Final LED bulb turns on when the batteries have been charged completely and a further load has been applied to them.

Solar Panel Specifications

- Specified power capacity (P_{max}) : 5W
- Potential across the circuit during open circuit open circuit (V_{oc}) : 21.6V
- Current in the line during short circuit condition (I_{sc}) : 0.33A
- Specified potential (V_{mp}) : 17.0V

3.3. *555 IC*

A semiconductor called the 555 Integrated circuit (IC) can be used to make oscillators, signal makers, and repeaters. 25 transistors, 2 diodes, and 15 resistors

are contained inside this basic 555 semiconductor IC chip, which has an 8-pin dual-in-line package (DIP-8).

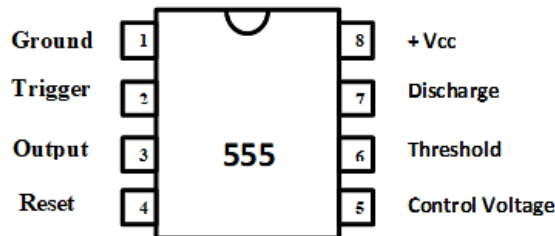


Figure 2. Pin diagram of 555 Timer

The voltage divider circuit, which typically consists of three 5k resistors linked in series, provides trigger values that really are one-third of VCC ($VCC/3$) as well as two-thirds ($2/3$) of the threshold voltage. Whenever necessary, the control voltage terminal (Pin 5) can be used to change the trigger and threshold settings. The requirements are adjusted by varying the control voltage at Pin 5, which also alters the trigger level and threshold voltage.

3.4. *Photo-electric Proximity Sensor*

It is an infrared sensor with an NPN output and a detection range of up to 30 cm. It is being used to detect obstacles in autonomous machines and mobile robots. It is, indeed, a scan that requires no interaction. Modulated IR signal implementations protect the sensor from interference induced by regular light from a light bulb or sunlight.

The sensor distance can be manually changed. It includes all sensors that detect objects without physically contacting them, as contrast to sensors, such threshold breakers, which sense the environment through manually touching them. The information regarding an element's motion or existence is transformed into an electrical signal using motion detectors.

Three different kinds of detection systems are employed to perform this transformation: one which employs magnetic fields to create eddy currents in metallic sensing objects; one that detects modifications in electrical characteristics as they get near to the detecting object; and the last one, which uses electromagnets and switching devices.

3.5. *Voltage Regulators*

Voltage regulators are meant to keep voltages consistent in the event of a power outage. The voltage regulator LM7805 is utilized. It belongs to the 78xx family of constant voltage regulator integrated circuits. It is impossible to deliver a constant output voltage since voltages in networks might oscillate. The terminal voltage is maintained steady by the voltage regulator IC. The LM7805 is a regulated power supply with a voltage of +5V. Capacitors are placed at the input and output levels based on the operating voltage.

The input voltage pin (PIN 1) has an operating voltage range of 5 to 16 volts. PIN 2 stands for the Ground PIN, and PIN 3 is the controlled output PIN with a 5 V voltage (in the voltage range of 4.8 V to 5.2 V).

3.6. Relays

The majority of supervisory apparatus or systems utilizes relays both as changeover and principal security features. Any relay can release or close associates or networks by reacting to one or more electrical qualities like voltage or current. A relay functions as a switching device by isolating or changing the state of an electrical circuits from one state to another.

Requirements for a relay

- Typical changeover currents of 7 A and 10 A
- Peak controlling voltage: 28 volts DC or 250 volts AC
- Dielectric strength V_{rms} : 750 V AC between open contacts and 1000 V AC seen between coil and the junctions
- the ambient 1000 V AC is present between the contacts; -40 to +85 °C is the ambient temperature is -40 to +85 °C and 10/8 ms is the operation/release time; and 10A 125V and 7A 250V are the contact capacities.

3.7. Battery

Two power supplies are required to control the grass cutter. One to power the control circuit and the other to power the motors. The battery's voltage rating and capacity must be chosen correctly. For ease of maintenance, both power supplies must be rechargeable. Due to the intended use of the batteries, sealed lead batteries with recharging capabilities were chosen. The motors are powered by a 12V battery. Because one battery is insufficient to drive the motors, it is more practical to use two parallel batteries.

Solar energy storage requires a battery with the following specific combination of qualities to be economically viable:

- Cheap price and high durability
- Relatively high efficiency and dependability

Battery packs details

- Model: AT12-1.3 (12 V 1.3 AH/20 Hr)
- Cycle use is 14.4–15.0 volts, while standby use is 13.5–13.8 volts.
- Preliminary current: under 0.39 A

3.8. *Motor*

The vehicle is primarily powered by three DC motors. Two of them are utilized for motion, while the other is used to cut the grass. As a result, the vehicle will be able to chop grass while running around the field. A DC motor with a rating of 300 W and 12 V is used in this experiment.

4. **HARDWARE IMPLEMENTATION**

4.1. *Hardware Implementation*

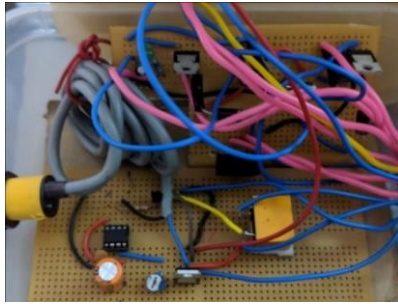


Figure 3. Control Circuit

The hardware is made up of two circuits. The first circuit is the timer circuit, which gives the necessary timing delay. The delay time is determined by the RC time constant. As a result, the capacitor and resistor values are chosen suitably. For the time delay in this circuit, 10K resistance and 1000 μ F capacitance are selected. Another circuit is the supply circuit, which provides power to allow the batteries to be recharged via the solar panel.

A photoelectric proximity sensor is used for obstacle detection. Through the battery, it receives 12V from the voltage regulator. It is made up of three wires, two of which are connected to the supply, and the other two to the regulator. The third wire is connected to the 555 timer's pin-2. When an impediment is recognized, pin 2 is lifted high, causing the relay to activate.



Figure 4 (a). Wheels for the robotic vehicle



Figure (b). Blade assembly

For forward motion, the entire assembly is mounted on a robotic vehicle with wheels. The motor shaft is connected to the wheels, which are powered by the

batteries. A blade is coupled to a high-speed motor that is used to cut the grass. As soon as the motor is switched on, the blades begin moving rapidly, cutting the lawn.

4.2. Torque Calculations and Hardware Output

$$\text{Power } P = 2\pi NT/60$$

Where N = Motor speed in RPM and T = Torque of the motor (N-m)

(i) Torque measurement in the absence of a load

Power (P) = 12 volts \times 25.2 Amps = 302.4 Watts, find torque

$$302.4 = (2 \times \pi \times 800 \times T) / 60, \quad \mathbf{T = 3.61 \text{ N-m}}$$

(ii) Torque measurement in loaded conditions

$$P = V \times I = 12 \times 28 = 336 \text{ W},$$

$$\text{find torque, } 336 = (2 \times \pi \times 620 \times T) / 60, \quad \mathbf{T = 5.17 \text{ N-m}}$$

In this work, three motors are used to power the vehicle. Two motors are employed to move things around, while the third one is used to mow the lawn. As a result, when running around the field, the vehicle will be able to chop grass. The automobile makes the turn when it detects an impediment using a proximity sensor. The solar panel charges the vehicle, which is then stored in a battery. The task was done satisfactorily.

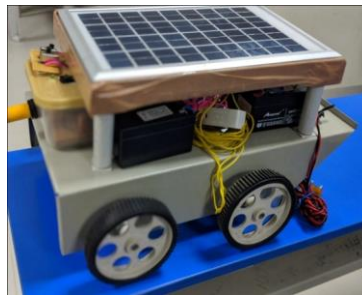


Figure 5. Prototype of fully automated solar grass cutter

5. CONCLUSION

The major goal of this work is to create a PV system-based automatic robotic lawn mower system that will assist in mowing the lawn in various designs while requiring less human labour. The system's benefits include the inexpensive cost of the components used. Because there is no need for fuel, this solar-powered lawn cutter will meet the demands of environmental protection and cheap operating costs. For use by homes and companies with lawns that cannot be mowed with tractor-driven mowers, a PV system based automatic mower vehicles has indeed been developed. The capacity of the machine is sufficient for its intended use. The machine has been shown to be a viable alternative to fuel-powered lawn mowers. A

succinct synopsis of the results and a precise description of the system represents advanced contribution in that field.

REFERENCES

- [1] J. Billingsley, 'Agricultural Robotics', IEEE Robotics Automation magazine, 2009.
- [2] T. Liu, B. Zhang, J. Jixing, 'Electromagnetic navigation system design of the green house spraying robot', Int. Conf. on Mechanic Automation and Control Engg., pp. 2140 – 2144, 2011.
- [3] G. D. Rai, 'Non-Conventional Energy Sources', Khanna Publishers, 1988.
- [4] D. Athina, K. Kumar, B. Kalyani, K. Vittal, 'Solar Grass Cutter Using Embedded Platform an Experimental Validation', IOP Conf. Series: Materials Science and Engg., pp.1057, 2021.
- [5] A.P. Pralhad, B.S. Bhagwan, K. S. Subhash, P. N. Vijay, R. U. Kale, 'Solar powered automatic grass cutter and pesticide spreading robot', Int. Res. J. Eng. and Tech., Vol. 4, Issue 5, pp 3372-3375, 2017.
- [6] D. T. Yashit, A. Hariya, A. Kadachha, D. Dethaliya, 'Fully automated solar grass cutter', Int. Journal of Sci. Tech. & Eng., Vol. 3, Issue 9, pp. 104-106 2017.
- [7] A. K. Chaudhari, 'Solar based grass cutter' Int. Journal of Electrical and Electronics Eng., Vol. 9, Issue 1, pp. 134-1389, 2017.
- [8] S. Jain, A. Khalore, S. Patil, 'Self-efficient and sustainable solar powered robotic lawn mower', Int. Journal of Trend in Research and Development, Vol. 5, Issue 2, pp. 294-297, 2015.
- [9] B. R. Patil, S. S. Patil, 'Solar based grass cutting', In. Res. J. Eng. and Tech., Vol. 5, Issue 2, 2017.
- [10] S. Akshay, V. Dhananjaya, G. I. Menezes, P. R. A. Kumar, 'Design & Fabrication of Remote-Controlled Solar Lawn Mower', Int. Research Journal of Engineering and Technology, Vol. 6, Issue 4, pp. 4106- 4112, 2019.
- [11] B. P. Dilip, N. B. Pagar, V. S. Ugale, S. Wani, M. Sharmila, 'Design and Implementation of Automatic Solar Grass Cutter', In. J. Adv. Res. in Elect., Electro. and Instru. Eng., Vol. 6, Issue 4, pp. 2433-2437, 2017.
- [12] B. Ibrahim, V. S. Brahmaiah, and P. Sharma, 'Design of smart autonomous remote monitored solar powered lawnmower robot', Materials Today: Proceedings, pp. 1-7, 2020.

Synthesis of Micro encapsulated Beeswax using in-situ polymerization and its characterization

¹K. Vijayakesh, ²S. Muthuvel, ^{3*}G. R. Gopinath, ⁴R. Sudhakar Pandian, ⁵G.R. Rajesh Kanna

^{1,2,3}Department of Mechanical Engineering, Kalasalingam Academy of Research and Education, Tamil Nādu, India.

⁴Department of Manufacturing Engineering, Vellore Institute of Engineering, Tamil Nādu, India.

⁵Department of Electrical and Electronics Engineering, Kalasalingam Academy of Research and Education, Tamil Nādu, India.

Email: vijayakeshk@gmail.com, s.muthuvel@klu.ac.in, gopinathradhakrishnan7@gmail.com, sudhakarapandian.r@vit.ac.in, iamrajeshkanna@gmail.com

Abstract

Application of Phase Change Material (PCM) in micro form increases more latent heat energy compare to macro form. This paper focuses on the microencapsulation of Beeswax PCM as core material and Urea-formaldehyde as shell material for utilizing them in thermal management applications using their latent heat storage. The in-situ polymerization method was adopted for microencapsulation Beeswax to obtain better surface morphology and minimum size. The microencapsulated Beeswax was characterized Scanning Electron Microscope (SEM), and Fourier infrared spectroscopy (FTIR). The thermal stability was evaluated using a Thermogravimetric analyzer (TGA). From the SEM analysis average diametrical size for the microcapsules was 0.23 μm . Chemical availability Beeswax core material and urea formaldehyde shell material was verified from absorption peaks in FTIR test. The maximum temperature of microencapsulated Beeswax was 210°C. The dynamic temperature was verified using Differential scanning calorimetry (DSC), the maximum temperature in the microcapsule was 62.5 °C, the cooling temperature was 59.7 °C.

Keywords. Beeswax, In-situ polymerization, Latent heat storage, Microencapsulation, Thermal management.

1. INTRODUCTION

The conservation of energy can be accomplished in two ways: by judicially using all the electrical equipment and disconnecting devices on idle condition from the power supply. Generally, PCMs are fatty acids or wax material. These materials are highly capable of storing a large amount of thermal energy. However, most of the PCM are less thermally conductive. In order to improve the thermal conductivity, the surface area of PCMs needs to be improved. There are several other chemical methods to microencapsulate the PCMs [1], namely the sol-gel

method, in situ polymerization, interfacial polymerization, suspension polymerization, complex coacervation, emulsion polymerization [2].

In the previous researches, many attempts done with Beeswax to use for latent heat storage by means of raw Beeswax in pouches and balls, Beeswax emulsion form, Beeswax with graphite, copper and silver nano particles for increasing thermal conductivity. The novelty of the present work is microencapsulated Beeswax using urea-formaldehyde as shell material. Since the previous researches reported that urea formaldehyde shell gives self-healing qualities to microcapsule while heating and also it improves encapsulation of the polymer shell [3].

In this paper, the in-situ polymerization method of microencapsulation is investigated for Beeswax. It is expected that the microcapsules obtained from this method will have better bonding strength [4]. The microencapsulated product is characterized for surface morphological analysis, functional group, and thermal behaviour.

2. MATERIALS AND METHODS

Beeswax ($C_{15}H_{31}COOC_{30}H_{61}$; melting temperature $64^{\circ}C$ and boiling temperature $85^{\circ}C$) was the PCM used in the study. Urea(CH_4N_2O – 99%) and formaldehyde (CH_2O – 37.4% w/v) were used as shell materials, as urea-formaldehyde rendered the shell with better thermal conductivity, i.e., 0.433 w/m $^{\circ}C$ [5] next to water (k_{water} 0.599 w/m $^{\circ}C$). Ammonium chloride was used as a nucleating agent, while sodium hydroxide (NaOH) and deionized water were used as general laboratory reagents. Hydrochloric acid (HCl) was used as an acidic liquid, and sodium hydroxide (NaOH) was used as a basic buffer for maintaining the pH level close to 5. Resorcinol ($C_6H_4(OH)_2$) was used as the crosslinking agent of microcapsules.

2.1. Extraction of Beeswax Phase-Changing Materials

Beeswax is extracted from a natural honeycomb. Initially, the honeycomb was collected and dried after removing the honey inside the individual holes. The powdered honeycomb was poured into the water, boiled at $100^{\circ}C$. For getting 100 g of Beeswax, 250g of honeycomb needs to be used. The water was maintained in the boiling state for 30 minutes. Then the melted wax started to float on the surface of boiling water. Once the liquid wax formed, it changed to a white or whitish-yellow colour, and the liquid was taken and filtered using a pure cotton cloth. Thus, the unwanted dust particles settled above the cloth. The water and melted wax were poured into the glass jar for cooling. The process flow chart for extracting Beeswax is shown in Figure.1.

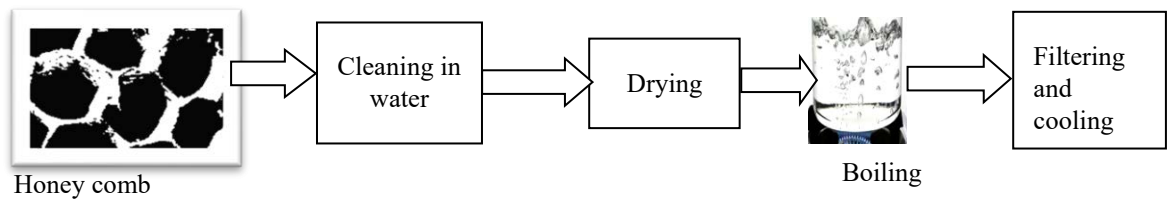


Figure.1 Stages of manufacturing Beeswax or Beeswax Phase-Changing Materials.

2.2. Selection of Chemical Polymerization method

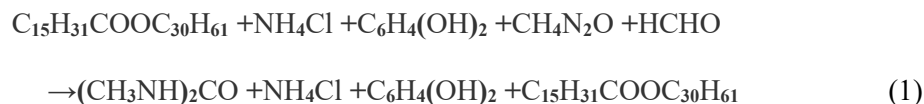
The in-situ polymerization method was recommended for improved bonding and tightness. In-situ polymerization method, which uses water-oil emulsion of shell material, and covers the core material after certain chemical processes. If larger particles are made into a smaller particle by stirring operation, the smaller amount of core material will be covered by shell material, which will create new microencapsulated particles; this process is known as microencapsulation [6].

2.3. Emulsification process

2.5 wt. % of Ethylene malic anhydride emulsifier was prepared for 10g of PCM. About 250 ml of Ethylene maleic anhydride was used for preparing the emulsion, wherein it was poured into 250 ml of water and stirred at 500 rpm using a magnetic stirrer. Another container of 200 ml capacity was filled with distilled water, and 0.5 g of resorcinol, 0.5g of ammonium chloride, and 5g of Urea were added. Then, 10 ml of Ethylene maleic anhydride solution was taken, added to the mixture, and stirred at 500 rpm. Hydrochloric acid and sodium hydroxide solutions were added dropwise for maintaining the pH level of the solution at 5.

2.4. Formation of Microcapsules

The prepared emulsion solution was heated to 70 °C because the Beeswax melting temperature was 64°C. 10g of Beeswax was added to the solution, followed by 10ml of formaldehyde solution, while the pH was maintained between 5-7 by adding one or two drops of sodium hydroxide solution and hydrochloric solution, as per the requirement. The stirring speed was increased to 1000 rpm and maintained for 5 hours at a constant temperature of 70°C. A smooth surface finish and smaller size can be obtained by maintaining constant stirring speed [7]. The chemical operation of the process is given below in Eq.1.



3. RESULTS AND DISCUSSION

An examination and understanding of the characteristics of microencapsulated PCMs, such as shape, size, surface morphology is essential to

determine their applicability. [9]. The SEM is used to observe the surface morphology, shape, and size; this will give the primary evidence of the formation of microcapsules. FTIR test was used to observe the functional groups of the chemical compounds formed in the microparticles. To assess the microcapsule's temperature stability, Thermogravimetric analysis (TGA) of the microcapsules was conducted [8].

3.1. SEM Analysis and FT-IR analysis for microencapsulated PCM

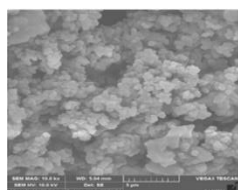


Fig. 2 (a)

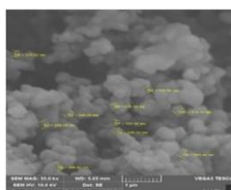


Fig. 2 (b)

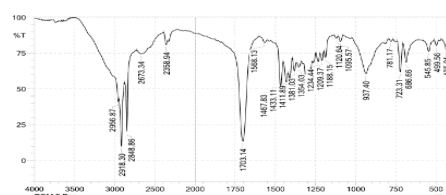


Fig. 2 (c)

Fig. 2 (a) and (b) SEM analysis 2 (c) FT-IR (Core, Shell, and microcapsule)

SEM test was done using ZEISS microscope. The fibrils were scanned for the different wavelength of the electron with different magnification varied from 100 X to 500 X, with the accelerated voltage of 20 KV. The images observed in the SEM are shown in Figs. 2 (a) and (b). From the SEM analysis, the shape of the microcapsules is spherical, as in-situ polymerization was used for microencapsulation. The maximum size observed in the microcapsule was 299.45 nm, while the minimum size of microcapsules measured in the image was 176.53 nm. The average diametrical size of the microcapsule was 0.23 μ m. The microcapsule surface had no dimples or depressions and exhibited a smooth texture.

FTIR test was done using SHIMADZU- instrument model (IR TRACER 100). The absorption peaks of Urea and the microcapsules were observed at 1020 cm⁻¹ to 1250 cm⁻¹ attributed to the stretching vibration of the C-N group. Similarly, the absorption peaks of formaldehyde measure from 1685 cm⁻¹ to 1710 cm⁻¹, which are observed as stretching bands of C=O bonds. Also, the peaks corresponding to the core material can be observed between 2500 cm⁻¹ to 3000 cm⁻¹. This result shows the presence of Beeswax, urea, and formaldehyde in microcapsules.

3.2. Thermogravimetric analysis and Differential Scanning Calorimeter (DSC)

A Thermogravimetric analyzer (TGA 4000, Pyris 6 machine) was used for this study. In this test, the temperature was increased, and the weight loss of the sample over the heating, holding, and cooling time was monitored. Fig. 4 a shows the TGA graph, where in the weight loss was gradual between 0 - 200 °C. At 210°C, there is a slight steep fall in the mass of the sample. Again, the mass loss was quite notable between 230°C and 350°C. Thus, the material began to decompose at 210°C. So, the maximum temperature the microencapsulated Beeswax can withstand without decomposition is 210 °C. Hence, the material can be operated within the regime of 0-200°C.

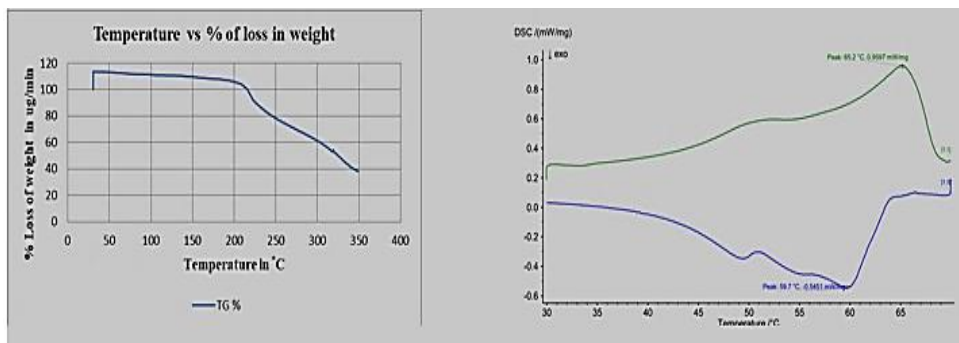


Figure. 4a TGA of microencapsulated Beeswax, Fig. 4b Heating and Cooling curve by DSC test.

In the DSC analysis the temperature was raised by about 10 °C until 350 °C cooled down to the initial temperature in the same manner. Fig. 4b shows the heat flow in the system during the heating-cooling of the microcapsule. The DSC results shows that the maximum heating temperature reached 65.2°C and enthalpy verified about 0.9597 mW/mg and the cooling temperature peak attained 59.7°C and enthalpy reaches 0.5451 mW/mg. So, the results revealed that usage of PCM for electronic component cooling can comfortably be done instead of air cooling done by fan.

4. Conclusion

Beeswax was successfully obtained from the honeycomb, and microencapsulation was done through the in-situ polymerization method. The microencapsulated Beeswax was spherical, smooth and the average size was between 0.2µm to 0.3µm. Chemical characterization of the encapsulated PCMs was conducted using FTIR spectroscopy to confirm the presence of PCMs in the Beeswax core material and Urea formaldehyde shell material. FTIR analyses confirmed the presence of Urea, formaldehyde, and the core materials with the peaks corresponding to their functional groups at 1020 cm⁻¹ to 1250 cm⁻¹, 1685 cm⁻¹ to 1710 cm⁻¹, and 2500 cm⁻¹ to 3000 cm⁻¹. The maximum temperature of microencapsulated Beeswax before decomposition was 210 °C. The cooling and heating curves of microencapsulated Beeswax were observed at 59 °C, and 65.2 °C. The microencapsulated Beeswax is used for latent heat storage systems for operating temperatures below 65 °C. The future work is plan to do the nano encapsulated PCM.

REFERENCES

- [1] J. Cust, A. Singh, K. Neuhoff, Rural Electrification in India: Economic and Institutional Aspects of Renewables, SSRN Electron. J. (2016). <https://doi.org/10.2139/ssrn.2760810>.
- [2] N. Putra, A.F. Sandi, B. Ariantara, N. Abdullah, T.M. Indra Mahlia, Performance of beeswax phase change material (PCM) and heat pipe as passive battery cooling system for electric vehicles, Case Stud. Therm. Eng. 21 (2020) 100655. <https://doi.org/10.1016/j.csite.2020.100655>.
- [3] T. Amberkar, P. Mahanwar, Synthesis and Study of Microcapsules with Beeswax Core and Phenol-Formaldehyde Shell Using the Taguchi Method, Mater. Proc. 7 (2021) 1. <https://doi.org/10.3390/iocps2021-11207>.
- [4] A.K. Raj, M. Srinivas, S. Jayaraj, A cost-effective method to improve the performance of solar air heaters using discrete macro-encapsulated PCM capsules for drying applications, Appl. Therm. Eng. 146 (2019) 910–920. <https://doi.org/10.1016/j.applthermaleng.2018.10.055>.
- [5] M. Amin, N. Putra, E.A. Kosasih, E. Prawiro, R.A. Luanto, T.M.I. Mahlia, Thermal properties of beeswax/graphene phase change material as energy storage for building applications, Appl. Therm. Eng. 112 (2017) 273–280. <https://doi.org/10.1016/j.applthermaleng.2016.10.085>.
- [6] Z.A. Qureshi, H.M. Ali, S. Khushnood, Recent advances on thermal conductivity enhancement of phase change materials for energy storage system: A review, Int. J. Heat Mass Transf. 127 (2018) 838–856. <https://doi.org/10.1016/j.ijheatmasstransfer.2018.08.049>.
- [7] D.Z. Chen, S.Y. Qin, G.C.P. Tsui, C. yin Tang, X. Ouyang, J. hua Liu, J.N. Tang, J.D. Zuo, Fabrication, morphology and thermal properties of octadecylamine-grafted graphene oxide-modified phase-change microcapsules for thermal energy storage, Compos. Part B Eng. 157 (2019) 239–247. <https://doi.org/10.1016/j.compositesb.2018.08.066>.
- [8] G. Alva, Y. Lin, L. Liu, G. Fang, Synthesis, characterization and applications of microencapsulated phase change materials in thermal energy storage: A review, Energy Build. 144 (2017) 276–294. <https://doi.org/10.1016/j.enbuild.2017.0>

A New Two Switch Non-Inverted Buck-Boost Converter for PV System

*¹J.N. Bhanutej, ²U. Hemalatha, ³B. Nagi Reddy

*^{1,2,3} Department of EEE, Vignana Bharathi Institute of Technology, Hyderabad, India
Email: bhanutej.mtech@gmail.com, udarihemalatha@gmail.com

Abstract

For photovoltaic-based systems, this study suggests a quadratic buck-boost converter with two active switches. The reduced redundant power processing (R^2P^2) concept serves as the foundation for the suggested converter. To achieve quadratic voltage gain, conventional boost and buck-boost cells are arranged in a non-cascading fashion. In order to obtain a high voltage conversion ratio and a low component count, the two active switches of the proposed converter operate concurrently. The effect on converter performance is also evaluated once the converter has been tested with varied sources and loads. Here, the voltage conversion ratio and semiconductor stresses of the proposed converter are described. Under steady-state conditions, the proposed converter's precise performance is assessed. With the help of MATLAB/SIMULINK, the suggested converter is evaluated.

Keywords. Two switch, PV, buck-boost, non-inverting, dc-dc converter.

1. INTRODUCTION

The proliferation of mobile systems and equipment over the past several decades has spurred innovation in portable power supply systems. This includes anything from powering IoT devices to overseeing renewable energy production. Increases in efficiency, conversion ratios, and power density are only some of the additional requirements placed on power electronics systems as a result of the industry's present direction. Because of its ability to process energy with the help of appropriate control schemes, the switching converter is essential to any contemporary power supply system [1].

In this regard, the design of novel switching converter topologies, as well as novel converter connectivity architectures and/or methods, is of interest. Similarly, low-voltage and/or low current semiconductor components are of relevance for this use. Numerous high transformation-ratio topologies based on isolated and nonisolated techniques have been devised recently, with implementation depending largely on the desired use case. Total harmonic distortion (THD) reduction, power factor improvement, output voltage control, and energy efficiency are some of the primary goals of switching converter-based AC power supply systems [2]. For these uses, it is preferable that the converter's output and input power supplies be completely isolated from one another. The first is the increasing need for DC power systems to serve portable and electronic devices, and the second is the development of DC power systems. Subsequently the voltage levels produced by fuel cells, solar systems, and/or batteries are just a few tens of volts, switching converters need to have high conversion ratios [3]. The ability to process energy at hundreds of volts, with or without galvanic separation, is necessary for this state to exist.

Recently, there has been a rise in interest for switching converters that can regulate the input voltage to meet the needs of certain devices. With the goal of achieving a low output voltage and a high-power factor. After introducing the quadratic buck & simple boost configurations [4], synthesized a switching converter that could be used in a solar system to modify the energy being fed into an inverter. As switching converter technology has advanced, converters with floating loads have emerged, limiting their usefulness. As an added bonus, certain circuit synthesis topologies merge the characteristics of quadratic converters with those of fundamental topologies [5]. Emergent topologies are being developed to solve real-world problems encountered by power supply for renewable energies systems [6]. This work introduces a non-cascade architecture for connecting basic converters as a switching converter configuration, based on the reduced redundant power processing approach. The output voltage is both multiplicatively increased and decreased, defining the achieved conversion ratio. The suggested converter has a low number of parts, produces a noninverting voltage at its output, shares a node with its input, and can accept a constant current input. The effect of the PV system on the converter's functioning is also studied by analyzing it with various source and load configurations.

2. PROPOSED NON-INVERTED BUCK-BOOST CIRCUIT

Block A's boost network with reversed output polarities is seen in Figure 1.a. This boost network causes storage element C1's voltage polarity to be reversed, which results in a negative voltage at block B's input port. The output port of the I-IIA structure is then supplied with a positive voltage by a buck-boost

network, as seen in Figure 1.b. Furthermore, E denotes the voltage source, while R denotes the load.

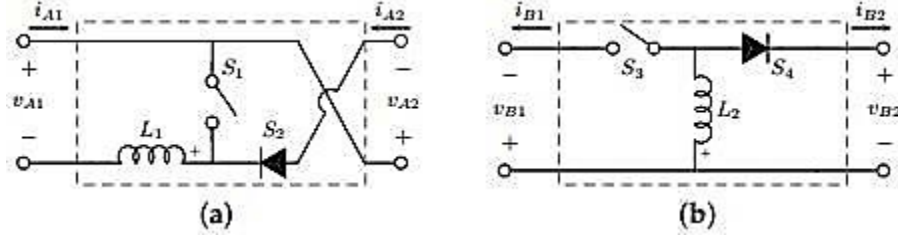


Figure 1. Basic switching cells that are not isolated: (A) buck-boost; (B) boost

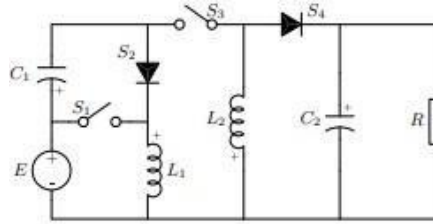


Figure 2. Proposed wide range buck-boost network

As previously mentioned, this kind of non-cascaded construction has been utilized to create various high-gain or secondary voltage conversion ratio devices topologies for PV applications. Nonetheless, there are several methods for designing topologies with specific high voltage gains. The planned converter steady-state analysis is expanded in this section by connecting the converter's inputport to a voltage source. The contributions of PV modules and converters are discussed in the following subsections. The states of the active switches define the converter's operating modes, and these assumptions are made:

- The converter is running continuously (CCM).
- To achieve high voltage gain, active switches S1 and S3 operate synchronously.
- The switching function q describes the mode of operation of active switches. An equation provides them (1).

$$q = \begin{cases} 1 & \rightarrow 0 < t \leq t_{on} \\ 0 & \rightarrow t_{on} < t \leq T_s \end{cases}, \quad q = \begin{cases} 0 & \rightarrow 0 < t \leq t_{on} \\ 1 & \rightarrow t_{on} < t \leq T_s \end{cases} \quad (1)$$

T_s denote the switching period, and T_{on} denotes the active switch conducting time. The converter's operating modes are indicated by the on- and off states of the active switches. In this situation, capacitor C1 powers load R while capacitor C2 powers inductor L2. The differential equations characterize the system's behaviour in this mode of operation:

$$L_1 \frac{di_{L1}}{dt} = E, \quad (2)$$

$$L_2 \frac{di_{L2}}{dt} = V_{C1} - E \quad (3)$$

$$C_1 \frac{dv_{C1}}{dt} = -i_{L2} \quad (4)$$

$$C_2 \frac{dv_{C2}}{dt} = -\frac{V_{C2}}{R} \quad (5)$$

Inductor L1 delivers energy to capacitor C1 via diode S2, and inductor L2 sends energy to the capacitors R-C2 via diode S4 while the switches are off (Figure 3b). The relevant differential equations are as follows:

$$L_1 \frac{di_{L1}}{dt} = E - V_{C1} \quad (6)$$

$$L_2 \frac{di_{L2}}{dt} = V_{C2}, \quad (7)$$

$$C_1 \frac{dv_{C1}}{dt} = -i_{L1} \quad (8)$$

$$C_2 \frac{dv_{C2}}{dt} = i_{L2} - \frac{V_{C2}}{R} \quad (9)$$

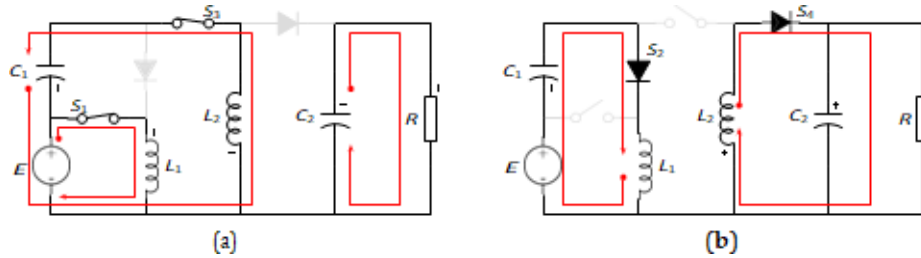


Figure 3. The proposed converter has 2 operating modes: q equals 1 in (a) and 0 in (b).

During one switching period, the voltages at the inductors' terminals and currents through the capacitors are defined by Equations (2) and (3). Equations (4) and (5) describe the converter's steady-state operation using the concepts of volt second and charge balances are applied to these voltages and currents (5).

$$\int_0^{T_s} v_L(t) dt = 0 \quad (10)$$

$$\int_0^{T_s} i_C(t) dt = 0 \quad (11)$$

$$I_{L1} = \frac{ED^3}{(1-D)^4 R} \quad (12)$$

$$I_{L2} = \frac{ED^2}{(1-D)^3R} \quad (13)$$

$$V_{C1} = \frac{E}{(1-D)}, \quad (14)$$

$$V_{C2} = \frac{ED^2}{(1-D)^2} \quad (15)$$

Where D is the converter's nominal duty ratio, the converter's voltage gain becomes quadratic with respect to duty ratio at that point, indicating a wide range of output step-up or step-down voltage conversion characteristics. Equation represents the voltage gain as a result (10). The steady-state operating condition and the voltage conversion ratio are the only applicable when the converter is in CCM mode. The conversion ratio is also positive, and the ports for input and output are both grounded.

$$M = \frac{V_{C2}}{E} = \frac{D^2}{(1-D)^2} \quad (16)$$

3. RESULTS

Finally, simulation of the converter in MATLAB/Simulink is done to obtain the response.

Table 1 Simulation values

Parameters or components	values
Input voltage (Vin)	24v
Output voltage (Vo)	200v
Output power (Po)	200W
Switching frequency (Fs)	80 KHz
Load resistance	200Ω
Duty ratio	0.7426
M(D)	8.32
L1(α=0.5A)	29.55 μH
L2(α=0.5A)	331.2 μH
C1(Δ=2V)	4.64 μF
C2(Δ=2V)	4.64 μF

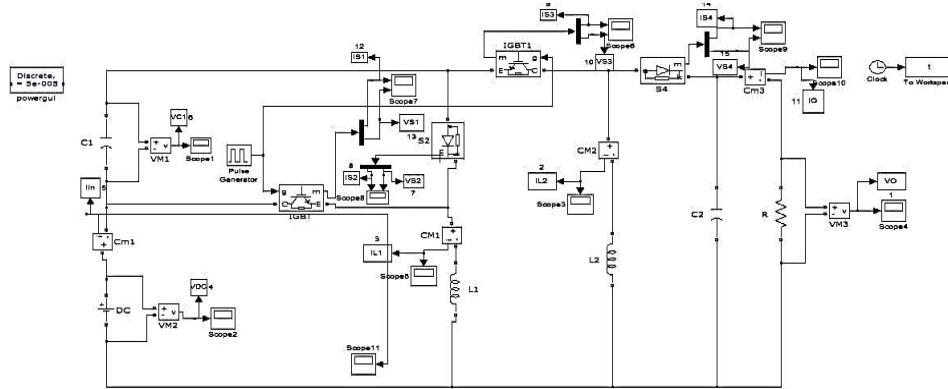
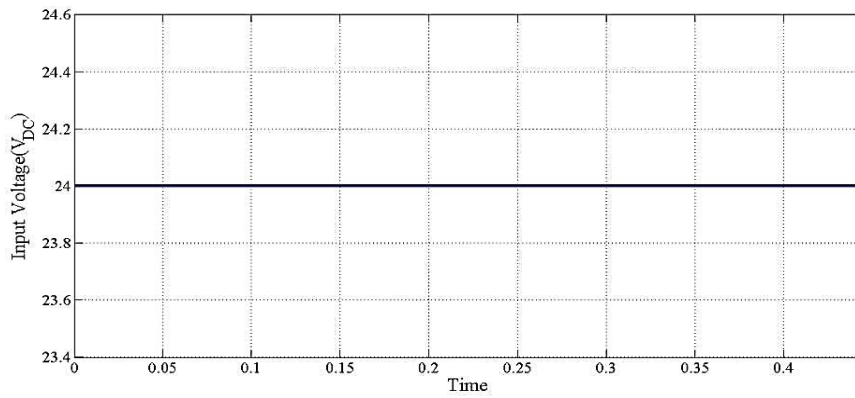
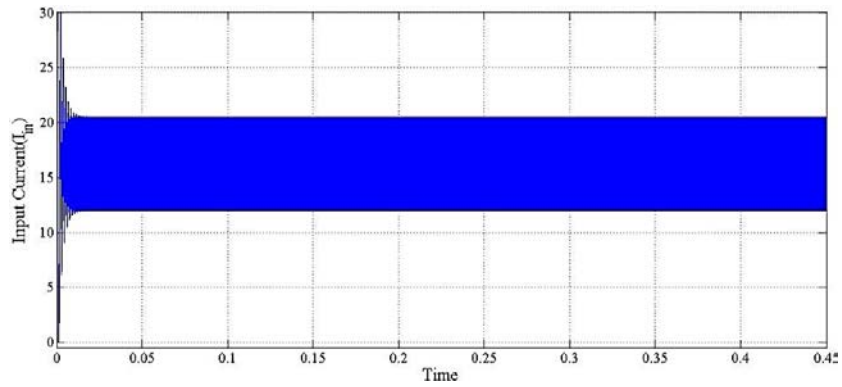


Figure 4. Simulation model

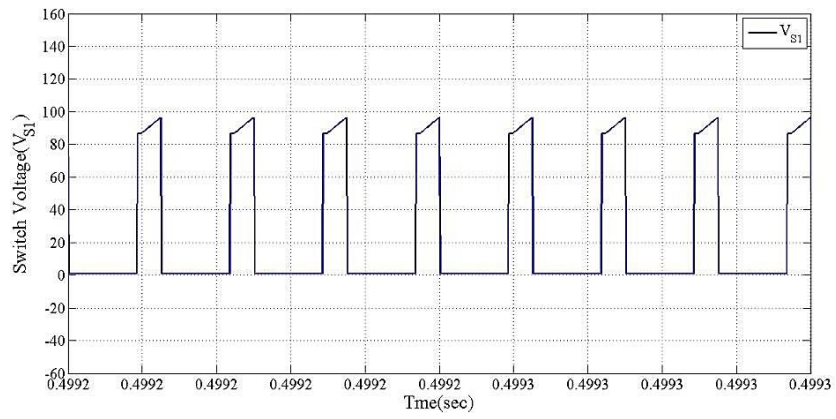


(a)

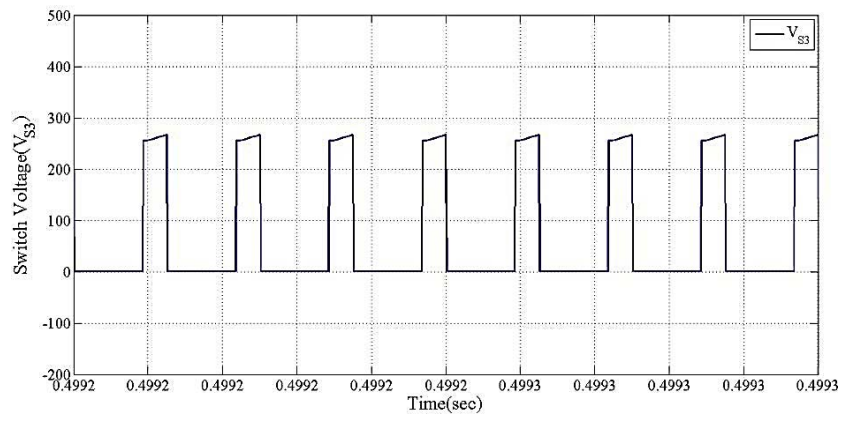


(b)

Figure 5. Input voltage and current



(a)



(b)

Figure 6. Switching voltages

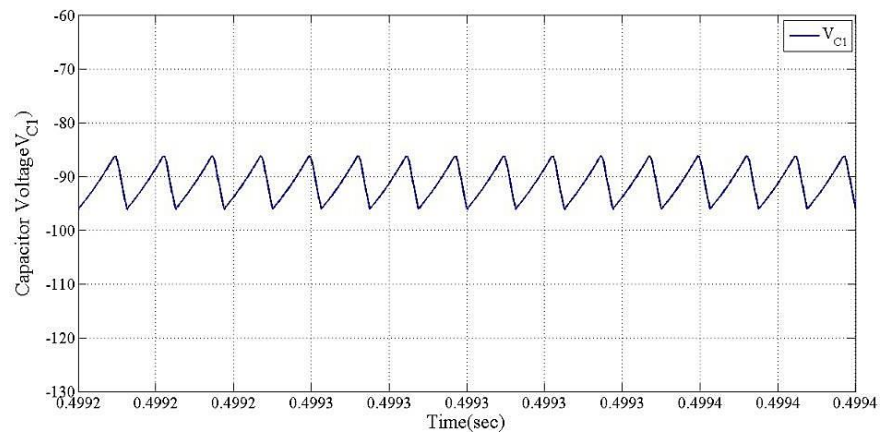
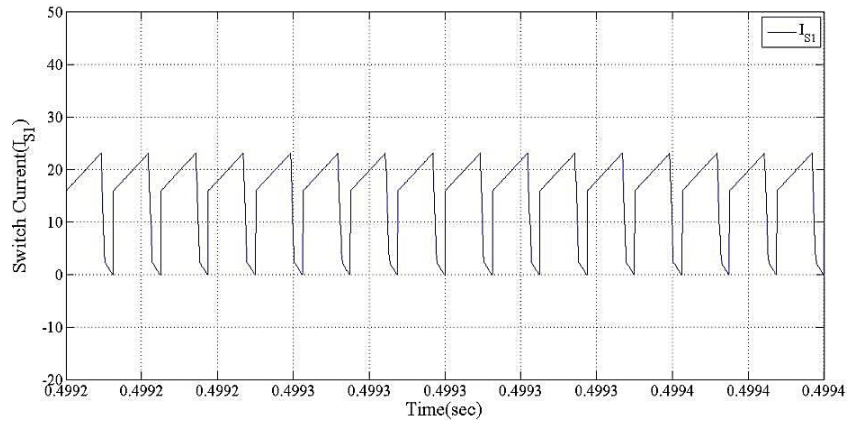
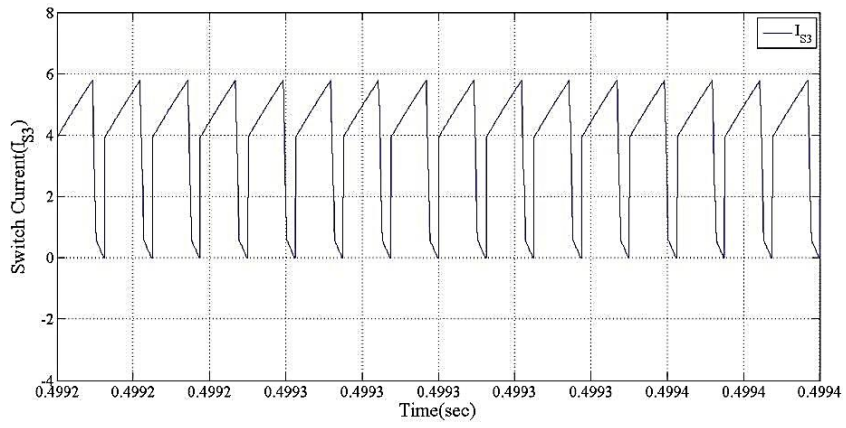


Figure 7. Capacitor voltage



(a)



(c)

Figure 8. Switching currents

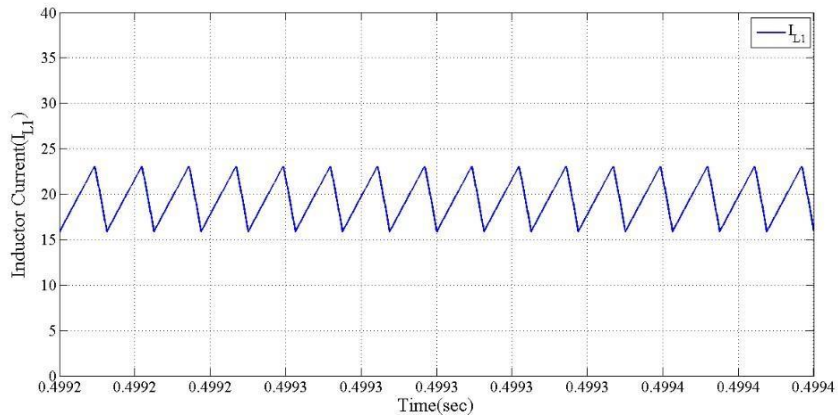
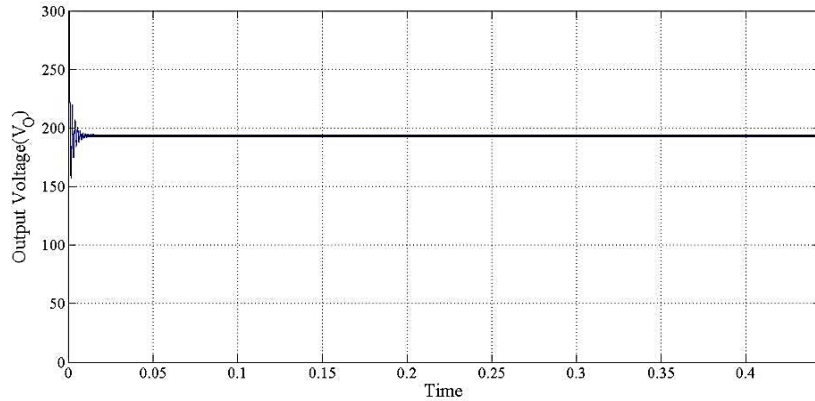
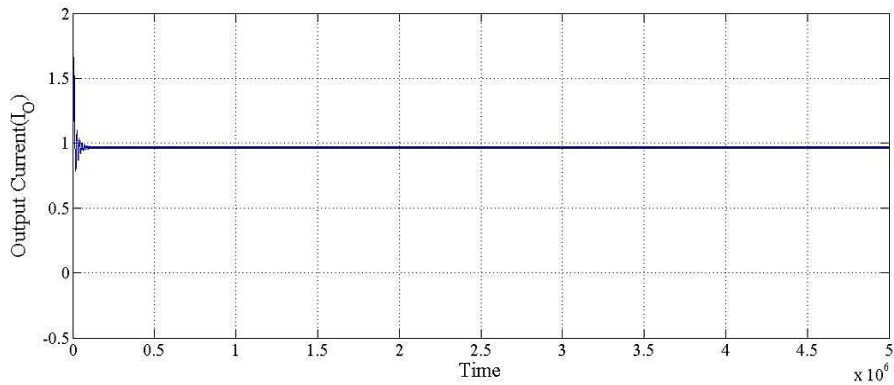


Figure 9. Inductor currents



(a)



(b) Output current

Figure 10. Output voltage and current

Global solar radiation varies greatly depending on fog. This is especially relevant to the amperage and power produced. The complexity of the P&O calculation will change the voltage at the PV module's terminals in tests; efficacy was greater than 80%. Using large components like SiC semiconductors and techniques like cooperative correction, in particular, will boost the effect. Nevertheless, replication evaluations were performed in this work to support hypothetical results regarding conversion rates, behavior, and potential use in PV applications. The mimicked response clearly predicted a strong response from the model converter and confirmed the correctness of the generated model.

4. CONCLUSION

In this article, a quadratic buck-boost converter that is based on the connection of two fundamental switch cells in an uncascaded design. Because the converter correctly connects PV devices to DC system connections, this is suitable for PV applications. PV applications behave differently than voltage source applications,

according to steady-state analysis. The voltage stress on the semiconductor is further greater in PV applications, but the current stress is lower. The simulation results show that the converter behaves properly under real-world conditions, with the duty cycle controlling the voltage at the PV module terminals and regulating the power produced. The converter has a high voltage conversion ratio, which enables it to handle wide input voltage swings while keeping the output voltage clamped. Inverters are suitable for grid-connected or micro-grid applications.

5. REFERENCES

- [1] Alonge, F.; Pucci, M.; Rabbeni, R.; Vitale, G. Dynamic modelling of a quadratic DC/DC single-switch boost converter. *Electr. Power Syst. Res.*, 152, 130–139, 2017.
- [2] Ozdemir, S.; Altin, N.; Sefa, I. Fuzzy logic based MPPT controller for high conversion ratio quadratic boost converter. *Int. J. Hydrogen Energy*, 42, 17748–17759, 2017.
- [3] Nagi reddy. B, sahithipriya. Kosika, manishpatel. Gadam, jagadhiswar. Banoth, ashok. Banoth, srikanthgoud. B, “Analysis of positive output buck-boost topology with extended conversion ratio”, *Journal of Energy Systems*, 6(1), pp. 62–83, 2022.
- [4] Al-Saffar, M.A.; Ismail, E.H.; Sabzali, A.J. Integrated buck-boostquadratic buck PFC rectifier for universal input applications. *IEEE Trans. Power Electron.*, 24, 2886–2896, 2009.
- [5] Zhang, N.; Zhang, G.; See, K.W.; Zhang, B. A single-switch quadratic buck-boost converter with continuous input port current and continuous output port current. *IEEE Trans. Power Electron.*, 33, 4157–4166, 2018.
- [6] Gorji, S.A.; Mostaan, A.; My, H.T.; Ektesabi, M. Non-isolated buck-boost DC-DC converter with quadratic voltage gain ratio. *IET Power Electron.*, 12, 1425–1433, 2019.
- [7] Nagi Reddy, B., Chandra Sekhar, O., Ramamoorthy, M. “Analysis and implementation of single-stage buck-boost-buck converter for battery charging applications *Journal of Advanced Research in Dynamical and Control Systems*, 2018, 10(4), pp. 446–457.

Optimized Energy Forecasting Using Hybrid Long Short-Term Memory Technique

P. Elumalaivasan¹, T. Munirathinam², G. Sasi³, R. Rajesh⁴, R. Pradeep⁵,
B. Rajmohan⁶

¹Department of Computer Science and Engineering, Vel Tech Rangarajan Dr. Sagunthala R&D Institute of Science and Technology, Chennai, India-600062. elumalaivasan1984@gmail.com

²Department of Computer Science and Engineering, Bannari Amman Institute of Technology, Erode, India-638401. munirathinamprg@gmail.com

³Department of Biomedical Engineering, Vel Tech Multi Tech Dr. Rangarajan Dr. Sakunthala Engineering College, Chennai, India-600062. gsasikumar75@gmail.com

⁴Department of Computer Science and Engineering, SRM Institute of Science and Technology, NCR Campus, Delhi, India-131029. rajeshrathnam84@gmail.com

⁵Department of Computer Science and Engineering, Rajalakshmi Engineering College, Chennai, India-602106. pradeeprajame@gmail.com

⁶Department of Computer Science and Engineering, Takshashila University, Tindivanam, India-604305. rajmohanit@gmail.com

Abstract

Energy needs are increased day to day, as the world is developing in all the sectors of energy. So, it is one of the vital factors for all the purposes of daily works and boundless demand for precise energy forecasting. It is to be provided for lower cost and also it should be stable, this will become the most challenging task for the energy service providers. Energy forecasting is typically available only for bigger regions. In this paper, we propose the hybrid Cat Swarm Optimization (CSO) with Long Short-Term Memory (LSTM) model for finding energy consumption to India by 2027. The proposed CSO-LSTM is designed by integrating with metaheuristic swarm-based optimization algorithm is applied on the dataset of Central electricity authority, Government of India. This approach is implemented in pycharm, colab software with the given time series data. Here, the optimal feature extractions are trained using LSTM model. Proposed method achieved best performance which can be understood from the metrics of Mean Square Error (MSE) reduced by 0.015 and Root Mean Square Error (RMSE). From the results that the implemented model CSO-LSTM is produced the best energy efficiency when compared with existing models.

Keywords: Energy Forecasting, Robustness, Scalability, CSO, LSTM

1. INTRODUCTION

Energy needs are increasing day by day, as the world is developing in all the sectors energy is one of the vital factors for all the purposes of daily works and boundless demand for precise energy forecasting. The proposed CSO-LSTM is designed by

integrating with meta heuristic swarm-based optimization. This algorithm is used to forecast the energy consumption in future with the growth dataset of Central electricity authority, Government of India. A hybrid strategy is effective for maximising the deep long-term memory approach, which results in a faster rate of convergence throughout the training phase and permits the development of small-scale decentralised systems. Time-series data can be handled well by deep learning methods like Long Short Term Memory (LSTM) and its variations.

2. RELATED WORKS

An in-depth analysis algorithm of the cat swarm optimization (CSO) which was motivated by the regular behaviour of cats. CSO is a strong and effective swarm-based metaheuristic optimization method that has gotten a lot of positive comments. The CSO algorithm is still a contender in the space [1]. The demand for energy and resources has grown more significantly as a result of the growing population and rising standard of living. The precise assessment of rising electricity energy demand is a requirement to planning tactics, boosting profits, avoiding electricity waste, and ensuring the energy demand management system runs steadily [2].

Created the cutting-edge, unique power demand forecasting system based on the LSTM Deep-Learning technique with relation to current demand patterns. Residential facilities, which are impacted by the weather, had a higher forecasting error rate than other facilities when using power demand data as input [3]. In order to predict and forecast the variable energy demand in decentralised power systems in overall and houses in specific and proposed idea to do the implementation with the feature selection. Improved forecasting of electricity demand with more predictors that is a greater risk of over-fitting in prediction models [4].

The system is made up of the two processes of extracting the highest peaks and load forecasting. It provides long-term forecasting, and the model is trained using data from prior years and serves an output. Reduce the requirement for last-minute non-renewable energy generation [5]. In order to develop the power generator sector and get ready for routine operations, anticipating electricity demand is crucial. Due to the intricacy of the available demand patterns, predicting future electricity demand can be difficult [6].

The main goals of implementing renewable energy in India are to encourage trade and industry development, improve energy security, and grow then trance to energy. It has also been determined what challenges the renewable sector is currently facing. The recommendations based on the review's findings give entrepreneurs, investors, industries, departments, researchers, and scientists vital information. Renewable technology uptake is hampered by a lack of thorough regulations and regulatory frameworks [7]. The straightforward defence system to guard against pollution and resource depletion in the environment. Using a photovoltaic (PV) system, solar energy is a renewable resource that may be transformed into electricity [8].

In order to address the unfavourable convergence behaviour of the optimization methods that is used to static sized windows of previous gradients to measure the gradient appripes to increase the performance [9].

3. PROPOSED METHODOLOGY

The proposed system is used to predict the energy consumption in the next 5 years using CSO with LSTM. In order to improve accuracy, it uses the dataset that was gathered at Central Electricity Authority (CEA), India to identify the best attributes.

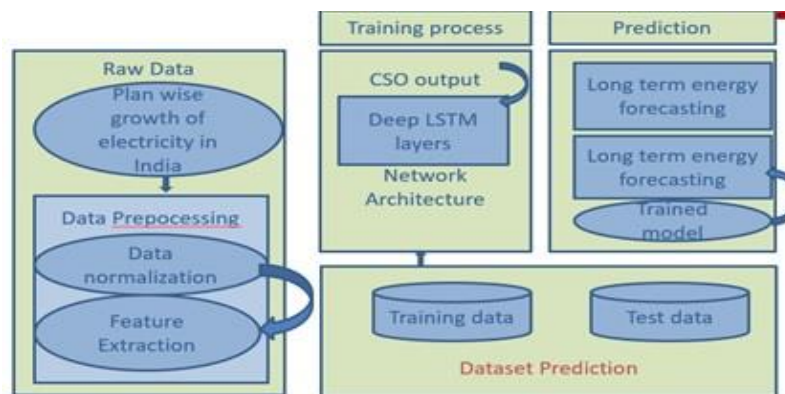


Figure 3.1. Architecture Diagram for Proposed Energy Forecasting System

Proposed schematic diagram for energy forecasting using CSO with LSTM shown in Figure 3.1. It is used in Pycharm, Jupiter, and Colab, and real-time data were used in the study. Deep LSTM model with CSO is used to train the ideal features. The findings of the proposed model are compared to those of the existing models in terms of set up capacity forecast, village electrification, hydro, coal, diesel, nuclear prediction, etc. The suggested model improves mean squared error (MSE) and root mean square error (RMSE) for LSTM by a percentage. Energy consumption is projected with a point of interval of 5 years' head using time series data sets from several utilities that have been educated using a hybrid model.

3.1 Data Pre-processing: The real-world datasets gathered may contain errors because to inconsistency of data. In order to prepare the data for future analysis, it is essential of the numerous pre-processing methods for handling unclean data.

3.2 Data Cleaning and Data Transformation: Data transformation is used to scale the properties. Redundancy data are eliminated and then number of attributes is decreased using data reduction procedures. Data should be standardized using the Min-Max scaler to prevent bias throughout the training phase. The data transformation phase is applied to the input values of time series data.

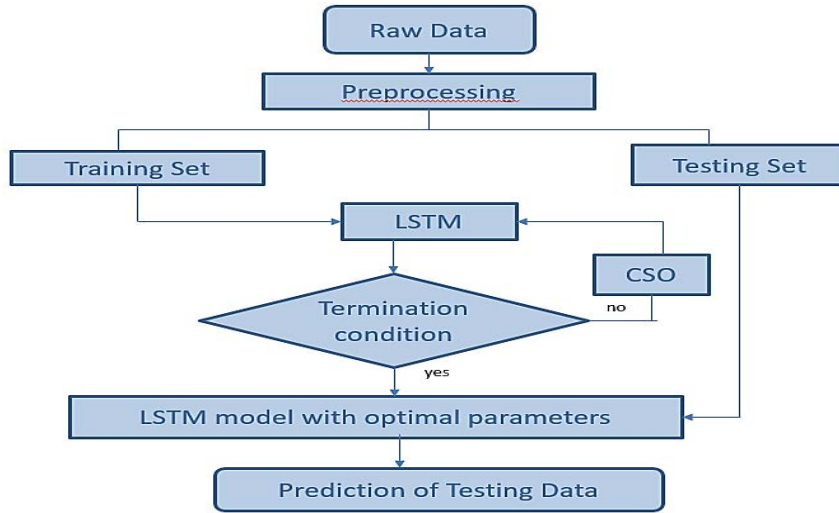


Figure 3.2. Data Flow Diagram

3.3 Data Extraction and Selection:

The output of data transformation procedure is subsequently sent into the extraction step of the technical indicators. In order to get the best forecast outcomes for electricity generation, technical indicators like the Simple Moving Average (SMA) and Exponential Moving Average (EMA) are successfully retrieved the efficient feature extraction and selection parameters.

3.4 Comparison of Energy Forecasting: Based on an LSTM classifier, the chosen feature N is utilised to forecast electricity demand or generation. However, the proposed CSO is used to carry out the LSTM training procedure. Figure 3.2 diagram shows the data flow of the proposed idea. Here, first the data is taken from growth dataset from Central Electricity Board India. The training and testing the data is done by applying the Deep learning techniques then condition is checked if condition gets satisfied then the output is displayed i.e prediction of energy consumption.

4. IMPLEMENTATION AND RESULTS

4.1 CSO with LSTM Algorithm

CSO with LSTM is a deep learning algorithm used to predict the energy consumption in next years. CSO is used to predict the best accurate values whereas the LSTM is used to take the data set and pre-process it.

4.2 Input and Output

Every year electricity board of India releases energy consumption dataset as a growth book [10]. The data contains the power consumption which has yearly power consumption, monthly power consumption, weekly power consumption and daily

power consumption. Taking that data as a data set and passing that data into CSO-LSTM deep learning algorithms to predict the amount of energy consumed in the future years. Forecasting of power consumption shown in Figure 4.1 and so proposed hybrid model achieved higher performance results for energy consumption is calculated to the next five years.

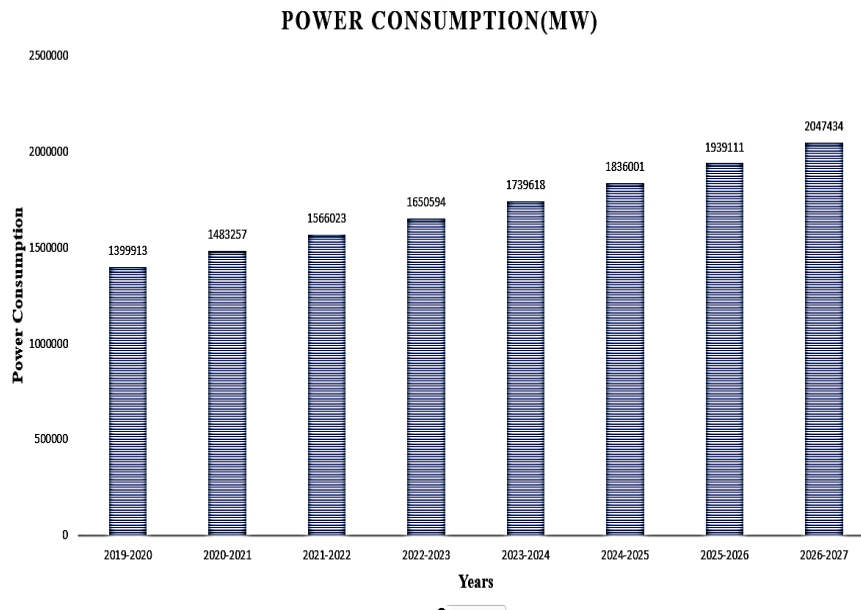


Figure 4.1 Forecasting of power consumption

5. CONCLUSION AND FUTURE WORKS

In this paper the four processes of the suggested approaches such as data transformation, technical indicators, feature extraction and selection, and power consumption of the predicted energy demands. A LSTM classifier that had been trained using the suggested CSO technique was used to anticipate the demand for electricity. Energy demand data is used to forecast future energy consumption using combined the CSO with LSTM deep learning algorithm by 2027. This strategy will reduce errors, result in a procedure that is cost-effective, and have a faster convergence rate, which will cut down on training time and increased accuracy. In future, the energy demand will be replaced with the various kind of renewable energy sources and also the long-term forecasting that will be possible to increase the arrangement of future energy demand, energy generation and consumption.

REFERENCES

- [1]. Aram M. Ahmed, Tarik A. Rashid, Soran Ab. M. Saeed, 'Cat Swarm Optimization Algorithm: A Survey and Performance Evaluation', Hindawi Computational Intelligence and Neuroscience, 2020.
- [2]. J. Bedi, D. Toshniwal, 'Energy load time-series forecast using decomposition and autoencoder integrated memory network', Appl. Soft. Comput. 2020, 93, 106390, 2020.
- [3]. E. Choi, S. Cho, D. K. Kim, 'Power Demand Forecasting Using Long Short-Term Memory (LSTM) Deep-Learning Model for Monitoring Energy Sustainability', Sustainability 12, 1109, 2020.
- [4]. A. Eseye, M. Lehtonen, T. Tukia, S. Uimonen, R. J. Millar, 'Machine Learning Based Integrated Feature Selection Approach for Improved Electricity Demand Forecasting in Decentralized Energy Systems', IEEE Access, 7, 91463–91475, 2019.
- [5]. J. Joaquin, M. Jimenez, L. Stokes, C. Moss, Q. Yang, V. N. Livina, 'Modelling energy demand response using long short-term memory neural networks', Energy Effic., 13, 1263–1280, 2020.
- [6]. T. Kang, D. Y. Lim, H. Tayara, K. T. Chong, 'Forecasting of Power Demands Using Deep Learning', Appl. Sci. 2020, 10, 7241, 2020.
- [7]. J. C. R. Kumar, M. A. Majid, 'Renewable energy for sustainable development in India: Current status, future prospects, challenges, employment, and investment opportunities', Energy Sustain. Soc., 10, 2, 2020.
- [8]. K. Padmanathan, U. Govindarajan, V. K. Ramachandaramurthy, A. Rajagopalan, N. Pachaivannan, U. Sowmmiya, 'A sociocultural study on solar photovoltaic energy system in India: Stratification and policy implication', J. Clean. Prod., 216, 461–481, 2019.
- [9]. Y. Yu, F. Liu, 'Effective Neural Network Training with a New Weighting Mechanism-Based Optimization Algorithm', IEEE Access, 7, pp. 72403–72410, 2019.
- [10]. Central Electricity Authority, Government of India, Ministry of Power, 2021. Available: www.data.gov.in

Monitoring and Security based Smart Wastebin for real time Application

Shuvendra Kumar Tripathy¹, G. Palai², K. P. Swain³

¹Department of EEE, Trident Academy of Technology, Bhubaneswar, Odisha, India

²Department of EEE, Gandhi Institute for Technological Advancement Bhubaneswar, Odisha, India

E-mail: shuvendra12478@gmail.com, gpalai28@gmail.com, kaleep.swain@gmail.com

Abstract

The overwhelming and massive augmentations in population procreate despondent all over the map in present day. Waste management is hulking ultimatum subsequently. An appropriate waste management structure is imperative to abstain from the prolonging diseases. In this system the ingenious dustbin is ubiquitously installed in the road side of the smart city. All tracked ingenious dustbin are carefully monitored and appropriate arbitration are considered as per the status of the bin through the IoT technology. The projected system will forewarn the real time status of individual dustbin to the concern authority of a particular region. The collection agency will have to send a vehicle only when the bins are full. This service will curtail the fuel cost as the route of the vehicle is determined from the Google map where red marks are showing full of the dustbin, yellow marks are going to full and green marks are empty dustbin. The works include, Raspberry Pi, Arduino Uno, Servo Motor, Ultrasonic Sensor, IR Sensor and Solar Panel. An internet connection is enabled through a WSN based modem. All the received distinctive sensor data of the different dustbin are figured out and processed in the cloud database. A pertinent web application as well as GUI is responsible for displaying status of the garbage inside the dustbin.

Keywords. Raspberry Pi, Arduino Uno, Servo motor, Ultrasonic Sensor, IR Sensor and Solar panel, Python programming language, Mobile APP.

1. INTRODUCTION

The staggering and gigantic growths in populace reproduce discouraged everywhere in show day. Squander administration is bulky final offer accordingly. A fitting waste administration structure is basic to go without drawing out infections [1], [2], [3] and [4]. In this proposed framework the brilliant dustbins are watch out for and the choices are taken according to the status of containers. Through a WSN IoT based web association, information is gotten, dissected and prepared in the cloud that shows the garbage status in the waste canister on the GUI on the internet

browser [5]. Data is collected from different sensor and stored in cloud [6]. A cloud-based analysis will take care. If the data are above the threshold level, then SMS will be sent to the concerned authority of Municipality Corporation and necessary action will be initiated. The analysis will be done in real time [7] [8]. A Mobile APP will be developed for the society people as well as to the concerned authority. They can control the respond from anywhere and anytime remotely [9].

The framework would manage two kinds of clients, i.e an official/administrator/overseer with special rights and community with constrained rights. The client's solitary method to collaborate with the framework is the web-based interface. An administrator client may have rights like checking status all bins then sending vehicles in the right time to right place and creating information for analysis report. While a native may just have the privilege to check the receptacle status of his region and enrol a protestation if any related with to the framework. Our proposed work can be actualized in our savvy city which is sufficiently enormous to tackle the issues with respect to waste management administration.

2. PROBLEM IN THE EXISTING TECHNOLOGY

Lack of data about the gathering time and region. and Lack of appropriate framework for checking, following the trucks and waste container that have been gathered continuously. There is no estimation to the measure of strong waste present inside the canister and the encompassing region because of the diffusing of waste. Lack of fast reaction to dire cases like truck mischance, breakdown and long time lingering. Odour issues and spoils the excellence of the city as well as Bad accumulation framework i.e., junk gathering vehicle is been sent to the territory every day twice or thrice relying on the separate populace here and there and there the dustbins may not be full.

3. SOLUTION TO THE PROBLEM

To plan a model which is a shrewd ready framework for savvy dustbin in the keen city and to incorporate diverse detecting and correspondence advancements utilizing IoT, constant strong waste container observing framework. When the dustbin is full then it naturally sends SMS to the concerning expert. It will likewise take care the filled level of dustbins. The primary objective in this proposed item is to decrease in cost, asset enhancement and compelling use of shrewd dustbins can be accomplished by actualizing this proposed framework. This will limit fuel cost as the path of the vehicle is as of now chosen. The concerned expert should send the trash gathering vehicle just when the dustbins are full.

4. PROPOSED SCHEME

A prototype model will be designed for Municipality Corporation and proficient enough and can be implemented in various street of the Bhubaneswar Smart City. A SMS signal will be given to the municipality authority so that they will be alerted and will send dustbin collection vehicle. The prototype model will be designed so that the authority as well as the society people can easily operate with the Mobile

App with a minor training. All the sensors will be interfaced with high performance Raspberry Pi development board. All the sensors' data will be uploaded to IoT Platform where cloud analysis will be carried out. In this proposed prototype model low power Raspberry Pi based embedded system will be used, so the power consumption will be greatly reduced. The block diagram of proposed prototype model is shown in Fig .1

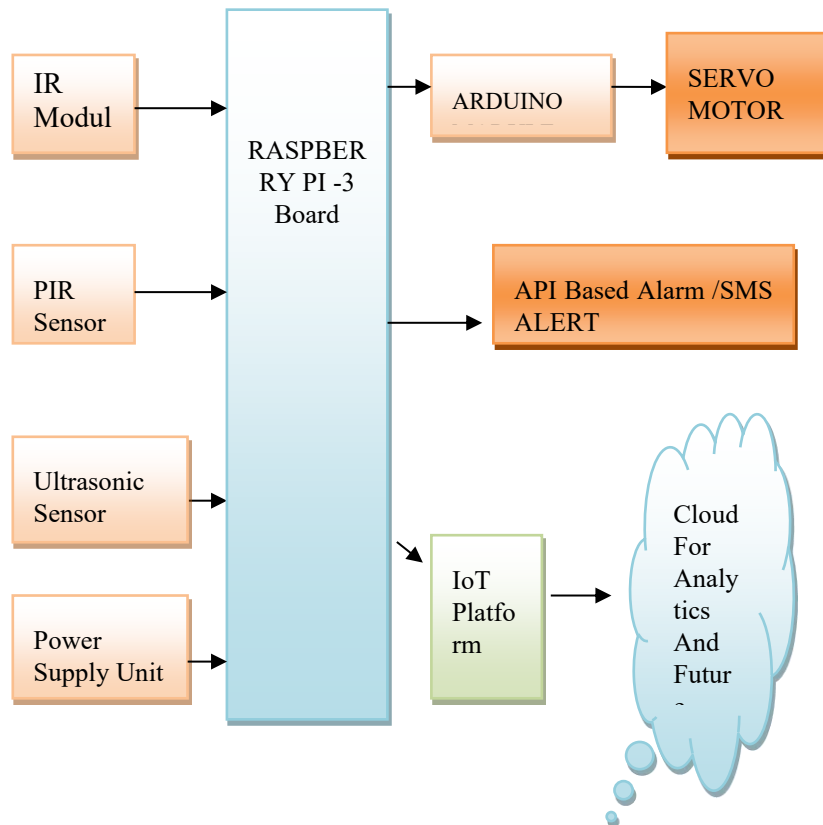


Fig.1 Block diagram of the proposed prototype model

5. METHODOLOGY

The ultrasonic sensors will be used to identify the person with garbage to be put in the dustbin. If the garbage level will be below the threshold level inside the dustbin, then the bin will be uncovered by a Servo Motor which will be connected through Raspberry Pi interface with the Arduino. The sensor output is fed to the input to Raspberry pi which will be programmed with NODE Red software in which algorithm will be designed for threshold levels for smart dustbin. The monitoring of bin will be shown in computer as well as a separate mobile application will be designed. The status of the dustbin will be hosted in cloud. If the dustbin level is more than the threshold level then a SMS will be sent to the BMC authority. Steps involved in designing the prototype model

Step-1 All the sensors i.e Ultrasonic and IR sensor will be interfaced with the analog to digital converter pins and then connected to Raspberry Pi.

Step-2 The prototype model will be designed in which the sensors will be exposed towards the inside of the bin. The signs created from the sensor will distinguish the level of the trash inside the dustbin. For the different concentrations of garbage, the corresponding values will be noted. The threshold level for bin to protect the overflow will be observed and will be written in the logical statements of the program.

Step-3 The WSN based embedded system will be interfaced with the IoT platform through which all the sensor data will be stored in cloud. The bin will be uncovered by a Servo Motor which will be connected through Raspberry Pi interface with the Arduino Uno, If the levels of garbage is above the threshold level, then an SMS signal will be generated and sent to the authority.

Step-4 An API will be designed for the mobile application. This portable application will be utilized by the administrator client who has rights to check the status of everything being equal and convey gathering vehicles and creates information examination report. In addition, a client may just have the privilege to check the canister status of his territory and enrol a protest. An SMS will be sent to the officer concerned, if the garbage levels are above the threshold level. Real Time field testing of the developed prototype model will be done which is shown in Fig.2.

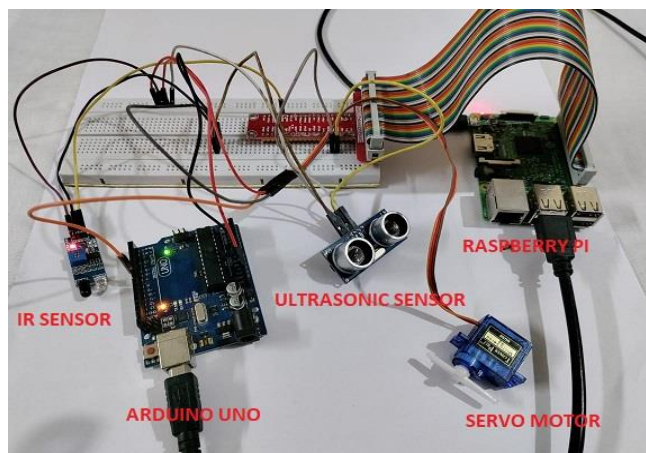


Fig 2. Interfacing the sensor module with Arduino and Raspberry Pi for Smart Dustbin

6. MODEL WITH CIRCUIT IMPLEMENTATION

The proposed work is done by utilizing Raspberry Pi for the WSN Technology for garbage monitoring using IoT. The garbage bin has sensors which check the level of garbage in the bin and informs the person about the status. All the sensors will be interfaced with the analog to digital converter pins and then connected to Raspberry Pi. The signals generated from the sensor will detect the level of the garbage inside the dustbin. The bin will be uncovered by a Servo Motor which will

be connected through Raspberry Pi interface with the Arduino. If the levels of garbage are above the threshold level, then an SMS signal will be generated and sent to the person concerned. An API will be designed for the mobile application. This mobile application will be used by the operator user who has rights to check the status of all bins.



Fig. 3 Prototype Model Side View



Fig. 4. Prototype Model Top View

FLOW CHART: The total strategy for module is clarified by a Flow Chart as appeared in fig 5.

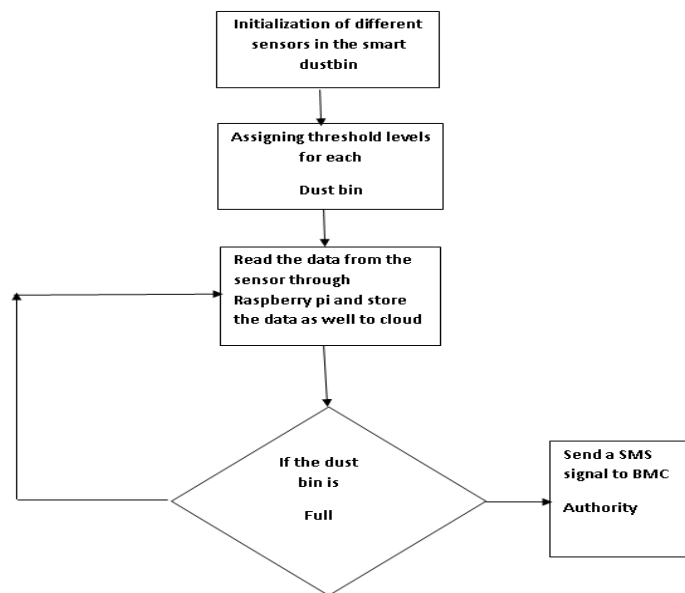


Fig. 5 Project implementation Flow Chart

7. RESULT

To evacuate the issues, numerous frameworks has been created. But IoT based smart dustbin has not introduce in the municipality corporation in the state of Odisha.

Through this mobile app we can monitor and control of smart waste bin in smart city.

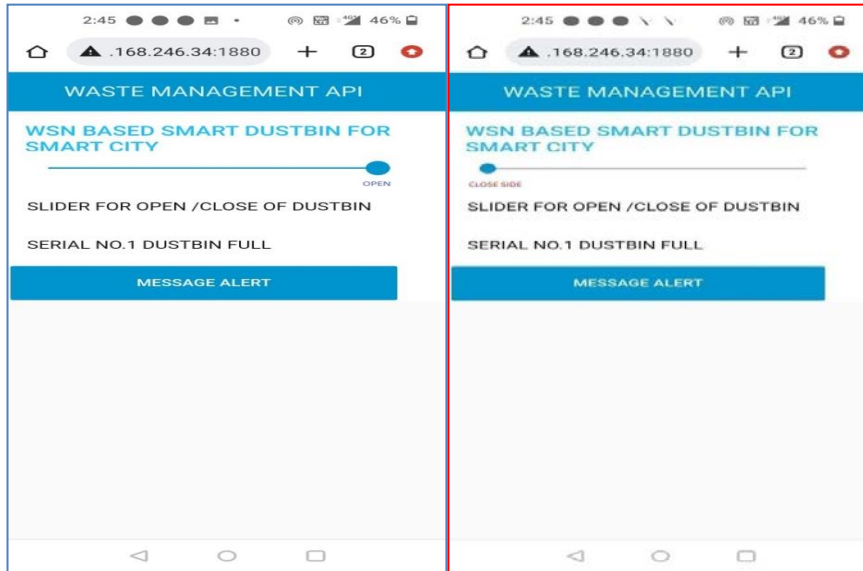


Fig.6 Mobile APP of the proposed prototype model for opening and closing the lid of the bin.

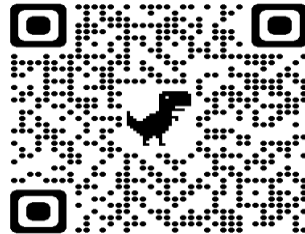


Fig. 7 This QR Barcode for the Application based URL (192.168.246.34:1880/UI) where the authority can send the alert message to the driver people.

8. CONCLUSION

A neoteric approach for checking out the Smart Dustbin system in the smart city using IoT is presented in this paper. This broadly impacts on the broader scientific community in terms of benefits to society along with the smart city application.

REFERENCES

1. Aldujaili, Ali & Dauwed, Mohammed & Meri, Ahmed & Sami, Safa. (2022). Smart internet of things kindergarten garbage observation system using Arduino

- uno. International Journal of Electrical and Computer Engineering. 12. 6820-6828.
2. Vishali, R. & Sarmila, R.V. & Priyadharshini, K.M. & Rajkumar, R. & Thiagarajan, D. & Menagadevi, M. (2022). Wireless Waste Management Monitoring System for Residential Society with Automatic Self-Navigated and Self- Sanitizing Trash Can. 1956-1960.
 3. Dr. Archana Shirbhate, Prof. Shahid Arafat, Dnyaneshwari Chhanikar, Yashraj Singh, Yash Patil, Manish Sharma, Shruti Khawase, " E-Waste Bin for Disinfection and Waste Management of Masks", International Journal of Scientific Research in Science and Technology (IJSRST), Volume 8, Issue 3, pp.613-617, May-June-2021.
 4. Abhishek Dev, Maneesh Jasrotia, Muzammil Nadaf, Rushabh Shah, "IoT Based Smart Garbage Detection System", in International Research Journal of Engineering and Technology (IRJET) Volume: 03 Issue: 12 — Dec -2016.
 5. P. Siva Nagendra Reddy, R. Naresh Naik, A. Amareshwar Kumar, S. Nanda Kishor, "Wireless Dust Bin Monitoring and Alert System Using Arduino", in 978-1-5090-3239-6/17/31.00©2017IEEE.
 6. Gaikwad Prajakta, Jadhav Kalyani, Machale Snehal, "Smart Garbage Collection System in Residential Area", IJRET: International Journal of Research in Engineering and Technology, Volume: 04 Issue: 03 — Mar-2015.
 7. Bharadwaj B, M Kumudha, Gowri Chandra N, Chaithra G "Automation of Smart Waste Management Using Iot To Support "Swachh Bharat Abhiyan" – A Practical Approach" in 2017 Second International Conference On Computing and Communication Technologies (ICCCT'17).
 8. Alexey Medvedev, Petr Fedchenkov, Arkady Zaslavsky, Theodoros Anagnostopoulos, and Sergey Khoruzhnikov, "Waste Management as an IoT-Enabled Service in Smart Cities" in Springer International Publishing Switzerland 2015 S. Balandin et al. (Eds.): NEW2AN/ruSMART 2015, LNCS 9247, pp. 104–115, 2015,
 9. Insung Hong, Sunghoi Park, Beomseok Lee, Jaekeun Lee, Daebeom Jeong, and Sehyun Park "IoT Based Smart Garbage System for Efficient Food Waste Management" in Scientific World Journal Volume 2014, Article ID 646953, 13 pages.

Modelling and Implementation of SEPIC Converter for Electric Vehicle Application

Chava Sunil Kumar¹, Udayini Vanga¹, Srilekha Akula¹

¹Department of Electrical & Electronics Engineering, BVRIT HYDERABAD College of Engineering for Women, Hyderabad, Telangana – 500090, India

Email: sunilkumar.ch@bvrithyderabad.edu.in

Abstract.

Converter is an important electronic component and plays a vital role in working of electric vehicle. Among all the converters Single-Ended Primary-Inductor Converter (SEPIC) has a unique feature that is, it gives constant output voltage irrespective of the varying input voltage because of this it is used for LED lightening system in electric vehicle. It also provides better voltage control, provides low input current ripple because of which harmonics can be reduced and large capacitor design is not required, it also has lesser electrical stress when compared with any other converter. This paper presents the design and implement of SEPIC converter for LED lightening system of electric vehicle by simulating it using MATLAB software. The proposed design technique is effectively validated using MATLAB/Simulink and implemented in hardware.

Keywords. SEPIC converter, PI controller, Electric vehicle.

1. INTRODUCTION

Converters are mostly used to enhance or buck voltage in response to demand. The resultant output voltage falls within the input voltage range of the SEPIC Converter. A converter that alters voltage is appropriate in this situation. Since buck-boost converters only need one inductor and one capacitor, they are less costly [1]. These converters do, however, contain a considerable amount of input current ripple. In many buck-boost converter applications, these ripples produce harmonics. A big capacitor LC filter is used to filter out these harmonics from the converter. However, this results in the converter becoming costly or ineffective. The fact that the output voltage is inverted by the buck boost converter complicates the use of the device further. The Cuk converter, however, overcomes these issues by including an extra capacitor and inductor. Cuk and buck-boost converter operation, however, put a lot of electrical strain on the parts, which might cause failure or overheating of the device. Both of these problems are addressed by SEPIC converters.

2. SYSTEM CONFIGURATION

Figure 2.1 depicts a simple SEPIC's schematic design. By stepping up or down the input voltage in accordance with the demand, a SEPIC converter takes a variable input and produces a constant output voltage. The amount of energy transported is

controlled by switch Q1, which is frequently a transistor like a MOSFET [2]. Compared to bipolar junction transistors (BJTs), MOSFETs have a substantially higher input impedance and a smaller voltage drop. Additionally, they do not need biasing resistors since, unlike BJTs, the switching of MOSFETs is controlled by a voltage difference rather than a current difference.

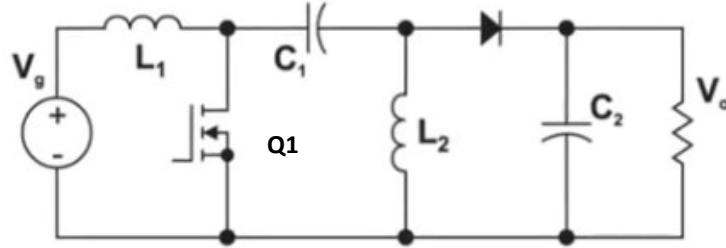


Figure 2.1. Schematic of SEPIC Converter

The converter shown in figure 2.2 contains an input capacitor, output capacitor, two inductors, a coupling capacitor, a control switch (MOSFET is considered here), an uncontrolled (Diode is considered here). The input terminal of SEPIC is connected to one terminal of the first inductor another terminal of L_{1A} is connected to capacitor C_p and drain of Q1. Second terminal C_p is connected to second inductor and anode of diode D1. Here L_{1A} is the first inductor and C_p is the coupling capacitor. The cathode of diode D1 is connected to the output capacitor. A PWM signal is given to gate of the Q1 and remaining terminals of the components are grounded as shown in figure 2.2.

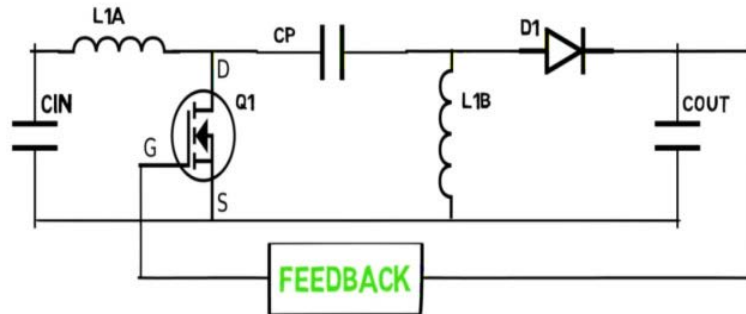


Figure 2.2. Schematic of SEPIC Converter with feedback.

3. ANALYSIS OF SEPIC DESIGN

Input Voltage consideration [3, 4, 8]

$$V_{IN} = V_{L1} + V_{C1} + V_{L2} \quad (3.1)$$

Where V_{L1} is the voltage across first inductor.

Inductor Selection

A good general rule of thumb for calculating inductance is to allow the peak-to-peak ripple current to be around 40% of the highest input current at the lowest input

voltage. Given by: The ripple current passing through inductors L1 and L2 of equal amplitude.

$$\Delta I_L = I_{IN} \times 40\% = I_{OUT} \times \frac{V_{OUT}}{V_{IN(\min)}} \times 40\% \quad (3.2)$$

The inductor value is computed as follows:

$$L1 = L2 = L = \frac{V_{IN(\min)}}{\Delta I_{IN} \times f_{sw}} \times D_{\max} \quad (3.3)$$

The switching frequency is f_{sw} , and the duty cycle at the minimum V_{in} is D_{\max} . To guarantee that the inductor does not saturate, the peak current is provided by:

$$I_{L1(\text{peak})} = I_{OUT} \times \frac{V_{OUT} + V_D}{V_{IN(\min)}} \times \left\{1 + \frac{40\%}{2}\right\} \quad (3.4)$$

$$I_{L2(\text{peak})} = I_{OUT} \times \left\{1 + \frac{40\%}{2}\right\} \quad (3.5)$$

Coupling Capacitor Selection

The SEPIC capacitor, C_s , is chosen based on the RMS current, which is provided by:

$$I_{C_s(\text{rms})} = I_{OUT} \times \sqrt{\frac{V_{OUT} + V_D}{V_{IN(\min)}}} \quad (3.6)$$

The peak-to-peak ripple voltage on C_s :

$$\Delta V_{C_s} = \frac{I_{OUT} \times D_{\max}}{C_s \times f_{sw}} \quad (3.7)$$

4. CONTROL STRATEGY

To regulate the SEPIC voltage, a control strategy for regulating the switch S1. Closed loop control is achieved with PI controllers. The following are the steps involved in tuning PI controllers:

- 1) Linearizing the plant
- 2) Identifying the new plant
- 3) Simulate data
- 4) Plant identification.

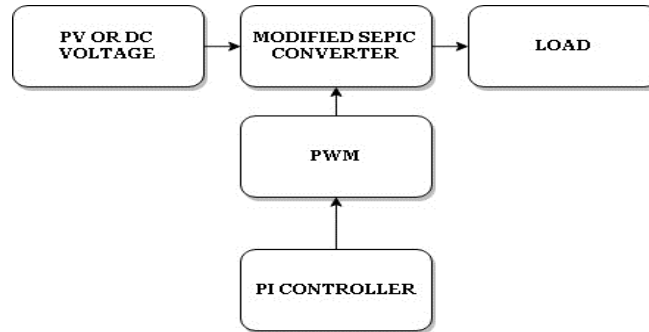


Figure 4.1. (a) Block diagram of PV system

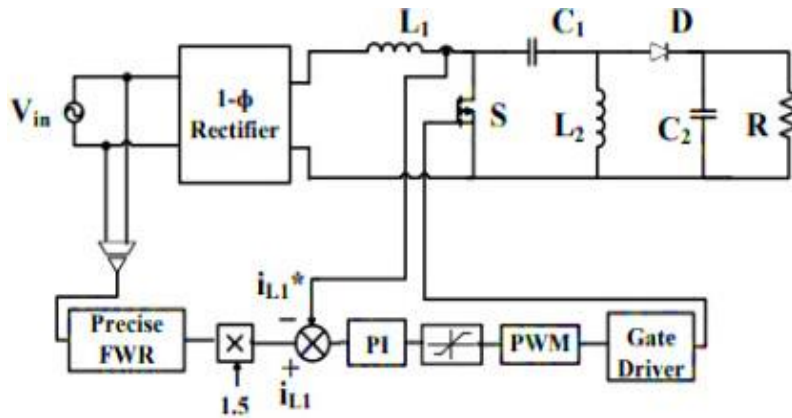


Figure 4.1. (b) Control diagram.

The control strategy for closed loop SEPIC converter is shown in figure 4.1. (a) & (b). In this configuration PI (Proportional Integrator) Controller is used to compare the output voltage with the required voltage. In closed loop configuration some part of the output is taken from the output and is given to a comparator. Reference signal as reference voltage is also given to comparator. The output of comparator is given to PI controller. The output of SEPIC is obtained by tuning the PI Controller (using plant identification method). According to the required output we get the output voltage.

5. SIMULATION RESULTS

The findings of the SEPIC converter employing the PI control scheme are shown in this part for two test scenarios. Table 1 shows the nominal parameters for the simulation research. MATLAB is used to implement the complete model. The following sections illustrate the two operational situations for a step change in source and load [5].

Table 1: Nominal Parameters for Simulation study

S. No	Parameters	Value
1	Input Voltage (V_{in})	20 V
2	Inductance (L_1 & L_2)	1.43mH
3	Capacitance (C_1 & C_2)	150 μ F
4	Resistance (R)	6.5 Ω

A. Source Voltage Step Change:

The simulation results for step change in source voltage for PI control schemes are shown in Fig. At $t=0.2$ sec, source voltage increases from 10V to 20V and bring back to 10V at $t=0.6$ sec. Due to sudden increase in source voltage results surge in load voltage. The load voltage is regulated in 3msec and 10msec at 0.2sec and 0.6sec respectively.

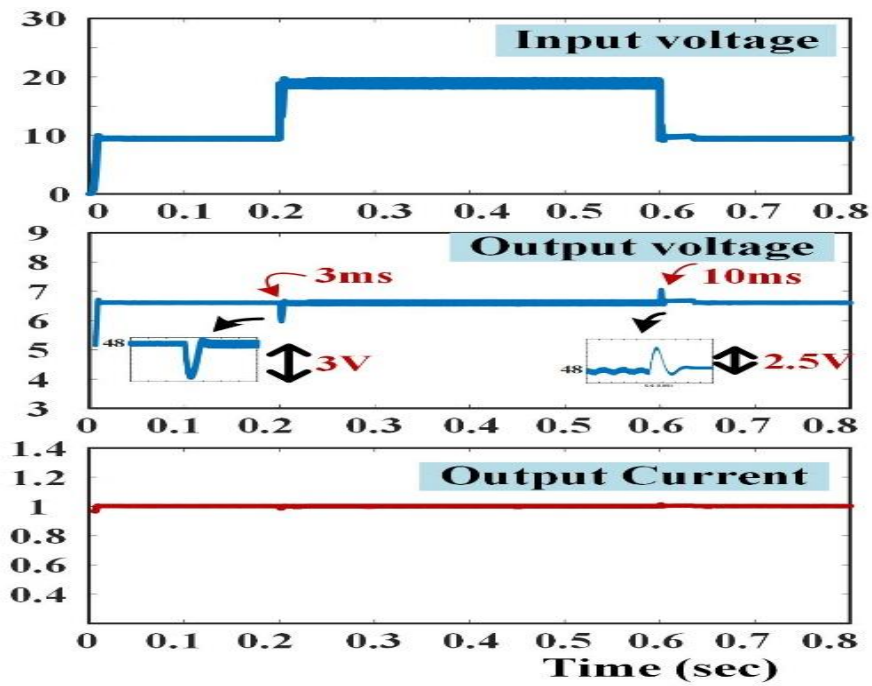


Figure 5.1. Results of simulation for a step change in source voltage

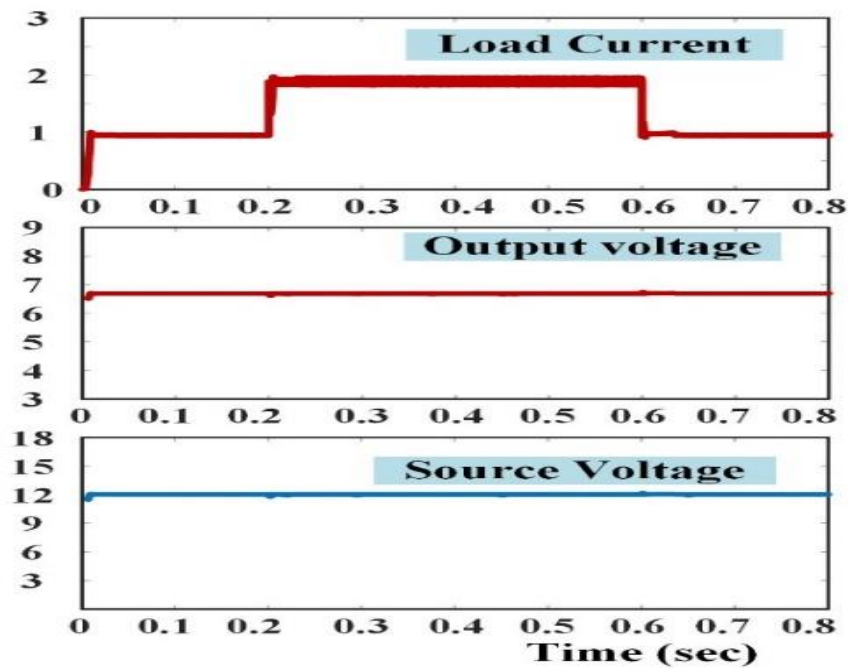


Figure 5.2. Simulation results for a load step change

B. Simulation results for step change in load:

The simulation results for PI control methods for a step change in load are shown in Fig. At $t=0.2\text{sec}$, load current increases from 1A to 2A and bring back to 1A at $t=0.6\text{sec}$. Due to sudden increase in load demand results surge in load voltage. The load voltage is regulated 6.5V.

6. HARDWARE IMPLEMENTATION

The TMS320F28069 controller board has been used in the development of the suggested method. The method is created in MATLAB with Simulink blocks. For the creation of high-speed, multi-variable digital controllers and real-time simulations in a variety of sectors, the TMS320F28069 controller board was created particularly. It is a whole real-time control system powered by a 250MHz, 603 PowerPC floating point processor. A/D and D/A converters are also available to handle analogue feedback signals. Users may debug the application, adjust settings, and track execution outcomes in real-time depending on the PC and DSP's connection capabilities.

There are two cases in the hardware output of SEPIC Converter they are:

i) When the headlight of electric vehicle glows with a bright light

The figure 6.1 shows the headlight that is used in the electric vehicles glowing with a bright light because of the output obtained from the closed loop SEPIC Converter which has a duty ratio of 0.4 with input voltage as 20 volts and output voltage of 12 volts using LAUNCHXL- F28069M board and subsequently firing pulses are generated [6, 7]. The pulses generated are given to MOSFET in the hardware circuit built. The constant output voltage obtained from the hardware circuit is given to headlight of electric vehicle.



Figure 6.1. Hardware setup for bright light

ii) When the headlight of electric vehicle glows with a dim light

The figure 6.2 shows the headlight that is used in the electric vehicles glowing with a dim light because of the output obtained from the closed loop SEPIC Converter

which has a duty ratio of 0.1 with input voltage as 20 volts and output voltage of 8 volts.



Figure 6.2. Hardware setup for dim light

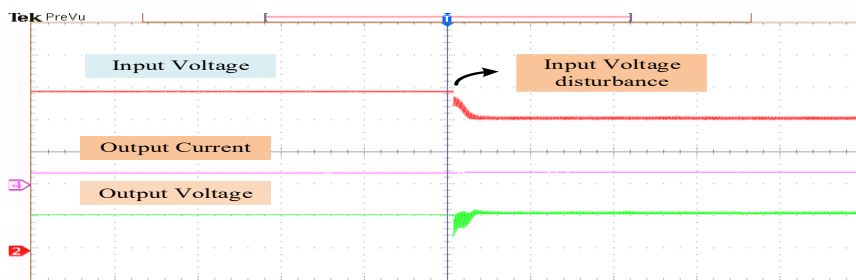


Figure 6.3 (a) Source side disturbances

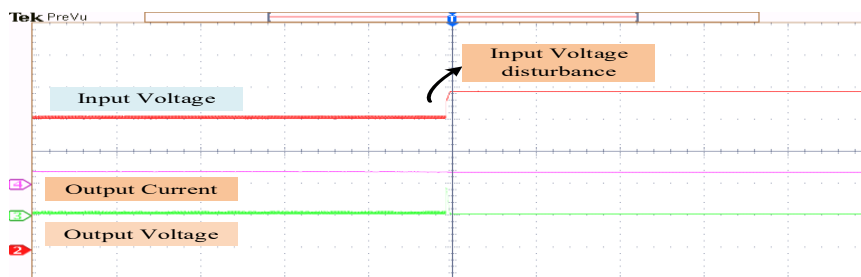


Figure 6.3(b) Source side disturbances

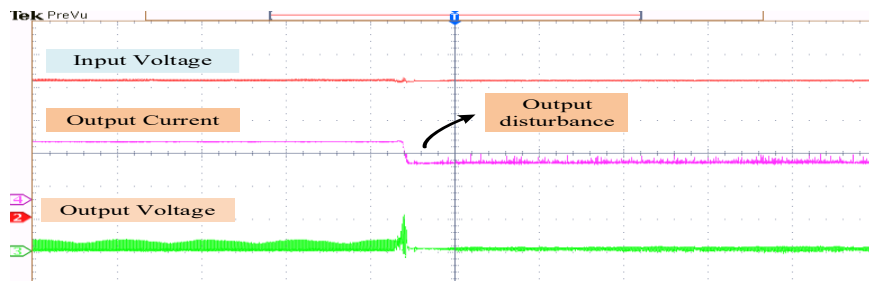


Figure 6.4 Load Side disturbances

The constant output voltage obtained from the hardware circuit is given to headlight of electric vehicle. Figure 6.3(a,b) and 6.4 shows the source and load disturbances.

7. CONCLUSION

The SEPIC may operate with input voltages that are more or lower than the output voltage's regulation. The SEPIC design has minimal active components, a straightforward controller, and clamped switching waveforms for low noise operation in addition to being able to function as both a buck and a boost. The simulation results for closed loop control show that the duty cycle may be adjusted to regulate DC output voltage as necessary. For the hardware implementation of the SEPIC Converter for the electrical vehicle lighting application from TEXAS instruments, the Simulink model of the SEPIC Converter with closed loop and open loop is completed and the results are seen.

REFERENCES

- [1] Reeto Jose. K, Anisha Shivanandan, Vani Venugopal and Kshemada Devi, 2015. V, DC-DC SEPIC Converter Topologies, *Int. Jnl. of Research in Engg. and Technology*, 04(05): 20-23.
- [2] Venkatanarayanan, S. and M. Saravanan, 2014. Proportional-integral Control for SEPIC Converter, *Research Jnl. of Applied Sciences, Engineering and Technology*, 8(5): 623-629.
- [3] Wael A. Salah, Dahaman Ishak, Basem Abu Zneid, Amir Abu Al Aish, Mohd Shawal Jadin and Anees Abu Sneineh, 2015. Implementation of PWM control strategy for torque ripples reduction in brushless DC motors, *Electr Eng.*, 97: 239-250.
- [4] Antonietta De Nardo, Nicola Femia and Walter Zamboni, 2012. Designing a mixed electrolytic/ceramic filter capacitor in DC-DC converters, *Analog Integr Circ Sig Process*, 73: 3-45.
- [5] Yuh-Shyan Hwang, An Liu, Chia-Hsuan Chen, Yi Tsen Ku, Jiann-Jong Chen and Cheng - Chieh Yu, 2014. A Continuous condition mode low-ripple high- efficiency charge-pump boost converter, *analog integer Circ Sig process*, 79: 355-369.
- [6] Uma maheswari, M.G., G. Uma and L. Annie Isabella, 2014. Analysis and design of digital predictive controller for PFC Cuk converter, *J Comput Electron*, 13: 142-154.
- [7] Dewei Jia, Yubo Duan and Jing Liu, 2009. Emerging technologies to power next generation mobile electronic devices using solar energy, *Front. Energy Power Eng. China*, 3(3): 262-288.
- [8] Anbu kumar Kavitha and Govindarajan Uma, 2010. Control of Chaos in SEPIC DC-DC Converter, *Int. Journal of Control, Automation and System*, 8(6):132.

Smart Anomaly Detection and Classification for Validation Process of Watch Gears Using LABVIEW

Boobalan S¹, Sanjeeve R¹, Thaqib K¹, Vignesh R S¹ and Vignesh S¹

¹ Sri Krishna College of Engineering and Technology, Coimbatore, India

Email: boobalans@skcet.ac.in

Abstract:

This project aims to automate the process of validation of miniature gears such as gears that are used in watches, clocks, etc., by using machine learning algorithms. These processes are carried out manually and hence the production speed is heavily dependent on the speed of validation of humans. This project aims to withdraw human support in this area by the use of machine learning. The gears are examined by using high-resolution cameras. The output of the camera is processed using NI LabVIEW's Vision Assistant which is pre-trained using ideal and defective gears. If the input gears are in coherency with those trained 'Ideal gears', such gears are sent for assembly. If the gears are defective, a signal is sent to an actuator (say a robot) to dispose of this defective gear for recycling. This way, the project when made as an industrial machine, could increase production and decrease the Cost-to-the-Company.

Keywords: Defect detection, image processing, computer vision.

1. INTRODUCTION

All manufacturing businesses try to create a variety of competitive products. The key determinants of competitiveness improvement are the productivity and quality of each industry's products. In this industry, defective items have resulted in numerous losses. Human inspection still detects the majority of faults that occur during the manufacturing process. Inspectors' work is arduous and time-consuming. Approximately 70% of defects can be identified manually. Furthermore, once a person becomes tired, the effectiveness of visual inspection decreases significantly. Because the bulk 2 of the gears are within a tenth of a millimetre of the specified size. Gear samples are increasingly being subjected to digital image processing techniques for product examination [1]. As technology advances, more and more products are being made with metals, particularly in robotics, which requires ultra-lightweight and modular components such as gears. Gears are composed of plastic material High-density polyethylene (HDPE) and other metals, according to industry statistics, which are prone to various sorts of defects (flash, warping, bubbles, empty portions, sink marks, ejector marks, and so on) when created using image processing [2]. As a result, we propose that a fully robust system based on image processing techniques (such as image segmentation and non-smooth corner detection) be investigated in order to develop a cost-effective solution for providing Total Quality

Management in manufacturing units, allowing for a continuous monitoring and improvement eco-system while lowering costs [3].



Fig 1.1 – Clock Gears

A gear is a rotating circular machine element with carved or inserted teeth (called cogs) which meshes with another (suitable) toothed part to transfer (convert) torque and speed. In terms of the underlying notion, gear action is analogous to lever action. Different-sized gears create a mechanical advantage by generating a difference in torque owing to their gear ratio, and so may be regarded a fundamental machine [9,10]. Two meshing gears have different rotational speeds and torques in proportion to their diameters. Both meshing gears have the same tooth shapes. The escapement, or wheelwork, of a clock is a set of turning wheels (gears) that transport motion from a weight or spring to the minute and hour hands. The accuracy of the wheels and pinions, as well as the tooth form, are critical for transferring power as consistently as feasible [11].

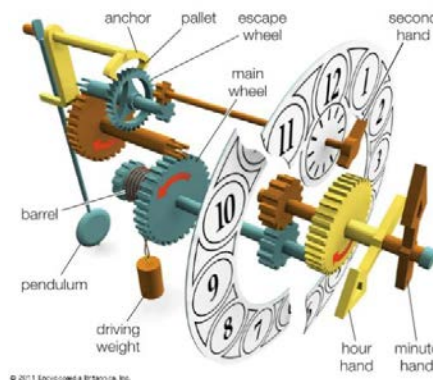


Fig 1.2 – A weight-driven clock featuring a pendulum's main components.
Encyclopaedia Britannica, Inc.

Before proceeding any further, let's have a quick glance at the common defects present in plastic materials like gears which is of course our material of interest [9]. The following are some examples of plastic gear faults that can be identified using image processing:

1. Flash: Excess moulding material that penetrates mould gaps, such as sliding push-out faces, inserts, and so on, is referred to as this fault.

2. Distortion: When the degree of shrinkage differs at different points inside the moulded component, this flaw causes deformation.

3. Bubbles: A manufacturing flaw has trapped an air bubble-like substance inside plastic gear.

4. Unfilled sections: This problem develops when injection moulding does not reach particular spots on the inside side of the die before solidifying.

5. Sink marks: On the outside surfaces of moulded components, they are markings or irregular patches on the surface.

6. Ejector marks: Flow markings are patterns left on the surface of moulded products by the flow tracks of molten plastic [4].

7. Missing Tooth: This fault refers to missing teeth/tooth in a plastic gear.

2. EXISTING METHODOLOGY

The existing methodology consists of examining and recording the condition of the functioning surfaces of gear teeth and bearings. Next, the gears are washed with solvents after the initial examination. The gears are again examined for defects. Because it is frequently the most essential aspect of the inquiry and may reveal vital information, this inspection is made as comprehensive as possible. For this investigation, a low-power magnifying lens and a pocket microscope are used.

A failure analysis report is made including all pertinent information discovered during the investigation, as well as inspections and testing, evidence weighing, findings, and suggestions. The information is thus documented in a concise manner, ideally in tables. The report normally includes suggestions for fixing the equipment or altering its design or operation to prevent future failures [5,6].



Fig 2 - Manual gear validation

However, the above-mentioned methodology suffers from various drawbacks such as

1. To make a written account of any significant observations, including drawings and pictures as appropriate.
2. To clearly identify and designate each component (including gear teeth and bearing rollers) in the textual description, drawings, and images.
3. The speed of production is purely dependent on the validation speed of employed humans.
4. The Cost-to-the-Company in case of human is far greater in comparison to a well-maintained machine.
5. As humans are liable to errors but machines, the end product will be more reliable and the defective pieces to ideal pieces' ratio will be very low

Considering the above drawbacks, an automated methodology using image processing is proposed to simplify, increase and modernize the process of validation and production [7].

3 PROPOSED METHODOLOGY

The proposed methodology consists of a High-Resolution Camera along with LabVIEW's Machine Vision Module to automate the whole process of validation of the gears before assembly [8]. As soon as the process starts, the gears are passed on to the validation stage via the conveyor. The gears are then examined by the camera (A phone camera in our case). The resolution of the camera is 108MP. The description of the apparatus used is depicted below.

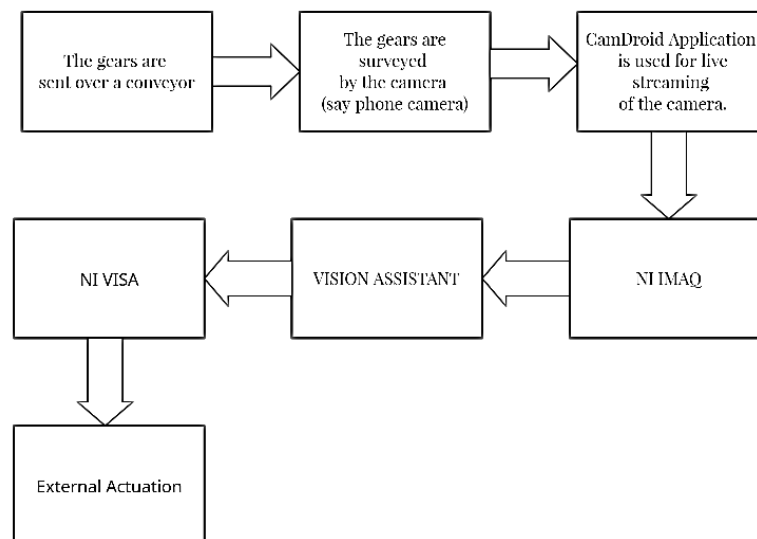


Fig 3.1 - Block Diagram of smart anomaly detection and classification for validation process of watch gears using LabVIEW

In order to decrease any noise, the camera is used under a dark environment. A flash is used to facilitate the imaging process. The image from the phone is telecasted to a Personal Computer with LabVIEW Software for further processing.

3.1 LabVIEW

The MAX and VISA toolsets include built-in support for NI hardware platforms including as Compact DAQ and Compact RIO. LabVIEW (Laboratory Virtual Instrumentation Engineering Workbench) is a platform and development environment for a visual programming language developed by National Instruments.

3.2 NI Vision Assistant

Vision Assistant is an image processing prototyping and testing tool. To design an image processing application, use the Vision Assistant scripting feature to create custom algorithms. The scripting feature records each stage of processing algorithm. The algorithm is saved as a script file that includes the processing functions and important parameters for the method you prototyped in Vision Assistant.

3.3 NI VISA

VISA is an application programming interface (API) that allows a programme to communicate with GPIB, VXI, GPIB-VXI, and serial interfaces in a consistent manner. The VISA API can be used instead of having distinct APIs for each interface. This enables the programmer to create code that can easily be converted to various interfaces [16].

3.4 Data-set Collection

The Data-set for training our model is made ready by capturing the images of both ideal and defective gears. A few of the captured images are presented below:



Defective
(Damaged at the centre)



Defective
(Damaged at the curvature)



Ideal
(No Defects)



Fig 3.2 – Gears Classification

The gears used for training model have their radii ranging from 1 cm to 1.75 cm. However, gears or parts of any dimensions can be trained effectively, as long as they are observable by the camera.

The defects which are currently observable by this project are missing teeth, dents, cracks, broken shaft and broken curvature.

The Work-Flow Diagram is presented below:

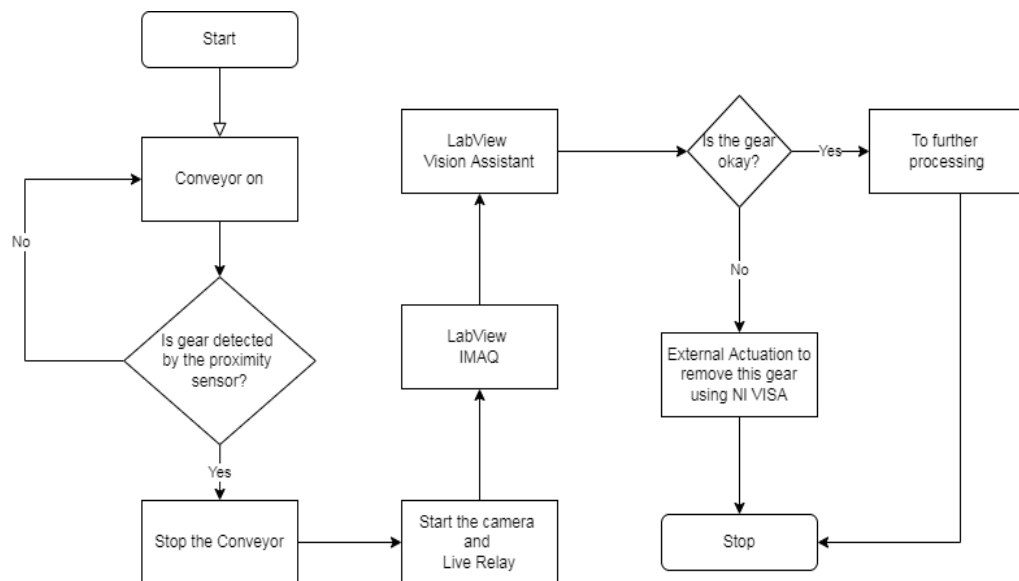


Fig 3.3 – Work flow chart of smart anomaly detection and classification for validation process of watch gears using LabVIEW.

The conveyor is loaded with the gears sequentially – one at a time. When the gear reaches the dark environment which can be focussed better by the camera, the proximity sensor outputs a signal to the controller which then stops the conveyor. The camera then live telecasts the gear to the LabVIEW using IMAQ module. This module grabs a frame from the live telecast and converts it into a

binary image by extracting the luminance features present in the image. This extracted feature is sent to the Vision Assistant which is preloaded with the trained images of both damaged and ideal gears. The Vision Assistant then clusters the input data with the trained models and outputs a signal depicting whether the gear is ideal or damaged. If the gear is devoid of damages, it can be sent for further processing. If the gear is found to be defective, a signal is sent to the external actuator (say a pick and place robot) to remove the defective gear.

4 RESULTS AND DISCUSSION

The above proposed method is implemented in the Robotics Automation Laboratory in our institution viz. Sri Krishna College of Engineering and Technology and the results are obtained. The gear models are trained using K-Nearest Neighbour clustering algorithm.

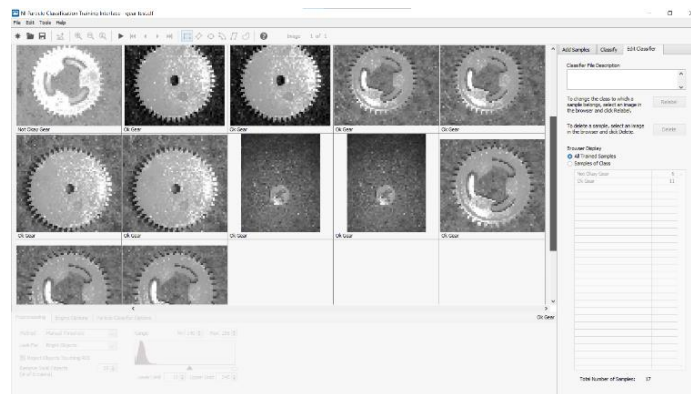


Fig 4.1 – Model Training

In Fig 4.1, the gear models used for training are depicted. For improving accuracy, one can train more models and classify them accordingly. Before training a picture, one has to choose the area of focus.

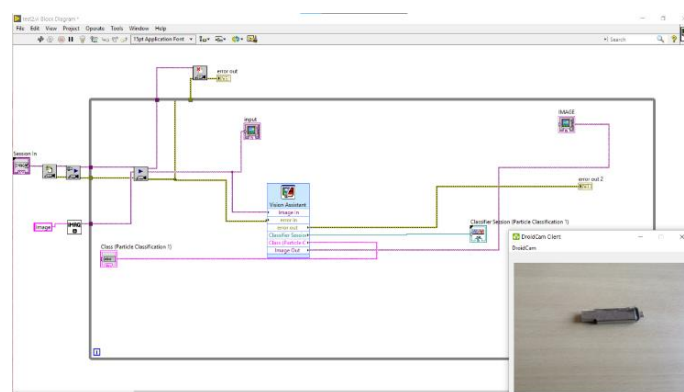


Fig 4.2 - LabVIEW Block Diagram

This can be done easily by adjusting the image histogram to select a particular feature such as luminance and omitting the others. The LabVIEW Block Diagram presented in Fig 4.2 has a NI IMAQ's Session in module via which the input camera which are connected to the PC can be selected. In our case, as we are using Droid Cam Client to telecast our phone camera to our PC. This telecasted phone camera is referred to as an external camera by the PC.

The next step which initializes the camera and grabs an image from the telecast, forwards the acquired image to the Vision Assistant Module. The forwarded image is visible to the user in the front panel. The image processed by the Vision Assistant is also visible to the user. These are shown in Fig 4.3.

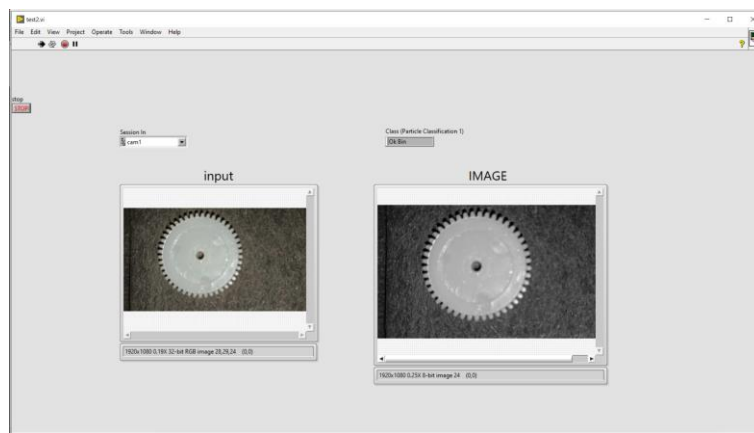


Fig 4.3 – LabVIEW Front Panel

The processed image is then classified based on the trained models and as seen from Fig 4.3, the Class (Particle Classification 1) string output shows “Ok Bin” meaning that the gear is free from defects.



Fig 4.4 Shows the Lab setup consisting of a conveyor, a ABB Robotic Arm, PLC and Servo Controllers and a PC with LabVIEW.

Let's have a look at the project's algorithm: One of the most essential Machine Learning algorithms is the K-Nearest Neighbour technique, which is based on Supervised Learning. When data has a high SNR, KNN is preferable to linear regression. The KNN method assumes that the new case/data and past cases are similar, and it allocates the new case to the category that is the most similar to the previous categories. The K-NN algorithm stores all available data and categorises incoming data points based on their similarity to existing data. This means that new data can be quickly sorted into well-defined categories using the KNN technique.

Assume there are two categories: A and B, and you receive a new data item x_1 . This data point belongs in which of the following categories?

This type of challenge necessitates the use of a K-NN algorithm.

We can simply determine the category or class of a dataset with the help of K-NN [12].

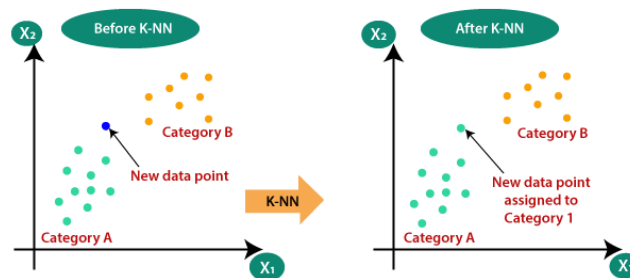


Fig 4.5 – K-NN

5 CONCLUSION

We can detect damaged gears with a number of teeth ranging from 64 to 120 using this proposed Methodology. The gear is declared defective and sent for recycling if the number of teeth is twisted, exceeds, or falls below the prescribed number. Second, using a range bound threshold that works on both colour and greyscale photos of the gears, we were able to identify some surface imperfections. This liberal technique can greatly limit the number of damaged gears transported to the assembly room by accident. Future approaches for improving the detection systems' performance include applying more complicated machine learning algorithms to identify problematic sections as they appear over time. The accuracy of the scenario machine techniques like as Support Vector Machine and neural network improves as a result of the adjusted parameter configuration. Thus, by automating a manually performed operation in an enterprise, the quality and quantity of output can be greatly enhanced.

6 FUTURE SCOPE

In future, the shaft radius and the gear radius can be included to the train model. If any part with radii different from that of the trained model is found, it would be classified as defective.

Currently, we were able to detect the defective gears with a specified number of teeth as mentioned above in this article. If the number of teeth is malformed or the gear is classified as defective by any means after processing by our system, a signal is sent to the robotic arm in the validation unit's conveyor in the future. The robotic arm is programmed to select and remove the faulty equipment based on the inputs given by LabVIEW [13].

For this purpose, we have planned to implement the above-mentioned process in the ABB Robotic Arm available in our institution's Robotics Automation Lab in Mechatronics Department. The image of the same is mentioned above: Fig 4.4.

If a defective part is found, reports can be generated automatically [14]. The report can withhold all the required information regarding the defective part such as defect classification, causes of the particular defect, number of defective parts with the same defect recognised so far etc. This information can be supervised by a manager which could facilitate improvising design and production methodologies to avoid faulty parts.

REFERENCES

1. S. LI.: Mesh Stiffness and Its Non-Linearity of a Pair of Spur Gears with Machining Errors, Assembly Errors and Tooth Modifications, The Proceedings of the Symposium on Motion and Power Transmission.
2. Prerna, Gaur., Poras, Khetrapal., Rajat, Sood., Abhijeet Bharadwaj.: Image Acquisition and Colour Based Segregation of Objects Using Labview, IEEE International Conference on Computing for Sustainable Global Development (2016)
3. Liu, L., Pines, D. J.: The Influence of Gear Design Parameters on Gear Tooth Damage Detection Sensitivity, Journal of Mechanical Design.
4. Moru. Desmond, K., Borro, D.: A Machine Vision Algorithm for Quality Control Inspection of Gears, The International Journal of Advanced Manufacturing Technology.
5. Mavi, A., Kaur, M.: Identify Defects in Gears Using Digital Image Processing. International Journal of Engineering Research and Development ISSN, pp. 49-55. (2012)
6. Tremaine, A.: Characterization of Internal Defects in Open Die Forgings. FIERF Grant Project for Undergraduate Research, 18. (2005)
7. Kamaruddin, S., Khan, Z. A., Foong, S. H.: Application of Taguchi Method in the Optimization of Injection Moulding Parameters for Manufacturing Products from

- Plastic Blend. *International Journal of Engineering and Technology*, 2(6), 574. (2010)
8. Szabó, R., Lie, I.: Automated Colored Object Sorting Application for Robotic Arms, (1 November 2012)
 9. Mahmoodi, M., James, L., Johansen, T.: Automated Advanced Image Processing for Micromodel Flow Experiments; An Application Using Labview, (1 August 2018)
 10. Rincon, A. F. D., Viadero, F., Iglesias, M., de-Juan, A., Garcia, P., Sancibrian, R.: Effect of Cracks and Pitting Defects on Gear Meshing. *Proceedings of the Institution of Mechanical Engineers, Journal of Mechanical Engineering Science*, 226(11), 2805-2815. (2012)
 11. Gaur, P., Khetrpal, P., Sood, R., & Bharadwaj, A.: Image Acquisition and Colour Based Segregation of Objects Using LabVIEW. In 2016 3rd International Conference on Computing for Sustainable Global Development (INDIACom) pp. 2461-2464. IEEE. (March, 2016)
 12. Posada-Gómez, R., Sandoval-González, O. O., Sibaja, A. M., Portillo-Rodríguez, O., & Alor-Hernández, G.: Digital Image Processing Using Labview. *Practical Applications and Solutions Using LabVIEW Software, InTech*, 297-316. (2011)
 13. Lee, J. M.: An Efficient kNN Algorithm. *The KIPS Transactions: PartB*, 11(7), pp. 849-854. (2004)
 14. Wang, S., Gao, L., & Zhang, C.: Image Processing Technology Based on LabVIEW Simulation System. In *Proceedings of the 2012 International Conference on Cybernetics and Informatics* pp. 1089-1094. Springer, New York, NY. (2014)
 15. Mouli, C. C., Jyothi, P., Raju, K. N., & Nagaraja, C.: Design and Implementation of Robot Arm Control Using LabVIEW and Arm Controller. *IOSR Journal of Electrical and Electronics Engineering*, 6(5), pp. 80-84. (2013)

An Effective Rapid Electric Vehicle Charger Using a Quasi-Direct Boost - Buck Converter

J. Sreedhar¹, U. Prashanth¹

¹Vignana Bharathi Institute of Technology, Hyderabad, India

Email: sreedharmtech@gmail.com

Abstract

This paper details a quick DC-type battery charger for electric vehicles, with reduced switching losses. A discontinuous PWM (DPWM) control is used, each phase-leg of a typical 3-phase, 2-level voltage source configuration with poor storage of capacitive energy switches off for 240 degrees of the grid essential duration, resulting in just one phase-leg switching every 60 degrees. Therefore, a buck-model DC-DC configuration is used in cascaded connection with the aim of supply current restriction and voltage control for the electric car charging process because the AC-DC network lacks the DC-link voltage controllability. While thinking about charging a Nissan Leaf, we simulated the provided circuit to various options for a built 50 kW battery charger power capability. The data demonstrates that the investigated technology is extremely power efficient.

Keywords. Electric vehicle, charging, battery, boost-buck.

1. INTRODUCTION

The charging market of electric vehicle (EV) is extremely fluid. Companies and organisations engaged in investigation and improvement of in these fields have greatly reduced his charging time for electric vehicles, making it the same as the time users spend charging an internal combustion engine vehicle (ICEV) at a gas station. Currently, most 50kW 400V electric vehicles comply with "CCS - up to 80kW" and "CHAdeMO - around 50kW" fast charging standards Rechargeable. New electric vehicles, alternatively, are built to withstand higher charging powers. As a result, scalability of output power using power electronics building blocks (PEBB) is an important feature of the EV charging system.

By using a parallel connection, total power can be scaled. This translates into manufacturing benefits because a single circuit package design can be used meet multiple companies and many charging standards. Connecting to the AC grid at medium voltage (MV) levels is becoming economically viable for EV chargers with 100s of kW capacity, as the 380V to 480V grid is most commonly used today. Where high-capacity chargers are installed, Battery banks and other local energy storage systems can be used to diminish power instabilities and AC grid quality problems. Native renewable power production organisations can also be utilised to

reduce power mandate and grid ingesting. In reality, the use of photovoltaic (PV) power generation has great potential. This is because the available area of EV charging station roofs and his buildings in the neighbourhood can exceed 1000 m2. It is also possible to integrate both the battery and the PV array as proposed in [1], into the charger itself.

Figure 1 depicts a bidirectional PEBB configuration suitable for connecting a huge power EV charger using DC type to an MV grid through a 50 Hz transformer. Battery chargers have the advantage of being fully equipped with half-span power modules making them accessible to countless manufacturers with little current rating or interference voltage. A closer look at the circuit in Figure 1 reveals a nice framework of two-stage power conversion. A DC circuit plus a three-stage AC-DC converter A three-channel PWM interleaved DC buck converter is implemented in the circuitry at the rear end. Instead of focusing on similarities with semiconductors, these highlights improved loss sharing between semiconductors or better current distribution amongst the same circuits.

This leads to absolute leadership potential and improved misfortune exchange. Furthermore, the symmetrical PWM interleaving activity compensates for the high repetitive noise compared to the amount of identical circuitry used In the two voltages and flows, the RMS currents in the DC capacitors C_f and C_o are reduced. To accomplish zero-voltage switching of the dynamic switch turn-on and low reverse recovery of the anti-DC diode, this component may be utilised to lengthen the duration waveform in each stage leg of the back-end circuit. Low-complexity and low-cost voltage source rectifier (2L-VSR) with 3-level, 3-wire, 2-level, and 6-level inputs is included into the front-end converter. If the voltage change rate between the AC grid and the EV battery is sufficient, the sustained pressure in the front-end and back-end circuits is enhanced.

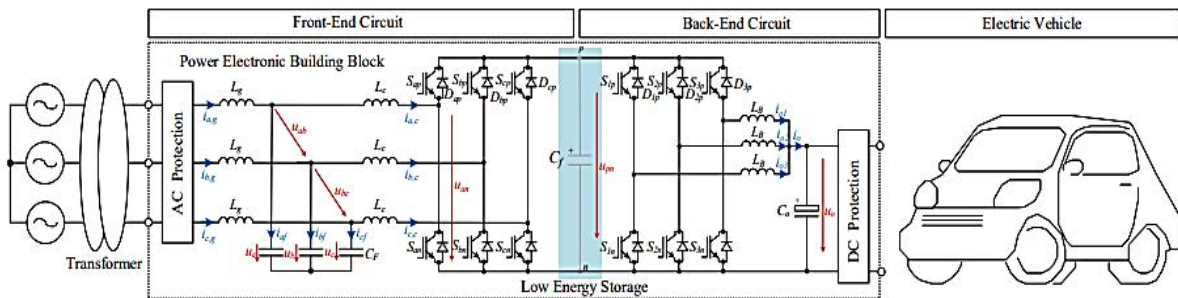


Figure 1. Concept of an EV charger with PWM interleaved buck converter for back-end power modification and a 6-switch two-stage bi-directional voltage source rectifier for front-end power modification. It's worth noting that the scaffolds are linked by low-energy DC connections.

This gives the advantage of assembly. In this document, front-end and Back-end circuits are purposefully linked by DC connections using capacitors with low energy storage. Capabilities, such as DC connections without electrolytic

capacitors. This deeply couples the activities of the two circuits. The DC connection or voltage between Figure 1 shows a modified encapsulation of the line voltage on an AC capacitor, which essentially corresponds to that achieved by a three-stage diode-span rectifier increase at terminals p and n (or upn). This enables the rectifier stage leg to operate with excellent intermittent PWM balance, allowing the swap to complete within 66 percent or 240° of the grid timeframe. Every 60° , one leg rotates.

This activity was recently revealed in [2], respecting the best exchange fault reduction among all known DPWM schemes, but the voltage of upn It comes at the cost of losing control. The back-end circuitry is critical to the voltage guidelines and current limits of the EV battery charging system. Additionally, if the backend converter is to guarantee consistent power operation, it must provide high power factor operation. He proposed a VIENNA-type front-end circuit in [3], and a DELTA-SWITCH-type front-end circuit with equivalent activity in [4]. The goal of this paper is to examine the benefits of performing DPWN with a 240° terminal switching section on a commonly used 2L-VSR when fast EV battery chargers are used. (e.g., those presented in [5]-[6])

Determining the fundamental characteristics of DC-type EV chargers on the market, appropriate fine-tuning techniques, including fewer replacement accidents, and key control strategies to ensure high-influence factor activity are based on semiconductor and Insightful conditions for determining load impact using passives. Given the converter's AC or DC current amplitude and voltage variation components. The circuit of Figure 1 compares in terms of viable performance [7] with other reasonable answers for a 50kW PEBB frame while considering quick charging of a 30kWh Nissan Leaf vehicle from 0% to 90% state of charge (SoC) will be possible.

2. THREE-PHASE EV BATTERY CHARGER

This section explains how the electric vehicle battery charger shown in Figure 2 works. As previously stated, the front-end Both the front-end and back-end circuits are connected via a DC link with limited energy storage capacity, resulting in highly coupled operation of both circuits. In reality, the circuit is a single-stage three-phase step-down AC-DC converter, with the two highest line-to-line AC voltages switched to the rear output. To regulate the output voltage u_0 used for charging electric vehicles, an end solid-state bridge and cascaded low-pass filtering (LB and C_0) are used. Similarly, the output voltage should ideally be adjustable from zero to any value.

$$u_0 < \sqrt{\frac{3}{2}} u_{g,l-l,rms} \quad (1)$$

Note that activity of the back-end circuit applying a (essentially) consistent power P_0 prompts a prerequisite of the ongoing I_x fluctuating in stage inverse as a result of the front-end circuit, to the six-beat rectifier voltage In a 3-wire framework, the

sinusoidal state of all AC is maintained for every 60° of mains voltage mains stage flows $i_{abc,c}$ is ensured by the superposition of cyclic I_x and current I_y . There is outright pressure in the front-end circuit, which is quickly most reduced.

To exhibit the sinusoidal controllability of the network current, the same circuit displayed in Figure 3 of the framework being scrutinized for lattice separating [0o, 30o] or $u_a > u_b > u_c$ (see Figure 3) is considered for examination. Increment. In a perfect world, there is no essential recurrence the voltage drop across the AC inductor causes the EV framework to act as a reasonable three-stage load to the network, with stage conductance G .

$$u_{Lc} = 0 \quad (2)$$

As a result, the value of the controlled current at phase b can be written as

$$\bar{I}_y = -i_{b,c} = -Gu_b \quad (3)$$

$$\bar{u}_y = u_b \quad (4)$$

$$\bar{u}_y = k_y \cdot u_b + (1 - k_y) \cdot u_c = k_y \cdot u_{ac} + ku_c \quad (5)$$

$$k_y = \frac{-u_{pos} - 2u_{neg}}{u_{pos} - u_{neg}} = \frac{u_{bc}}{u_{ac}} \quad (6)$$

$$u_{pos} = \max(u_a, u_b, u_c) \text{ and } u_{neg} = \min(u_a, u_b, u_c) \quad (7)$$

$$\overline{i_{sbp}} = k_y \cdot \bar{I}_y = -k_y \cdot i_{b,c} = -k_y \cdot G \cdot u_b = -G \cdot u_b \cdot \frac{u_{bc}}{u_{ac}} \quad (8)$$

$$i_{a,c} = G \cdot u_a, i_{b,c} = G \cdot u_b \text{ and } i_{c,c} = G \cdot u_c \quad (9)$$

$$\bar{I}_x = k_x \frac{P_o}{u_o} \quad (10)$$

$$k_x = \frac{u_o}{u_{pos} - u_{neg}} \quad (11)$$

$$\bar{I}_x = \frac{P_o}{u_{ac}} = \frac{i_{a,c} \cdot u_{ac} + i_{b,c} \cdot u_{bc}}{u_{ac}} = G \cdot \frac{u_a \cdot u_{ac} + u_b \cdot u_{bc}}{u_{ac}} \quad (12)$$

$$i_{a,c} = \bar{I}_x + \overline{i_{sbp}} = G \cdot u_a \quad (13)$$

$$i_{a,c} + i_{b,c} + i_{c,c} = 0 \text{ and } u_a + u_b + u_c = 0 \quad (14)$$

$$i_{c,c} = \overline{i_{sbp}} - \bar{I}_x = (1 - k_y) \cdot \bar{I}_y - \bar{I}_x = G \cdot u_c \quad (15)$$

$$M_a = \frac{V_{as}}{V_{at}} \quad (16)$$

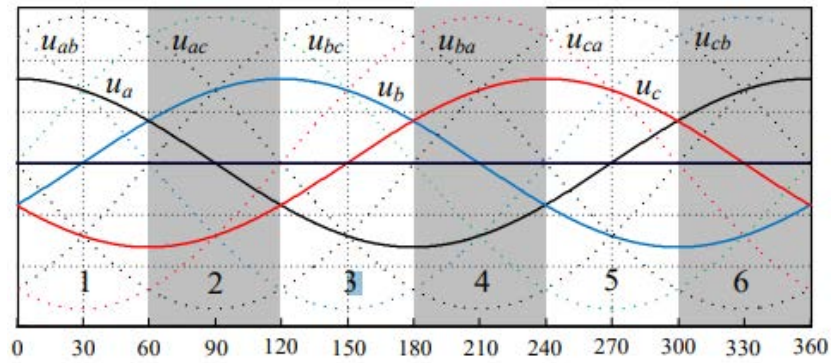


Figure 2. Grid sectors are defined by the various relationships between the instantaneous values of the grid phase voltages $u_{a,b,c}$.

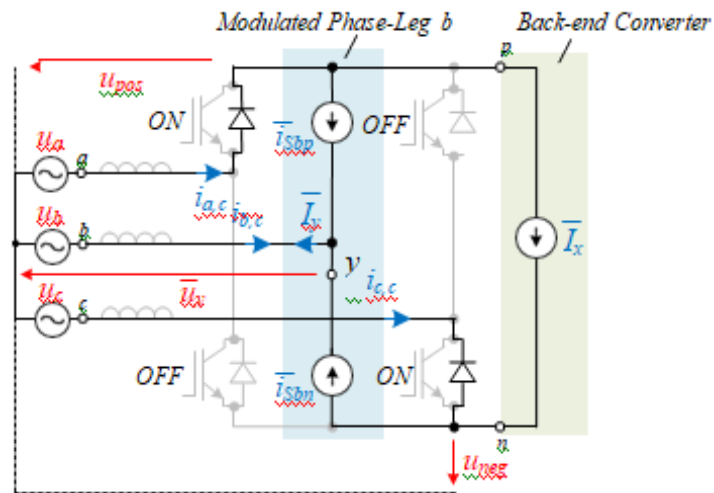


Figure 3. Equivalent circuit of the front-end convert operation for $u_a > u_b > u_c$

$$M_{fr} = \frac{f_{ct}}{f_{rs}} \quad (17)$$

$$v_r > v_c \text{ } S11 \text{ is on, } V_{out} = \frac{v_d}{2}$$

$$v_r < v_c \text{ } S12 \text{ is on, } V_{out} = -\frac{v_d}{2}$$

$$m_f = \frac{f_t}{f_m} \quad (18)$$

3. SIMULATION RESULTS

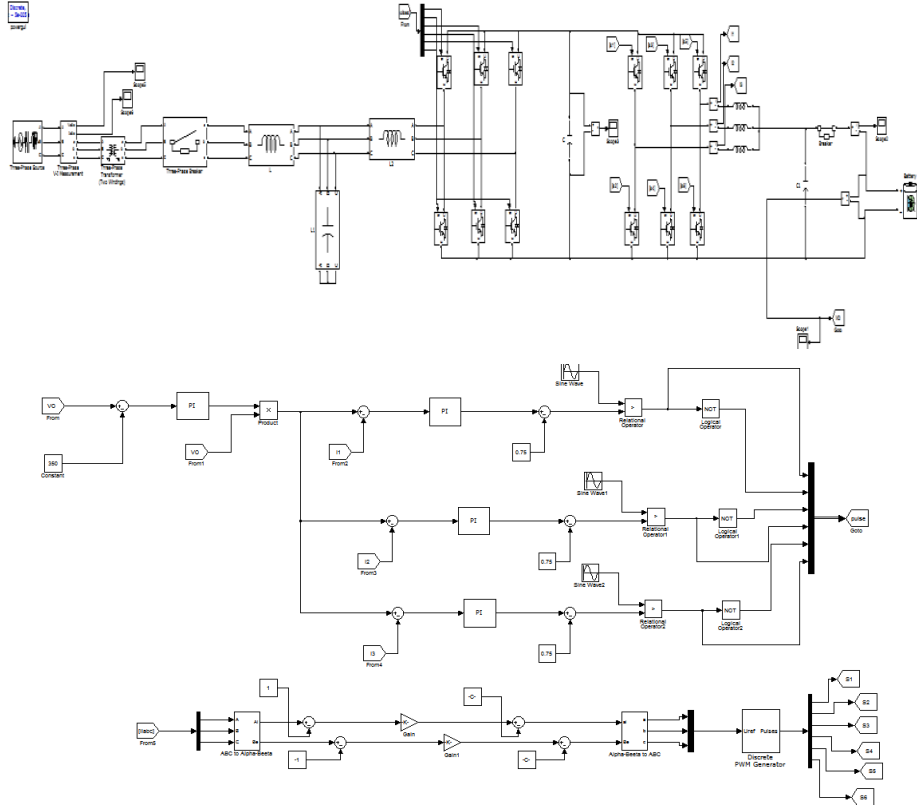


Figure 4. Proposed system circuit configuration

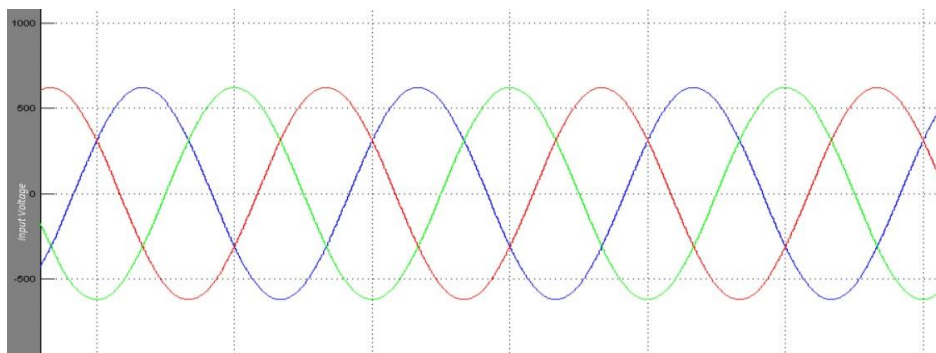


Figure 5. Input voltage for proposed system

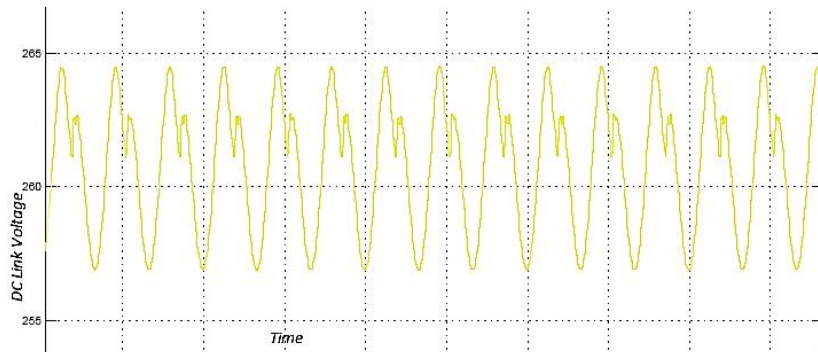
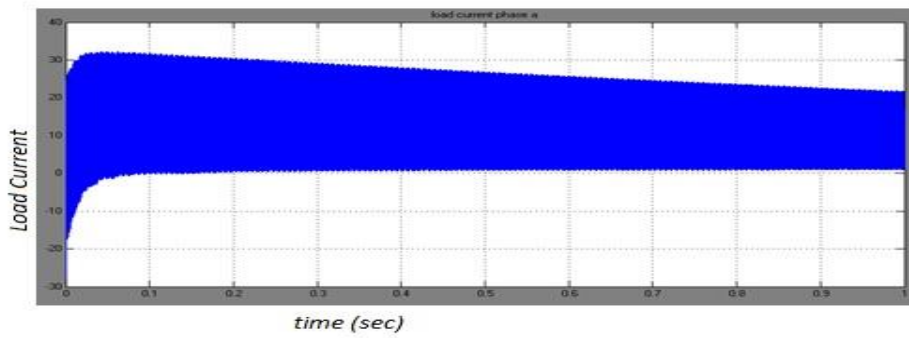
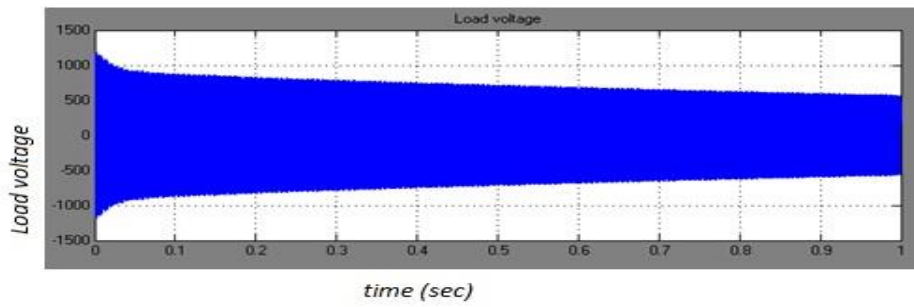


Figure 6. DC-link voltage for proposed system



(a)



(b)

Figure 7. Load voltage and load current

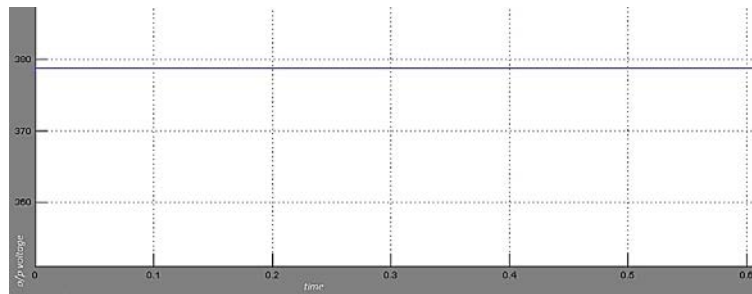


Figure 8. Battery voltage

The findings indicate that the AC flows i_{ac} , i_{bc} , i_{cc} on the converter side can follow the sinusoidal information step voltage u_{abc} , as can be seen very well in Figure 4.6. The same buck converter is running smoothly, so the PEBB-focused circuit and control strategy makes sense. The converter voltage between the step's AC terminal and the DC link's terminal n , confirming that the scaffold leg can complete the exchange for 66 percent of the power grid timeframe increase. The running stresses of scaffold parts, the repetition of appropriate replacements, and the accuracy tests of determined conditions representing the benefits of potential parts were selected. An alternating repetition of $f = 16$ kHz is allocated because it divides well the difference between high productivity, high power density, and high data transmission capacity for control Table II shows the results of the top primaries.

4. CONCLUSION

A three-phase DC battery concept for electric vehicles was studied using a PWM interleaved buck converter for the back end and a two-stage bidirectional voltage source rectifier with six switches for the front end He described his own DPWM modulation implementation. This ensures high power factor operation while also allowing the phase leg to suspend switching for two-thirds of its line cycle, or 240° resulting in significant switching losses in the semiconductor is reduced to this project covered the working principle, the main design equations, suitable modulation schemes and its PWM control. A benchmark of the semiconductor power consumption figures achieved in his The Nissan Leaf charging session from 0 to 90% was demonstrated. Underneath, a 50kW DC EV charger will be developed using commercially available Wolf Speed SiC MOSFET and Infineon Si IGBT power modules, as well as an appropriate air-cooling system. The analysis also considers the behaviour of grid-tied power conversion using other established modulations, namely SVPWM and DPWM120, as well as his DPWM240 under investigation. The DPWM240 calculations perform admirably in terms of loss reduction and energy savings, as expected.

REFERENCES

- [1] S. Bai and S. M. Lukic, "Unified active filter and energy storage system for an mv electric vehicle charging station," *IEEE Trans. Power Electr.*, 2013.
- [2] J. A. Anderson, M. Haider, D. Bortis, J. W. Kolar, M. Kasper, and G. Deboy, "New Synergetic Control of a 20 kW Isolated Vienna Rectifier Front-End EV Battery Charger," *Proc. of 20th IEEE Workshop on Control and Modeling for Power Electronics (COMPEL)* June 17-20, 2019.
- [3] T. B. Soeiro, and P. Bauer, "Three-phase unidirectional quasi-single- stage delta-switch rectifier + dc-dc buck converter," in *Proc. of 39th Ann. Conf. of the Ind.Electr. Soc., (IECON)*, 2019.
- [4] Ahmet Masum Hava, "Carrier based pwm-vsi drives in the overmodulation region." PhD thesis, 1998.
- [5] M. Hava, R. J. Kerkman, and T. A. Lipo. "A high performance generalized discontinuous pwm algorithm." *IEEE Trans. Ind. Appl.*, pages 1059–1071, 1998.
- [6] L. Schrittwieser, J. W. Kolar and T. B. Soeiro, "99% efficient three- phase buck-type SiC MOSFET PFC rectifier minimizing life cycle cost in DC data centers," in *Proc. Intern. Telecommunications Energy Conference (INTELEC)*, Austin, TX, 2016, pp. 1-8.
- [7] Nagireddy B, sahithipriya. Kosika, manishpatel. Gadam, jagadhishwar. Banoth, ashok. Banoth, Srikanth goud. B, "Analysis of positive output buck-boost topology with extended conversion ratio", *Journal of Energy Systems*, 6(1), pp. 62–83, 2022.

Design of IoT Based Smart, Portable and Low-Cost Massage Band

J. Naga Vishnu Vardhan¹, K. Deekshitha², S. Tejaswini Harshitha³ K. Devi Saranya⁴,
S. Harika⁵, G. Srinivasa Rao⁶

^{1,2,3,4,5,6} Department of ECE, BVRIT HYDERABAD College of Engineering for Women,
Hyderabad, India

Email: jnvvardhan@gmail.com

Abstract

Every person at some point in their life might experience muscular pains. Especially, women during menstrual cycle and elderly people experience heavy muscular pains. These pains can be very straining and may not have adequate resources to manage. A good massage can calm muscles and soothe the nerves to let body pain go away. Hence a portable, safe, self-operated, user-friendly cost-effective massage band is developed that provides relief and helps in reducing muscular pains. The massage band developed is integrated with an App named Smart Massager through which one can control the features like Start, Stop, Timer, Speed and Pressure. Because of this app integrated with device, it is an advantage for the user not to apply any force physically, no need to depend on others and can totally control in App. The amount of air pressure applied can be varied according to requirement. The periodical pressure applied helps in contraction and relaxation of muscles. The speed of inflation and deflation of pressure cuff can also be varied according to the user requirement. Moreover, one more major feature unlike some devices available in the market which can be for certain parts in the body; this band can be used for most of the parts. It is a simple model and portable.

Keywords. Massage Band, Portable, Flexible.

1. INTRODUCTION

Muscle aches (myalgia) are generally common. Almost, everyone experiences discomfort in their muscles some times. As muscle tissues are in nearly all parts of the body, this type of pain can be felt. However, there's no single cause for muscle aches and pains. Often, most instances of myalgia result from too much stress, tension, or physical activity. Most of the existing solutions or massage bands available in the market provides relief. But they may be too expensive and are not plausible to use without the help of another person. When there is no one to help, we have to press or hold with other hand for longer time which causes stress to hand.

The model developed is an attempt to build a device that helps in providing relief to reduce joint and muscle pain. The model developed will be controlled via mobile application which is user friendly where the start and stop of the device,

speed, and pressure can be adjusted easily. It has two important parts like pressure cuff and control unit. When experiencing pain, people can just wear the cuff and plug it to the controller unit. The user can also choose the suitable speed they need and can set time accordingly. The device inflates and deflates within the rate at which it is operating. Speed can be controlled using Arduino. A 5V, 2A power adapter is used to power this device. As this is of low-cost, it can be made available to a larger market. The massager provides a relaxing and soothing that relieves from pain. As the speed and pressure are set within the normal limits, it is safe to use.

2. LITERATURE SURVEY

In the market, large variety of massage bands is available [1, 2]. Some of them are bulky; some of them are costlier; some are not self-operated and need support of others etc. An ancient practice of Manual massage is the one that needs the intervention of a trained physiotherapist. On the other side, automated massage is carried out using devices without or with minimal need of a trained human and the effects of automated massage is presented in [3]. Multispecialty Massage belt to improve their skeletal support of the users/patients to for the betterment and relief of pain was discussed in [4].

In paper [5], percussion massages guns that are commonly used by athletes and others for physical recovery were discussed. It is mentioned that no evidence or clinical reports are published. The effect of massage therapy on patients seeking Pain that can be addressed through a holistic approach and meta-analysis to analyze the quality of massage therapy is presented in [6].

The study of various massage bands mentioned above have their own limitations in terms of being bulky or costlier or depends on others or need to apply physical force or restricted to few parts etc. The model proposed overcomes all the mentioned limitations and has a novelty of smaller in size (Portable), less cost, can be operated through App and not required to apply physical force, suitable for most of the parts.

2.1 Massage Chair: A chair designed for massage. It is of two types, Traditional chair (Fig 1) that helps a masseur to have an easy access to head, shoulders and back of the recipient but that needs a support of trainer.



Fig 1: Traditional Chair

Fig 2: Robotic Chair

Other is robotic massage chair (Fig 2) which contains electronic motors and gears to massage the recipient. Though they provide a deep relaxation, reduce blood pressure, lowers the pulse rate, increase metabolism, they are very costlier and bulky in size.

2.2 Neck and Shoulder: It is a massaging product solely designed for neck and shoulder, which helps in relieving the muscular pains. These work by applying pressure to particular points of the body to relax muscles and soothe the pain. Few may also use heat to ease the pain. These cannot be used for more than 20 minutes, Skin redness and bruising may cause and can be used only for neck and shoulder pains.



Fig 3: Neck and Shoulder Massage band

2.3 Hand-held Massagers: A portable hand-held massager which uses vibrations to warm the muscle tissues and increase blood flow to the area is shown in Fig 4. These are the electric massagers which have changeable massage heads to

customize the massage. It is a portable one, light in weight. But one needs to apply more pressure.



Fig 4: Hand-Held Massager

2.4 Leg Foot Massager: A leg foot massager machine (Fig: 5) with rubber kneading pads is used for effective massage for foot ankle and calf. It is effective in promoting blood circulation. This model also has a limb-circulator device. Depending on foot sensitivity, it can cause electric shock if used with wet feet may cause burns and is a chance of



Fig 5: Leg Foot Massager

3. PROPOSED MODEL

The Block diagram of Proposed Massage band is as given below. The above Fig 6 depicts the block diagram of the proposed system. The framework used for the proposed system is the Arduino Nano ATMEGA 328P. HC-05 Bluetooth module is used to interact with the user application on mobile phone, is connected to Arduino Nano ATMEGA 328P microcontroller board. ULN2803A driver is the Darlington transistor array that consists of eight NPN transistors. This ULN2803A is connected to both mini air pump and solenoid air valve. Both solenoid air and mini air pump valve are driven by this ULN2803A driver according to input received by the Arduino Nano board from the user application via Bluetooth module. Pressure cuff is connected to a mini air pump via pressure tube. The pressure sensor BMP 180 is connected to the pressure cuff through this tube is used to monitor the pressure that is applied using the mini air pump. For both Arduino Nano board

and ULN2803A driver to function 5V, 2A DC power is to be supplied and rechargeable batteries can also be used.

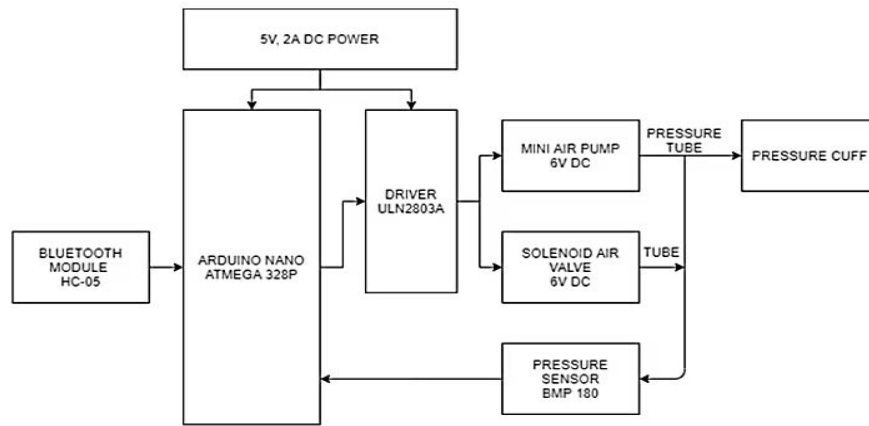
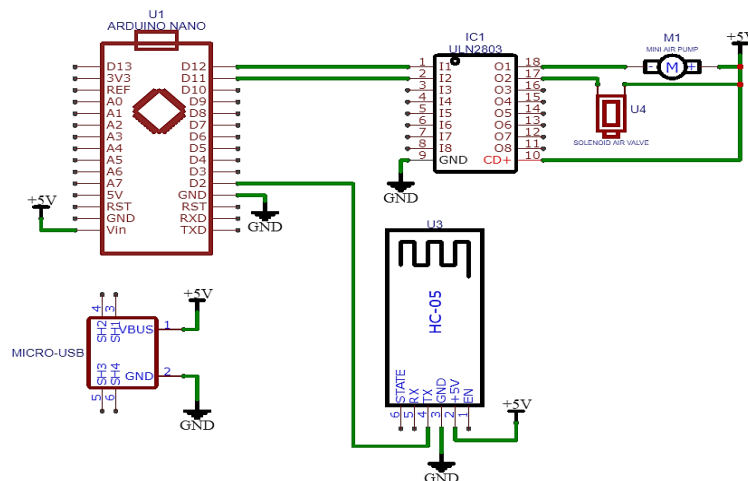


Fig: 6 Block Diagram of Proposed Model



inflates pressure to that level only. Mapping of pressure value with actual value is done on the control unit. The Sequence of the operation is represented diagrammatically as below.

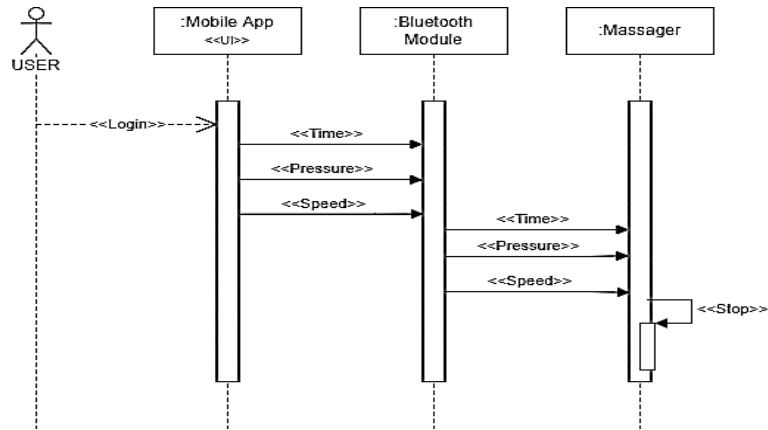


Fig. 8 Sequence diagram of the device

Speed can also be controlled through APP among three levels like Low, Medium, and Fast that correspond to inflate and deflate of pressure cuff. The pressure cuff inflates and deflates according to speed value. The value that sent from the APP to Arduino would be 0, 1, and 2 respectively. The mapping of the speed is done using Arduino. The below Fig: 9 depict the waveforms for various speeds

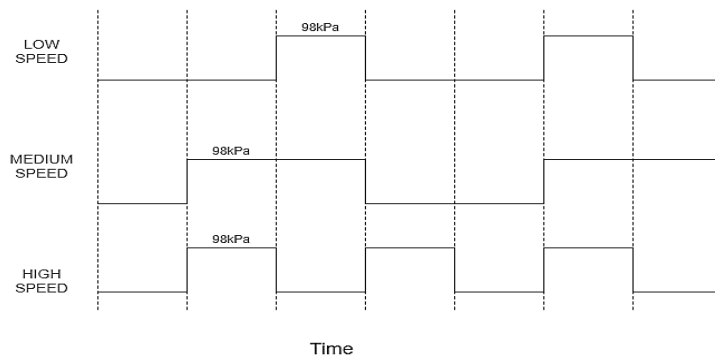


Fig: 9 Waveform of speed values

The below Fig's 10 & 11 shows the user module of the APP where the time can be set, speed and pressure can be controlled and device can be start and stop.

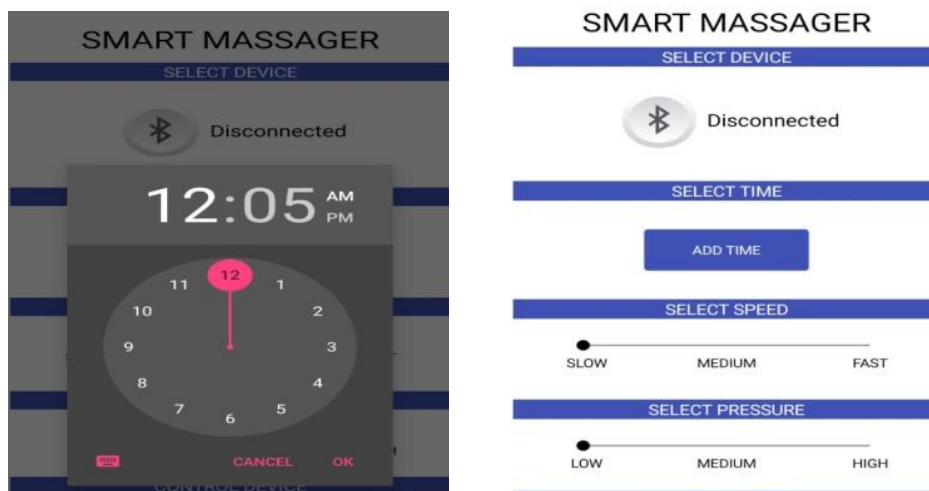


Fig: 10 Time Setter in APP

Fig: 11 Speed and Pressure controls, Stop – Start buttons

Once all the pressure, time and speed values are selected, then click on the START button to initiate the process. In this model, an Arduino Nano microcontroller board that has Atmega328P is used and programmed using Arduino IDE. For driving the solenoid air valve and the mini air pump, an L293D driver module is used. This module needs 5V input and need upto 500mA on every output pin. The Arduino gives control signals to the driver according to the configurations set in the app. For establishing communication, Bluetooth module is used.

A solenoid air valve is driven by L294D and controlled by Nano acts like a gateway. When activated it doesn't let the air out and therefore increases pressure within the cuff, making it inflate. BMP180 pressure sensor was used. Because of I2C interface, it was easily interfaced with Arduino using the four pins (+3.3V, GND, SCL, SDA). The sensor module was kept inside a box with a nozzle for connecting the tube and sealed on all sides to obtain consistent pressure readings. The process ends once the selected time is completed, or we can also end the process by clicking the STOP button.

A Mobile App was developed using Kodular.in that allows creating Android apps easily with a blocks-type editor and requires no coding skills. It is a free online tool for the development of mobile apps. It mainly provides an online drag-and-drop Android app creator, by which everyone can create any kind of app.



Fig: 12 Prototype of Proposed Massage Band Fig: 13 Applying at different Parts in a body

As the Pressure cuff is flexible, a single band can be accommodated for massaging at different parts in a body like Hand, leg, shoulder, back, neck etc. where it not possible with most of the existing models and totally can be controlled by a App without need of applying any physical force.

4. CONCLUSION

Massaging has many benefits like reducing stress, relieving body pains, helps with insomnia problems etc. Massage bands are really popular due to the many benefits they provide. But many massage bands that are available now in the market have their own limitations as discussed.

The Safe and cost-effective massage band is an attempt to overcome all these limitations. This device is portable and has some technological touch to automate the process which is programmed using Arduino. The device consists of pressure cuff which inflates and deflates to create pressure. This pressure can be easily controlled with the mobile application developed using Kodular.in according to the preference of the user. A pressure sensor is used to measure the exact pressure to feed to the Arduino. It has a blue tooth module to enable wireless operation. The device can also be powered by rechargeable batteries which make it safe from any electrical shocks.

In future, for the introduction of this product in the market better features can be added. For example, voice alerts can be included for better feedback. Voice alerts can help enhance the customer satisfaction. Analytics can also be included to predict the most comfortable pressure for each and every one and appropriate pressure for a certain kind of muscular pain can also be recommended.

REFERENCES

- [1] Electronic Massage Devices Market - Global Industry Analysis, Size, Share, Growth, Trends and Forecast 2019-2027
- [2] Best Massagers, "Medically reviewed by Jenneh Rishe, RN - Written by Suzy Davenport on September 29, 2021
- [3] Paul, A., Usman, J., Ahmad, M.Y. et al. Health efficacy of electrically operated automated massage on muscle properties, peripheral circulation, and physiological variables: a narrative review. EURASIP J. Adv. Signal Process. 2021, 80 (2021). <https://doi.org/10.1186/s13634-021-00788-6>
- [4] Panda, Kunal & Anupriya, M & Naveen, C & Ravi, Sandhiya. (2020). An Eminent Design of Multipurpose (All-In-One Kneading Belt) for Lumbar Massage. IOP

Conference Series: Materials Science and Engineering. 993. 012165.
10.1088/1757-899X/993/1/012165.

- [5] Jian Chen, MD, PhD, Fan Zhang, MD, MSc, Haizhu Chen, NB, Hui Pan, MD, MPH, Rhabdomyolysis After the Use of Percussion Massage Gun: A Case Report, *Physical Therapy*, Volume101, Issue 1, January 2021.
- [6] Crawford C, Boyd C, Paat CF, Price A, Xenakis L, Yang E, Zhang W; Evidence for Massage Therapy (EMT) Working Group. The Impact of Massage Therapy on Function in Pain Populations-A Systematic Review and Meta-Analysis of Randomized Controlled Trials: Part I, Patients Experiencing Pain in the General Population. *Pain Med.* 2016 Jul 1;17(7):1353-1375.

Comparative study on Sudoku using Backtracking algorithm

¹T Navya, ¹T J Mounika, ¹S Tharun, ¹Kaladevi R, ²Hariharan S, ²Bhanuprasad A

¹Saveetha Engineering College, Department of Computer Science and Engineering,
Chennai, India

²Department of Computer Science and Engineering, Vardhaman College of
Engineering, Hyderabad, India

navyachowdary.thellapati@gmail.com, tjmounika01@gmail.com,
tharuns9492@gmail.com, kaladevi@saveetha.ac.in,
mailtos.hariharan@gmail.com, a.bhanuprasad@vardhaman.org

Abstract

Sudoku puzzles appear in magazines, newspapers, internet pages or in books on day basis. In truth, humans across the arena apprehend a way to play Sudoku. The technology behind this game is tons extra complex than it appears. This is the main strength of investigation for researcher community to have positioned a extraordinary quantity of attempt to generate green algorithms to remedy these puzzles. Some researchers might even advise that an algorithm to remedy Sudoku games without trying a large quantity of variations does now not exist. Within this decade, fixing the Sudoku would be expected to in everyone's ardour. The simpler and more challenging requirement would be the mathematical skills which cause people to have huge hobby in accepting challenges that encounters to solve the puzzle. Consequently, researchers attempted to find good procedure to generate puzzles that could be solved through very simple programming. At this venture there is a fixed of policies known as naïve primarily based on essential hassle solving. The motive is to put into impact an extra green algorithm and then observe it with every other Sudoku solver set of guidelines named as lower back tracking. Backtracking set of regulations is a stylish algorithm that may be hired in to any troubles. The outcomes have proved that the backtracking set of rules solves the puzzle faster and more powerful than the naïve set of policies.

Keywords. Sudoku, Backtracking Algorithm, Running time, Naive Bayes Algorithm.

1. INTRODUCTION

Currently, Sudoku puzzles have become more and more popular the various humans all over the world. The game has turned out to be more successful among human mankind in variety of countries. Efforts have also been taken to attempt to generate even more complex and thrilling games that entertain humans. In the

proposed study, algorithm for solving Sudoku namely naïve bayes is used along with backtracking approach is used to solve the puzzles for finding the best strategy. The naïve set of rules is formulated based totally on human strategies which implies that a set of rules is applied primarily based on human perceptions. The returned monitoring algorithm is then used to evaluate with this set of rules with the intention to evaluate the performance of the proposed algorithm.

The backtracking is well known with a set of rules than may is implemented to find a feasible and efficient solution in terms of running time is concerned. The proposed procedure aims at generating possible solutions that finds best solution. The simple principle of a backtracking algorithm with reference to Sudoku is to move forward one square at a time and to supply a working Sudoku grid. When a trouble takes place, the set of rules takes itself returned one step and tries a unique route. It's almost not possible to supply a legitimate Sudoku through randomly plotting numbers and trying to cause them to match. Likewise, backtracking with a random placement technique is equally useless.

Backtracking exceptional works in a linear technique. it's far rapid, powerful if executed successfully. The reason of the machine is to research the backtracking set of rules and the naïve algorithm. Later these two techniques are compared analytically. it's far predicted here to locate an efficient technique to clear up the Sudoku puzzles. This study aims at implementation of the returned tracking set of rules that simulate answer of the puzzle. The reason of the machine is to research the backtracking algorithm and the naïve algorithm. its miles predicted here to locate an efficient technique to solve the Sudoku puzzles.

The proposed work is organized as follows, while section 1 discusses on some general aspects on the ideology and importance of the proposed study, section 2 describes the related study that exists on Sudoku Puzzle implemented using various algorithms. Section 3 elaborates on the research basics and discusses on the naive bayes and backtracking algorithms, followed by proposed work with an architecture in section 4. Section 5 concludes the study analyzing the performance of research work using time complexity metric.

2. LITERATURE SURVEY

Backtracking set of regulations is less complicated than extraordinary algorithms that guarantees a choice to the maximum tough puzzles. games and puzzles were a platform for utility of mathematics, artificial intelligence and exclusive diverse techniques. The past years have delivered into hobby a completely popular puzzle known as Sudoku. The common Sudoku puzzle grid is a nine-through-9 cells into nine three-by way of manner of-3 squares. The suggestions of the game are: each row, column, and square (of three-by-3) should be filled with every of the numbers 1 until 9 and that range cannot seem extra than as quickly as in any of the row, column, or rectangular. The initial grid is populated with some

digits, known as clues. In evaluation to magic squares and other numeric puzzles, no arithmetic is worried; the elements in a Sudoku grid must just as well be letters of the alphabet or some other symbols. Sudoku has led exclusive researchers to three advances in set of rules design and implementation. These paintings modified into largely inspired by means of the interesting mathematical requirements behind it. This paper describes the development of a Sudoku solver using MATLAB.

A few authors are presenting a search-based answer through the usage of some heuristic elements in a changed steepest hill ascent. some researchers, are suggesting the format of a genetic algorithm via manner of representing the puzzle as a block of chromosomes, extra specific as an array of eighty-one integers. Any crossover appears a number of the 3x3 grids and any mutations arise only within the 3x3 grids. Geem is proposing a Sudoku solver model based totally on concord are trying to find those mimics the tendencies of a musician. Santos-Garcia and Palomino are suggesting a way for fixing Sudoku puzzles the usage of easy precise judgment with rewriting regulations to mimic human intelligence. Others are suggesting neural networks thru modeling an power pushed quantum (Q'tron) neural community to resolve the Sudoku puzzles. Barlett and Langville are imparting an answer based totally mostly on binary integer linear programming (BILP). To formulate in a simple manner the approach, we are able to say that it makes use of binary variables to select a digit for any cellular in a Sudoku puzzle. Our MATLAB software uses most effective one pattern—singletons—collectively with a primary laptop technological know-how technique, recursive Backtracking [3].

The backtracking set of rules is an improvement of the brute pressure algorithm that finds out the answers to issues amongst all possible solutions systematically. Backtracking is a normal form of recursive set of rules and is primarily based on DFS (Depth First Search) in locating the proper solution. Backtracking policy works with several opportunities that cause the solution till it finds the optimum ones. So, there is no want to check all feasible solutions, however it's miles enough that most effective results in the answer, specifically by using sorting pruning the nodes that do not purpose the answer. The distinction with the brute stress algorithm is the fundamental concept, particularly, in backtracking, all solutions are made inside the form of an answer tree \, after which the tree may be traced in DFS (intensity-First are seeking for) to locate the first-rate-favoured answer.[4]

The essential precept of a backtracking set of regulations, with regard to Sudoku, one mobile at a time, to supply a running Sudoku grid. Sudoku become advanced with the aid of the use of an American architect, Howard Garnes, in 1979, as a numerical combinatorial puzzle. The puzzle acquired popularity in 2004, when Wayne Gould glad the times in London to submit it. There are 6,670,903,752,021,072,936,960 possible combos for completing a nine-via-9. Sudoku grid, but simplest 5,472,730,538 of them truly count number for great solutions and for this reason one needs a handful of lifetimes to clear up all of them.[5]

Sudoku is a superb judgment-primarily based definitely, combinatorial number placement puzzle. The word “Sudoku” is brief for Suji wadoku shinnikagiru (in Japanese), which means that “the numbers should be unmarried”. The set of guidelines is also the correct method to find out a solution quicker and greater efficient. Sudoku is a puzzle undertaking played on a grid that consists of 9 x 9 cells each belonging to three corporations: considered one of 9 rows, genuinely certainly one of nine columns and one among nine sub grids (now and again referred to as regions). the sport of Sudoku is basically based on Latin squares. The Sudoku became incepted within the 12 months 1979 and emerge as first posted within the Dell Magazines as “variety region” in the year 1984. The time period Sudoku manner a single quantity. the game begins with numbers already revealed in a few cells. The player needs to fill inside the empty cells with the numbers 1 to 9 such that every column, row and area carries that range precisely as soon as. there are various Sudoku packages that have already been evolved by means of many programmers around the world. in this paper, we provide an overview of the paintings that we have completed at the development of the sport of Sudoku that generates a 9 x nine puzzle grid with numerous trouble stages.

The utility additionally permits customers to go into their very personal puzzle and to be solved with the aid of the computer [6]. The superior software additionally consists of advanced abilities which encompass maintain, load and speedy input validation. The solving set of policies of the developed Sudoku utility has additionally been as compared to some present Sudoku programs for assessment. Many methods as well as their hybrids are available to solve Sudoku puzzles. However, those techniques have several shortcomings at the side of not being capable of clearing up the puzzles. This overlook constraints violations in Sudoku policies have several steps similarly to missing capacity possibilities for finding feasible solution. The research study advises on hybrid backtracking set of rules and pencil and paper technique to conquer the constraints of the existing techniques [7]. Experimental consequences show that the proposed approach is greater powerful further to green in solving puzzles of different hassle levels than the opportunity to be had technique.

3. RESEARCH BASICS

3.1. Backtracking algorithm

The backtracking set of policies makes use of an array of the crook numbers inside the cellular to attempt a answer earlier than it moves directly to the subsequent mobile. If an answer cannot be observed, it backtracks and attempts to remedy the board once more with a extraordinary wager choice. The greater errors the solver makes, the greater backtracks it have to carry out, which decreases its commonplace efficiency and will growth its effective runtime. exams of the fixing set of rules have been completed using 195 base solutions with more than one preliminary board configurations were carried out to investigate the distinction in

the set of rules performance via using comparing the variety of recursive backtracks among sequential and randomly distributed guesses [10].

3.2. Naïve Bayes algorithm

Naïve Bayes set of policies is a easy probabilistic algorithm in class method which gets its opportunity price based at the calculation of frequency and price combos from the associated series [8]. This set of rules assumes that each one attributes are unbiased [9]. The class technique of Naïve Bayes wishes numerous clues or recommendations to determine the magnificence of the data to be analyzed.

4. PROPOSED APPROACH

The proposed approach right here is the backtracking algorithm with an incomplete board. The architecture is presented in Fig 4.1. The steps involved are:

1. Locate a few empty areas.
2. Attempt to place the digits 1-9 in that area
3. Take a look at if that digit is valid in the modern-day spot primarily based at the modern board.
 - a. If the digit is legitimate, recursively try to fill the board the usage of steps 1-3.
 - b. If it isn't legitimate, reset the Square you simply stuffed and move again to the previous step.
4. Once the board is full by the definition of this algorithm there's an answer.

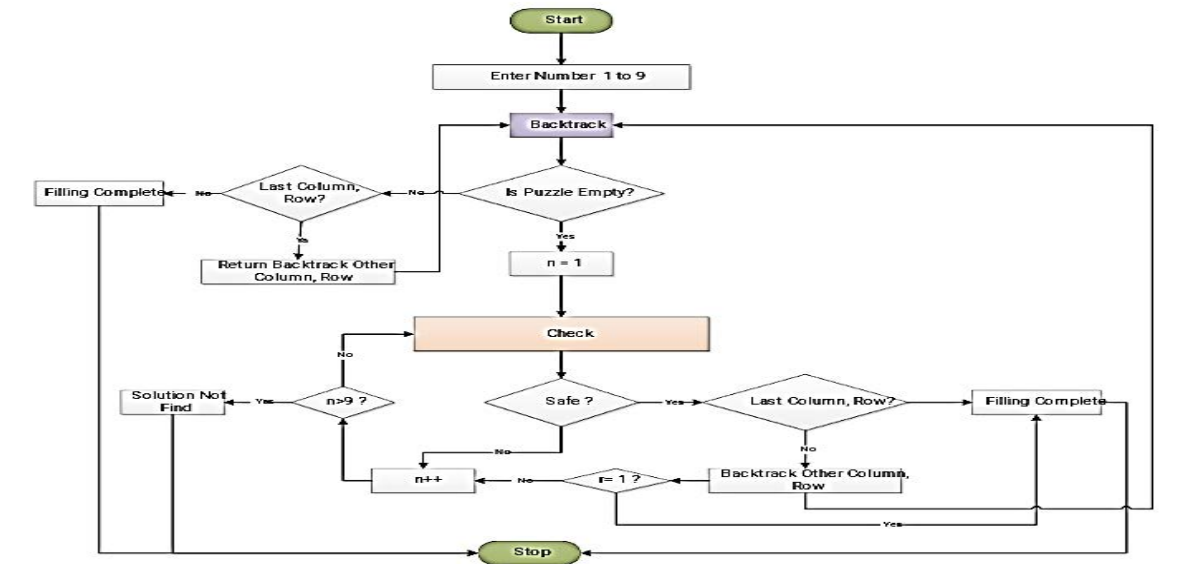


Fig 4.1 Proposed architecture work flow diagram

The results are compared with the algorithms presented in section 1 and the running time is measured and results are presented in Fig 4.2. The time complexity is presented in equation 4.1. For each unassigned index, there are 9 possible options so the time complexity is $O(9^{(n*n)})$. The time complexity stays the same but there might be some early pruning so the time taken can be an entire lot less than the naive set of regulations but the upper certain time complexity remains the equal. The naïve bayes (shown in blue colour) and backtracking algorithm (shown in red colour) is presented in Fig 4.2.

$$O(9^{(n*n)}) \quad (4.1)$$

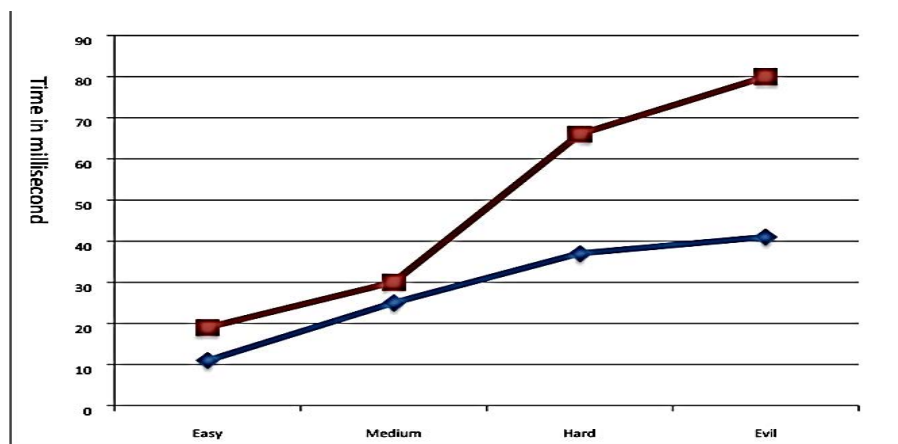


Fig 4.2 Running time of naïve bayes and backtracking algorithm

5. CONCLUSION

The paper has ended with result to solve sudoku board which shows that the backtracking with set of rules is a best approach. The set of guidelines is likewise the proper technique to find a solution faster and extra inexperienced compared to the naïve algorithm. The performance of monitoring set of rules is better than the naïve algorithm with appreciate to the computing time to treatment any puzzle which is found out from the time complexity calculation. The naïve algorithm also gives a completely unique output. However, naïve set of rules isn't inexperienced due to the truth the extent of problems is irrelevant to the set of rules. This set of guidelines exams all possible answers to the puzzle until a legitimate solution is located that is a time-ingesting procedure resulting an inefficient solver. The future work may be enhancement of the Backtracking algorithm to growth its performance. This look at shows that Backtracking algorithm is greater possible to resolve any Sudoku puzzles, additionally the quality technique to find a solution faster and additional green in fixing capability, illustration, and performances with any level

of difficulties. This have a look at can also be useful in statistical tests and method to find out a few greater consequences for comparing.

REFERENCES

1. Pouria Kaviani, Sunita Dhotre, 2017, Short Survey on Naive Bayes Algorithm, International Journal of Advance Engineering and Research Development.
2. H. Lloyd and M. Amos 2019 Solving Sudoku with Ant Colony Optimization, IEEE Trans. Games, pp. 1–1, 2019.
3. Charu Gupta, 2017, Solving Sudoko using Backtracking algorithm, international journal of Modern Trends and Research
4. T. H. Cormen, Ed., 2009, Introduction to algorithms, 3rd ed. Cambridge, Mass: MIT Press.
5. Lekha. K, Vadivu. G, 2017, Performance Analysis of Sudoku Puzzle Solver, International Journal of Pure and Applied Mathematics
6. Abhishek Majumder, Abhay Kumar, Nilu Das and Nilotpal Chakraborty, 2010, International Journal of Computer Science and Network Security, VOL.10 No.8, August 2010
7. Abdullah-Al-Wadud, 2021, An Improved Hybrid Method Combining Backtracking for solving Sudoku puzzles, ISEIEE Conference
8. T. R. Patil and S. S. Sherekar, "Performance Analysis of Naive Bayes and J48 Classification Algorithm for Data Classification," Int. J. Comput. Sci. Appl., vol. 6, no. 2, pp. 256–262, 2013.
9. R. Abraham, J. B. Simha, and S. S. Iyengar, "A Comparative Analysis of Discretization Methods for Medical Datamining with Naïve Bayesian Classifier," in Proceedings - 9th International Conference on Information Technology, 2007, pp. 235–236.
10. Moriel Schottlender, 2014, The effect of guess choices on the efficiency of a backtracking algorithm in a Sudoku solver, IEEE Long Island Systems, Applications and Technology (LISAT) Conference 2014
11. Atilla Ergugen, Erdal Erdal, 2020, Sudoku Solution Using Backtracking Algorithm, International Journal of Advances in Electronics and Computer Science.

Composite and Microencapsulated Phase Change Materials: A Brief Review

¹B. J. Ashok kumar, ²S. Muthuvel, ³ N. Rajini, ^{4*} G.R. Gopinath, ⁵R. Sudhakara Pandian, ⁶G.R. Rajesh Kanna

^{1,2,3,4} Department of Mechanical Engineering, Kalasalingam Academy of Research and Education, Krishnankoil, Tamilnadu, India-626126.

⁵Department of Manufacturing Engineering, Vellore Institute of Engineering, Tamilnadu, India.

⁶Department of Electrical and Electronics Engineering, Kalasalingam Academy of Research and Education, Tamil Nādu, India

¹bjashokkumar1980@gmail.com, ²s.muthuvel@klu.ac.in, ³rajiniklu@gmail.com,
⁴gopinathradhakrishnan7@gmail.com, ⁵sudhakarapandian.r@vit.ac.in

Abstract

Phase change materials (PCMs) play a valuable part in thermal management solutions. The immense benefits of PCMs towards energy savings have increased its market demand in all developing and developed economies. Emerging progress in the properties of PCMs can overcome numerous limitations of conventional heat storage systems, such as low thermal conductivity, thermal stability, only energy changing model, etc. The combination of the composite material with Micro-Encapsulated Phase Change Materials (MEPCM) was utilised by employing a low-cost, small-scale procedure to exploit the better thermal transport features of the hybridized PCMs. Composite and microencapsulated PCMs offer high thermal conductivity, thermal stability and avoid leakages during phase transition due to their high latent heat storage properties. Shape-stabilized composite PCMs have been showcasing admirable thermal performance and effective encapsulation for Thermal Energy Storage (TES) applications. Many research articles have been published on evaluating different TES systems. This review aims to serve as a consistent, reliable, and helpful reference for future research on eco-friendly and energy-efficient TES containing PCMs.

Keywords. Microencapsulation, Phase Change Materials (PCM), Composites, Thermal Energy Storage (TES), Thermal Stability

1. INTRODUCTION

The increase in temperature has a detrimental effect on the routine activities on earth, and in some cases, due to the drop of the average temperature, there is a huge need for supplemental energy. In order to compensate for the fluctuating temperatures and stabilize the condition for specific applications, a high volume of investment is also required [1].

The PCM is a good energy packing material to achieve obtainable heat energy that is kept or available in excess. These TES methods are eco-friendly, and their capacity to store heat and the extensive use of temperature-controlled packing in industries such as bio-medical, pharmaceuticals, and food and beverage are encouraging their implementation [2]. TES is a simple yet effective way to decrease energy consumption and optimise its utilization. In recent years, PCMs have found application in many industries such as solar dryers in agricultural industries, electronic industries, solar cooling, solar power plant, photovoltaic electricity generation system, waste heat recovery systems, domestic hot water, and building envelopes. [3]. Most of the studies focused on the upper volumetric TES capabilities with minimal consideration given to the semi-permanent escape features. In the indirect incorporation method, a leakage problem may occur, and the PCM would be incompatible with PU [4].

This article provides a detailed review of composite PCM from the outlook of synthesis procedures, microencapsulation of PCM, thermal stability, and thermal conductivity. Thus, this review can benefit new research by highlighting the limitations, challenges, and gap that needs to be bridged. The review paves the way for expanding the prospects and applications of composite PCMs.

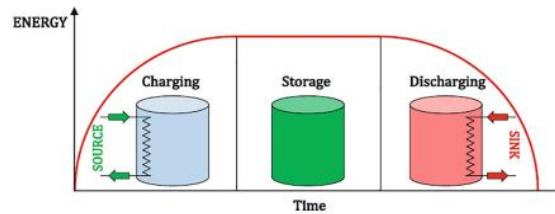


Fig 1.1: Thermal Energy storage stages [5].

2. Phase Change Materials

2.1. Composite PCMs

PCMs are incapable of efficiently storing and releasing thermal energy. Providentially, composite PCMs comprising photothermal materials can respond rapidly to light and actively meet the necessities in an exact environment [6]. In polyurethane foam, the TES capacity is improved by integrating a fatty acid ester-based PCM for latent heat storage. The PU- PCM composite material improved heat absorption capacity by 34% compared to the PU rigid foam. The composite materials demonstrated the buffering function in the case of temperature variations by improving the heat sinks. The PU- PCM composite rises in density and thermal conductivity [7].

2.2. Microencapsulated PCMs

Microencapsulation is a method used to present a core material as PCM (energy-storage) and a shell material as organic or inorganic polymers. It retains the thermo-mechanical performance, avoids PCM from leakages, improves the protection from the environment, and it widens the surface area for heat transfer. The heat transfer features

of the MEPCM will be affected by the encapsulation ratio. It specifies the efficiency of the PCM inside the shell, and it is calculated by following relation [8].

$$\text{E.R.} = \frac{(\Delta H)_{mpcm}}{(\Delta H)_{pcm}} \times 100 \quad (1)$$

where $(\Delta H)_{mpcm}$ and $(\Delta H)_{pcm}$ is the latent heat of the MEPCM and the PCM respectively. The encapsulation will depend upon the shell material width, wherein the encapsulation ratio lowers for thicker shell material [9]. Various methods of microencapsulation have been developed and well evaluated by researchers. Regarding the low thermal conductivity of PCMs, several matrices, such as compacted graphite matrix, thin aluminum sheets, honeycomb-like shapes, have been used with low thermal conducting paraffin to improve the thermal conductivity [10].

2.3. Thermal energy storage (TES)

The effective utilization of both organic and inorganic PCMs as TES is influenced by the thermal conductivity which describes these materials. The phase transition of PCM is crucial in latent heat energy storage by solid-liquid transition. In the phase change composite material, the energy stored/ liberated is dependent on the molecular interaction. The energy is released by the response between moisture and dehydrated salt [11].

The energy storage density of SHS material, like rock, is concerning 5, or 7 times fewer than the storage density of paraffin or sodium sulfate decahydrate PCM. During the heating process, the PCM will absorb energy, and when the surrounding temperature lowers, the PCM will release energy in the form of solid-liquid phase change, wherein latent heat storage is the most effective method for TES. Coconut coir fiber reinforced PCM composite material was used in making envelopes, which can also be used as a TES material. Henceforth, the addition of carbon fibers to these systems demonstrates a combined effect on improving the heat transfer abilities [12].

2.4. Thermal conductivity of PCMs

The solid state PCM have the low thermal conductivity when compared to PCM and MEPCM foam composite material. The degree of positioning of the MEPCM in the foam matrix and the improper spreading of PCM to the foam matrix will affect the heat transfer rate. Conductive particles are joined to bridge the gap for the discontinuous heat flow path. The chemical belongings of the PCM are not affected when supportive materials are added, they offer a ceaseless design with a decent way for-heat transfer [13]. The G foam composite with P-wax is ascribed to high thermal conductivity of the G- foam matrix which permit the rapid heat transfer throughout P-wax. In the solid phase the thermal conductivity is somewhat decreases with increasing temperature. Addition of EG to the CPCM was significantly improved the thermal conductivity when the EG content is higher. The inorganic PCM, calcium chloride hexahydrate was encapsulated with EG to attain 14 times higher the thermal conductivity [14].

Thermal properties of CPCM determined by impregnation method

S. No	PCM	Melting temperature (°C)	Freezing temperature (°C)	Enthalpy (kJ/kg)	Thermal conductivity (Wm ⁻¹ K ⁻¹)	Application	Ref.
1.	Polyethylene glycol	60.4	37.9	164.9	-	Energy storage	1
2.	Polyethylene glycol	57.5	34.8	142.6	0.45	TES	3
3.	Polyethylene glycol	63.5	34.7	160.7	0.79	Microelectronic device	4
4.	Polyethylene glycol	60.2	41.6	136.8	4.764	Energy conversion and storage	6
5.	Paraffin	36.4	35.5	157.4	-	TES	8

Table 2.1 Thermal properties of CPCM

2.5. Thermal stability of PCM

The thermal stability accounts for the strength, leak resistance, and thermal degradation of the PCM. These characteristics determine the nature of application of thermal energy-storage systems made of composite PCMs. Paraffin is the most familiar PCM used to reduce temperature variations in various applications. They are utilized in applications that require non-corrosive systems, wherein small volume variations in the phase change process are handled with good thermal stability. The thermal stability of diatomite/ paraffin exhibited steadiness up to 95°C. Composite PCMs generally have good thermal stability [15].

3. Recent applications and advancements of CPCM

The CPCMs are also used in some high technology fields like Aeronautics Space Administration, and smart drug delivery. In the medical field, CPCMs like 1-tetradecanol are filled into hollow mesoporous CuS₂ by impregnation and are used to eliminate the tumor and multimodal cancer treatments. In the building application, the shape stabilized PCM with supporting materials can be used, and it is utilized in the different parts like interior and exterior walls, ceiling, roof, and floor [16].

4. Conclusion

To conclude, a brief review has been showed on the thermal features of recently explored composite PCM directed on the thermal attributes of composite PCMs. As of now, different investigations have been conducted to synthesis shape-stabilized

organic composite PCMs. The synthesized PCMs, their performance, design, and overall system have been observed to provide a several useful applications.

In the composite PCM the thermal physical characteristics like thermal stability, thermal conductivity is suitable for integrated TES material. The addition of composite PCM is the incorporation of composites in porous material to prevent leakages during the phase transformation. Thermal characterization of the composites revealed that the temperature of melting and freezing point of the composite was not affected with properties of the incorporated material, but had a negative effect on the latent heat storage capacity in all cases.

References

- [1] Shahid, U. B., & Abdala, A. (2021). A critical review of phase change material composite performance through Figure-of-Merit analysis: Graphene vs Boron Nitride. *Energy Storage Materials*, 34, 365-387.
- [2] Nie, B., Chen, J., Du, Z., Li, Y., Zhang, T., Cong, L., ... & Ding, Y. (2021). Thermal performance enhancement of a phase change material (PCM) based portable box for cold chain applications. *Journal of Energy Storage*, 40, 102707.
- [3] Piselli, C., Castaldo, V. L., & Pisello, A. L. (2019). How to enhance thermal energy storage effect of PCM in roofs with varying solar reflectance: Experimental and numerical assessment of a new roof system for passive cooling in different climate conditions. *Solar Energy*, 192, 106-119.
- [4] Al-Jethelah, M., Ebadi, S., Venkateshwar, K., Tasnim, S. H., Mahmud, S., & Dutta, A. (2019). Charging nanoparticle enhanced bio-based PCM in open cell metallic foams: An experimental investigation. *Applied Thermal Engineering*, 148, 1029-1042.
- [5] Ma, T., Yang, H., Zhang, Y., Lu, L., & Wang, X. (2015). Using phase change materials in photovoltaic systems for thermal regulation and electrical efficiency improvement: a review and outlook. *Renewable and Sustainable Energy Reviews*, 43, 1273-1284.
- [6] Subramanian, M., Hoang, A. T., Kalidasan, B., Nižetić, S., Solomon, J. M., Balasubramanian, D., ... & Nguyen, X. P. (2021). A technical review on composite phase change material based secondary assisted battery thermal management system for electric vehicles. *Journal of Cleaner Production*, 322, 129079.
- [7] Ohayon-Lavi, A., Lavi, A., Alatawna, A., Ruse, E., Ziskind, G., & Regev, O. (2021). Graphite-based shape-stabilized composites for phase change material applications. *Renewable Energy*, 167, 580-590.
- [8] Yousefi, A., Tang, W., Khavarian, M., & Fang, C. (2021). Development of novel form-stable phase change material (PCM) composite using recycled

- expanded glass for thermal energy storage in cementitious composite. *Renewable Energy*, 175, 14-28.
- [9] Zou, D., Liu, X., He, R., Zhu, S., Bao, J., Guo, J., ... & Wang, B. (2019). Preparation of a novel composite phase change material (PCM) and its locally enhanced heat transfer for power battery module. *Energy Conversion and Management*, 180, 1196-1202.
- [10] Rathore, Pushpendra Kumar Singh, and Shailendra Kumar Shukla. "Enhanced thermophysical properties of organic PCM through shape stabilization for thermal energy storage in buildings: A state of the art review." *Energy and Buildings* 236 (2021): 110799.
- [11] Ren, S., Li, J., Huang, K., Bai, Y., & Wang, C. (2021). Effect of composite orders of graphene oxide on thermal properties of $\text{Na}_2\text{HPO}_4 \cdot 12\text{H}_2\text{O}$ /expanded vermiculite composite phase change materials. *Journal of Energy Storage*, 41, 102980.
- [12] Luo, J., Zou, D., Wang, Y., Wang, S., & Huang, L. (2022). Battery thermal management systems (BTMs) based on phase change material (PCM): A comprehensive review. *Chemical Engineering Journal*, 430, 132741.
- [13] Amaral, C., Pinto, S. C., Silva, T., Mohseni, F., Amaral, J. S., Amaral, V. S., ... & Vicente, R. (2020). Development of polyurethane foam incorporating phase change material for thermal energy storage. *Journal of Energy Storage*, 28, 101177.
- [14] Liu, H., Wang, X., & Wu, D. (2019). Innovative design of microencapsulated phase change materials for thermal energy storage and versatile applications: a review. *Sustainable Energy & Fuels*, 3(5), 1091-1149.
- [15] Shao, Y. W., Hu, W. W., Gao, M. H., Xiao, Y. Y., Huang, T., Zhang, N., ... & Wang, Y. (2021). Flexible MXene-coated melamine foam-based phase change material composites for integrated solar-thermal energy conversion/storage, shape memory and thermal therapy functions. *Composites Part A: Applied Science and Manufacturing*, 143, 106291.
- [16] Wang, Z., Zhu, S., Zhao, X., Huang, L., & Zou, D. (2022). Preparation and thermal performance of a novel alloy microencapsulated phase change material (MEPCM)/ceramic composite. *International Journal of Thermal Sciences*, 176, 107478.

Hardware Implementation of Electric Spring Converter in a PV and Wind based Smart grid for Power Quality Improvement

M. S. G. Smitha¹, Md Asif²

¹Department of EEE, Anantha Lakshmi Institute of Technology and Sciences, Andhra Pradesh, India

²Department of EEE, Vardhaman College of Engineering, Hyderabad, Telangana, India
Email: msgsmitha@gmail.com, asif_eee@vardhaman.org

Abstract

In this paper, an electric Spring based Converter is proposed for the improvement of power quality in a PV and wind based smart grid. Permanent Magnet Synchronous Generator is used for conversion of wind energy into electrical energy. An electric Spring has the characteristic feature of fast recovery of the performance of the electrical system. It modulates the Voltage, frequency, THD of voltage and current. It improves the power factor during abnormal conditions of wind and solar energies. An effective control scheme has been developed with the Back-to-Back inverter to obtain stability in difficult weather conditions also. The prototype of the proposed converter is developed and its performance is verified with the results obtained from the simulation. The result shows that the Electric Spring Back-to-Back converter effectively stabilizes voltage and frequency and the reactive power is compensated.

Keywords. Electric Spring, MPPT, PMSG, Back-to-Back Converter, Smart Grid.

1. INTRODUCTION

A review of recent research works shows the efficient distribution of renewable energy in a smart grid system. In addition to diesel generators, several renewable inputs like photovoltaic (PV) and wind turbine have been regarded for efficient distribution of renewable energy. It is extremely difficult to determine the size of photovoltaic, wind and diesel generators in the efficient distribution of renewable energies. Renewable energy grid integration is difficult because the power factors of voltages and currents change with changing weather conditions. This is mainly due to many factors related to this problem, instability because of renewable resources. Consequently, renewable energy system control strategies are primarily designed to detect maximum power, optimize the management of energy supplies as well as the control of demand voltage and frequency. Therefore, to meet this challenge, a comprehensive smart grid infrastructure is required to offer a workable resolution.

The ability of a power grid to address current grid difficulties, such as increasing demand for electricity, aging infrastructure and the infiltration of distributed energy sources into supply. With the invention of latest technologies, it is proposed to change the existing power grids to smart grids. Compared to conventional centralized power plants, renewable energy source power generation devices may be located nearer to main grid and they are more compact and economical. Electricity grids are being modernized to a smart grid to improve reliability and to make it easier to integrate renewable energies and to effectively manage energy usage.

2. ELECTRIC SPRING CONVERTER

Electric Spring Converter hardware is designed with two back-to-back converters with a storage battery connected between the Converters as a storage device. A grid supplied by renewable energies may maintain voltage and power stability using the latest electronic grid component known as Electric Spring. A demand side planning strategy to produce voltage and power control has been presented.

The restoring force of an optimum mechanical spring, according to Hooke's law, is inversely proportional to its deviation from the equilibrium point.

$$F = -kx \quad (1)$$

F Restorative force of spring which tries to get its equilibrium position, x displacement from the equilibrium position, k spring constant.

Potential energy which is stored in the mechanical spring given as

$$PE = \frac{1}{2}kx^2 \quad (2)$$

Similar to a physical spring, an electrical spring can sustain the required electrical tension, store electrical power, and dampen electric vibrations brought on by transitory circumstances. The definition of an electric spring is

$$q = C\vartheta_a \text{ inductive mode} \quad (3)$$

$$q = -C\vartheta_a \text{ capacitive mode} \quad (4)$$

$$q = \int i_c dt \quad (5)$$

i_c is the current flowing through the capacitor having the electric charge q with a potential difference of ϑ_a .

Here the capacitor's stored electric charge can control the electric spring's voltage regulation function by injecting or by absorbing the voltage. By using a current controlled source, charge through the capacitor can be regulated. Consequently, an electrical spring may be thought of as a supply voltage with control scheme. An electrical spring can regulate amplitude along a maximum stress by linking to non-critical loads in line, as illustrated in Fig. 1. Here the current source is a voltage source with command strength. Just as a mechanical spring develops mechanical force from a neutral position, an electric spring adjusts voltage drop and operates a constant or managed voltage at critical loads.

By adjusting the electrical potential difference across the capacitor via the current source, an electrical spring voltage may be produced. The electrical dock's dynamic voltage support is made possible via closed loop control, which has the ability to change the main supply value in the power grid. The electric spring may also be used for electric noise damper, which linking words another device in series with the electric spring to dissipate the electric charge. As demonstrated in fig. 1, non-critical demands could be linked in serial. The series linked electric load, as shown in the power system difference, wastes electrical power for damper and can be beneficial to manage the tension across the electrical spring to ensure that the electricity usage of non-critical loads varies with the power grid. Hybrid generation systems having wind, PV as generating sources are unstable as these renewable energy sources depend on weather conditions. Due to this, ac voltage across critical loads dynamically changes with power generation of hybrid system. By connecting electric spring with a dissipative non critical load, critical loads which are connected in parallel with power system will get required well-regulated mains voltage.

For improving stability of hybrid system with substantial renewable generation, novel smart load electric spring technology is highly distributed solution. Using this Electric spring technology more diverse control options and wider operating range is achievable. In addition, with voltage support and electric oscillations damping, some other favourable features of this technology are primary frequency control, power quality improvement and power balancing.

A back-to-back converter with Electric Spring (ES) technology is introduced in [9]. Compared with battery storage or capacitor storage, back-to-back converter-based ES technology has an extended range of compensation and independent of battery storages. ES with back-to-back converter consists of one series converter and one shunt converter. Series converter regulates load voltage or frequency and shunt converter maintain stable DC voltage across DC link.

Stabilized DC link voltage of back-to-back converter can instantaneously balance active power flow between shunt and series converters. Individual controlling of both converters is possible because of independent reactive power capacity of both converters. Active and reactive power characteristics of the back-to-back converter can be described as

$$P_{sh_es} = |V_s| |I_{sh_es}| \cos \theta \quad (6)$$

$$P_{se_es} = |V_{se_es}| |I_{ns}| \cos \alpha \quad (7)$$

$$P_{sh_es} = P_{se_es} \quad (8)$$

$$Q_{sh_es} = |V_s| |I_{sh_es}| \sin \theta \quad (9)$$

$$Q_{se_es} = |V_{se_es}| |I_{ns}| \sin \alpha \quad (10)$$

$|V_s|$, $|V_{se_es}|$, $|I_{ns}|$, $|I_{sh_es}|$ are the RMS values of mains voltage, series converter voltage, non-critical load current and converter shunt current respectively, θ is the phase difference between mains voltage and shunt converter current, α is the phase difference between non critical load current and series converter voltage

The shunt converter current and the series converter voltage must be within the operating range of the rear converter. The maximum amount of reactive power must be delivered by both converters during any serious voltage sag to keep the voltage constant at the critical load. In addition, the shunt converter must also maintain a constant voltage on the DC link.

The symbol for non-critical grid voltage is

$$|V_{nc}| = \sqrt{|V_{se_es}|^2 + |V_s|^2 - 2|V_s||V_{se_es}| \cos(\theta_{se_es})} \quad (11)$$

$$\theta_{V_{nc}} = \cos^{-1} \left(\frac{|V_s| - |V_{se_es}| \cos(\theta_{se_es})}{|V_{nc}|} \right) \quad (12)$$

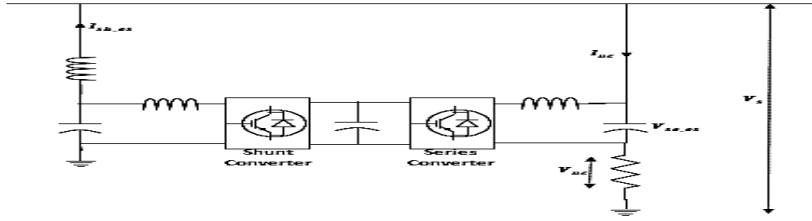


Fig. 1. Back-to-back converter for an electrified spring

For non-critical demand, assuming constant impedance it is possible to write its current as

$$I_{nc} = \frac{|V_{nc}|}{|Z_{nc}|} \angle(\theta_{V_{nc}} + \cos^{-1}(\text{pf})) \quad (13)$$

The actual and reactive energy of a series converter may be calculated based.

$$P_{se_es} = |V_{se_es}| |I_{nc}| \cos \alpha \quad (14)$$

$$Q_{se_es} = |V_{se_es}| |I_{nc}| \sin \alpha \quad (15)$$

$$\alpha = \theta_{se_es} + \theta_{V_{nc}} - \cos^{-1}(\text{pf}) \quad (16)$$

Real and reactive power for Shunt converter's can be derived as

$$P_{sh_es} = P_{se_es} \quad (17)$$

$$Q_{sh_es} = |V_s| \sqrt{I_{sh_eslim}^2 - \left(\frac{P_{sh_es}}{|V_s|} \right)^2} \quad (18)$$

Back-to-back converter, Total reactive power is

$$Q_{es} = Q_{se_es} + Q_{sh_es} \quad (19)$$

Under these circumstances, the peak power value for the entire apparent power from the equations [20, 21] is feasible.

$$\frac{\partial Q_{es}}{\partial \theta_{V_{se_es}}} \quad (20)$$

$$\frac{\partial Q_{es}}{\partial |V_{se_es}|} = 0 \quad (21)$$

The series converter maintains a steady regulated voltage across the vital load while connecting the output in series with the output of the non-critical load to handle voltage variations caused by the meteorological conditions of the hybrid model. The shunt converter compensates for the actual power demand of the shunt converter and maintains the DC link voltage. The voltage fluctuation on the input side can be balanced by a series converter and a non-critical load, and can therefore be called as Smart load.

Therefore, the purpose of controlling the series converter is to control the voltage on a non-critical demand while adjusting the voltage level. The clever coupling of an electrified spring demand and a non-critical demand can do this by altering the actual and reactive power usage. The control structure of series converters with hanging control is shown in Fig. 3 shown. Droop control has the advantage of coordinated control of reactive power compensation and voltage control between multiple electric springs without communication. Reference voltage and measured voltage can be deducted and delivered to PI controller to produce the needed real power $P_{(se_es)}$ and $Q_{(se_es)}$ is taken as 0. Using real power and reactive power and series converter current I_{nc} , reference injected voltage ($V_{(es_ref)}$ and $\theta_{(es_ref)}$) by series converter can be calculated as shown in Fig. 3. Reference voltage is modified using a droop gain to match the feeder voltage

3. HYBRID SYSTEM

Hybrid generation system with application of electric spring back-to-back converter for reactive power compensation and voltage regulation at load side is shown in Fig. 2. A rechargeable battery device, two generation modules (breeze and sun), and a common DC connection are used to supply power to the grid side through an inverter.

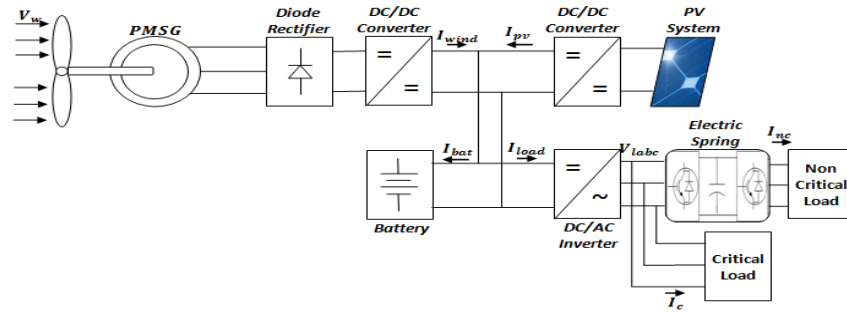


Fig. 2. Hybrid System

Case 1. Electric Spring Converter Hardware results

Hardware implementation of a Hybrid generation system with Electric spring back-to-back converter is designed and hardware results are compared with the simulation. A Hybrid

generation system hardware is designed and the results are tabulated as below for variable wind and solar conditions.



Fig. 3. Hardware Implementation of Wind and solar based Smart Grid

Case 2: Critical load of 170 W and 130 VAR and non-critical load of 170 W and 10 VAR are coupled to an electric spring

In this system, a back-to-back commutating electric spring is connected between the inverter and the critical load in line with the non-critical load. The AC voltage after changing the inverter after the LC filter is shown in the figure. 9. The load current after a series electric spring converter is shown in the figure. 10.

The RMS voltage of the load is shown in the figure. 11 and is nearly constant and is more variable, ranging from 0.98 to 1.02 with no electrified spring (0.5 to 1.2 pu). As seen in Fig., the load's active and reactive power.

Figure 13 displays the voltage at a steady load. The THD of the load voltage and current are shown in Figures 14 and 15. Table 1 is shown to compare simulation

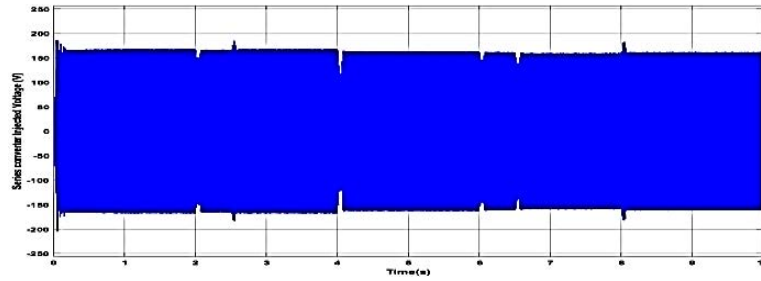


Figure 9. Inverter Filtered voltage

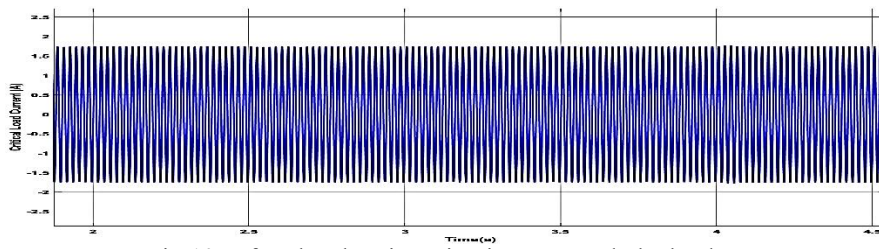


Fig 10. After the electric spring is connected, the load current

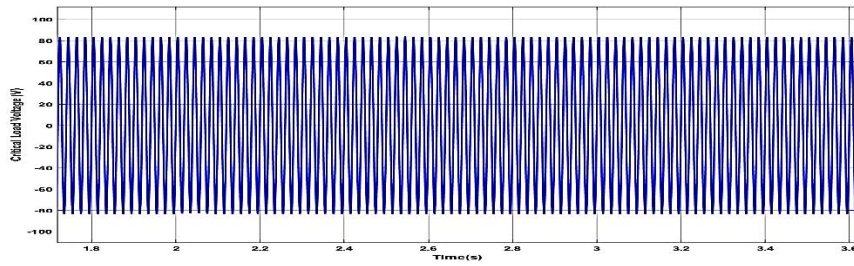


Fig11 With an Electric Spring, RMS Load Voltage

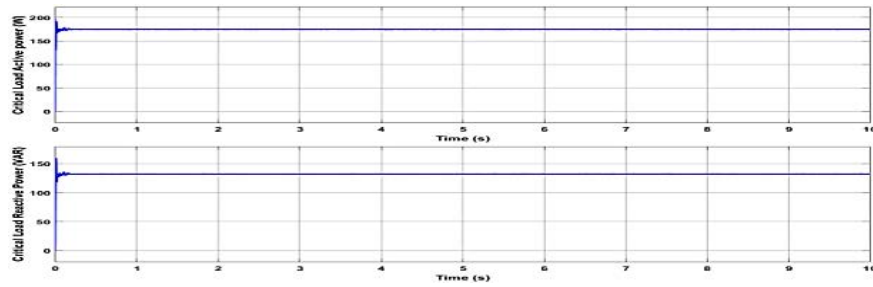


Fig 12. Reactive as well as Active Loading

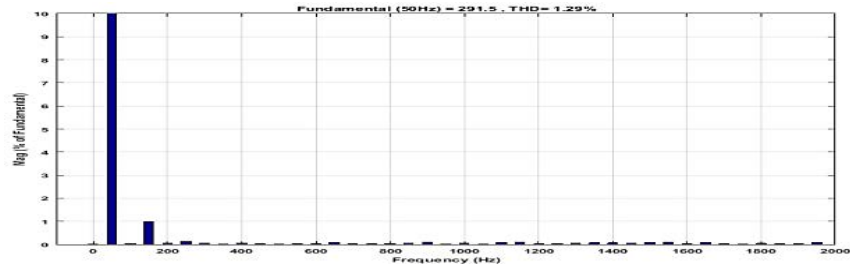


Fig13. Voltage Series Converter

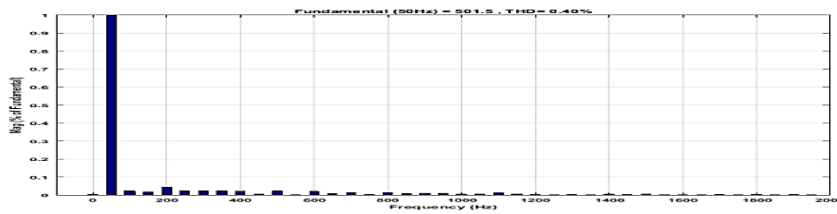


Fig 14: Charge current THD

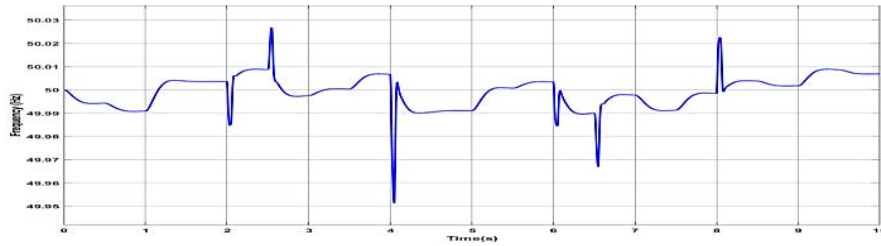


Fig 15. Voltage at Load Cycles

Table:1-Comparison of Hardware and simulation results

Parameter	Hardware results of Electric Spring	Simulation Results of Electric Spring
Voltage THD at Load	0.8	0.4
Current THD at Load	2.1	1.29
Power Factor	0.92	0.9826
% Voltage Variation	4.2%	2 %
%Frequency Variation	0.3%	0.1%

3. CONCLUSION

The back-to-back electric spring is connected to a hybrid system to improve voltage and frequency stability for critical loads and compensate for reactive power. The sun and wind are considered as energy sources and the line voltage is linked to the battery. The battery

storage device is connected to withstand the maximum load. Since both renewable energy sources are sensitive to weather, the common DC bus voltage of the two energy sources is unstable. This affects the stability of critical and non-critical loads connected to the DC bus through the inverter. To improve voltage and frequency stability and to compensate for reactive power, an electric spring is connected to the converter between the inverter and the critical load. To achieve the electric spring effect, a control scheme is applied to both converters. Simulated findings with equipment and those from MATLAB/SIMULINK are used to validate the proposed converter in the hybrid model. The findings demonstrate that perhaps the electric spring back-to-back converter successfully balances reactive power while stabilizing frequencies and voltages.

References

1. Md Asif, Dr Sardar Ali, Dr N Sambasiva Rao, Voltage & Frequency Regulation, Power Factor, THD Of Load Voltage and Current Improvement of an Electric Spring Based Smart Grid, International Journal of Advanced Research in Engineering and Technology, Volume 11, Issue 12, December 2020, pp.2320-2340
2. Md Asif, Dr Sardar Ali, Dr N Sambasiva Rao, Wind and PV Based Smart Grid Power System Analysis Using MPPT and PSO Technique, International Journal of Advanced Science and Technology Vol. 29, No. 5, (2020), pp. 7439-7450
3. Md Asif, Dr Sardar Ali, Dr N Sambasiva Rao, Power quality of a smart grid using MPPT and PWM technique, International Journal of Electrical Engineering & Technology (IJEET) Volume 11, Issue 2, March – April 2020, pp. 95-105
4. N. Arghira, I. Stamatescu, I. Făgărășan, G. Stamatescu, V. Calofir and S. S. Iliescu, "Demand dispatch framework for smart distribution grids," 2017 12th IEEE Conference on Industrial Electronics and Applications (Siem Reap, 2017, pp. 48-52.
5. S. M. A. Mahmud and P. Sant, "Real-time price savings through price suggestions for the smart grid demand response model," 2017 5th International Istanbul Smart Grid and Cities Congress and Fair (ICSG), Istanbul, 2017, pp. 65-69
6. H. F. Jamahori and H. A. Rahman, "Hybrid energy storage system for life cycle improvement," 2017 IEEE Conference on Energy Conversion (CENCON), Kuala Lumpur, 2017, pp. 196-200.
7. Z. Akhtar, B. Chaudhuri and Shu Yuen Ron Hui, "Smart loads for voltage control in distribution networks," 2016 IEEE Power and Energy Society General Meeting (PESGM), Boston, MA, 2016, pp. 1-1.

8. D. Santos-Martin and S. Lemon, "Simplified Modeling of Low Voltage Distribution Networks for PV Voltage Impact Studies," in *IEEE Transactions on Smart Grid*, vol. 7, no. 4, pp. 1924-1931, July 2016.
9. V. Yaramasu, B. Wu, P. C. Sen, S. Kouro and M. Narimani, "High-power wind energy conversion systems: State-of-the-art and emerging technologies," in *Proceedings of the IEEE*, vol. 103, no. 5, pp. 740-788, May 2015.
10. N. Neyestani, M. Y. Damavandi, M. Shafie-khah, J. P. S. Catalão and G. Chicco, "Uncertainty characterization of carrier-based demand response in smart multi-energy systems," 2015 IEEE 5th International Conference on Power Engineering
11. F. Blaabjerg and K. Ma, "Future on Power Electronics for Wind Turbine Systems," in *IEEE Journal of Emerging and Selected Topics in Power Electronics*, vol. 1, no. 3, pp. 139-152, Sept. 2013
12. S. Tan, C. K. Lee and S. Y. Hui, "General Steady-State Analysis and Control Principle of Electric Springs with Active and Reactive Power Compensations," in *IEEE Transactions on Power Electronics*, vol. 28, no. 8, pp. 3958-3969, Aug. 2013.
13. S. Y. Hui, C. K. Lee and F. F. Wu, "Electric Springs—A New Smart Grid Technology," in *IEEE Transactions on Smart Grid*, vol. 3, no. 3, pp. 1552-1561, Sept. 2012